2003

Development of a polymer-based, pro-apoptotic cancer therapeutic

Rachel A. Jones
University of Wollongong, rachelj@uow.edu.au

DEVELOPMENT OF A POLYMER-BASED, PRO-APOPTOTIC CANCER THERAPEUTIC

A thesis submitted in fulfilment of the

requirements for the award of the degree of

Doctor of Philosophy

From

The University of Wollongong

By

Rachel Anne Jones (B. Biotech. Hons. Class 1)

Department of Biological Sciences

2003

Acknowledgments

This thesis would not have been possible without the support of many people.

Firstly, I would like to thank Associate Professor Mark Wilson for his continual support, guidance, encouragement and knowledge over the past 4 years. He always had time to answer all my questions and help me in every way possible. He has graciously put up with my continual laughter and jokes. Thanks Mark for fighting my battles with Leica in Germany and letting me have sing-a-long Tuesdays. I feel privileged to have worked in your lab and would certainly recommend you as a supervisor to future students.

Thankyou also to all the past and present students in Lab 110, 112 and 120: Kerry, Dave, Matt, Marc, Stevie, Alison, Juzzy, Elise, Kara, Helen, Carolyn, Leonie, Nicole, Maree, Jovanka, Sarah, Fay, Timra and Cindy. The fond memories of this lab (e.g. Stewie, Leroy and Tyson the Siamese fighting fish, the lab gymnastics, and the never ending lab photos) will stay with me for a long time to come. Thankyou especially to Alison Smail and Christine Gillen who have made these last 4 years extremely entertaining and exciting. I have no doubt that our friendship will last for many years.

Thankyou to Stephen Pine, Alison Ung and the many other students in the Pine Lab. Thankyou for allowing me to work into your lab. Thankyou for your patience and willingness to answer all my questions, especially about the Rotovap! Working in a chemistry lab was like learning a new language!

Thankyou, also to the many friends that have supported me over the past 4 years. Thankyou to Katie Jones and Marianne Rietveld for graciously proof reading my thesis. Thankyou also to Marianne for ringing me on numerous occasions just to tell me to keep on going and that I would finish.

Lastly, I would like to thank my family, especially my Mum and Dad. Without their continual support, guidance and 100% confidence that I would finish, this thesis would not have been possible.

Abstract

This thesis documents work directed towards the development of a novel cancer therapeutic that uses a synthetic polymer to deliver a pro-apoptotic peptide into the cytosol of cancer cells and in turn induce death by apoptosis. This was approached by (1) testing the ability of a range of synthetic polymers (poly(2-alkyl acrylic acid)s (PAAAs) and poly[1-(dimethylamino)ethyl methacrylate] (pDMAEMA)) to facilitate the release of molecules from endosomes to the cytosol, (2) conjugating a pro-apoptotic peptide (Bad(140-165)) to a suitable endosomal-disruptive polymer, and (3) testing the ability of the polymer-peptide conjugate to enter the cytosol following endocytosis and to trigger apoptosis.

PAAAs were shown to be endocytosed into cells and transported to late endosomes, where acidification of the lumen by the membrane H^+-ATPase triggered polymer-mediated vesicle disruption and release of endosomal contents to the cytosol. pDMAEMA was shown to induce rapid necrosis and to be endocytosed into cells where it induced morphological changes in late endosomes/lysosomes. However, pDMAEMA did not have the ability to disrupt endosomes, and was thus not used in further experiments. In addition, the very high toxicity of pDMAEMA could also pose a significant risk of bystander cell damage in cancer therapies. A hydrazide-linker (X) was synthesised and conjugated to PAAAs. Results showed that (1) the membrane disruptive ability of PAAAs was retained following conjugation with hydrazide linker, and (2) the carboxcyclic-hydrazide bond incorporated within the linker was stable at pH 7 but not at pH 5. Finally, PAAA-X was conjugated to Bad(140-165) to form PAAA-X-Bad(140-165). Immunofluorescence assays showed that PAAA-X-Bad(140-165) partially co-localised with early endosomes and induced disruption

of endosomes and release of their contents into the cytosol in a time-dependent manner. Surprisingly, cell viability was retained following uptake of PAAA-X-Bad(140-165). The reasons why apoptosis was not induced following uptake of PAAA-X-Bad(140-165) are currently unknown, however possibilities include incomplete cleavage of the linker and/or insufficient release of Bad(140-165) into the cytosol. Future experiments, such as increasing the number of linkers and/or Bad(140-165) molecules attached to molecules of PAAA, may aid in the understanding of why apoptosis was not induced.

As an adjunct to studies of the effects of polymers and PAAA-X-Bad(140-165) on cells, a new technique was developed to measure mitochondrial permeability transition (MPT) in intact cells. In this method, calcein is introduced into cells by pinocytic loading. Polarised mitochondria are visualised as darkened voids within a bright green fluorescent cytosol. MPT is measured as an in-filling of calcein fluorescence into these darkened voids. This method is free of disadvantages associated with earlier developed techniques and will be valuable in studies of MPT in intact cells. However, unfortunately, technical limitations prevent the use of this method to measure MPT in cells undergoing apoptosis.

Taken together, results presented in this thesis provide a firm foundation for the future development of a novel cancer therapeutic that (1) directly targets cancer cells, (2) induces apoptotic death, and (3) avoids disadvantages associated with traditional cancer therapeutics.

Table of Contents

Abbreviations

$\Delta\psi_{mit}$	disruption of mitochondrial transmembrane potential
μg	microgram
μg/ml	micrograms per millilitre
μl	microliter
μm	micometer
μM	micromolar
%	percent
C	degrees Celsius
AEMA	aminoethylmethacrylate
AIF	apoptosis inducing factor
ANT	adenine nucleotide translocator
AO	acridine orange
ATP	adenosine triphophate
BA	bongkrekic acid
BAF	bafilomycin
Bcl-2	B-cell leukemia/lymphoma 2
BH	Bcl-homology domains
BIR	baculovirus IAP repeat
b-pDMAEMA/AEMA	biotinylated pDMAEMA/AEMA
b-PEAA	biotinylated PEAA
BSA	bovine serum albumin
Calcein-AM	calcein-acetoxymethyl ester
Capases	cysteinyl asparate-specific proteinases
Cat B	cathepsin B
cDNA	complementary DNA
$CoCl_2$	cobalt chloride
CO_2	carbon dioxide
cm/h	centimetres per hour
Da	Dalton
dATP	deoxyadenosine triphosphate
DCC	N,N-Dicyclohexylcarbodiimide
DFF	DNA fragmentation factor
Diablo	direct IAP binding protein with low PI
$DiOC_6(3)$	3,3'-dihexyloxacarbocyanine Iodine
DISC	death-inducing signaling complex
DMAP	4'dimethylaminopyridine
DMEM:F12	dulbeccos modified eagles medium: hams F1
DMF	dimethyl formamide
DMSO	dimethylsulfoxide
DNA	dioxyribonucleic acid
DOTAP	dioleyltrimethylammonium propane
Dox	doxorubicin
EDTA	ethylenediamine-tetraacetic acid

EEA1	early endosomal antigen 1
EGFP	enhanced green fluorescent protein
EPR	enhanced permeability and retention effect
FADD	Fas-associated death domain protein
FBS /FCS	foetal bovine serum/ foetal calf serum
FITC	fluorescein isothiocyanate
FL1	green fluorescence
FL2	orange fluorescence
FL3	red fluorescence
FSC	forward scatter
g	grams
Grf	globular region of fluorescence (Lamp1 staining)
H_2O	water
HCl	hydrochloric acid
HEPES	N-(2-hydroxyethyl)piperazine-Ní-(2-ethanesulfonic acid)
HPMA	N-(2-Hydroxypropyl)methacrylamide)
HSD	honestly significant difference
IAP	inhibitor of apoptosis family of proteins
Ig	immunoglobulin
K_D	binding affinity
kb	kilobase
kDa	kilodaltons
Lamp-1	lysosomal-associated membrane protein-1
M	molar
mM	millimolar
Mab	monoclonal antibody
MBA	4-maleimidobenzoic acid
ml	milliliter
ml/min	milliter per minute
mg	milligrams
mg/ml	milligrams/milliliter
mm	milimeter
mM	Milimolar
MPT	mitochondrial permeability transition
MSDH	O-methyl-serine dodecylamide hydrochloride
N_2	nitrogen gas
NaCl	sodium chloride
NAD/H	nicotinamide adenine dinucleotide
NaOH	sodium hydroxide
NCS	neocarzinostatin
ng/ml	nanograms/mililiter
nm	nanometer
nM	nanomolar
NMR	nuclear magnetic resonance
PAAA	poly(2-alkylacrylic acid)
PAAA-X	PAAA conjugated to the hydrazide linker

PAAA-X-Bad(140-165)	PAAA conjugated to hydrazide linker and Bad(140-165)
PB	polymer buffer
PBS	phosphate buffered saline
pDMAEMA	poly[1-(dimethylamino)ethyl methacylate]
PEAA	poly ethyl acrylic acid
PEAA-X	PEAA conjugated to the hydrazide linker
PEG	polyethylene glycol
PF	paraformaldehyde
PI	propidium iodide
PK1	N-(2hydroxypropyl)methacrylamide copolymer-doxorubicin
PL	pinocytic loading
PMAA	poly methyl acrylic acid
PMT	photomultiplier tubes
PNU	HPMA copolymer-pacitaxel
ppm	part per million
PPAA	poly propyl acrylic acid
PPAA-X	PPAA conjugated to the hydrazide linker
PS	phosphatidylserine
PT	permeability transition
PTP	permeability transition pore
RA	13-cis-retinoic acid
RBC	red blood cells
RME	receptor mediated endocytosis
ROI	regions of interest
ROS	reactive oxygen species
Smac	second mitochondria-derived activator of caspases
SMANCS	SMA-NCS conjugate complex
SAMSA	5-((2-(and-3)-S-(acetylmercapto)succinoyl)amino)fluorescein
SDS-PAGE	sodium dodecyl sulfate-polyacrylamide electrophoresis
SE	standard error
SFM	serum free media
SMA	poly(styrene-co maleic acid/anhydride)
S.R.	substitution ratio
SSC	side scatter
TAPS	(N-tris[Hydroxymethyl]methyl-3-aminopropane-sulfonic acid)
TEMED	N,N,N,N-tetramethylethylenedaime
TFA	trifluoroacetic acid
TLC	thin layer chromatography
TMRM	tetrmethylrhodamine methyl ester
TNFR1	tumour necrosis factor receptor 1
Tris	tris(hrdroxymethyl)aminomethane
TX-100	triton X-100
UV	ultra violet
VAD-FMK	valyl-alanyl-aspartyl-[o-methyl]-fluormethylketone
VDAC	voltage dependent anion channel

v/v	volume per volume
V	volts
w/v	weight per volume
X	hydrazide linker
XK469	2-[4-(7-chloro-2-quinoalinyloxy)phenoxypropionic acid)

List of Figures

List of Tables

Chapter 1

Introduction

This chapter gives a review of the current understanding of apoptosis. Details of the molecules and processes involved and the mechanisms of regulation are described. The development of pH-sensitive polymers and their use in cancer therapies are then described. The final section of this chapter describes a novel cancer therapeutic, involving pH-sensitive polymers that directly target cancer cells and induce death by apoptosis.

1.1 Apoptosis

Apoptosis, or programmed cell death, represents a physiological form of cell death and is thought to be involved in every homeostatic and pathological process in the body (Gastman, 2001; Wilson, 1998). It is the dominant form of cell death especially in the organs and tissues of the immune system and is genetically controlled by an internally encoded suicide program (Steller, 1995; White, 1993).

The apoptotic pathway is divided into three functionally distinct phases: initiation, execution and degradation. During the initiation phase the cell receives a death-inducing signal, which can result from various chemical and biological agents (Gastman, 2001). Examples of initiating signals include a shortage of nutrient supply or ligation of death signal-transmitting receptors (Kroemer *et al.*, 1997). Apoptosis can be initiated by many different pathways but it is in the execution phase where these different signals are translated into a common molecular pathway. During the execution phase a 'point of no return' is passed and the cells become irreversibly programmed to die (Kroemer *et al.*, 1995; Kroemer *et al.*, 1997). The final degradation phase is accompanied by a distinct set of morphological and physiochemical changes including:

1. Cellular and nuclear shrinkage, which is accompanied by internucleosomal DNA fragmentation (Patel *et al.*, 1996; Vander Heiden *et al.*, 1997).
2. Protein degradation and blebbing of the membrane into apoptotic bodies (which contain intact cytoplasmic organelles and nuclear fragments). This occurs just before phagocytosis by macrophages or adjacent cells (Shi, 2001; Villa *et al.*, 1997), preventing the leakage of noxious cellular contents into the surrounding tissue. Figure 1.1 depicts major cytostructural changes that occur during apoptosis.

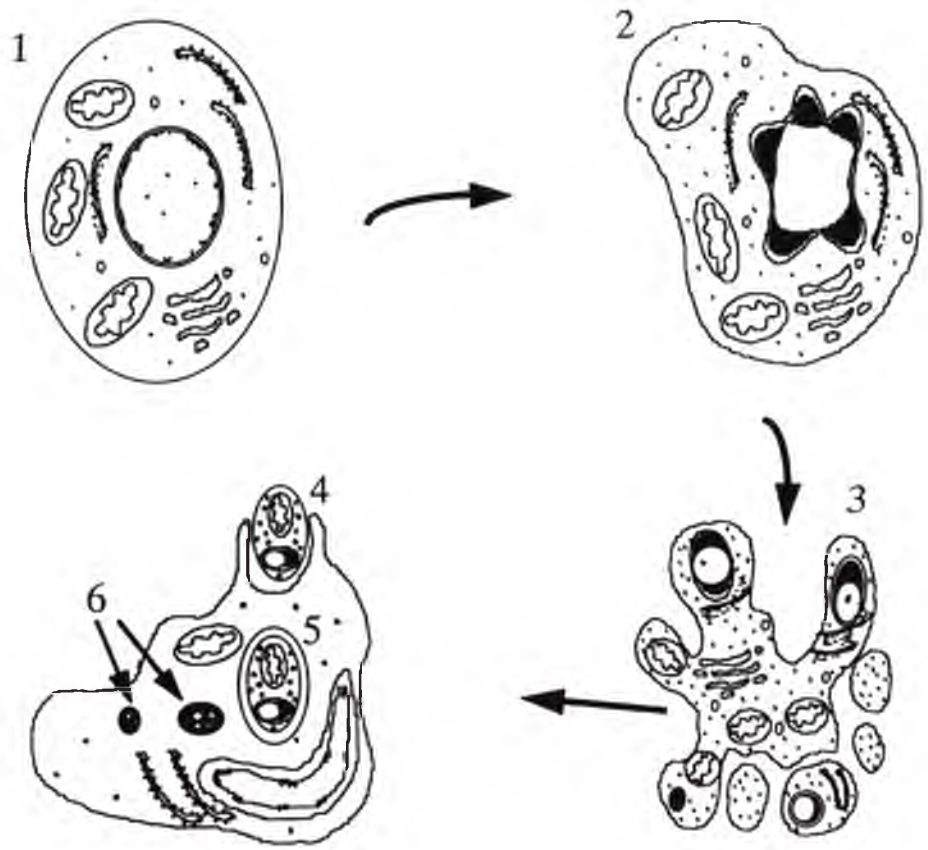

Figure 1.1: The major cytostructural changes that occur during apoptosis. (1) Shows a normal cell. In the early stages of apoptosis the cytoplasm starts to condense, the chromatin becomes very dense and compact, forming uniform, fine granular masses on the nuclear envelope, and the nuclear and cellular outlines become mildly ruffled and convoluted (2). This is then followed by rapid chromatin condensation and convolution of the nuclear and cellular outlines. The nucleus breaks up into discrete membrane enclosed fragments, and the cell buds to produce membrane-bound apoptotic bodies containing well-preserved organelles (3). The apoptotic bodies are phagocytosed by adjacent cells (4) and degraded within lysosomal vacuoles (5) to form compact debris (6) (Adapted from Kerr, 1995).

1.2 Organelles Involved in Apoptosis

In the evolution of eukaryotic cells, mitochondria have for a long time played a prominent role (Scheffler, 2001). They (1) are essential for cellular energy metabolism (Rutter and Rizzoto, 2000), (2) reduce and detoxify free radicals, such as reactive oxygen species (ROS) (Mignotte and Vayassiere, 1998), (3) serve as a cellular calcium buffer (Orth and Schapira, 2001), and (4) are sites of electron transport and generators of cellular ATP (Harris and Thompson, 2000). A growing body of evidence from many independent research groups, now supports a role for mitochondria as crucial participants in the induction and execution phases of apoptosis (Finucane *et al.*, 1999; Wilson, 1998; Green and Reed, 1998; Kroemer *et al.*, 1998; Bernardi *et al.*, 2001; Desager and Martinou, 2000, Gottlieb *et al.*, 2000; Parone *et al.*, 2002).

In recent years, several controversial reports have suggested that lysosomes may also play a crucial role in apoptosis, particularly in the initiation phase. In a number of cell types, apoptosis is associated with an early destabilisation of lysosomal membranes and subsequent release of lysosomal enzymes into the cytosol (Terman *et al.*, 1999; Neuzil *et al.*, 1999; Roberg *et al.*, 1999). It was suggested that rupture of the lysosomal membrane may be an early upstream event in apoptosis (Antunes *et al.*, 2001). Despite these recent findings, the involvement of lysosomes in apoptosis is still poorly understood (see section 1.7), and probably because of this, not generally accepted (Hengartner, 2000).

It has also been suggested that the endoplasmic reticulum may be involved in the execution phase, independent of mitochondria (Ng *et al.*, 1997). Ng *et al.* (1997) suggested that caspase-mediated generation of an N-terminal 20 kDa fragment of the

human protein p28 Bap31 in the endoplasmic reticulum induces apoptotic nuclear changes. It is also possible that other organelles may be involved. For example, Mancini and colleagues (2000) have suggested that the Golgi complex may be involved in the execution phase, while Li *et al.* (2000) suggest the involvement of the nucleus in the execution phase. However, to date, evidence is limited and further research will be needed to confirm these suggestions.

1.3 Proteins Involved in Apoptosis

Extensive research has revealed many of the crucial components involved in apoptosis, however ongoing research indicates the potential for many more. Some of the vital components of the apoptotic pathway discovered to date include: (1) cytosolic-based proteins such as caspases and inhibitor of apoptosis (IAP) family proteins and (2) mitochondria-associated proteins such as Bcl-2 family proteins, cytochrome c, Smac/DIABLO, apoptosis inducing factor (AIF) and Omi/HtrA2.

1.3.1 Cytosolic Proteins

1.3.1.1 Caspases

Caspases (cysteinyl aspartate-specific proteinases) are a family of intracellular cysteine proteases that cleave substrates adjacent to aspartic acid residues and that can themselves be activated by cleavage at similar sites (Mignotte and Vayssiere, 1998; Green and Evan, 2002). They are produced in cells as catalytically inactive zymogens and are activated by either truncation or dimerization. Three general mechanisms of caspase activation have been described thus far:

1. Processing by an upstream caspase – This type of activation results from pro-caspases being exposed to a previously activated caspase. It is the simplest mechanism of caspase activation and is used specifically for the activation of downstream caspases, such as caspase-3, -6 and –7.

2. Induced Proximity – Muzio *et al.* (1998) suggest that the formation of a death-inducing signalling complex (DISC), comprised of tightly clustered specific ligands (e.g. Fas), receptor molecules, adaptor proteins (e.g. FADD) and pro-caspase-8, is sufficient to allow the pro-enzyme molecules to mutually cleave and activate each other, thereby producing active caspase-8.

3. Association with regulatory subunits – This activation process is the most complex. The only known example involves the formation of a large complex, comprised of Apaf-1, cytochrome c, ATP and pro-caspase-9. The specific combination of these proteins results in the activation of caspase-9, however, the exact mechanism of activation remains unclear (Hengartner, 2000).

Over a dozen caspases have been identified and are divided into three subgroups, based on their substrate preference, extent of sequence homology and structural similarities (Hengartner, 2000). Table 1.1 shows the groupings of all known caspases. The cysteine containing sequence glutamine-alanine-cysteine-arginine-glycine (QACRG) is a conserved motif common to all caspases; if the cysteine is mutated, then the proteases are inactivated (Vaux and Strasser, 1996).

Group	Caspase
I	Caspase-1, -4, -5
II	Caspase-2, -3, -7
III	Caspase-6, -8, -9, -10
Structurally related to group I	Caspase-11, -12, -13
Structurally related to group II	Caspase-14

Table 1.1: – Caspases and their subgroups (Gastman, 2001).

1.3.1.2 IAPS

The inhibitor of apoptosis (IAP) family of proteins inhibit the enzymatic activity of mature caspases (Miller, 1999). In the past few years several distinct IAPs have been identified, all of which exhibit anti-apoptotic activity. Table 1.2 summarises the known IAPs. All IAPs contain a highly conserved functional region known as the baculovirus IAP repeat (BIR), which contains approximately 80 amino acids folded around a zinc atom (Shi, 2001). Most IAPs have more than one BIR region, with the various BIR domains exhibiting different functions. Caspase inhibition occurs through precise interactions between the BIR domains of IAPs and the mature caspase.

XIAP	BRUCE	Survivin	ML-IAP
CIAP-1	CIAP-2	NAIP	Livin
Apollon			

Table 1.2: Members of the IAP Family (Gastman, 2001).

1.3.2 Mitochondria-Associated Proteins

1.3.2.1 Bcl-2 Family

In recent years, extensive research has been conducted on the Bcl-2 family proteins, as they have been strongly implicated as important regulators of apoptosis. A primary mechanism by which these proteins regulate apoptosis is probably by controlling cytochrome c release, however, further research is needed to determine the exact function of these specialised proteins. A number of Bcl-2 family members have been identified and are summarised in Table 1.3. Each family member contains at least one of the four conserved functional regions called Bcl-2 homology domains (BH1-BH4), schematically shown in Figure 1.2. These domains enable the different members of the family to form homo- or hetero-dimers with each other, thereby enhancing or antagonising their functions (Mignotte and Vayssiere, 1998; Kelekar *et al.*, 1997). They are divided into three different groups based on Bcl-2 homology and function. The anti-apoptotic members, such as Bcl-2, harbour at least three, but generally four, BH domains, while the pro-apoptotic members have between one and three BH domains. The pro-apoptotic group is subdivided into two groups – those with only one BH domain and those that possess up to three domains. Many of the pro-apoptotic family members, such as Bax, Bid and Bad, are synthesised in the cytosol, however, following an apoptotic stimulus, they undergo a conformation change and are translocated to mitochondria (Dengy and Wu *et al.*, 2000; Datta *et al.*, 2000).

Anti-apoptotic	Pro-apoptotic	
	Multi-domain	**BH3 domain Only**
Bcl-2	Bcl-x_S	Bad
Bcl-x_L	Bok/Mtd	Bid
Bcl-w	BAX	BIM/BOD
Mcl-1	BAK	Harakiri/DP5
A1/Bfl-1	Bcl-Gl	BLK
Boo/Diva		NIX/BINP3
Nr-13		Noxa
		Bcl-Gs
		MAP-1

Table 1.3 : Functional groupings of Bcl-2 family members (B-cell leukemia/lymphoma 2). (Gastman, 2001; Cory and Adams, 2002).

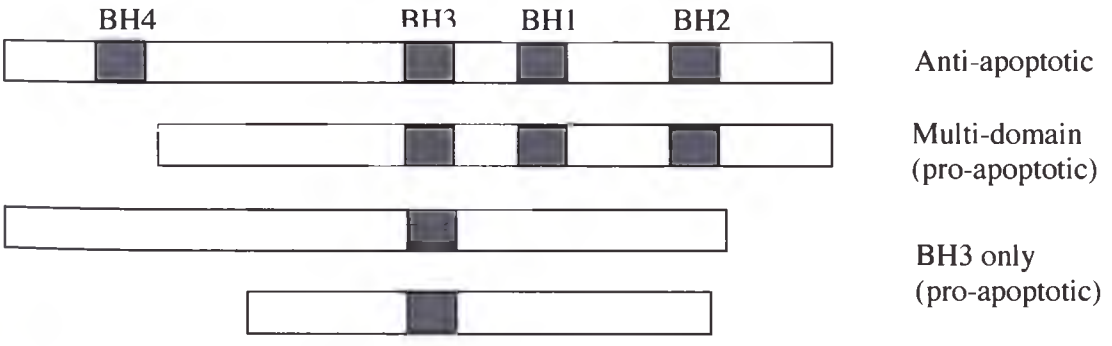

Figure 1.2: Schematic representation of the BH domains contained within the Bcl-2 family members (Adapted from Hengartner, 2000; Cory and Adams, 2002).

1.3.2.2 Cytochrome c

Cytochrome c is a 12.3 kDa extrinsic membrane protein, normally associated with the outer surface of the inner membrane of mitochondria (Gastman, 2001). It is encoded by a nuclear gene and is translated by cytosolic ribosomes as apocytochrome c. Apocytochrome c is subsequently translocated into mitochondria where a haeme group is attached covalently to form holocytochrome c (Yang *et al.*, 1997; reviewed by Waterhouse *et al.*, 2002). The release of holocytochrome c from mitochondria has been implicated as one of the critical steps in apoptosis; much debate continues over the mechanism and the order of events that lead to the release of the protein. The Bcl-2 proteins are thought to be involved in this process. This is supported by Gross *et al.* (1999) and others, who have shown that the addition of pro-apoptotic Bcl-2 family members to isolated mitochondria is sufficient to induce cytochrome c release, whereas the over-expression of anti-apoptotic Bcl-2 family proteins inhibits cytochrome c release. In addition to Bcl-2, mitochondrial lipids (e.g. cardiolipin) have also been suggested to be involved in the release of cytochome c. Cardiolipin is thought to induce the detachment of cytochrome c from the inner mitochondrial membrane (Ott *et al.*, 2002).

1.3.2.3 Smac / DIABLO

Smac (second mitochondria-derived activator of caspases), also known as DIABLO (direct IAP binding protein with low pI) is a recently discovered mitochondrial protein. It is comprised of 239 amino acids, including an N-terminal 55 residue-long targeting sequence that is cleaved upon transport into mitochondria (Du *et al.*, 2000; Verhagen *et al.*, 2000, Reed, 2002). During apoptosis, Smac/DIABLO is released, in conjunction with cytochrome c, from the intermembrane space of mitochondria. However, it is yet to

be determined if these two proteins are released by the same mechanism. Smac interacts with multiple IAPs, thereby preventing their inhibitory effect on both initiator and effector caspases (Chai *et al.*, 2000). The interaction between Smac and various IAPs is thought to involve the four N-terminal residues of Smac and the BIR domains of the IAPs (Liu *et al.*, 2000; Wu *et al.*, 2000).

1.3.2.4 Omi/HtrA2

The serine protease Omi is the most recent mitochondrial protein implicated in apoptosis to be identified. Like Smac, Omi is localised predominantly in the intermembrane space of mitochondria but is released into the cytosol, in conjunction with Smac and cytochrome c, during apoptosis (Hegde *et al.*, 2002). As yet, it is not known if Omi, cytochrome c and Smac are released by the same mechanism (Martins *et al.*, 2002). In the cytosol, the N-terminal 133 amino acids are cleaved from the rest of the protein and mature Omi protein is generated (van Loo *et al.*, 2002). To date the function of Omi remains unclear, however, it is thought to interact with the BIR domains of IAP proteins, thereby promoting caspase activity (van Loo *et al.*, 2002; Martins *et al.*, 2002; Verhagen *et al.*, 2002). Hegde *et al.* (2002) have also shown that Omi can induce cell death in mammalian cells independent of caspases, Apaf-1 or IAP, via its serine protease activity; they suggest that it may be involved in a caspase-independent mechanism of cell death.

1.3.2.5 AIF

AIF (apoptosis inducing factor) is a 50 kDa protein which is normally confined to the intermembrane space of mitochondria but translocates to the nucleus following induction of apoptosis (Susin *et al.*, 1999a; Daugas *et al.*, 2000). Once inside the

nucleus, it induces chromatin condensation and cleavage of DNA into 50 Kb fragments, however the mechanism involved remains unresolved (Ye *et al.*, 2002). AIF has now been shown to induce caspase-independent peripheral chromatin condensation and DNA fragmentation when added to purified nuclei. In addition to its apoptogenic action on nuclei, AIF can also participate in the regulation of apoptotic mitochondrial permeabilisation (reviewed by Cande *et al.*, 2002).

1.4 Pathways Involved in Apoptosis

There are two major apoptotic pathways known to date: the intrinsic pathway, which is initiated by mitochondria, and the extrinsic pathway, initiated by cell surface receptors. The extrinsic pathway, or death receptor pathway, is triggered by members of the death receptor family, such as CD95 and tumour necrosis factor receptor 1 (TNFR1). The binding of a specific ligand to these receptors results in the formation of a death-inducing signalling complex. This complex, together with an adaptor molecule known as FADD (Fas-associated death domain protein), associates with multiple pro-caspase-8 molecules to cause caspase-8 activation (Hengartner, 2000). The activation of caspase-8 in turn activates other downstream caspases and causes apoptotic death (Figure 1.3).

The intrinsic pathway occurs in response to a wide range of death stimuli, including the activation of tumour suppressor proteins and oncogenes (Shi, 2001). It is thought that these diverse pathways converge on mitochondria, possibly via the action of pro-apoptotic Bcl-2 proteins. This is followed by the release of many proteins from the intermembrane space, such as cytochrome c, AIF (Lorenzo *et al.*, 1999), Smac/DIABLO (Du *et al.*, 2000; Verhagen *et al.*, 2000) and several pro-apoptotic

caspases, including pro-caspase-2,-3, and -9 (Loeffler and Kroemer, 2000). Exactly how these proteins are released and the order of release is still greatly debated and will be discussed later (Sections 1.5 and 1.6). Once in the cytosol, cytochrome c is thought to bind tightly with Apaf-1; this binary complex then associates with dATP or ATP and pro-caspase-9 to form a complex known as the apoptosome (Zou *et al.*, 1999; Saleh *et al.*, 1999; Green and Evan, 2002), which in turn activates pro-caspase-9 to form caspase-9. Interestingly, caspase-9 remains bound to the apoptosome as a holoenzyme, as caspase activity is only retained while it is bound in this conformation (Rodriguez and Lazebnik, 1999). The holoenzyme caspase-9 activates caspase-3 and subsequent apoptotic events (Hengartner, 2000; Desagher and Martinou, 2000). The final events include the activation of DNA fragmentation factor 45 (DFF45) which, when activated, functions as a nuclease and degrades chromatin into nucleosomal fragments.

The intrinsic and extrinsic pathways converge at the level of caspase-3 activation. The activation of caspase-3 is inhibited by IAP proteins, which are themselves antagonised by Smac/DIABLO following release from mitochondria (Hengartner, 2000). These pathways are linked by the action of Bid, a pro-apoptotic Bcl-2 family member (Yin, 2000). The activation of caspase-8, in the extrinsic pathway, increases the pro-death activity of Bid and its translocation to mitochondria, where it promotes release of cytochrome c and Smac (Yin 2000; Li *et al.*, 2002). Figure 1.3 schematically represents the extrinsic and intrinsic pathways.

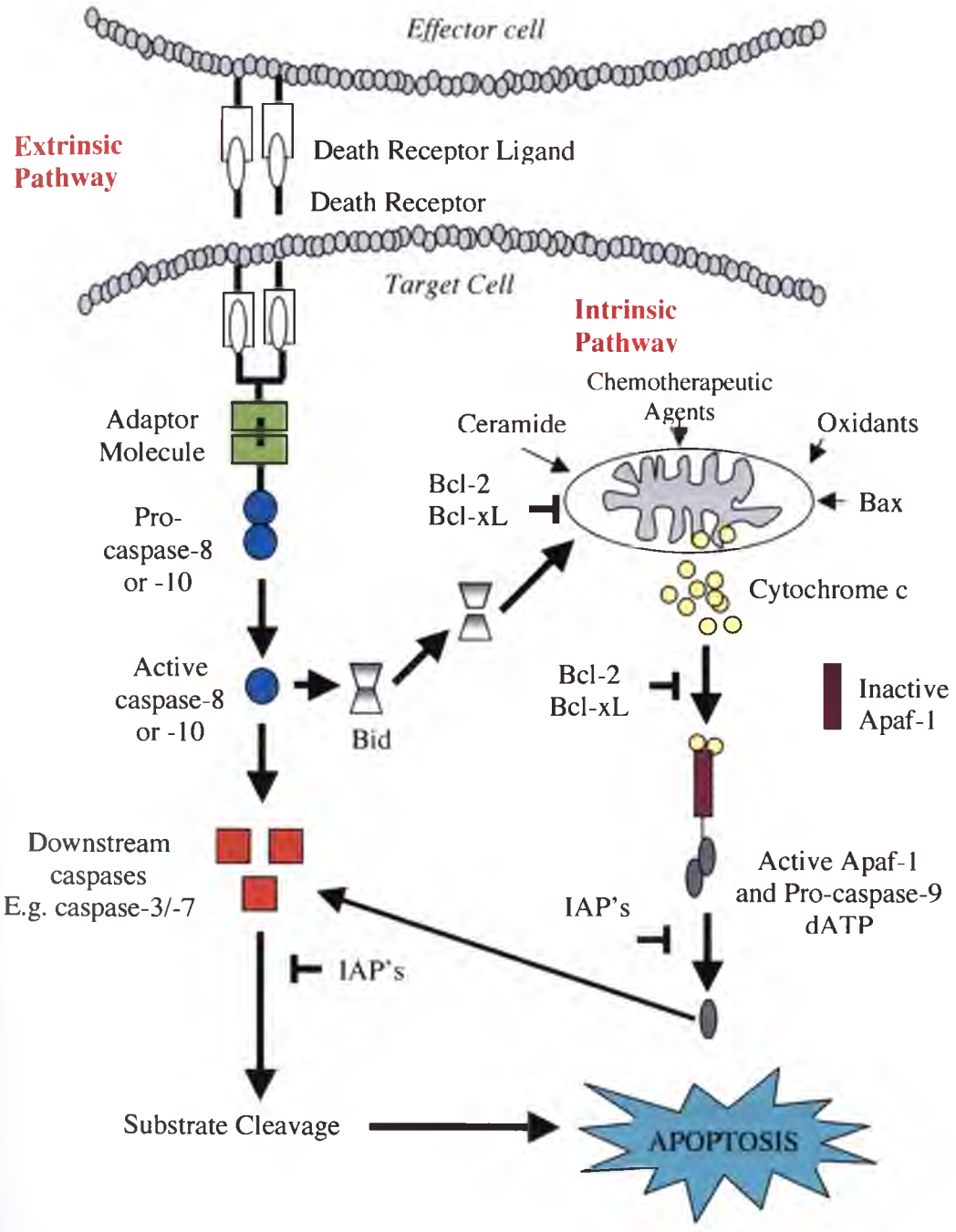

Figure 1.3: Schematic representations of the two major pathways of apoptosis. In the extrinsic pathway, death receptor ligands bind to death receptors and in turn activate caspase 8 and further downstream caspases, thereby causing apoptotic death. In contrast, the intrinsic pathway can be triggered by various cell death stimuli, which cause mitochondria to release proteins, such as cytochrome c. This then triggers a cascade of events, including the activation of caspases and DNA fragmentation (Adapted from Gastman, 2001).

1.5 Mitochondria and Apoptosis

Mitochondria are now accepted as key players in the execution phase of apoptosis. The culmination of results from many independent research groups has led to this conclusion. Some of these results are summarised below:

1. Kroemer and others (reviewed by Loeffler and Kroemer, 2000) have shown that mitochondrial membrane permeabilization often precedes the signs of advanced apoptosis and necrosis, irrespective of the cell type or death-inducing stimulus. They have also shown that inhibition of mitochondrial membrane permeabilization by specific pharmacological interventions (i.e. agents acting on mitochondrial proteins) prevents or retards cell death.
2. Balakirev and Zimmer (1998) reported major changes to mitochondrial integrity prior to the classical sign of apoptosis, and also mitochondrial depolarisation preceded DNA fragmentation.
3. Pastorino *et al.* (1998) and Zamzami *et al.* (1998a,b) have shown that the Bcl-2 family of proteins act on mitochondria to regulate apoptosis.
4. Green and Kroemer (1998), Kroemer and Reed (2000) and Boya *et al.* (2001) have shown that several pro-apoptotic signals converge on mitochondria to induce mitochondrial membrane permeabilisation and this phenomenon is under the control of Bcl-2 related proteins.
5. Gilmore *et al.* (2001) have shown that pinocytic loading of the pro-apoptotic mitochondrial protein cytochrome c in to intact cells induces activation of caspase-3 and –9 like enzymes, and a loss of mitochondrial depolarisation coincident with an increase in mitochondrial permeability.
6. Numerous proteins, such as Smac, Omi and cytochrome c, which have downstream apoptotic functions, are primarily localised in mitochondria (Du *et*

al., 2000; Verhagen *et al.*, 2000; van Loo *et al.*, 2002; Martins *et al.*, 2002; Verhagen *et al.*, 2002).

Two models for the involvement of mitochondria have been proposed:

1. The first model was initially proposed by Kroemer *et al.* (1997) and involves the phenomenon referred to as mitochondrial permeability transition (MPT). MPT results in the opening of mega channels or pores (permeability transition pores-PTP), which are formed under specific conditions at points where the inner and outer membranes of mitochondria touch. The opening of the pores allows for the equilibration of ions and respiratory substrates (<1500 Da) between the cytosol and the mitochondrial matrix, leading to the reduction of mitochondrial transmembrane potential ($\Delta\psi_{mit}$) (Mignotte and Vayssiere, 1998). $\Delta\psi_{mit}$ results from the asymmetric distribution of protons and other ions on either side of the inner mitochondrial membrane, which gives rise to a chemical (pH) and electrical gradient which is essential for mitochondrial function (Kroemer *et al.*, 1997). Following $\Delta\psi_{mit}$, water moves into the mitochondrial matrix, causing swelling and the outer mitochondrial membrane is broken (Sklachev, 1996). As a result, mitochondrial proteins (cytochrome c, AIF, Smac and Omi) are released into the cytosol, promoting caspase activation and triggering DNA fragmentation and chromatin condensation (Ferri and Kroemer, 2001) (Figure 1.4). This MPT-dependent model has been supported by studies of many cell types in response to various toxic stimuli (Zamzami *et al.*, 1997; Petit *et al.*, 1996; Boise and Thompson, 1997; Hirsh *et al.*, 1997; Zamzami *et al.*, 1998a,b; Cassarino *et al.*, 1999; Fulda *et al.*, 1999; Heiskanen *et al.*, 1999).

2. The second model of mitochondrial involvement in apoptosis proposes the release of mitochondrial proteins through an MPT-independent mechanism (Liu *et al.*, 1997). Many studies have suggested that cytochrome c release occurs in the absence of or prior to mitochondrial depolarisation (Goldstein *et al.*, 2000; Kluck *et al.*, 1997). For example, in Jurkat and FL5.12 cells, the release of cytochrome c was shown to coincide with swelling of the outer mitochondrial membrane. This change was apparent before the loss of Ψ_{mit}, which is normally associated with MPT (Kluck *et al.*, 1997). To date, four alternative mechanisms have been suggested for the MPT-independent release of mitochondrial proteins, however none of these have been established. These include: (1) formation of a lipid-pore complex in the outer mitochondrial membrane (Vander Heiden *et al.*, 1997), (2) Bcl-2 family members (e.g. Bax) forming channels in the outer mitochondrial membranes, thereby allowing cytochrome c and other proteins to be released but not damaging mitochondria (Shimizu *et al.*, 1999; Antonsson *et al.*, 1997), (3) direct action of upstream caspases on mitochondria (Susin *et al.*, 1997) and (4) Bcl-2 family members (e.g. Bax), in conjunction with mitochondrial permeability transition pores proteins (e.g. voltage dependent anion channel (VDAC)), forming pore in the outer mitochondrial membrane.

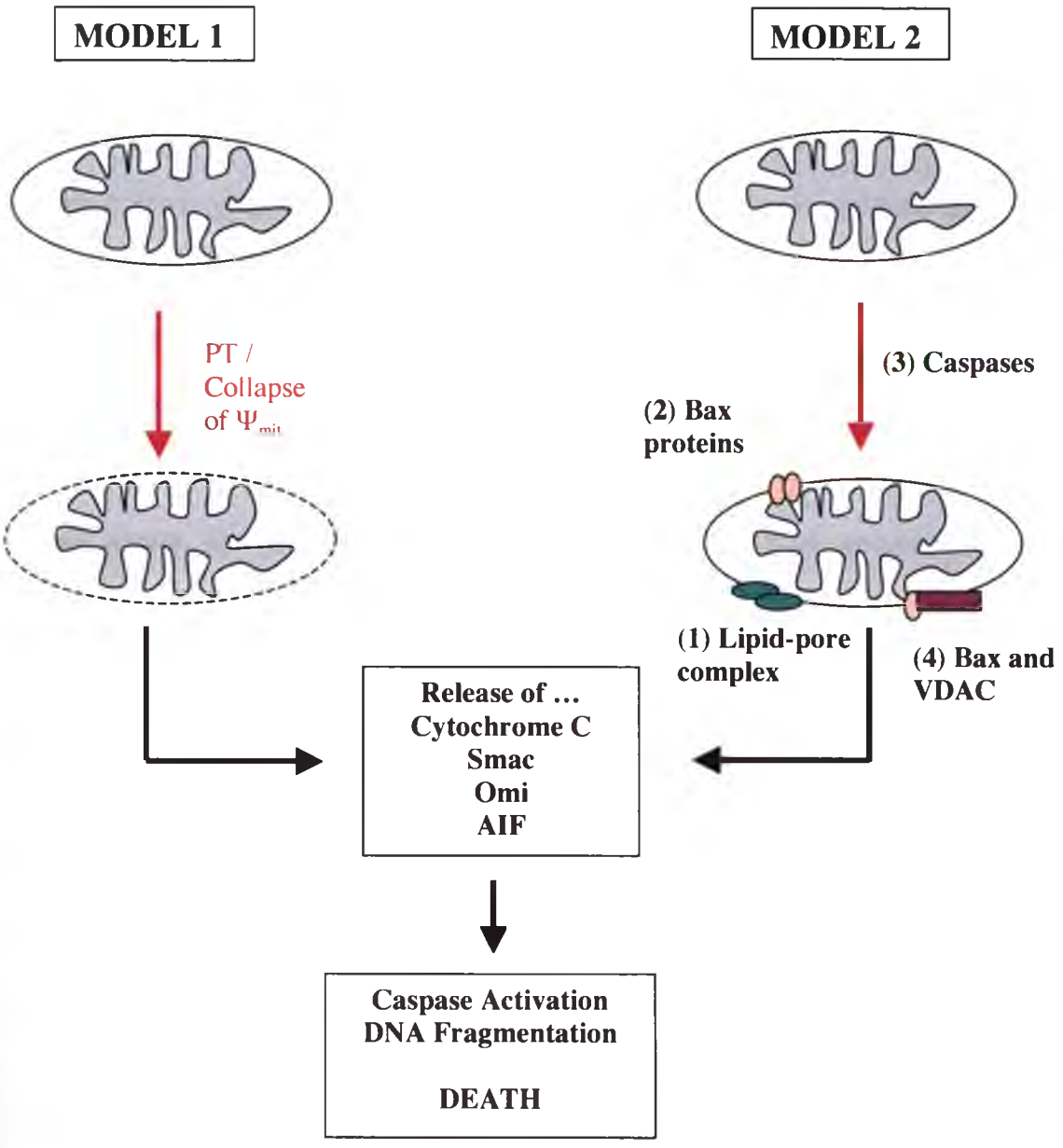

Figure 1.4: Schematic representation of two models of the involvement of mitochondria in apoptosis. In model 1, PTP open causing MPT, collapse of Ψ_{mit} swelling of mitochondria and release of mitochondrial proteins, such as cytochrome c, into the cytosol. This is followed by caspase activation and DNA fragmentation. In model 2, mitochondrial proteins are released by an MPT-independent mechanism. Many MPT-independent mechanisms have been proposed, including (1) formation of a lipid-pore complex, (2) Bax proteins forming large pores in the outer mitochondrial membrane and releasing proteins, (3) caspases acting directly on mitochondrial membranes, and (4) Bax forming pores in conjunction with VDAC.

1.6 Regulation of Apoptotic Pathways

Slight alterations in the apoptotic process can have drastic consequences. For example, abnormal down-regulation of apoptosis is a contributor to cancer and autoimmune diseases, whereas up-regulation of cell death is implicated in neurodegenerative disorders such as Alzheimer's disease (Thompson, 1995). Therefore, the apoptotic process must be highly regulated. In a wide variety of cell types, Bcl-2 and Bcl-2-related proteins are critical in preventing cells from undergoing apoptosis induced by various stimuli. The mechanism(s) by which these proteins modulate apoptosis is not yet known but several theories have been proposed:

1. One of the unique characteristics of the Bcl-2 family members is their ability to form homo- and hetero-dimers. One of the first theories advanced to account for the effects of Bcl-2 family members on apoptosis focussed on the interaction between Bax and Bcl-2 related proteins. Sedlak *et al.* (1995) reported that the formation of Bax homo-dimers promotes apoptosis and the formation of hetero-dimers between Bcl-2 related proteins and Bax prevents apoptosis in murine FL.5.12 cells. However, in some cell systems, the binding of Bax to Bcl-2 was not sufficient to prevent apoptosis (Knudson and Korsmeyer, 1997). It was suggested that the process of hetero-dimerization may inhibit apoptosis by preventing the translocation of Bax to mitochondria (Gross *et al.*, 1998; Nomura *et al.*, 1999).

2. Bcl-2 and Bcl-x_L may inhibit apoptosis by preventing the over-production of ROS and shifting the redox potential to a more reduced state. The mechanism for this effect is not known but it has been suggested that Bcl-2 may act in an antioxidant pathway (Mignotte and Vayssiere, 1998).

3. Pro-apoptotic Bcl-2 proteins may also regulate apoptosis through interaction with caspases. In mammalian cells a complex between caspase-9, Bcl-x_L Apaf-1 and cytochrome c is formed in many different types of cells induced to undergo apoptosis, including murine thymocytes (Hsu *et al.*, 1997). Caspase-9 and Bcl-x_L bind to distinct domains in the Apaf-1 molecule (Pan *et al.*, 1998). It has been suggested that the formation of this complex may regulate mammalian cell death (Pan *et al.*, 1998). Regulation is achieved by the binding of the Bcl-x_L to Apaf-1, which blocks the ability of Apaf-1 to promote the activation of caspase-9, hence preventing activation of other caspases and DNA fragmentation. Bcl-2 related proteins such as Bax, Bak and Bik are able to disrupt the interaction between Bcl-x_L and Apaf-1 by forming hetero-dimers with Bcl-x_L (Pan *et al.*, 1998: Mignotte and Vayssiere, 1998), allowing apoptosis to proceed.

4. Reed (1997) suggested that the Bcl-2 family inhibits apoptosis by inserting, following a conformational change, into the outer mitochondrial membrane, forming channels or even large holes. Muchmore *et al.* (1996) originally reported the ability of Bcl-x_L to form channels with discrete conductances in synthetic lipid membranes. Recently, Zhai *et al.* (2000) and Basanez *et al.* (1999) showed that Bid and Bax are also able to form pores in liposomes and release encapsulated molecules such as cytochrome c. However, this pore forming ability does not establish a corresponding function *in vivo*. The synthetic membranes used in these studies do possess a similar negative charge to the outer mitochondrial membrane. Therefore, it is possible that Bcl-2 proteins and mitochondrial membranes might interact in a similar manner.

5. It is hypothesised that the Bcl-2 family members may be involved in the formation of large pores through the recruitment and interaction of other outer mitochondrial membrane proteins. Bcl-2 family members have been shown to interact with a large mitochondrial protein called the voltage dependent anion channel (VDAC). In electrophysiological studies, Shimizu and colleagues (1999 and 2000) have shown that Bax and VDAC specifically interact in synthetic membranes to form novel ion channels, which are bigger than pores formed by VDAC or Bax alone.

6. It is possible that Bcl-2 family members may regulate the release of cytochrome c by controlling the opening and closing of the PTP and in turn MPT. The precise molecular composition of the PTP remains elusive, however, it is thought to be a multi-protein assemblage, incorporating proteins such as the VDAC, the adenine nucleotide translocator (ANT), the benzodiazapine receptor and cyclophilin D. Bax has been shown to interact specifically with two of these proteins, VDAC and ANT (Tsujimoto and Shimizu, 2000). Therefore, this model suggests that Bcl-2 family members, in particular Bax, may control MPT and the release of cytochrome c.

1.7 Lysosomes and Apoptosis

Lysosomes, together with late endosomes, are the main cellular compartment for intra-cellular degradation and contain a large number of enzymes, particularly non-specific proteases. Accumulating evidence suggests that lysosomes, perhaps in conjunction with mitochondria, may be intimately involved in apoptosis. However, the role of lysosomes in apoptosis is still poorly understood.

Many researchers believe that lysosomes are sturdy structures whose integrity remains intact until the final stages of cell death (reviewed by Antunes *et al.*, 2001; Brunk and Svensson, 1999; Li *et al.*, 2000; Helliquist *et al.*, 1997), thereby contributing little to the process. Despite this common opinion, it is now known that in certain pathological situations, as well as in normal aging (Bi *et al.*, 2000), lysosomal integrity may be compromised, causing leakage of lysosomal proteases into the cytosol. It has also been shown that minor lysosomal destabilisation produces degenerative alterations that are efficiently repaired by autophagocytic processes, suggesting that minor lysosomal leakage might be a common and reversible occurrence (reviewed by Brunk and Svensson, 1999). Many independent research groups have now reported that partial rupture of lysosomes seems to be an early and consistent event preceding apoptosis, caused by a variety of agonists, including oxidative stress, growth factor withdrawal, FAS receptor ligation, and exposure to low density lipoprotein, photo-oxidative damage, vitamin E (in particular α-tocopheryl succinate) and a synthetic lysosomotrophic detergent, O-methyl-serine dodecylamine hydrochloride (MSDH) (Roberg *et al.*, 1999; Kagedakl *et al.*, 2001; Antunes *et al.*, 2001; Brunk and Svensson, 1999; Hellquist *et al.*, 1997; Neuzil *et al.*, 1999; Li *et al.*, 2000).

Rupture of lysosomal membranes is thought to result in the release of many hydrolytic proteases, for example cathepsins, to the cytosol. Cathepsins are proteases that are present in nearly all animal cells (Roberg *et al.*, 1999). They have various functions, however, their most interesting role in relation to the field of apoptosis is their ability to activate pro-caspases (Gardner *et al.*, 1997). This activation may be upstream to the mitochondrial release of cytochrome c (Roberg, 2001). The precise mechanism of caspase activation by cathepsins is currently not known. Kagedal and associates (2001)

suggest that cathepsin D may activate caspases directly, through proteolytic interaction, or indirectly, through proteolytic attack on mitochondrial membranes, thereby ensuring the release of pro-apoptotic factors. Also, cathepsin B was previously shown to contribute to bile-salt induced apoptosis by a caspase-8-dependent process and is thought to be involved in the activation of specific proinflammatory caspases (Guicciardi *et al.*, 2000; Schotte *et al.*, 1998).

Oxidative stress induces apoptosis in many cell lines. In fibroblast cells, oxidative stress induces relocation of cathepsin D from lysosomes to the cytosol. This was observed to be an early event, preceding other apoptotic changes, such as the release of cytochrome c to the cytosol (Roberg *et al.*, 1999). This sequence of events is consistent with lysosomes being involved in the initiation of apoptosis. Recently, Antunes *et al.* (2001) and Olejnicka *et al.* (1999) have reported lysosomal membrane rupture in Jurkat and NIT-1 cells following exposure to hydrogen peroxide. A similar sequence of events to that found in fibroblast cells was observed in both Jurkat and NIT-1 cells. Partial lysosomal membrane rupture was the initial event, followed by mitochondrial depolarisation, cytochrome c release and activation of downstream caspases. These events did not occur until 1-2 hours after the removal of hydrogen peroxide. Antunes *et al.* (2001) noted that following treatment of Jurkat cells with hydrogen peroxide the number of lysosomes decreased. This decrease is thought to result from a feed-back loop, where the early release of lysosomal enzymes feed-back to activate further lysosomal rupture. Interestingly, over-expression of Bcl-2 was found to inhibit this feed-back loop and further apoptotic changes in J774 cells following oxidative stress. It is possible that Bcl-2 somehow blocks down-stream events that result in later lysosomal

rupture (Zhao *et al.*, 2000) and cytochrome c release. Thus, this is another putative function for Bcl-2 (see Section 1.6).

Until recently, it was agreed in much of the published literature that death caused from lysosomal rupture was the result of direct pro-caspase activation by lysosomal proteases. However, some research groups were unable to detect caspase activation. Vandenabeele's group argue that the primary role of released cathepsins may be related to an inflammatory response, as opposed to an apoptotic response. Their results suggest that lysosomal proteases, in particular cathepsin B, efficiently process pro-caspase 1 and 11 (caspases involved in inflammation) but only weakly process the precursors of caspase-2, -3, -6, -7 and –14. Stoka and colleagues (2001) have recently proposed an alternative model in which proteases released from lysosomes following lysosomal injury are involved in the activation of Bid. As previously discussed, Bid is a pro-apoptotic member of the Bcl-2 family that is typically activated by proteolysis. Stoka *et al.* (2001) reported the ability of proteases, such as cathepsin D, to cleave and activate Bid. Once Bid is activated, it is translocated from the cytosol to mitochondria, thereby causing release of cytochrome c (Stoka *et al.*, 2001). It is currently unclear if proteases released from lysosomes directly activate caspases or specific members of the Bcl-2 family. It may be that both the activation of caspases and Bid by proteases are required for the onset of apoptosis. Irrespective of the precise action of lysosomal proteases, the recent literature strongly suggests that lysosomal rupture may (at least under some conditions) be extremely important in the initiation of apoptosis. Figure 1.5 depicts a hypothetical scheme of how early lysosomal rupture may initiate downstream apoptotic events.

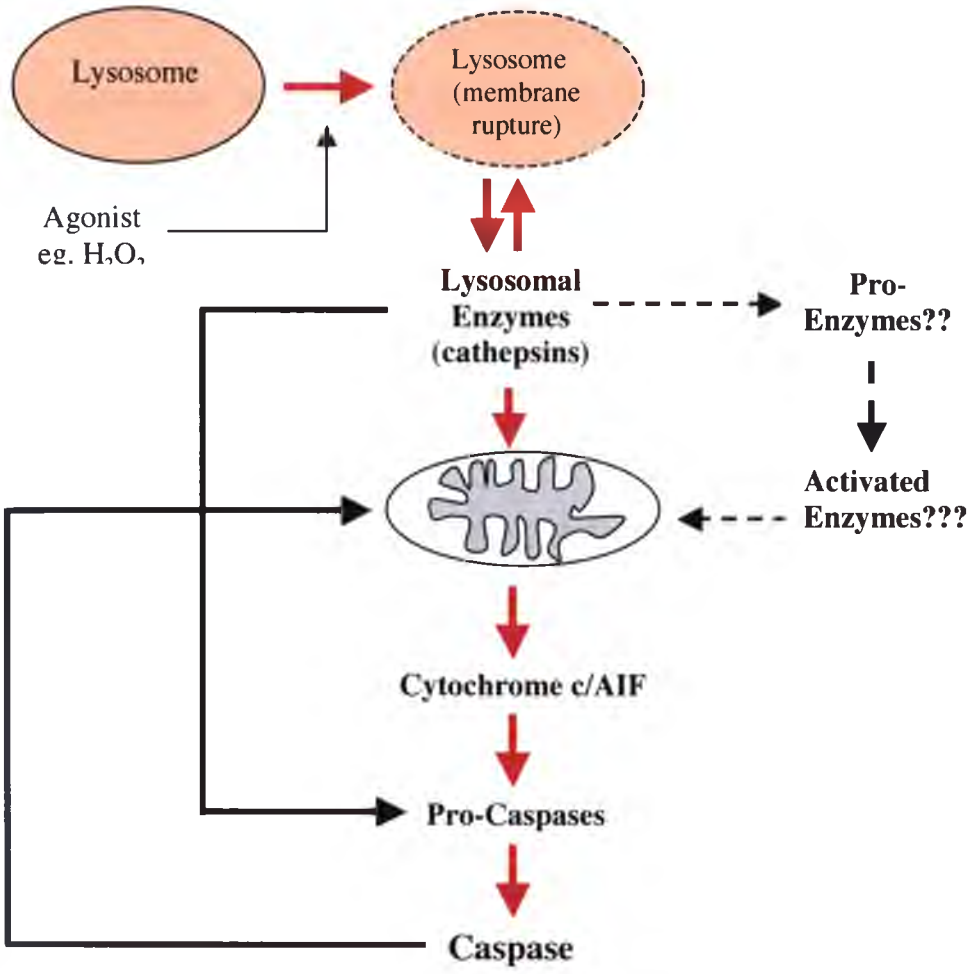

Figure 1.5: Proposed pathway of lysosomal involvement in apoptosis. Under some conditions, lysosomal rupture is thought to be an early event, preceding many apoptotic events such as cytochrome c/AIF release and caspase activation. It has been suggested that cathepsins may activate pro-caspases, thereby forming active caspases, or interact with Bcl-2 proteins to induce apoptosis, however, the exact mechanism is not known. Other undiscovered enzymes may also be involved (adapted from Zhao *et al.*, 2000).

1.8 Cancer Therapeutics

As previously mentioned, dysfunctions of apoptosis have been implicated in the pathogenesis of many serious diseases, including cancer. Cancer is the second most common cause of death in highly developed countries (Szekeres and Novotny, 2002). For many years now, clinical treatment for cancer has typically involved chemotherapy,

radiotherapy and surgery. Despite the extensive use of these therapies, there are still many disadvantages associated with them, such as a lack of specificity that often causes many harmful side effects (Luo and Prestwich, 2002). In addition, cell death caused by chemo- and radiotherapy is through an indirect mechanism, that is, cell death results from interference with DNA replication or metabolic processes, not by the direct induction of apoptosis (Baell and Huang, 2002). This mechanism of killing is sometimes insufficient to kill all cancer cells and, furthermore, makes it possible for cancers to develop radio-or chemo-resistant sublines that survive successive rounds of treatment and ultimately result in patient mortality (Ali *et al.*, 1999; Igney and Krammer, 2002). Therefore, a need exists to develop therapeutic approaches that can overcome these disadvantages.

Over the last five years, a diverse range of experimental therapeutic strategies have been developed. Typically, these involve targeted delivery of anticancer drugs to cell surface proteins specifically expressed by tumour cells. These types of approaches have significant potential to improve efficacy and minimise toxicity to normal healthy cells (Kreitman, 1999; Trail and Bianchi, 1999; Luo and Prestwich, 2002). The most promising strategies involve monoclonal antibody (Mab) fragments, hormones or growth factors conjugated to drugs, toxins, radionuclides, enzymes, photosensitizers or cytokines. A small number of these are being trialled clinically. For example, the use of radio-labelled Mab 17-1A has resulted in improved survival of patients with Dukes C collateral cancer (Trail and Bianchi, 1999), while immunotoxins using anti-CD22 and anti-CD19 Mabs have been used to target B-cell lymphoma and leukaemia (Kreitman, 1999). Immunotoxins are constructs of either a plant or bacterial protein toxin bound to an antibody. Although these newly developed treatment methods signify a marked

improvement in the area of cancer therapeutics, problems involving specificity, immunological reactions and the treatment of solid tumours still remain. Furthermore, the majority of these new treatments require parallel treatments in order to be successful.

A non-immunogenic complex that delivers the killing agent or toxin specifically to cancer cells in order to directly activate apoptosis, in the absence of bystander cell damage would be an ideal cancer therapeutic. Currently, there are few cancer therapeutics available that directly manipulate apoptosis. However, in the past few years, cancer research has started to focus on therapeutic agents that directly affect the apoptotic pathway. Mai *et al.* (2001) and Arap *et al.* (2002a) have recently reported a novel peptide (comprised of a protein transduction domain) which, when coupled to an antimicrobial peptide ($(KLAKLAK)_2$) and injected, induces apoptosis. This conjugate, known as DP1, has greater efficiency than other potential therapeutics such as the immunotoxins. Unfortunately, disadvantages are still associated with it: for example (1) it can't be used alone, other therapies would still be required, and (2) it must be injected directly into the tumour. Kessel and Horwitz (2001) also recently reported another synthetic anti-tumour agent, XK469, (2-[4-(7-chloro-2-quinoxalinyloxy) phenoxypropionic acid), which induces apoptosis in solid tumours *in vitro*. These researchers suggested that this drug may induce apoptosis by interacting with the peripheral benzodiazepine receptor (which is thought to form part of the PTP); however, further experiments are required to confirm this.

1.9 Potential Applications of Synthetic Polymers in Cancer Therapy

Despite continued efforts to find more potent and selective compounds for treating cancers, advances have been disappointing, particularly for the treatment of commonly occurring solid tumours (Duncan, 1997). Major limitations include the inability to (1) specifically target cancer agents to tumour sites, and (2) induce apoptosis only within cancer cells. Ideally, cancer drugs need to be concentrated preferentially in tumour cells, in order to maximise tumour cell death and minimise bystander cell damage.

In recent years many synthetic polymers have been investigated as potential drug delivery agents for cancer therapy, some of which are currently in clinical trials. These include pH-sensitive polymers, and HPMA (N-(2-hydroxypropyl)methacrylamide) and SMA (poly(styrene-co maleic acid/anhydride)) polymers.

1.9.1 pH-Sensitive Polymers

Linhardt and Tirrell (2000) investigated the behaviour of three polymers from a family of polymers referred as polyacrylic acids (Figure 1.6). These have a simple chemical structure with a carbon backbone conjugated to either a methyl (polymethylacrylic acid - PMAA), ethyl (polyethylacrylic acid - PEAA) or propyl side chain (polypropylacrylic acid - PPAA).

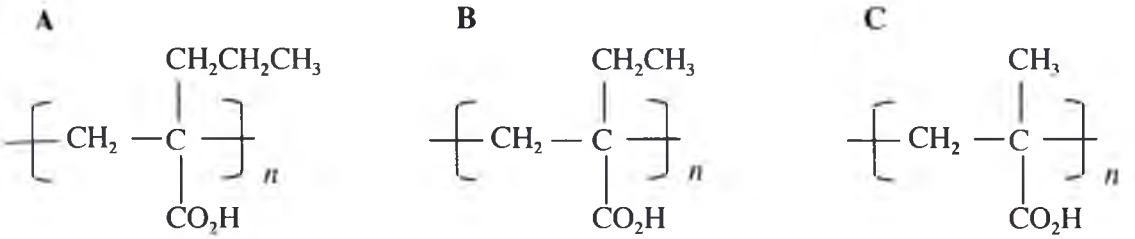

Figure 1.6: Chemical structures of pH-sensitive polyacrylic acid polymers (A) polypropylacrylic acid (B) polyethylacrylic acid (C) polymethylacrylic acid (adapted from Kim and Tirrell, 1999).

The most striking feature of these polymers is their ability to disrupt membranes in a pH-sensitive manner. The pH is not constant throughout a cell for example, the pH within an endosome is lower than that of the cytosol by 1 or 2 pH units, depending on the stage of endosomal development (Murthy *et al.*, 1999). Anti-tumour drugs introduced into cells are trafficked from early endosomes to late endosomes and eventually to lysosomes where they are degraded (Mukherjee *et al.*, 1997). Unfortunately, this trafficking process prevents the release of the internalised drug into the cell cytosol, inhibiting its cytotoxic action. Endosome-destabilising peptides (Tolstikov *et al.*, 1997) and pH-triggered bispecific antibodies (Raso *et al.*, 1997 a and b) have previously been used to release internalised drugs into the cytosol. Linhardt, Tirrell and associates suggest that the variation of pH in endosomes and lysosomes must be considered when investigating possible delivery of cancer drugs *in vivo* (Linhardt *et al.*, 1999). They suggest that the use of pH-sensitive polymers, such as PEAA and PPAA, would be ideal as part of a membrane-disruptive system which could enhance the release of drugs from endosomes into the cell cytosol. Such polymers would need to disrupt lipid bilayers at pH 6.5 and below but should be non-lytic at physiological pH (pH 7.4) (Murthy *et al.*, 1999).

Despite the similar structures of PEAA, PMAA and PPAA, they have significantly different pKa values (Stayton *et al.*, 2000). This results in each of the polymers disrupting membranes at different pH values (the "critical pH"). Linhardt *et al.* (1999) suggest that control of the critical pH can be attained either by altering the properties of the lipid bilayer or by variation of the polymer chain structure. Polymer side chains have been modified in length and chemical composition (by copolymerisation with methacrylic acid) (cited by Linhardt *et al.*, 1999). In order to determine the critical pH, initial experiments were conducted using red blood cells (RBC). Synthetic polymers such as PEAA have also been shown to disrupt liposomes and synthetic vesicles (Meyer *et al.*, 1998; Hughes *et al.*, 1996). With RBC, PPAA produces maximum haemolysis at approximately pH 6.0, whereas maximum haemolysis for PEAA is reached at pH 5.0 (Stayton *et al.*, 2000). On a molar basis, PPAA is 15 times more effective than PEAA at pH 6.0 (Murthy *et al.*, 1999).

Recently, Lackey and colleagues (1999) have demonstrated the ability of PPAA to retain haemolytic ability following conjugation with streptavidin. PPAA-streptavidin complexes not only retain the capacity to lyse RBC lipid bilayers at low pH but the haemolytic activity is similar to that of unmodified PPAA (Lackey *et al.*, 1999). The ability of these synthetic polymers to lyse membranes at specific pHs and to retain this function after conjugation could be valuable in the development of novel polymer-based cancer therapeutics.

Another pH-sensitive polymer that has potential for use as a membrane-disruptive agent is pDMAEMA. pDMAEMA was originally described by Van de Wetering and colleagues and has previously been used in gene therapy (Van de Wetering *et al.*, 1999).

The ability of pDMAEMA to deliver genes into cells is consistent with it doing this by disrupting endosomes. The mechanism of putative pDMAEMA-mediated endosomal disruption is probably different from that of PAAA. At physiological pH, the polymer is partially protonated. However, Van de Wetering *et al.* (1999) suggests that, at low pH, the polymer acts as a 'proton sponge'. They propose that, when inside endosomes, pDMAEMA causes massive ATPase-driven proton accumulation, which is followed by passive chloride influx into the endosomes to prevent the build up of a charge gradient. In this model water is then absorbed into endosomes as a result of the increased osmolarity (due to the uptake of protons and chloride ions), causing osmotic swelling and endosomal membrane rupture (Van de Wetering *et al.*, 1999). However, there is no direct experimental evidence to support this model. There are very few previous studies that have examined the effects of pDMAEMA on intact cells. pDMAEMA has not previously been conjugated to other compounds, including anti-tumour agents. The ability of derivitized pDMAEMA to disrupt endosomes remains unknown.

1.9.2 HPMA and SMA Polymers

In recent years, extensive research has implicated HPMA and SMA synthetic polymers as potential cancer therapeutic agents, in particular for treating solid tumours (Maeda *et al.*, 2001; Duncan *et al.*, 2001). *In vivo*, many cancer drugs, in particular those of low molecular weight, rapidly penetrate many types of cells to cause extensive bystander cell damage. Furthermore, these drugs can be quickly removed from circulation via the action of the kidneys, thereby reducing tumour killing potential. Duncan (1997) and Etrych (1999) have shown that conjugating a potent anti-tumour agent to a polymeric carrier, such as HPMA or SMA, temporarily inactivates the drug and increases its distribution in the body, as the conjugate can only gain entry into cells via endocytosis.

The increased circulation of the drug-polymer conjugate results in enhanced accumulation of the drug in tumours and thus enhanced cancer cell killing. This phenomenon is known as the enhanced permeability and retention effect (EPR - Figure 1.7) (Maeda *et al.*, 2001; Duncan, 1997).

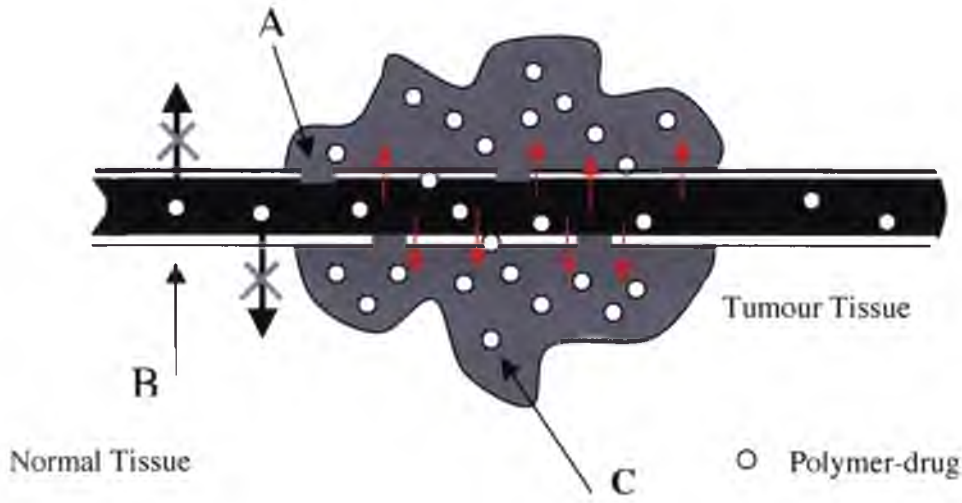

Figure 1.7: Schematic representation of the enhanced permeability and retention effect (EPR). **A.** Due to the higher permeability of tumour blood vessels, the drug-polymer conjugate is easily able to escape into the tumour. **B**. The low permeability of blood vessels in normal tissue prevents the drug-polymer conjugate from escaping to areas where it is not needed. **C**. Tumour tissues have poor lymphatic drainage and thus tend to retain drug-polymer conjugate (adapted from Duncan, 1997; Duncan *et al.*, 1996).

HPMA has been conjugated to a variety of drugs but the most promising is doxorubicin (Dox), an anthracycline antibiotic with activity against a broad range of tumours (Seymour, 1991). Duncan (1997) reported studies of the first Dox–HPMA conjugate. HPMA and Dox were conjugated by a Gly-Phe-Leu-Gly-peptidyl side-chain, which is cleaved intracellularly by lysosomal thiol-dependent proteases, releasing free Dox into the cell. Proteases, like cathepsin B, are known to be present at higher levels in some human tumours. The Dox-HPMA conjugate, now known as PK1, is a 25 kDa complex

which successfully capitalises on the EPR effect to concentrate up to 70 times more than free Dox in mouse melanoma tumours *in vivo* (Duncan, 1997; Pimm *et al.*, 1996; reviewed by Luo and Prestwich, 2002). Pre-clinical tests revealed that PK1 was 5-10 times less toxic than free Dox and displayed improved antitumour activity, particularly in solid tumour models (Duncan *et al.*, 1992; Ulbrich *et al.*, 1996). In recent years, PK1 has been trialled on a broad range of tumours, for example MAC15A and MAC26 (Loadman *et al.*, 1999). These tumours display distinctly different morphology and vasculature, leading to the suggestion that PK1 may have therapeutic potential for a variety of cancers. PK1 is currently undergoing Phase II evaluation for treatment of breast, colon and non-small cell lung cancer (Duncan *et al.*, 2001).

Many variations of the simple PK1 construct, including changes in (1) the chemical bond used to produce the conjugate, (2) the overall mass of the conjugate, and (3) the structure and length of the spacers (Ulbrich *et al.*, 1996) have been made, in order to improve the EPR effect and the toxicity to tumours. Etrych *et al.* (2001) constructed a conjugate between HPMA and Dox, using a hydrolytically unstable hydrazone linkage. This spacer is stable under physiological conditions (pH 7.4) but is hydrolytically degraded in mildly acidic environments (e.g. the lumen of endosomes at pH 5.0). Initial *in vitro* experiments indicate that the complex is relatively stable at physiological pH and that the drug activity increases under mildly acidic conditions (pH 5) (Etrych *et al.*, 2001). Compared with PK1, this conjugate is significantly more efficient at treating EL4 T-cell lymphoma in mice (Ertych *et al.*, 2001).

There are now at least seven HPMA polymer-drug conjugates that have entered phase I/II clinical trials as anticancer agents, including N-(2-hydroxypropyl)methacrylamide

further 4 hours. For these latter experiments, cells were analysed by confocal microscopy and flow cytometry.

3.2.2.6 Identification of Intracellular Vesicles Disrupted by PAAA Polymers

Immunofluorescence assays were used to examine the morphology and distribution of both early and late endosomes and lysosomes following endocytosis of polymers. This enabled determination of the specific intracellular vesicle/s that the polymer/s disrupted. Monoclonal antibodies reactive with early endosomal antigen 1 (EEA1), lysosomal-associated membrane protein-1 (Lamp-1), and Golgin-97 were used. EEA1 is thought to only be associated with early endosomes. Lamp-1 is associated with various vesicles, however, it seems to predominately accumulate in late endosomes and lysosomes (Akasaki, 1995). Anti-golgin-97 recognizes a 97 kDa protein called Golgin-97, which is a member of the granin family of proteins localised on the cytoplasmic face of the Golgi apparatus.

U937 cells were treated as described for measuring the release of calcein from endosomal vesicles (section 3.2.2.3), except that calcein was deleted from the initial incubation mixture. Following uptake, the cells were incubated for 4 hours at 37°C in 10% FBS/DMEM:F12 before processing for immunofluorescence. In some experiments, polymers were omitted from the initial incubation buffer but 70 μM MSDH (an acidotropic detergent known to disrupt lysosomes (Li *et al.*, 2000)) was added to the medium used for the subsequent 4 hour incubation. The cells were then centrifuged for 5 minutes at 300 *g*, resuspended in 0.4 ml of 4% (w/v) paraformaldehyde in PBS, pH 7.4, and incubated with shaking at room temperature for 30 minutes. The fixed cells were then washed with PBS and permeabilised

results, cited by Maeda *et al.*, 2001). Also, encouragingly, SMANCS treatment has been associated with minimal side effects, the major one being a low-grade fever.

1.10 Development of a Novel Cancer Therapeutic

The recent development of pH-sensitive polymers (section 1.9.1) and consideration of what was known about apoptotic signal transduction pathways, particularly the involvement of Bcl-2 family members (sections 1.3.2.1 and 1.4) and lysosomes (section 1.7), led to the formulation of two strategies that offered the potential to develop new kinds of cancer therapeutics. These strategies were;

1. To test whether endocytosed pH-sensitive polymers would disrupt lysosomes and thereby induce apoptosis.
2. If strategy 1. was not feasible, to begin development of a trimolecular construct that was designed to be taken up by cancer cells via receptor-mediated endocytosis, and to subsequently release a pro-apoptotic peptide into the cytosol where it would induce apoptosis.

These strategies are further elaborated below.

1.10.1 Lysosomal Destabilisation

As previously discussed, partial destabilisation of lysosomal membranes is thought to be an early event in some apoptotic pathways. It was hypothesised that the gradual decrease in pH in endosomes/lysosomes might cause (1) endocytosed PAAAs to undergo a change to a membrane-disruptive conformation or (2) endocytosed pDMAEMA to become a 'proton sponge' which would destabilise lysosomes and

release their lumenal proteases into the cytosol to induce apoptosis. These hypothetical effect(s) of PAAAs and pDMAEMA on cells have not been studied before.

1.10.2 Development of a Pro-Apoptotic Trimolecular Construct

If polymer-mediated destabilisation of lysosomes is not feasible then the alternative approach adopted will be to develop a trimolecular construct, incorporating three components:

1. A killing peptide to induce apoptosis.
2. A targeting ligand that, by binding to a specific receptor on the surface of cancer cells, induces receptor-mediated endocytosis.
3. An endosomal disruptive polymer that will release the construct from endosomal vesicles into the cytosol.

Currently, very few cancer therapeutics target apoptosis directly. However, this is an ideal mode of killing because apoptotic cells are naturally engulfed and degraded by phagocytes, preventing the release of toxic cellular contents into adjacent healthy tissue. Thus, apoptotic killing would (1) result in a reduced number of side effects, and (2) eliminate potentially dangerous inflammatory reactions. Figure 1.8 depicts the proposed construct.

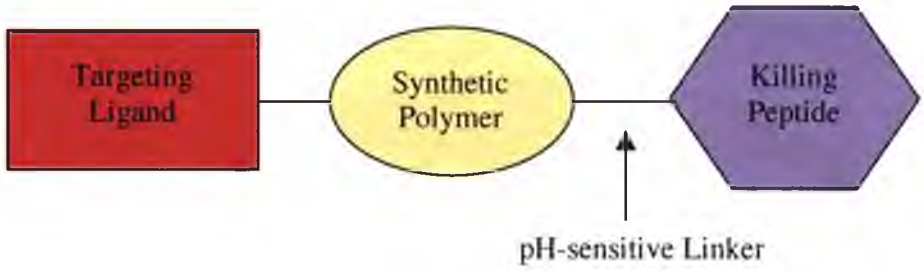

Figure 1.8: The proposed trimolecular construct. The construct is designed to enter the target cell via receptor-mediated endocytosis. Once inside the endosome/lysosome, the polymer and the pH-sensitive linker are designed to facilitate release of a pro-apoptotic peptide into the cytosol.

In theory, this construct offers many potential advantages compared to other cancer therapeutics, including (1) efficient cell killing (i.e. direct induction of apoptosis in target cells), (2) high specificity - the combination of the action of the targeting ligand and the tendency of the polymer to accumulate at sites of solid tumours (via the EPR effect) would significantly reduce bystander cell damage, and (3) repeated cycles of treatment will be feasible, due to the construct being poorly immunogenic. A proposed pathway of action for the trimolecular construct is schematically represented in Figure 1.9.

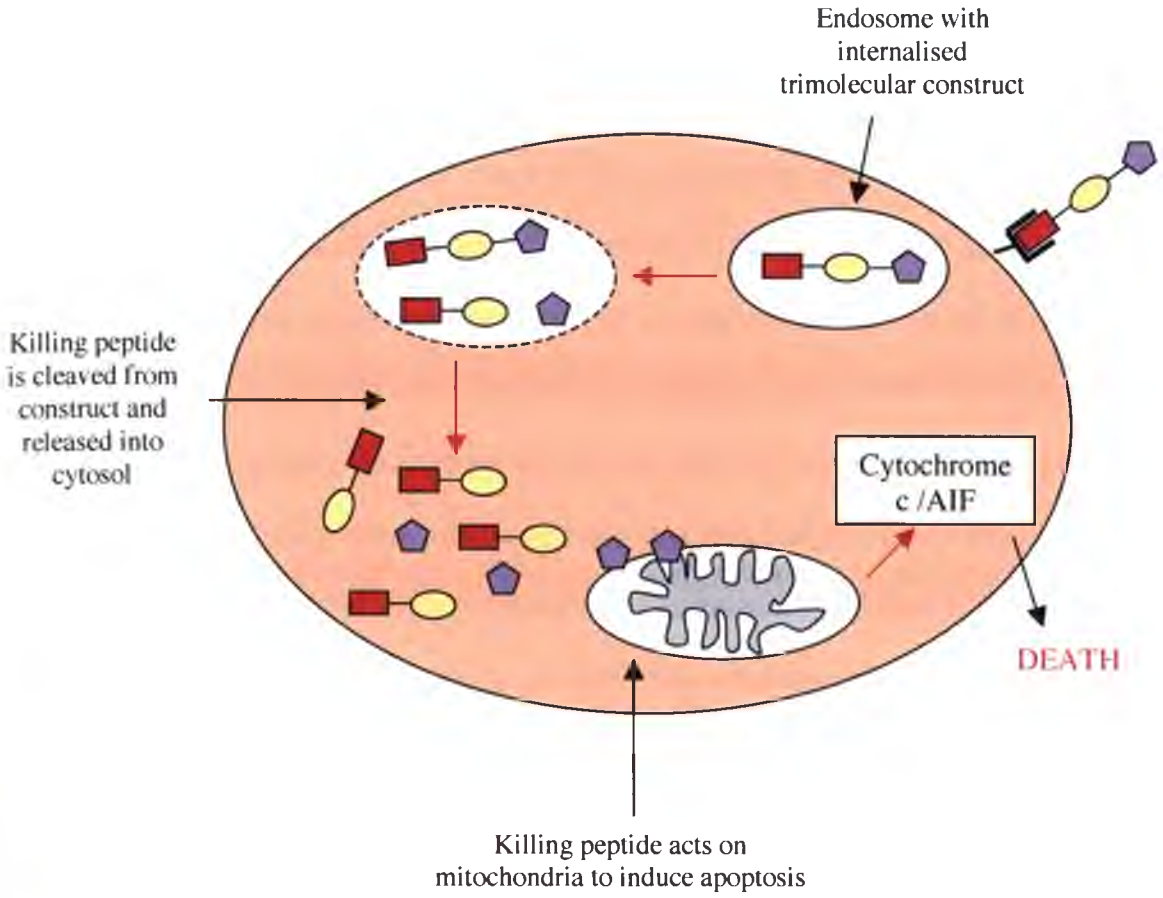

Figure 1.9: Proposed pathway of action of the trimolecular construct on a target cell. It is hypothesised that the construct will enter the cell via receptor-mediated endocytosis. Once inside an acidified endosome, the linker between the killing peptide and the polymer will be cleaved and the polymer will disrupt the endosomal membrane. The released killing peptide will then target mitochondria and induce apoptosis.

1.10.2.1 Pro-apoptotic Peptide

Bcl-2 family members are known to play an important role in the release of cytochrome c from mitochondria, to initiate downstream apoptotic events. In recent years, it was discovered that the BH3 domain is critical for hetero-dimerisation of Bcl-2 family members and appears to be essential for death promoting activity (Polster *et al.*, 2001). Since this discovery, many BH3 peptides have been developed as potential apoptosis

inducing agents. The Bad(140-165) peptide, developed by Kelekar *et al.* (1997) was one of the first BH3 peptides to be synthesised. *In vitro* experiments showed that this peptide binds to Bcl-x_L and induces characteristic features of apoptosis. Truncated forms of pro-apoptotic Bak and Bax consisting of only the BH3 region are also sufficient to induce apoptosis and antagonise the effects of anti-apoptotic members of the Bcl-2 family of proteins in prostate carcinoma cell lines (Finnegan *et al.*, 2001). Finnegan and co-workers believe that BH3 peptides interact with Bcl-2 at sites where pro-apoptotic proteins normally bind, thereby inhibiting binding of Bak and Bax-like proteins. As a result, BH3 peptides promote the formation of pro-apoptotic Bak/Bax homodimers, thereby inducing cell death. Polster *et al.* (2001) recently developed a Bax peptide, comprised of amino acids 53-86 that includes the BH3 domain.

Theoretically, if used *in vivo* to induce apoptosis of cancer cells, pro-apoptotic peptides have several advantages when compared with other toxic agents. Firstly, pro-apoptotic peptides must be introduced into the cytosol to have a cytotoxic effect. Since the peptide is membrane impermeable, it can't easily enter the cytosol of non-target cells, thus limiting damage to adjacent, healthy cells. Second, once in the cytosol of a target cell, the peptide will remain there until it is naturally degraded (or the target cell membrane loses integrity). Finally, systemic exposure to the peptide is unlikely to elicit an immune response as it represents a human amino acid sequence. Therefore, a variety of recently developed BH3 peptides could be used as suitable killing agents in the proposed trimolecular construct.

To confirm that Bcl-2 peptides induce apoptosis in intact cells, processes associated with apoptosis (e.g. MPT) must be measured. Two techniques have previously been

employed to measure MPT in intact cells, however both have significant disadvantages. Therefore a need exists for the development of a method to measure MPT in intact cells that is free of the disadvantages associated with the other techniques. The development of a novel technique to measure MPT in intact cells is discussed in chapter 6.

1.10.2.2 Targeting Ligand

Receptor-mediated endocytosis (RME) is the process by which a ligand makes contact with a specific receptor on the cell surface and elicits internalisation of the ligand within the cell. This type of uptake is highly efficient when cells display a high density of ligand-specific receptors (Duncan *et al.*, 1996). Many receptors, including those for transferrin, low-density lipoprotein and growth factors have been proposed as candidates for tumour targeting and used in many experiments. The transferrin receptor has frequently been used in these studies. Transferrin is a 77 kDa human blood glycoprotein with a broad cellular distribution. It regulates iron availability in the body and mediates the transport and uptake of iron into cells, via RME (Ali *et al.*, 1999; Luo and Prestwich, 2002). The number of transferrin receptors on the cell surface is in direct relationship to the amount of iron required by a cell. The iron requirement of most human cells is generally minimal hence few transferrin receptors are present on the plasma membrane. However, it has been found that rapidly dividing cells, like cancer cells, express transferrin receptors at significantly higher levels. This has led to the proposal that the transferrin uptake pathway could be exploited for targeted delivery of chemotherapeutic agents *in vivo* (Ali *et al.*, 1999). Thus, transferrin would be a suitable prototype for initial studies.

1.10.2.3 Synthetic Polymer

Following RME, the trimolecular construct must be released from the endosome into the cytosol in order to cause mitochondrial changes and induce apoptosis. Non-viral (i.e. immunological compatible *in vivo*) and inexpensive endosomal disruptive agents would be ideal to use in the proposed trimolecular construct. Synthetic polymers, such as PAAAs and pDMAEMA have been suggested as possible endosomal disruptive agents.

1.10.2.4 Covalent Linkage Between Polymer and Peptide

It is likely that a pro-apoptotic peptide will have to be released from the construct to allow it to act on mitochondria and induce apoptosis. A wide variety of linkers that facilitate peptide release have previously been employed. The most popular are (1) spacers that are degraded by proteases such as cathepsins, and (2) a pH-sensitive linker that releases the drug on entry into acidic endosomes or lysosomes. Various acid-sensitive linkages, including the carboxylic-hydrazone, the *cis*-aconityl and the trityl, have been investigated (Kratz *et al.*, 1999). The carboxylic-hydrazone linkage system is the most extensively used and has produced promising results (Kratz *et al.*, 1999). This type of linkage will be used in the initial studies described in this thesis.

1.11 Aims

The aims of this thesis were to:

1. Determine if any of the available pH-sensitive polymers can disrupt lysosomal membranes and thereby directly induce apoptosis.

If the polymers tested were incapable of this, then proceed to:

2. Identify the most efficient endosomal-disruptive polymer.

3. Synthesise a hydrazide pH-sensitive linker and conjugate it with an endosomal-disruptive polymer.
4. Conjugate a linker-derivatised endosomal-disruptive polymer with a pro-apoptotic peptide.
5. Determine if the conjugate produced in 4. induces apoptosis in cultured cells.
6. Develop an improved technique to directly measure mitochondrial permeability transition in intact cells.

If results from 5. are promising, then (if time permits)

7. Conjugate transferrin to the conjugate formed in 5. (to form a trimolecular construct) and test its ability to be internalised via RME and kill cancer cells via apoptosis.

Chapter 2

Materials and Methods

This chapter contains general materials and methods that were used throughout the work described in this thesis. Other chapter-specific materials and methods are described in the corresponding chapters.

2.1 Materials

Many general chemicals were purchased from Sigma (MO, USA). Details of chemicals purchased elsewhere are provided below.

2.1.1 Tissue Culture

Dulbecco's Modified Eagles Medium: Hams F-12 (DMEM:F12) was from Life Technologies (MD, USA) and Foetal Bovine Serum (FBS) and Trypsin-EDTA were from Trace (Melbourne, Australia). $NaHCO_3$ was from Ajax (Sydney, Australia) and HEPES was from United States Biochemical Company (USB, OH, USA). Most cell lines used were obtained from the American Type Culture Collection (ATCC, MD, USA) and included: Jurkat (human leukemia T cells), U937 (human myelomonocytic cell), HL60 (human promelocytic leukima cells) and HeLa (human epitheloid carcinoma cells). Hek 293 (human embryonic kidney) cells were a kind gift from P. Poronick (University of Sydney, Sydney, Australia). Sterile Greiner Labortechnik plasticware was obtained from Interpath Services (Melbourne, Australia).

2.1.2 Purification of Annexin V

Acrylamide, tris(hydroxymethyl)aminomethane (Tris), and glycine were from ICN Biochemicals (Sydney, Australia). Bradford reagent, ammonium persulphate, FITC (fluorescein isothiocyanate), N,N,N',N'-tetramethylethylenedaime (TEMED) were from

Sigma (Syndey, Australia). N,N'methylene-bis-acrylamide and sodium dodecyl sulphate (SDS) were from BDH (Dorset England). Annexin-V-FLUOS was from Roche (IN, USA). N-(2-hydroxyethyl)piperazine-N'-(2-ethanesulfonic acid) (HEPES) was from United States Biochemical Corp. (OH, USA). DEAE-Sephacel was from Amersham Biotech (Melbourne, Australia). The Econo pump system was purchased from Bio-Rad (Sydney Australia). Ultrafree concentration devices were from Millipore (MA, USA). Hoeffer Scientific "Tall-Mighty-Small" Minicell (CA, USA) was used for electrophoresis of proteins. All other chemicals were of reagent grade and were from either Sigma (Syndey Australia) or Ajax Chemical Co. (Sydney Australia).

2.2 Methods

2.2.1 Tissue Culture

Cells were cultured in complete medium, consisting of DMEM:F12 medium supplemented with 10% (v/v) FBS. The cells were incubated in a Forma Scientific humidified incubator at 37°C and 5% (v/v) CO_2. Passage of suspension cells involved most of the culture being discarded and replaced with complete medium twice a week. Passage of adherent cells was conducted similarly except that all the culture medium was discarded. Pre-warmed, sterile trypsin-EDTA was then added to the flask, ensuring that the base of the flask was covered. Cells were then incubated (37°C and 5% (v/v) CO_2) for 2-3 minutes or until most of the cells became suspended. Following this, trypsin-EDTA was discarded and replaced with complete medium. All procedures were carried out in a laminar flow hood with sterile techniques and reagents.

2.2.2 Flow Cytometry

A Becton Dickinson (CA, USA) FACSort flow cytometer and CellQuest software (version 3.1f) were used to analyse cells. A flow cytometer is an instrument used to analyse large numbers of cells collecting information about the size, granularity and fluorescence of each cell (Darzynkiewicz and Li, 1996). In the FACSort, cells are delivered upwards in a stream of liquid and are intercepted by a laser that excites the cells at 488 nm. As shown in Figure 2.1 the signals produced include forward scatter (FSC, relating to the size of the cell), side scatter (SSC, measuring the granularity of the cell), and three different fluorescent signals: FL1 (green fluorescence), FL2 (orange fluorescence) and FL3 (red fluorescence), all of which are measured by dedicated detectors (Darzynkiewic and Li, 1996). A series of three dichroic mirrors allows for the detection of three fluorescent signals. Dichroic mirrors discriminate between wavelengths, allowing specific wavelengths to pass through but reflecting others (Carter and Meyer, 1994; Mechtold and Radbruch, 1992).

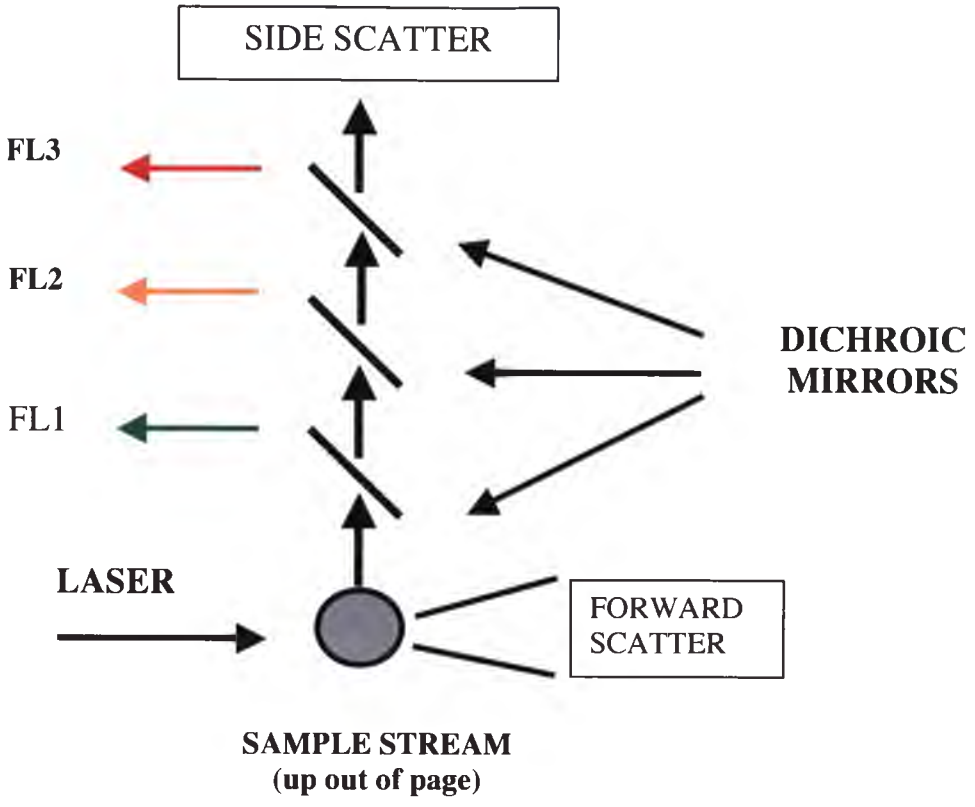

Figure 2.1: A schematic diagram of the operation of a flow cytometer. A stream of cells is intercepted by a laser beam. The size, granularity and fluorescence of each cell are measured.

2.2.3 Confocal Microscopy

A Leica TCS SP confocal microscope mounted on a Leica DM IRBE inverted microscope (Leica Microsystems, Heidelberg, Germany) was used to analyse cells. Confocal microscopy is used to image either fixed or living tissues that have been labelled with one or more fluorescent probes. Confocal microscopes are built around a conventional microscope but use lasers rather than a lamp for a light source. They also have sensitive photomultiplier tube detectors (PMTs) that detect the points of light produced by the specimen and a computer to control the scanning mirrors and to facilitate the collection and display of images (Paddock, 1999). Images are subsequently stored and analysed via software. Leica TCS NT software was used (Version 1.6.587:

Leica Microsystems, Heidelberg, Germany). The images produced have greater resolution than those achieved by conventional microscopy. In all confocal image analyses signals collected were adjusted to remain within the linear range of the detectors.

2.2.4 SDS-Polyacrylamide Gel Electrophoresis (SDS-PAGE)

A Hoeffer Scientific "Tall-Mighty-Small" vertical slab-casting unit connected to a Bio-Rad model 1000/500 power supply was used for electrophoresis. Melted agar (1%) was used to seal the bottom of the chamber. The separating gel (10% acrylamide) was placed in the chamber and allowed to set. The stacking gel was then added to the chamber. Immediately following loading of the stacking gel, a comb (used to form the sample wells) was placed in the top of the chamber. The stacking gel was then left to solidify while the comb was in place. Once the stacking gel was set, the comb was removed and the chamber placed in the electrophoresis unit.

For each sample, approximately 10 μg of protein in PBS was mixed with an equal volume of sample buffer. Samples were then boiled for 5 minutes before loading into the wells. Running buffer (250 mM TRIS, 1.9 M Glycine, 1% SDS) was subsequently poured into the buffer chambers before the gel was electrophoresed at a constant 180 V until the dye front had reached the bottom of the gel (approximately 2 hours). Following completion of electrophoresis, gels were placed into a Coomassie Blue staining solution (0.1% Coomassie Blue, 40% methanol, 10% glacial acetic acid) and left to stain, on a platform rocker, for 1 to 1.5 hours. Gels were then destained using 'destain' solution (50% methanol, 50% glacial acetic acid) until the bands were clearly visible (data not shown).

2.2.5 Bradford Assay

To a clean 96-well microtitre plate, 100 μl of BSA protein standards were added to the wells in the first three columns (setting up a triplicate series), in order of increasing concentration (i.e. from 0.05 mg/ml to 1 mg/ml) down the plate. To the next three columns, a series of binary dilutions of the "unknown" protein sample was performed down the plate (giving a final volume of 100 μl/well). To each well, 100 μl of Bradford reagent was added and mixed. The plate was incubated at room temperature until a blue colour developed in wells containing protein (usually between 5 and 60 minutes). The plate was subsequently read at 595 nm using a spectrophotometer. A plot of absorbance versus concentration for the BSA standards was generated and used to interpolate the concentration of "unknown" proteins.

2.2.6 Purification of Annexin V from Chicken Liver

Crude annexin V protein, isolated from chicken liver, was supplied by a previous colleague. It was isolated by homogenisation and density gradient centrifugation as described by Boustead *et al.* (1993). The crude annexin V protein was then purified by ion-exchange chromatography. A DEAE-Sephacel column was connected to an Econo pump system, including UV detector and chart recorder (running speed 2 cm/h). The column was equilibrated with 20 mM HEPES buffer pH 7.4. Following equilibration, the crude annexin V solution was passed over the column. The unbound protein was eluted and a linear gradient of 0-0.6 M NaCl in 20 mM HEPES buffer pH 7.4 was applied to the column. The column was eluted at 1 ml/min and 5 ml fractions were collected. Elution of annexin V was expected at 0.1 M NaCl (Clarke, 1998). Fractions were analysed by SDS PAGE (section 2.2.4) and annexin V was identified based on molecular weight. Fractions containing annexin V were pooled together and

concentrated, using Ultrafree concentration devices (cut off 20 kDa) to a final volume of 1.5 ml. The final concentration of the purified annexin V protein was determined by a Bradford protein assay (section 2.2.5).

2.2.7 Conjugation of Annexin V with FITC

An aliquot of a stock solution of FITC (40 mg/ml in DMSO) was added to the protein to give a final concentration of 250 μg FITC per mg of protein. The reaction mixture was then incubated (protected from light) at room temperature for 2 hours on a platform rocker. Following incubation, the reaction mixture was placed in dialysis tubing and dialysed against several changes of PBS, pH 7.4, over 24 hours. Unconjugated FITC was removed from the reaction mixture by dialysis performed at 4°C protected from light. The protein concentration and the substitution ratio were determined by taking A_{280} and A_{295} absorbance readings of the dialysed protein.

The protein concentration and substitution ratio (S.R.) were determined using the following formulas, respectively.

$$[\text{protein}]\ \text{mg/ml} = \frac{A_{280} - (0.35 \times A_{495})}{A_{280} - (0.35 \times A_{495})} \qquad \text{S.R.} = \frac{2.87 \times A_{495}}{A_{280} - (0.35 \times A_{495})}$$

2.2.8 Staining Cells with Annexin V-FITC

Annexin V labelling solution was made by diluting 1:100 annexin V-FITC in annexin V buffer (10 mM HEPES, pH 7.4, 140 mM NaCl, 5 mM $CaCl_2$). $1x10^6$ cells were centrifuged at 300 *g* for 5 minutes. The cells were resuspended in 1 ml of 1x PBS and re-centrifuged. Cells were then drained thoroughly and resuspended in 50 µl of the

annexin V labelling solution, followed by a 15 minute incubation at room temperature in the dark. Immediately before flow cytometric analysis of the cells, 500 µl of annexin V buffer was added to the cells. FSC, SSC and FL1 signals were acquired. Increased exposure of phosphatidylserine (PS) on the surface of the cells was measured by an increase in FL1. Manufacturer's instructions were followed when cells were stained using annexin-V-FLUOS.

2.2.9 Comparison of Annexin-V-FLUOS and Purified Annexin V Conjugated to FITC

The ability of purified annexin V conjugated to FITC (annexin V-FITC) to detect exposed PS was compared to annexin-V-FLUOS (commercial annexin V-FITC). U937, HL60 and Jurkat cells were induced to undergo apoptosis using three different stimuli, respectively: TNFα/cycloheximide (10 ng/ml and 10 µg/ml respectively, 4 hours), etoposide (20 µg/ml, 6 hours) and α-Fas antibody (100 ng/ml, 4 hours). Following incubations, cells were stained with either annexin-V-FLUOS or annexin V-FITC. Cells were also stained with PI to ensure that only viable cells were analysed (see section 3.2.2.1). All experiments were performed in triplicate to ensure reproducibility. In all cases, annexin V-FITC and annexin V-FLUOS gave comparable detection of exposed PS. The results shown in Figure 2.2 are representative.

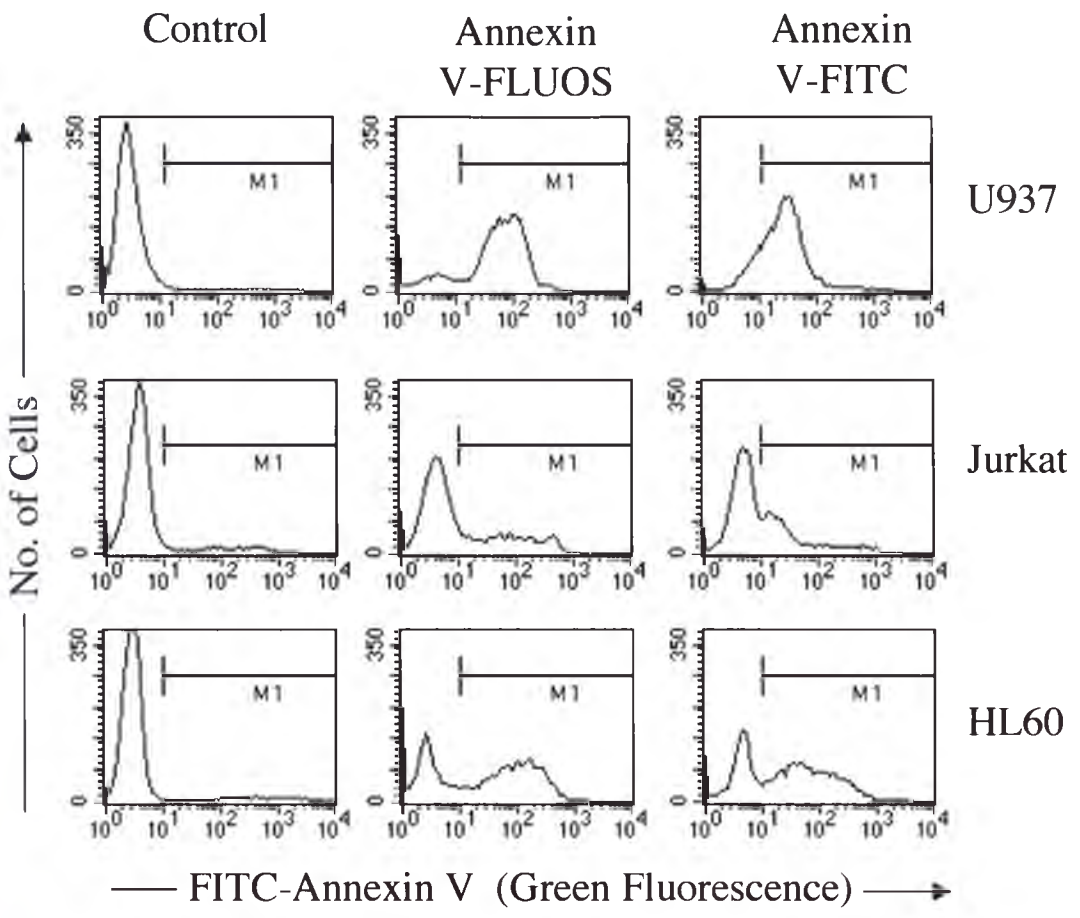

M1 values (%)	Control	Annexin V-FLUOS	Annexin V-FITC
U937	4.79	83.07	81.81
Jurkat	10.56	33.22	36.76
HL60	8.22	60.39	63.18

Figure 2.2: Flow cytometry histograms showing comparisons of annexin V-FLUOS (commercial annexin V-FITC) and annexin V-FITC. Comparable detection of PS, detected as an increase in FL1 fluorescence, was found for both reagents in all cases (see table).

Chapter 3

Poly(2-Alkylacrylic Acid) Polymers Deliver Molecules to the Cytosol by pH-Dependent Disruption of Endosomal Vesicles

3.1 Introduction

In recent years, many attempts have been made to improve cancer therapy, for example, by the development of synthetic polymers as macromolecular carriers. Synthetic polymers have significant potential for the delivery of molecules and drugs to cells both *in vitro* and *in vivo*. They offer several advantages in therapeutic situations, including (1) increased plasma half-life (because their size is above that required for renal exclusion), (2) controlled release of the drug at lower drug doses, and (3) enhanced accumulation of drugs at sites of solid tumours (due to the "enhanced permeability and retention" effect) (Luo and Prestwich, 2002).

Poly(2-alkylacrylic acid) (PAAA) polymers have recently been suggested as a possible delivery agent for anti-cancer drugs. Three PAAA polymers have been synthesized. Polypropyl(2-alkylacrylic acid) (PPAA), polyethyl(2-alkylacrylic acid) (PEAA) and polymethyl(2-alkylacrylic acid) (PMAA) are distinguished by the length of the hydrocarbon side chain. To date, few studies have examined the effects of PAAAs on intact cells. Murthy *et al.* (1999) have reported the ability of these polymers to disrupt red blood cells in a pH-dependent manner. The precise molecular mechanism(s) by which these polymers disrupt lipid bilayers is not known, although it is thought that the polymer undergoes a conformational transition from an expanded coil shape to a more complex shape upon acidification (Linhardt *et al.*, 1999). This change in conformation is most likely related to the increased hydrophobic character when the many carboxylate ions become protonated at low pH. At low pH, partitioning of the polymer into cell membranes increases significantly, resulting in membrane rupture (Murthy *et al.*, 1999). Cheung *et al.* (2001) have also shown that when PPAA is incorporated into lipoplexes

(mixtures of lipids, DNA and PPAA) formed with dioleyltrimethylammonium propane (DOTAP) it facilitates the delivery of genes into cells.

Currently, the effects of PAAAs on nucleated mammalian cells are not known. It has been hypothesised that PAAAs may be endocytosed by cells into acidified vesicles and are there triggered by low pH to disrupt endosomes and release their contents to the cytosol. However, the ability of PAAAs to disrupt specific endosomal compartments, and the pH dependence of this action, has not previously been measured.

The following chapter investigates the effects on cells of constitutively endocytosed PAAAs. Cells continually endocytose materials and particles from their extracellular environment. The cell membrane invaginates and forms specific vesicles called early endosomes. The contents of early endosomes then transit to more acidic compartments, late endosomes and lysosomes. The toxicity and pH-dependent lytic activity of each polymer was initially determined. Further investigations were carried out to (1) test the ability of PAAAs to disrupt endosomes and/or lysosomes in cultured human cells, and (2) determine whether this action was dependent upon vesicle acidification. Similar studies of pDMAEMA were also carried out; these results are presented in chapter 4. We predicted that if the PAAAs disrupted lysosomal membranes, apoptotic death would result (see section 1.7). Many independent research groups have shown that partial lysosomal rupture induces apoptosis; enzymes released from lysosomes are thought to produce this effect by interacting with proteins associated with mitochondria (Brunk and Svensson, 1999). If the PAAAs disrupt lysosomes and induce apoptosis it is feasible that they could themselves be used as cancer therapeutics.

3.2 Materials and Methods

3.2.1 Materials

Poly(2-alkylacrylic acid) (PAAA) polymers were supplied by P. Stayton (University of Washington, WA, USA). Lipofectamine was from Invitrogen (Melbourne, Australia). Propidium iodide, acridine orange, bafilomycin and calcein were from Sigma (MO, USA). Monoclonal antibodies reactive with early endosomal antigen 1 (EEA1), lysosomal-associated membrane protein-1 (Lamp-1) and Golgin-97 were from Pharmingen-Transduction Laboratories (CA, USA). Alexa 488-conjugated goat-anti-mouse Ig, streptavidin-Alexa 546 and LysoTracker Yellow DND-68 were from Molecular Probes (OR, USA). O-methyl-serine dodecylamide hydrochloride (MSDH) was a kind gift from G. Dubowchik (Bristol-Myers Squibb. CT USA). The pEGFP-N1 plasmid, encoding enhanced green fluorescent protein, and the pCMVβ plasmid, encoding β-galactosidase, were obtained from Clontech (CA, USA). The pCat-EGFP plasmid, encoding green fluorescent protein was a generous gift from G. Gores (Mayo Medical School, Minnesota, USA). All other chemicals were of reagent quality and were obtained either from Sigma Chemical Co. (MO, USA) or Ajax Chemical Co. (Sydney, Australia).

3.2.2 Methods

3.2.2.1 Viability of Cells Following Constitutive Endocytosis of Synthetic Polymers

The cytotoxicity of endocytosed PAAAs is unknown. The viability of cells was determined by staining cells with propidum iodide (PI), at intervals during 24 hours following uptake of PAAAs. PI is a cell-impermeant fluorescent stain. Loss of cell viability coincides with a decrease in membrane integrity, allowing PI to enter the cell and stain the DNA, which is detected as an increase in red fluorescence.

Cells ($2x10^6$) were centrifuged (5 minutes, 300 *g*) and resuspended in 500 μl of polymer buffer (PB, 145 mM NaCl, 5 mM KCl, 0.5 mM HEPES) containing 200 μg/ml polymer (added from a stock solution of 2 mg/ml in 0.1 M NaOH). Cell suspensions were incubated for 30 minutes at 37°C and then washed 3 times with DMEM:F12 before being resuspended in 10% FBS/DMEM:F12. Cells were then incubated for 24 hours at 37°C. Cell viability was determined at 2, 4, 8 and 24 hours, following the initial incubation with polymer. Immediately before flow cytometric analysis, cells were stained with PI (1 μg/ml). 10,000 cells were analysed for each sample and FSC, SSC and FL3 signals were collected.

3.2.2.2 Confirming Endocytic Entry of Polymers into Cells

Endocytosis is the process by which all mammalian cells internalise macromolecules and particulates from the extracellular environment. Internalised materials are initially held within vesicles known as early endosomes. We reasoned that PAAAs, internalised by endocytosis, would be localised in early endosomes. To confirm this, we traced the

initial movements of PEAA through the cell. This was achieved by biotinylating PEAA (b-PEAA, details below) and staining permeabilised cells with anti-EEA1 antibody (EEA1 is used for the detection of early endosomes). b-PEAA was detected by streptavidin-Alexa 546 and anti-EEA1 antibody was detected by Alexa 488-conjugated goat anti-mouse Ig antibody.

PEAA was biotinylated as follows; 5.1 mg PEAA was dissolved in 0.5 ml anhydrous dimethylsulfoxide (DMSO). This was mixed with biotin-x-hydrazide (0.7 mg dissolved in 0.5 ml anhydrous DMSO and 2 mg of 4'dimethylaminopyridine (DMAP)). This mixture was then mixed with 2.7 mg of N,N'-dicyclohexylcarbodiimide (DCC) on a shaker for 2 hours at room temperature. The solution was diluted with 10 ml of 0.1 M NaOH and incubated for a further 10 minutes at room temperature. The precipitate was then collected by filtration and 1 ml of 3 M sodium acetate was added (pH approximately 4.5). This mixture was then incubated for 10 minutes at room temperature to allow a precipitate to form, and filtered through a glass filter. The precipitate was washed with 3x1 ml of 60 mM sodium acetate (pH 5), filtered again and air dried, giving biotin–x-PEAA as a product.

Biotin-x-PEAA (2.3 mg) was dissolved in 100 μl of DMSO. U937 cells were centrifuged (5 minutes, 300 *g*) and resuspended in 500 ml polymer buffer containing 200 μg/ml of biotin-x-PEAA and incubated for 30 minutes at 37°C. The cells were then centrifuged for 5 minutes at 300 *g*, resuspended in 0.4 ml of 4% (w/v) paraformaldehyde in phosphate buffered saline (PBS), pH 7.4, and incubated with shaking at room temperature for 30 minutes. The fixed cells were then washed with PBS and permeabilised by incubation with 0.4 ml of 0.5% (v/v) triton X-100 in PBS for

15 minutes on ice. Fixed, permeabilised cells were washed with 0.1% (w/v) bovine serum albumin (BSA) in PBS (0.1% BSA/PBS), then suspended in 50 μl of anti-EEA1 antibody (diluted 1:50 in 1%BSA/PBS) and incubated on ice for 1 hour. The cells were then washed with BSA/PBS, suspended in 50 μl of goat-anti-mouse Ig-Alexa 488 (diluted 1:50 in 1% BSA/PBS) and streptavidin Ig-Alexa 546 (diluted 1:50 in 1% BSA/PBS). Cells were then incubated on ice for 1 hour. Finally the stained cells were washed with PBS and examined by confocal microscopy. Cells were excited at 488 and 543 nm and fluorescence collected simultaneously using emission windows set at 500-540 nm and 550-600 nm.

3.2.2.3 Measuring Polymer-Mediated Release of Tracer Molecules from Intracellular Vesicles

Endocytosed molecules are transported within cells via a series of vesicular compartments, namely endosomes and lysosomes. Vesicular traffic can be traced using fluorescent markers. Calcein, a 622 Da membrane-impermeable fluor, was used as a tracer molecule to follow the uptake of external medium by constitutive endocytosis, and, in turn, trace the effects of synthetic pH-dependent polymers on internalised vesicles.

In these experiments, $2x10^6$ U937 cells were centrifuged for 5 minutes at 300 *g*. Cells were resuspended in 0.5 ml of polymer buffer (PB) containing 2 mg/ml calcein with or without the addition of polymers from stock solutions at 6 mg/ml in 0.1 M NaOH. Following the addition of the polymer, and prior to adding to cells, the pH of PB/calcein/polymer solution was re-adjusted to pH 7.4. Cell suspensions were incubated for 30 minutes at 37°C and then washed 3 times with DMEM:F12 before

being resuspended in 10% FBS/DMEM:F12. Subsequently, the distribution of calcein within cells was examined by confocal microscopy. Cells were excited at 488 nm and fluorescence collected using an emission window set at 500-540 nm. In some experiments, calcein distribution was determined each hour over a 4 hour time period.

The TCS NT software was also used to calculate the average pixel intensity of calcein fluorescence within regions of interest (ROI) drawn onto collected images. In these cases, for each treatment, images of 15-25 individual cells were analysed as follows. For each cell, the mean fluorescence intensity was determined for three ROI drawn to represent (1) cytoplasm (these were drawn to exclude any calcein-containing vesicles), and (2) background (drawn outside the cell). The values for each set of three ROI were averaged. The mean background value was then subtracted from the mean value for cytoplasm and the results for each cell obtained in arbitrary fluorescence units. Differences between treatments were analysed using Oneway ANOVA (JMP software, v3.0.2, SAS Institute Inc., Cary, NC, USA).

3.2.2.4 Transient Transfection of Hek293 Cells with a Plasmid Encoding Cathepsin B-EGFP Fusion Protein

Cathepsin B (Cat B) is a 38 kDa lysosomal cysteine protease, primarily involved in protein degradation within lysosomes. Roberts *et al.* (1997) constructed a plasmid encoding a fusion protein comprised of rat Cat B fused at its C terminus to an enhanced green fluorescent protein (EGFP). A rat cDNA fragment containing the coding sequence for amino acids 1-334 of rat Cat B was excised from the pRSG-2A vector and ligated into the pEGFP-N1 expression vector, which has a multiple cloning site adjacent to its EGFP sequence (Cat-B-EGFP). Transfection of this plasmid DNA into mammalian

cells was used to show that cat B is translocated to the nucleus during bile salt-induced apoptosis (Roberts *et al.*, 1997).

To determine if synthetic polymers release macromolecules from endosomes, Hek293 cells were transiently transfected with Cat-B-EGFP prior to polymer loading. Hek293 cells were seeded into 6 well plates ($2x10^5$ cells in 2 ml of 10% FBS/DMEM:F12 per well) and incubated for 24 hours at 37°C. Cells were then transfected with either pEGFP-N1 (used as a control) or Cat-B-EGFP, using lipofectAMINE, according to the manufacturer's instructions (Invitrogen, Melbourne, Australia). Seeded cells were washed with 2 ml of serum-free medium (SFM). 200 μl of transfection mixture (24 μl plasmid DNA/transfection, 18 μl lipofectAMINE reagent and 158 μl SFM) was then added to each well. Cells were then incubated for 5 hours at 37°C in a 5% CO_2 incubator. The transfection mixture was subsequently removed and replaced with 2 ml of complete medium. Cells were assayed for gene expression by confocal and epifluorescence microscopy at 48 hours post transfection.

Once expression had been confirmed, complete medium was removed and replaced with 500 μl of PB containing 50 μg/ml of PPAA. The cells were then returned to a 37°C, 5% CO_2 incubator and 2 and 4 hours later analysed by confocal microscopy for the release of Cat-B-EGFP to the cytosol.

3.2.2.5 Determining if Polymer-Mediated Endosomal Disruption is pH-Dependent

The ability of PAAAs to disrupt membranes in a pH-dependent manner was determined using three assays. Each assay is described below.

1. Whole cell experiments were conducted to determine the ability of PAAAs to disrupt membranes in a pH-dependent manner. Cells were incubated in different buffers at various pH levels in the presence of 200 μg/ml of polymer. The pH-dependence of membrane-lytic activity was determined by measuring the proportion of non-viable cells at different pHs. $1x10^6$ U937 cells were pelleted and resuspended in 400 μl of 100 mM MES buffer (100 mM NaCl, 100 mM MES, 5 mM KCl) at various pH levels. The pHs used were 5, 5.5, 6, 6.5 and 7. PPAA, PEAA or PMAA was added from a 10 mg/ml stock solution in 0.1 M NaOH, to give a final concentration of 200 μg/ml (no additions were made to the control tubes). The samples were then incubated at 37°C for 30 minutes and stained with propidum iodide (PI) immediately before flow cytometric analysis. For each sample, FL3 (red fluorescence) was acquired for 10 000 cells.

2. Bafilomycin was then used to determine the ability of PAAAs to disrupt membranes in a pH-dependent manner. Bafilomycin is a specific inhibitor of the endosomal/lysosomal H^+-ATPase (Ohkuma, 1993). H^+-ATPase is responsible for the acidification of endosomes. In these experiments, 1 mM bafilomycin was added to cell suspensions during calcein uptake (section 3.2.2.3) and the subsequent 4 hour incubation.

3. Finally, the ability of PAAAs to disrupt membranes in a pH-dependent manner was determined by increasing the concentration of Hepes buffer in the PB; this is known to alkalinize the contents of endosomes (Sullivan, 1987). In these experiments calcein was again constitutively endocytosed into cells as described in section 3.2.2.3. Control cells were incubated in 0.5 mM Hepes-buffered PB (that had been adjusted to an equivalent osmotic pressure by the addition of 75 mM sucrose) and PAAA-exposed cells were incubated in 50 mM Hepes-buffered PB. Following uptake, cells were incubated for a

further 4 hours. For these latter experiments, cells were analysed by confocal microscopy and flow cytometry.

3.2.2.6 Identification of Intracellular Vesicles Disrupted by PAAA Polymers

Immunofluorescence assays were used to examine the morphology and distribution of both early and late endosomes and lysosomes following endocytosis of polymers. This enabled determination of the specific intracellular vesicle/s that the polymer/s disrupted. Monoclonal antibodies reactive with early endosomal antigen 1 (EEA1), lysosomal-associated membrane protein-1 (Lamp-1), and Golgin-97 were used. EEA1 is thought to only be associated with early endosomes. Lamp-1 is associated with various vesicles, however, it seems to predominately accumulate in late endosomes and lysosomes (Akasaki, 1995). Anti-golgin-97 recognizes a 97 kDa protein called Golgin-97, which is a member of the granin family of proteins localised on the cytoplasmic face of the Golgi apparatus.

U937 cells were treated as described for measuring the release of calcein from endosomal vesicles (section 3.2.2.3), except that calcein was deleted from the initial incubation mixture. Following uptake, the cells were incubated for 4 hours at 37°C in 10% FBS/DMEM:F12 before processing for immunofluorescence. In some experiments, polymers were omitted from the initial incubation buffer but 70 μM MSDH (an acidotropic detergent known to disrupt lysosomes (Li *et al.*, 2000)) was added to the medium used for the subsequent 4 hour incubation. The cells were then centrifuged for 5 minutes at 300 *g*, resuspended in 0.4 ml of 4% (w/v) paraformaldehyde in PBS, pH 7.4, and incubated with shaking at room temperature for 30 minutes. The fixed cells were then washed with PBS and permeabilised by

incubation with 0.4 ml of 0.5% (v/v) triton X-100 in PBS for 15 minutes on ice. Fixed, permeabilised cells were washed with 0.1% (w/v) bovine serum albumin (BSA) in PBS (0.1% BSA/PBS), then suspended in 50 μl of either, anti-EEA1, anti-Lamp-1 or anti-golgin-97 antibodies (diluted 1:50 in 1%BSA/PBS) and incubated on ice for 1 hour. The cells were then washed with BSA/PBS, suspended in 50 μl of goat-anti-mouse Ig-Alexa 488 (diluted 1:50 in 1% BSA/PBS) and incubated on ice for 1 hour. Finally the stained cells were washed with PBS and examined by confocal microscopy. Cells were excited at 488 nm and fluorescence collected using an emission window set at 500-540 nm.

In experiments analysing the effects of treatments on Lamp-1 immunofluorescence, TCS NT software was used to measure for 50 randomly chosen cells from each treatment, in a constant arbitrary plane, the diameter of globular areas of fluorescence within cells (see Figure 3.11). The measurement taken was used to score each cell as being in one of four categories: (1) no globular regions of fluorescence (i.e. diameter (grf) = 0 mm), (2) diameter (grf) = 0.1-1.5 mm, (3) diameter (grf) = 1.6-3.0 mm, or (4) diameter (grf) > 3.0 mm. Histograms were then plotted from these scorings. In the small number of cases in which there was more than one globular area of fluorescence within a cell, only the largest was measured.

3.2.2.7 Lysosomal Assays

To further test the effects of polymers on lysosomes, in addition to the immunofluorescence assay with Lamp-1 antibody, cells were stained with the fluorescent acidotropic probes acridine orange and LysoTracker Yellow. Acridine orange accumulates to high concentrations in the lysosomal lumen where it forms red fluorescing dimers (Zelenin, 1999). An increase in dimer formation can be detected by

flow cytometry. The LysoTracker dyes are thought to partition into lysosomal membranes. The morphology and distribution of lysosomes was determined, following staining, by confocal microscopy.

Polymers were loaded by constitutive endocytosis into U937 cells as previously described (section 3.2.2.3). Following the 4 hour incubation, cells were centrifuged for 5 minutes at 300 *g* and resuspended in DMEM:F12 containing 5 μg/ml acridine orange, incubated for 20 minutes at room temperature in the dark, and finally analysed by flow cytometry. The cells were excited with a 488 nm Argon laser and red fluorescence collected using a 650 nm long pass filter. For each sample, 10,000 events were acquired.

Similarly, for LysoTracker Yellow staining, cells were loaded with polymers by constitutive endocytosis and incubated in 1 ml of 10% FBS/DMEM:F12 for 4 hours at 37°C. After 3 hours, LysoTracker Yellow (75 nM - from 1 mM stock) was added to the cell suspension and cells were incubated for a further hour. Cells were then centrifuged (5 minutes, 300 *g*), resuspended in DMEM:F12 and analysed by confocal microscopy. Cells were excited at 543 nm and fluorescence collected using an emission window set at 550-600 nm.

In experiments analysing the effects of treatments on LysoTracker fluorescence, the TCS NT software was used to draw a line in a constant arbitrary plane across the entire diameter of images of individual cells and the "profile" function used in each case to obtain a histogram plot of the level of fluorescence along the length of the line drawn. A constant arbitrary "baseline" level of fluorescence was selected and the number of

continuous regions with fluorescence above this baseline was counted for each cell. For each treatment, this was performed on 40 randomly chosen cells.

3.3 Results

3.3.1 Viability Assays

Following uptake of PPAA, PEAA or PMAA by constitutive endocytosis, cell viability was determined. During the ensuing 24 hour period, like control cells, more than 95% of cells treated with PPAA remained viable. Similar results were obtained for cells treated with PEAA and PMAA (data not shown).

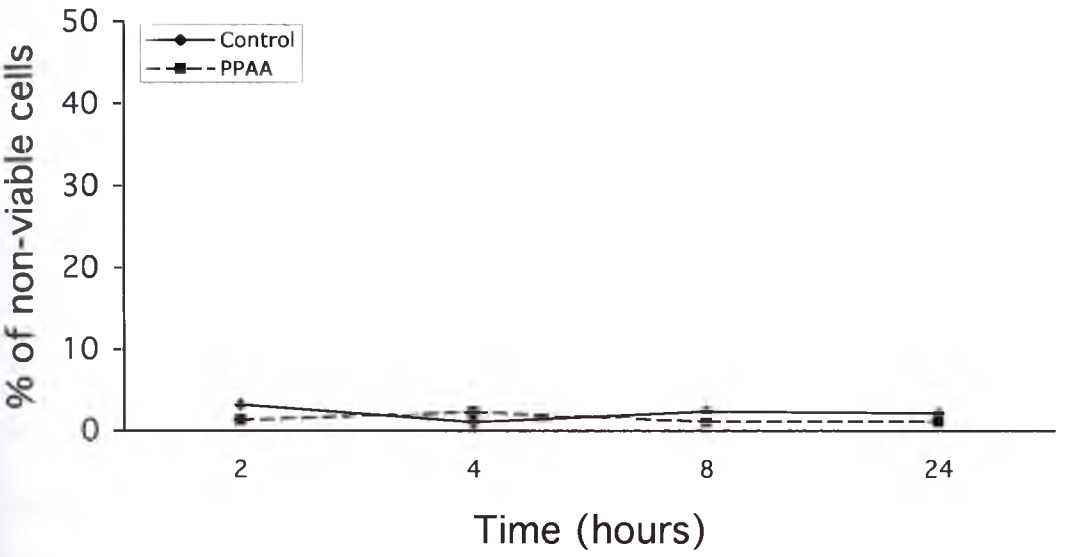

Figure 3.1: Line graph showing the viability of PPAA-treated (dashed line) and control U937 cells (solid line) over a 24 hour period following uptake of PPAA by constitutive endocytosis. Over the 24 hour time period, no significant change in cell viability was detected in either PPAA-treated or control cells. Each data point represents the mean of 3 independent experiments. Error bars are too small to be seen.

3.3.2 Testing the pH-Dependent Lytic Activity of PPAA, PEAA and PMAA

Whole cell experiments were conducted to determine the pH-dependent lytic activity of the polymers; cell lysis was measured as a function of pH. Cytolysis was detected by flow cytometric analysis of PI-stained cells (Figure 3.2). At all pH levels tested, little cell lysis (approximately 5%) was detected in control and PMAA-treated cells. In contrast, at some pHs, cell viability was significantly reduced following treatment with PPAA and PEAA. Following exposure to PPAA, the percentage of non-viable cells increased considerably between pH 7.0 and 6.5, but gradually decreased with further reductions in pH (Figure 3.2). At pH 7.0 neither PPAA nor PEAA induced significant loss of cell viability. However, at pH 6.5, exposure to PPAA lysed nearly 90% of cells (Figure 3.2). At progressively more acidic pH, the proportion of cells lysed by PPAA decreased slightly. In contrast, the proportion of cells lysed by PEAA did not increase significantly until the pH was reduced to 6.0 (where about 15% of the cells were lysed). At pH 5.5 and 5.0, PEAA lysed more than 90% of cells. For unknown reasons, PMAA does not have the ability to disrupt cell membranes, regardless of the pH level tested.

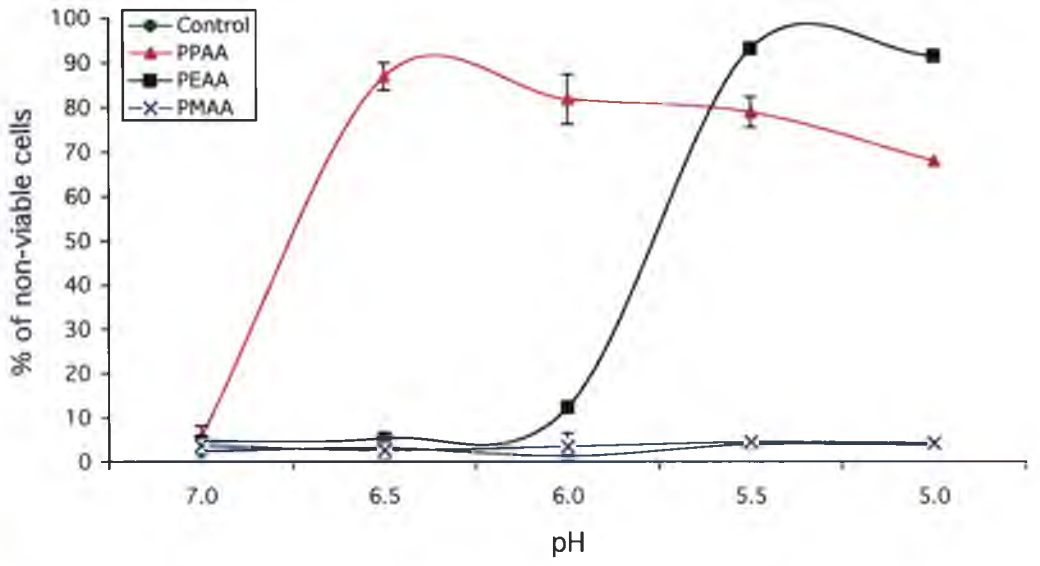

Figure 3.2: Line graph showing the percentage of non-viable U937 cells following exposure to either 200 μg/ml PPAA (▲), PEAA (■) or PMAA (×). Each data point represents the mean values for three independent experiments. Errors bars represent the standard errors of the mean in each case.

3.3.3 Polymers are Endocytosed and Release Calcein from Intracellular Vesicles

Following a 30 minute incubation in polymer buffer containing b-PEAA, U937 cells were stained with anti-EEA1 antibody and Alexa 488-conjugated goat anti-mouse Ig; b-PEAA was detected using streptavidin-Alexa 546. Confocal microscopy showed the polymer (b-PEAA) in punctate structures, many at the periphery of the cell. Many of these punctate structures co-stained with anti-EEA1 antibody. This pattern of fluorescence suggests that the polymer, which is hydrophilic at pH 7.4, enters the cell via the process of endocytosis (Figure 3.3).

Figure 3.3: Confocal microscopy images of U937 cells incubated in PB containing b-PEAA (red fluorescence). Images show cells stained with (a) anti-EEA1 antibody only (green fluorescence), (b) streptavidin-Alexa 546, and (c) an overlay of the two fluorescence images. In many cells, vesicles show co-localisation of green and red fluorescence (white). This result is representative of four independent experiments. 40-50 cells were scanned to ensure reproducibility. Bar = 10 μm.

When U937 cells were incubated in PB containing the membrane- impermeable fluor calcein, they subsequently showed fluorescent intracellular vesicles, consistent with constitutive endocytosis of the external medium. Numerous fluorescent intracellular vesicles were detected (Figure 3.4). When PPAA was included in the buffer together with calcein, there was a time-dependent release of calcein from vesicles to the cytosol. The pattern of intracellular fluorescence significantly changed during a 4 hour period following the initial uptake. Immediately following constitutive endocytosis of calcein and polymer, intracellular fluorescence was punctate. Two hours after uptake, larger fluorescent vesicles were clearly seen in many polymer-treated cells (Figure 3.4, panel b, indicated by arrow) but were absent in control cells, suggesting that PPAA induced vesicle fusion. At the same point in time, some cells showed partial release of calcein to the cytosol (Figure 3.4, panel b). At 4 hours following loading, fluorescence was considerably more diffuse, suggesting movement of calcein from vesicles to the cytosol (Figure 3.4, panel c). A similar pattern of fluorescence was detected when PEAA was

used. PEAA-treated cells also showed vesicle fusion and cytosolic calcein release, although this occurred later then in PPAA-treated cells. After 4 hours, calcein release was also detected in cells treated with PMAA, however the extent of this was less than in PPAA or PEAA-treated cells.

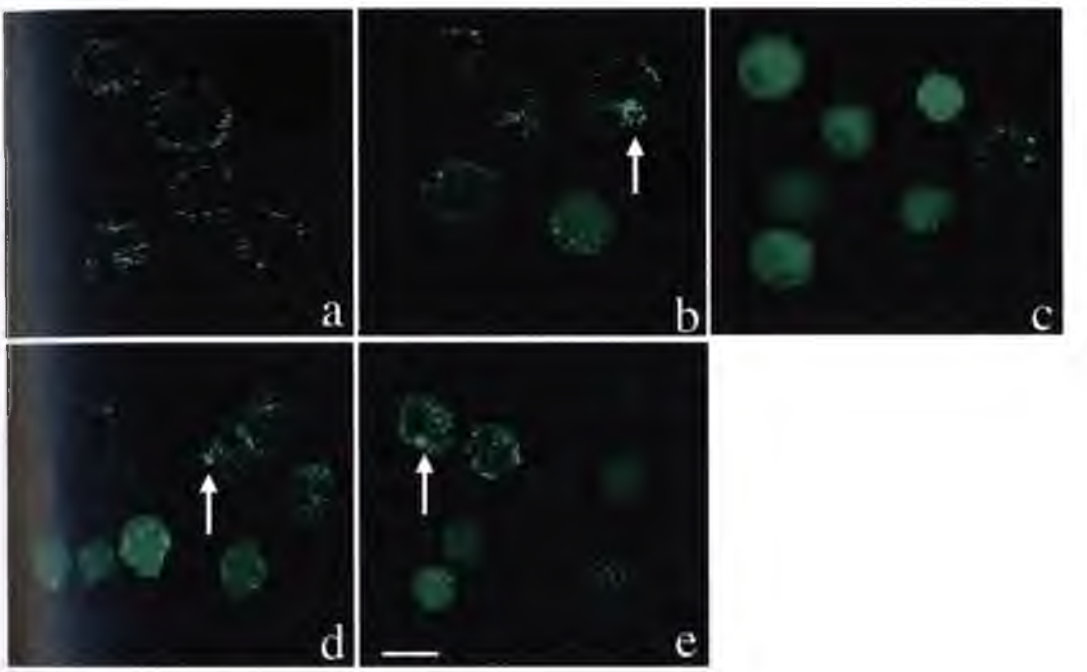

Figure 3.4: Confocal microscopy images of U937 cells incubated in PB containing 200 μg/ml of polymer and 2 mg/ml calcein. (a) Image of U937 cells immediately following PPAA treatment. Fluorescence is largely in punctate regions. (b) U937 cells 2 hours following PPAA-treatment. (c-e) Images of U937 cells 4 hours after loading of PPAA (c), PEAA (d), and PMAA (e) by constitutive endocytosis. In some cells vesicles have fused (arrows) and in others fluorescence is diffuse. This result is representative of six independent experiments. 40-50 cells were scanned to ensure reproducibility. Bar = 10 μm.

These interpretations are supported by quantitative analysis. For all polymers tested there was an increase in cytosolic fluorescence over time. At 4 hours following PPAA exposure the average cytosolic fluorescence (in arbitrary units) was 107. The corresponding level of fluorescence was 96 for PEAA-treated cells and 58 for PMAA-

treated cells. All these readings are significantly higher than those of control cells (Figure 3.5).

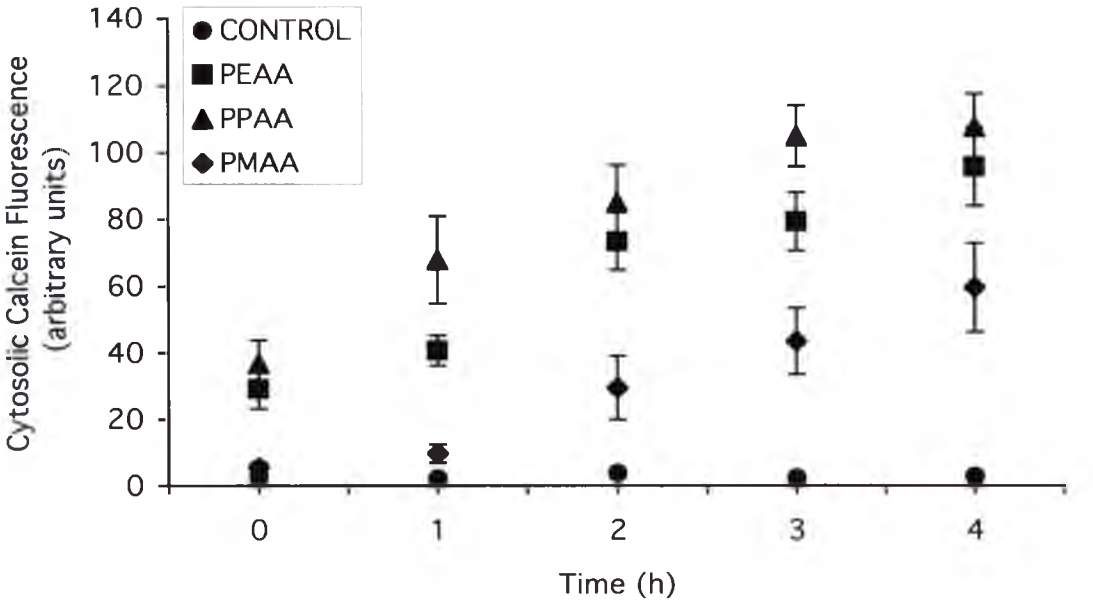

Figure 3.5: Plot showing the cytosolic calcein fluorescence of U937 cells, following constitutive endocytosis of media containing 2 mg/ml calcein and either 200 μg/ml PPAA, 200 μg/ml PEAA or 200 μg/ml PMAA. Over time, cytosolic calcein fluorescence increased by 60-70 arbitrary units in all treatments. 50 randomly chosen cells were analysed for each treatment. Error bars represent the standard error of the mean cytosolic calcein fluorescence in each case.

The ability of polymers to mediate calcein release showed a biphasic dependence on polymer concentration (Figure 3.6). For any one polymer, the level of calcein release was comparable for polymer concentrations of 5-25 μg/ml but increased to a higher similar level at either 50 or 200 μg/ml of polymer. The level of calcein release obtained following exposure of cells to either 50 or 200 μg/ml PPAA was significantly greater than that obtained with 25 μg/ml PPAA ($P<0.001$, $F_{4,50}=13.87$, pairwise Tukey-Kramer comparisons). Significant differences between either of the higher concentrations of

PEAA or PMAA (i.e. 50 μg/ml or 200 μg/ml) were not observed. In further experiments, 50 or 200 μg/ml of polymer was used.

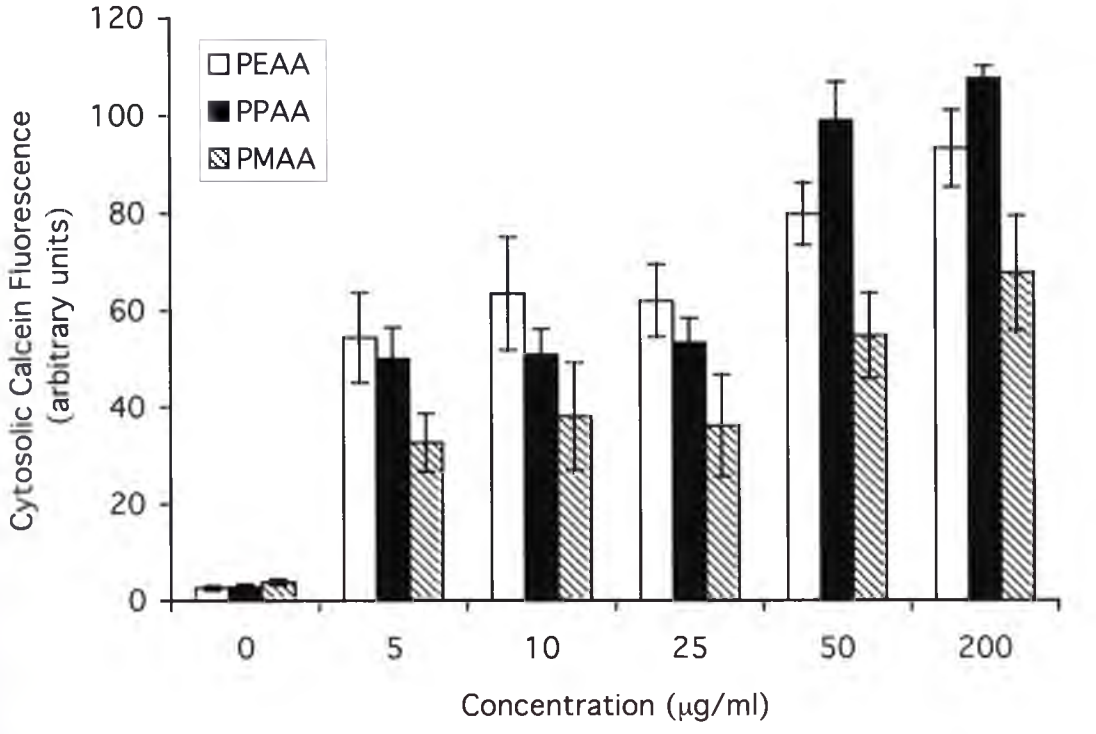

Figure 3.6: Dependence of endosomal calcein release on the concentration of poly(2-alkylacrylic acid)s. Plots show the level of cytosolic calcein fluorescence in U937 cells (determined as described in section 3.2.2.3), 4 hours after a 30 minute incubation in PB containing 2 mg/ml calcein and the indicated concentrations of PEAA, PPAA or PMAA. Each data point represents the mean values determined for 15 cells. The error bars shown are standard errors of the mean.

3.3.4 Polymers Release a Cathepsin B-GFP Fusion Protein from Intracellular Vesicles

Results in section 3.3.3 demonstrate that PAAAs can mediate release of a 622 Da fluor, calcein, from intracellular vesicles. To investigate whether the polymers could also mediate the release of macromolecules from vesicles, Hek293 cells were transiently

transfected with pCatB-EGFP plasmid encoding a fusion protein consisting of cathepsin B fused at its C-terminus to enhanced green fluorescent protein. Cathepsin B is an enzyme that is concentrated in lysosomes but is also found in early and late endsomes (Seaman, 2001). Control cells were transfected with control DNA (pEGFP-N1). Cells expressing EGFP showed a homogeneous distribution of green fluorescence within the entire cell (Figure 3.7A, panel a). In contrast, cells expressing Cat B-EGFP showed a restricted distribution of intracellular fluorescence consistent with the fusion protein being localized within endosomes/lysosomes (Figure 3.7A, panel b). When these latter cells were incubated in PB containing 50 μg/ml PPAA for 30 minutes, and subsequently examined by confocal microscopy, the intracellular fluorescence was more diffuse (Figure 3.7A, panel c), indicating partial release of cathepsin B-EGFP to the cytosol. Quantitative image analysis (as described in section 3.2.2.3) indicated that under the conditions tested, uptake of PPAA caused a statistically significant 2.4-fold increase in the cytosolic level of green fluorescence in pCatB-EGFP transfectants ($p<0.001$, Students t-test; Figure 3.7B). Similar changes in the distribution of fluorescence were also found when pCatB-EGFP-transfected cells were treated as above with PEAA or PMAA, but not when they were treated the same in the absence of any polymers (data not shown).

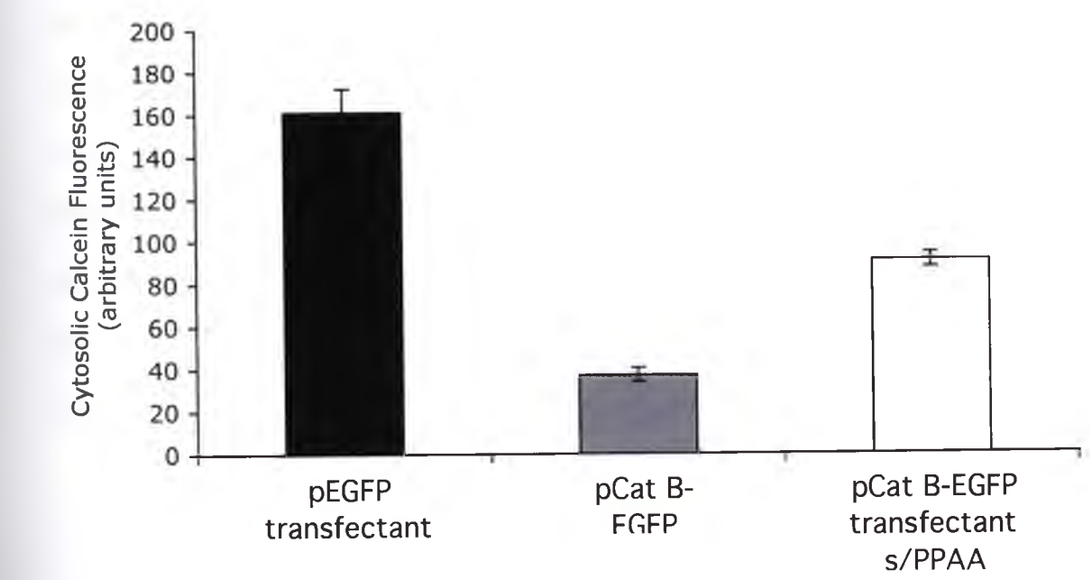

Figure 3.7: **A**. Confocal microscopy images of transiently transfected Hek293 cells showing (a) diffuse cytoplasmic fluorescence in cells transfected with a plasmid encoding (cytosolic) EGFP, (b) fluorescence restricted to intracellular vesicles in cells transfected with a plasmid encoding a cathepsin B-EGFP fusion protein, and (c) the same type of transfectants shown in (b) 4 hours after incubation in PB containing 50 μg/ml PPAA, showing release of cathepsin B-EGFP from vesicles to the cytosol. Release of cathepsin B-EGFP to the cytosol was also visible at earlier time points following polymer uptake (data not shown). PEAA and PMAA were also able to mediate release of cathepsin B-EGFP to the cytosol; this release did not occur in cells treated similarly but in the absence of PAAAs (images not shown). Bar = 10 μm. **B**. Histogram plots summarising the results of quantitative image analysis of cytosolic calcein fluorescence in Hek293 cells following transient transfection with (i) p-EGFP or (ii) pCatB-EGFP (with or without a subsequent 4 hour exposure to 50 μg/ml PPAA). Results are representative of 2 independent experiments and for each treatment 30 cells were analysed. Error bars represent the standard error of the mean cytosolic calcein fluorescence in each case.

3.3.5 Polymer-Mediated Disruption of Intracellular Vesicles is pH-Dependent

Stayton (2000) previously reported that PAAAs disrupt membranes in a pH-dependent manner and their membrane disruptive ability is significantly enhanced at acidic pH. The intra-vesicular pH of the major vesicles involved in the endocytic pathway gradually decreases from approximately 6.5 (early endosomes) to 4.5 (lysosomes). The progressive acidification of these vesicles is achieved primarily by the operation of an H^+-ATPase pump found in the vesicle membrane. Acidification can be inhibited by membrane-permeable vacuolar ATPase inhibitors such as bafilomycin (Vandeurs *et al.*, 1996; Schoonderwoert *et al.*, 2000).

Results discussed in sections 3.3.3 and 3.3.4 suggest that PAAAs are able to mediate the release of small and macro-molecules from endosomes to the cytosol. Bafilomycin significantly inhibits the release of calcein from intracellular vesicles mediated by PPAA, PEAA or PMAA (Figure 3.8). In each case, the effect of bafilomycin was statistically significant ($p<0.02$, Student's t-test). These result suggest that acidification of endosomal contents effected by the H^+-ATPase is required for PAAA-mediated disruption of endosomes.

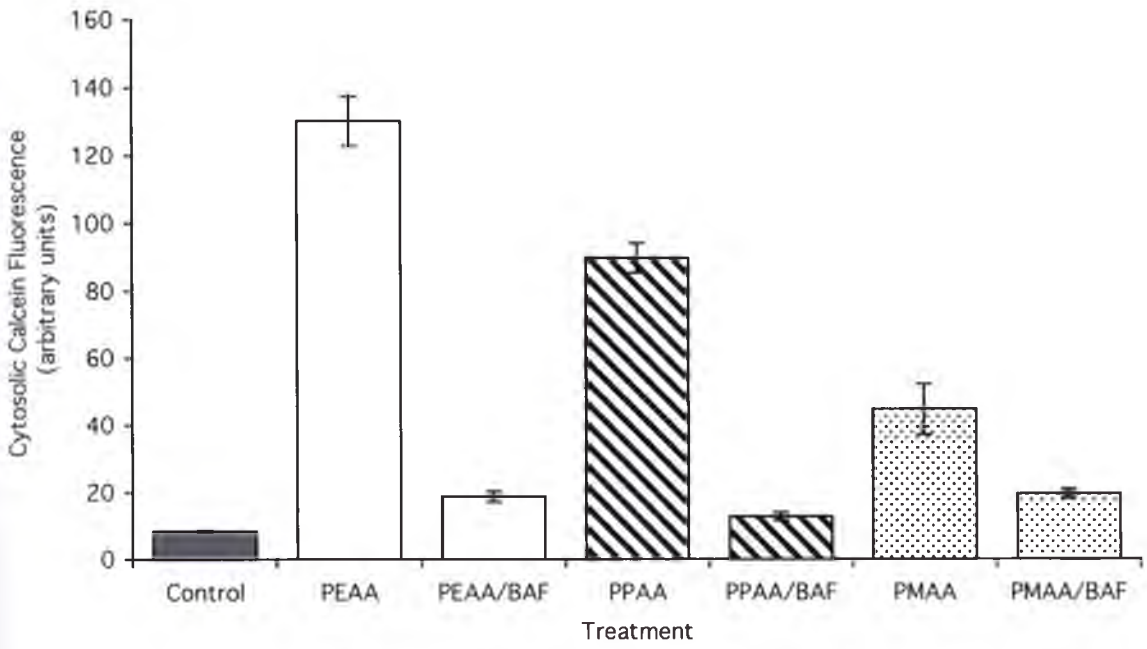

Figure 3.8: Plot showing that bafilomycin-mediated alkalinization of endosomes inhibits PAAA-mediated release of calcein to the cytosol. Quantitative results of confocal microscopy analyses of U937 cells measuring calcein release into the cytosol (see section 3.2.2.3 for details), 1.5 hours after a 30 minutes incubation in PB containing 2 mg/ml calcein and (where indicated) other additions. The histogram plots show results for cells incubated only with calcein (control) or with calcein and other additions (e.g. PEAA, cells incubated with calcein and 200 μg/ml PEAA). Where indicated (e.g. PEAA/BAF), cells were also treated with 1 μM bafilomycin to inhibit H^+-ATPase-mediated acidification of endosomal vesicles. Data points represent the mean of 25 cells and error bars represent the SE of the mean in each case.

This result was confirmed by showing that strong buffering of the solution from which cells endocytosed calcein and polymers inhibited the subsequent release of calcein into the cytosol. A 50% decrease in calcein release was detected in cells incubated in the strongly buffered solution, containing 200 μg/ml PPAA, compared to those incubated in the control buffer (Figure 3.9, $p<0.001$, Students t-test).

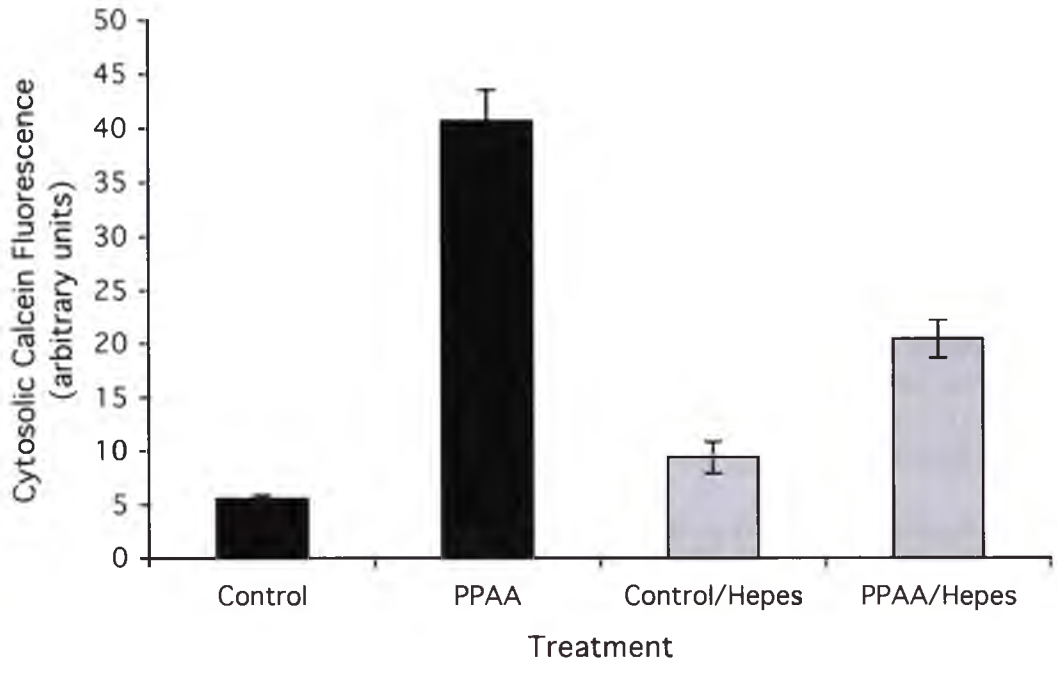

Figure 3.9: Buffer-mediated alkalinization of endosomes inhibits PAAA-mediated release of calcein to the cytosol. Plots show quantitative results of confocal microscopy analyses of U937 cells measuring calcein release into the cytosol (see section 3.2.2.3 for details). Cells were analysed 1.5 hours after a 30 minute incubation in PB containing 2 mg/ml calcein and where indicated (Hepes), the buffering of PB was increased from 0.5 mM to 50 mM Hepes. The histograms show results for cells incubated with calcein only (control) and cells incubated with calcein and 200 μg/ml PPAA (PPAA). Where indicated (Control/Hepes and PPAA/Hepes), cells were incubated in PB containing 50 mM Hepes. Pairwise comparisons indicated that 50 mM Hepes significantly inhibited the release of calcein ($p<0.001$, Student's t-test): the small difference between Control/Hepes and Control is not statistically significant. This data are representative of three independent experiments and error bars represent the standard error of the mean in each case.

3.3.6 Effects of Polymer Uptake on EEA1 and Lamp-1 Immunofluorescence

Results thus far indicate that PAAAs, particularly PEAA and PPAA, disrupt intracellular vesicles in a pH-dependent manner. Immunofluorescence was used to examine the effects of individual polymers on the morphology and distribution of different vesicle populations. Early endosomes were identified by staining cells with anti-EEA1 antibody. In both control and polymer-treated cells, fluorescence was in distinct punctate regions, generally towards the periphery of the cell (Figure 3.10), suggesting that the uptake of polymers did not affect the morphology or distribution of early endosomes. The lysosomal disruptive agent MSDH also had no effect on early endosomes (data not shown).

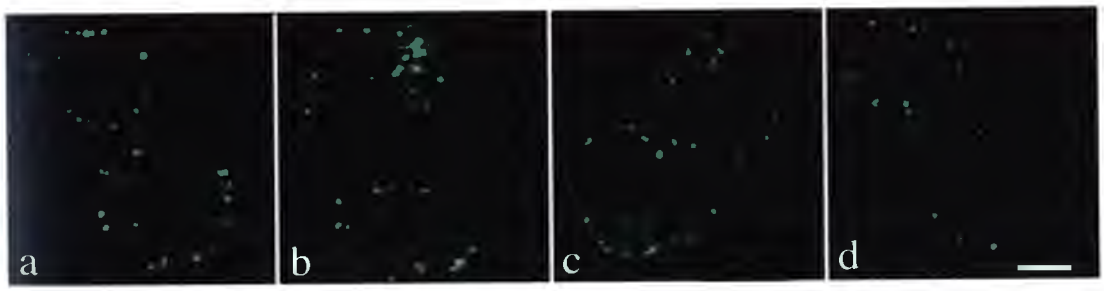

Figure 3.10: Confocal microscopy images showing U937 cells stained with anti-EEA1 antibody following constitutive endocytosis of PAAAs. A similar punctate pattern of fluorescence was detected in both control cells (a) and polymer-treated cells; PEAA (b), PPAA (c) and PMAA (d), suggesting that internalised polymers have no effect on early endosomes. These images are representative of cells analysed from 4 independent experiments. Bar = 10 μm.

Late endosomes and lysosomes were detected by staining cells with anti-Lamp-1 antibody. In control cells, one or two regions of bright concentrated fluorescence were

detected. These concentrated regions were approximately 2-4 μm in diameter and were surrounded by smaller fluorescent vesicles distributed throughout the cell (Figure 3.11A Panel a). In polymer-treated cells, these bright fluorescent globular regions were significantly reduced in size and in many cells these regions were not identifiable at all. Interestingly, the smaller fluorescent vesicles distributed throughout the cell were unaffected by polymers. This notable change in fluorescence was most obvious in cells treated with MSDH. In the majority of MSDH-treated cells, no globular regions of Lamp-1 specific fluorescence were detected (Figure 3.11A). These interpretations were confirmed by quantitative image analysis (Figure 3.11B).

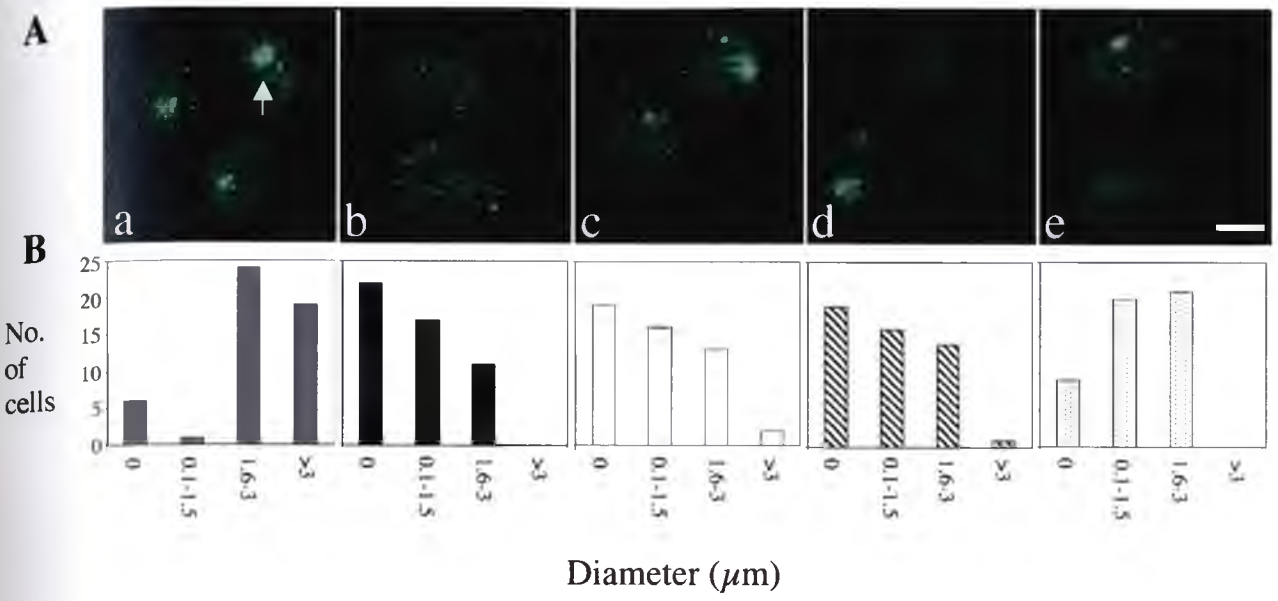

Figure 3.11: **A**: Confocal microscopy images of U937 cells following uptake of PAAAs by constitutive endocytosis and staining with anti-Lamp-1 antibody. Images show: Lamp-1 positive globular regions of fluorescence (grf; arrow) in cells incubated with (a) no added polymer, (b) 70 μM MSDH (to disrupt lysosomes), or 200 μg/ml of (c) PEAA, (d) PPAA or (e) PMAA. **B**: Histogram plots summarising the results of quantitative image analysis of the diameter of grf of 50 randomly chosen cells from each treatment (see section 3.2.2.6 for more details regarding this analysis). Bar = 10 μm.

3.3.7 Identifying the Specific Intracellular Vesicle Compartment(s) Disrupted by PAAAs

Lamp-1 is a major lysosomal protein but is also found in the membranes of late endosomes and the trans Golgi network (Akasaki, 1995). Thus, the changes in the pattern of Lamp-1 immunofluorescence induced by uptake of PAAAs might result from changes to one or more of these compartments. To eliminate the possibility that PAAAs might be transported from endosomes to the trans-Golgi and there disrupt the Golgi, following uptake of polymer, U937 cells were stained with anti-golgin 97 antibody.

Anti-golgin-97 antibody recognizes a 97 kDa protein called golgin–97 that is located on the trans-Golgi network. Golgin-97 is not located in any other compartment. Cells were analysed by confocal microscopy following polymer uptake and antibody staining. In both the control cells and polymer-treated cells, fluorescence was in distinct elongated clumps around the periphery of the cell (Figure 3.12), suggesting that the uptake of PAAAs did not affect the morphology or distribution of the trans-Golgi apparatus.

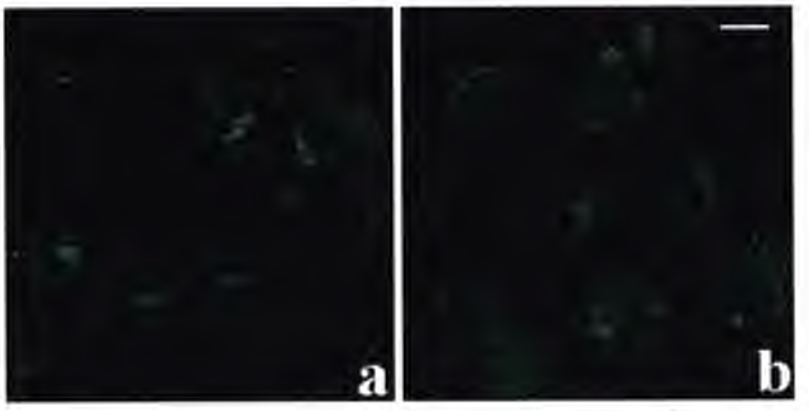

Figure 3.12: Confocal microscopy images of U937 cells showing Golgin-97 positive vesicles (trans-Golgi apparatus). Four hours after a 30 minutes incubation in PB alone (a) or PB containing 200 μg/ml PPAA (b), U937 cells were fixed, permeabilized and then stained with anti-golgin-97 antibody. Images are representative of two independent experiments. Bar = 5 μm.

To investigate the effects of polymer uptake on lysosomes, LysoTracker Yellow and acridine orange were used. Control cells stained with LysoTracker Yellow showed one or a small number of patches of peri-nuclear fluorescence (Figure 3.13, panel a). In cells treated with MSDH, the areas of fluorescence were smaller in size and more punctate (Figure 3.13, panel b), indicating changes in lysosomal morphology. However, the effects of the polymers were less pronounced. Polymer-exposed cells showed a more irregular pattern of staining with LysoTracker Yellow than control cells (Figure 3.13,

panels c-d). Uptake of PEAA produced a pattern of fluorescence that was similar to that of MSDH-treated cells. Cells that had taken up PPAA or, particularly, PMAA showed lesser effects but the pattern of fluorescence was still more dispersed than that of the controls. Image analysis (see section 3.2.2.7) confirmed that MSDH and the polymers had induced changes in the pattern of LysoTracker fluorescence (Figure 3.13B). Flow cytometric analysis of cells treated with either MSDH or polymers and stained with acridine orange indicated that MSDH induced loss of lysosomal integrity but that uptake of any of the polymers did not (Figure 3.14). Collectively, these results suggest that polymers were causing changes in lysosomal morphology but were not causing physical disruption of the lysosomal membrane.

panels c-d). Uptake of PEAA produced a pattern of fluorescence that was similar to that of MSDH-treated cells. Cells that had taken up PPAA or, particularly, PMAA showed lesser effects but the pattern of fluorescence was still more dispersed than that of the controls. Image analysis (see section 3.2.2.7) confirmed that MSDH and the polymers had induced changes in the pattern of LysoTracker fluorescence (Figure 3.13B). Flow cytometric analysis of cells treated with either MSDH or polymers and stained with acridine orange indicated that MSDH induced loss of lysosomal integrity but that uptake of any of the polymers did not (Figure 3.14). Collectively, these results suggest that polymers were causing changes in lysosomal morphology but were not causing physical disruption of the lysosomal membrane.

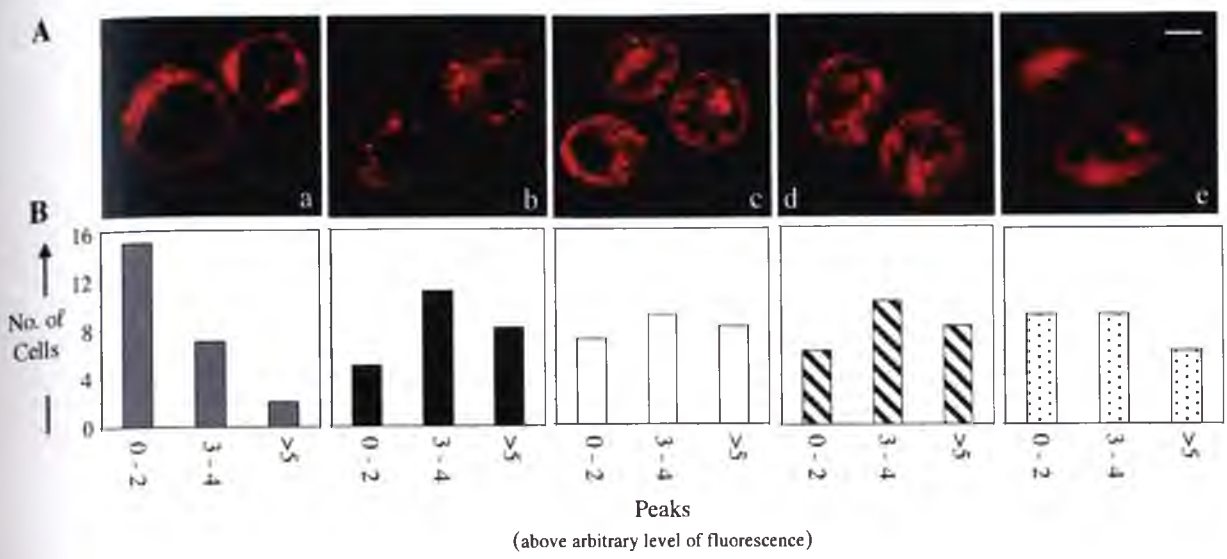

Figure 3.13 **A**: Confocal microscopy images of U937 cells loaded with PAAAs by constitutive endocytosis and stained with LysoTracker Yellow. U937 cells were incubated in PB containing various additions for 30 minutes. Cells were then washed and resuspended in complete medium and incubated for a further 4 hours. LysoTracker Yellow was added directly to the cells 1 hour before confocal analyses (see section 3.2.2.7 for more details). Images show: (a) control cells (no added polymer); (b) MSDH-exposed cells (MSDH disrupts lysosomes); (c) PEAA-treated cells (200 μg/ml), (d) PPAA-treated cells (200 μg/ml) and (e) PMAA-treated cells (200 μg/ml). For each treatment, the images shown are representative of 40 cells analysed in three independent experiments. Bar = 10 μm. **B**: Each histogram plot summarises the results of quantitative image analysis (performed as described in section 3.2.2.7) of 25 cells treated as in the image above. Cells from three independent experiments were analysed.

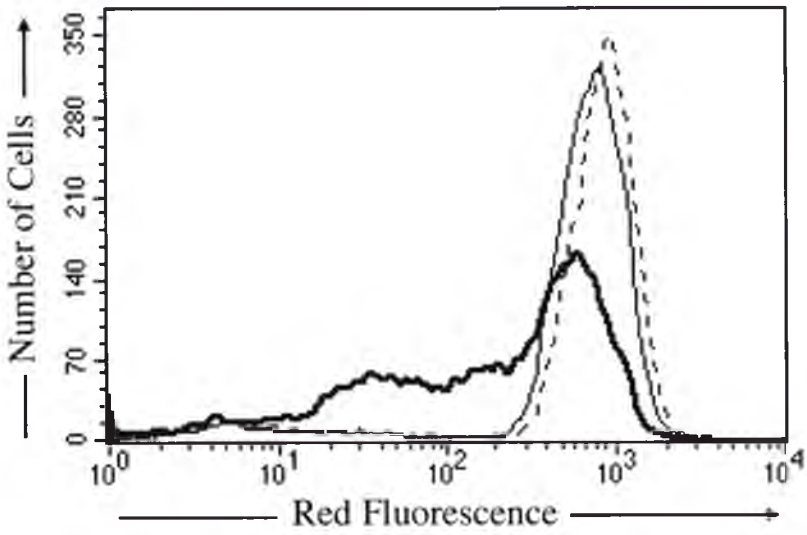

Figure 3.14: Overlay flow cytometry histograms showing U937 cells stained with acridine orange 4 hours after a 30 minute incubation in PB containing no additions (thin solid line) or 200 μg/ml PEAA (dashed line), or after 4 hours incubation in culture medium containing 70 μM MSDH (thick solid line). The results shown are representative of four independent experiments. In similar experiments, the uptake of PPAA and PMAA also had no effect on the level of red fluorescence associated with acridine orange-stained cells (data not shown).

3.4 Discussion

This chapter describes work in which PAAAs were introduced into cells via constitutive endocytosis and the effects on cells were characterised. No significant decrease in cell viability was detected over a 24 hour time period following polymer uptake. Whole cell experiments indicated that both PEAA and PPAA destabilize membranes at mildly acidic pH. The membrane-disruptive activity was greatest at pH 5.5 for PEAA and pH 6.5 for PPAA. Interestingly, the membrane-disruptive activity of PPAA appeared to decrease at pH<6.5. At these pHs, PPAA has a tendency to precipitate from aqueous solution. It has been suggested that at pH 5 and 5.5, PPAA may form micro-aggregates with a reduced ability to disrupt membranes (Jones *et al.*, 2003). Thus, the greater hydrophobicity of PPAA may explain why it had reduced lytic efficiency at lower pH. Previous work has suggested that PAAAs are likely to deliver molecules into cells by endocytic uptake followed by low pH-induced disruption of endosomes/lysosomes to release their contents to the cytosol (Murthy *et al.*, 1999). The membrane-disruptive activity results suggest that PPAA might achieve maximum membrane-disruptive activity during the earlier stages of endosomal acidification, whereas PEAA might only achieve this in the final most acidic endosomal compartments. In these whole cell experiments PMAA did not display any membrane-disruptive activity. The reason(s) for this are unknown.

Results displayed in Figure 3.3 show U937 cells with biotinylated PEAA (b-PEAA) in punctate structures located primarily at the periphery of the cell; some of the punctate structures are co-stained with anti-EEA1 antibody. This suggests that PEAA (which is hydrophilic at pH 7.4) is taken up by endocytosis and transits through early endosomes before moving onto other vesicular compartments. Similarly, when U937 cells were

incubated in buffer containing the membrane-impermeable fluor calcein, they subsequently showed fluorescent intracellular vesicles, consistent with constitutive endocytosis of the external medium (Figure 3.4). Uptake of PAAAs induced fusion of calcein-containing endosomes followed by release of calcein to the cytosol (Figure 3.4). This effect appears similar to the PEAA-induced fusion of phosphatidylcholine vesicles observed *in vitro* at mildly acidic pH (Linhardt and Tirrell, 1999).

Time course studies conducted over a 4 hour period showed a time dependent release of calcein from intracellular vesicles into the cytosol. PPAA produced more rapid disruption of vesicles than PEAA. PMAA produced the least disruption of vesicles and its effect was the slowest of the three polymers tested. The faster kinetics and greater extent of vesicle disruption mediated by PPAA and PEAA compared to PMAA may result from the greater hydrophobicity of PPAA and PEAA.

In contrast to the results reported here, Plank *et al.* (1994) previously showed that pH-sensitive endosomal disruptive peptides were able to induce significant release of fluorescent dextran from intracellular vesicles 15 minutes after endocytic uptake. However, in these experiments no measurements of the time dependence of release were reported. Both PPAA and PEAA mediated measurable release of calcein from vesicles immediately after uptake, however, the extent of release increased progressively with time, reaching a maximum at approximately 4 hours after uptake. It appears that, once endocytosed, PAAAs may disrupt endosomes more slowly than pH-sensitive peptides. It has been suggested that endosomal-disruptive peptides only require protonation of a small number of side-chain groups (e.g. 3) to bring about transition to a membrane-disruptive conformation (Plank *et al.*, 1994). In contrast,

PAAA are polyanions at physiological pH: when internalised within endosomes they will act as polyvalent buffers and will require the transport of hundreds of H^+ ions per polymer molecule before becoming membrane-disruptive. Another possible reason for the apparently slower kinetics of vesicle disruption mediated by PAAAs versus peptides may be that PAAAs appear unable to disrupt lysosomes (Figure 3.14). Mellman (1996) suggests that undegraded endocytosed material is continually recycled between late endosomes and lysosomes. Therefore, the PAAAs may only mediate the release of molecules when they are intermittently and transiently resident in late endosomes.

The default pathway for endocytosed materials is to be carried through vesicle compartments towards lysosomes for eventual degradation. During this trafficking the contents of the vesicles become progressively acidified, reaching a pH of less than 5.0 in lysosomes. We reasoned that endocytosed PAAAs would probably follow this pathway and when the vesicle contents became sufficiently acidic, the polymers would adopt a conformation competent to disrupt membranes. Acidification of the lumen of endososomes/lysosomes is effected by an H^+-ATPase found in the vesicle membrane, which can be specifically inhibited by bafilomycin (Vandeurs *et al.*, 1996). Results shown in Figures 3.8 and 3.9 show that disruption of intracellular vesicles was significantly decreased following bafilomycin-mediated inhibition of the endosomal/lysosomal H^+-ATPase or strong buffering of the medium from which polymers were endocytosed. These results indicate that endocytosed PAAAs are triggered by the progressive acidification of endosomal/lysosomal contents to become membrane-disruptive.

The ability of PAAAs to mediate calcein release showed a biphasic dependence on concentration (Figure 3.6). Cytosolic calcein fluorescence was comparable when cells endocytosed PAAAs from concentrations of 5-25 μg/ml increased significantly to a similar higher level when either 50 μg/ml or 200 μg/ml PAAA were used. The reason why this occurs is not known, however, it is possible that at higher concentrations in an acidic environment, individual polymer molecules may co-operate in some way to more efficiently disrupt membranes.

PAAAs disrupt intracellular vesicles to release both small molecules (e.g. 622 Da calcein) and macromolecules (e.g. a 64 kDa fusion protein) (Figure 3.4 and 3.7, respectively). In addition, Lackey *et al.* (2002) have shown that PPAA similarly mediated release of a large (approximately 264 kDa) polymer-antibody-streptavidin complex to the cytosol. These results suggest that PAAAs are capable of sufficiently disrupting intracellular vesicles to effect the indiscriminant release of their contents to the cytosol.

There are three major types of acidified intracellular vesicles through which most endocytosed materials pass through. These are early and late endosomes and lysosomes. These vesicles are thought to be the location of expressed Cat B-EGFP (Guicciardi *et al.*, 2000). Results shown here indicate that Cat B-EGFP is released from intracellular vesicles following polymer treatment (Figure 3.7). Therefore, it was reasoned that one of these three compartments would be the site(s) disrupted by endocytosed PAAA polymers. There was no measurable effect of polymer uptake on the pattern of EEA1 immunofluorescence, suggesting that early endosomes were unaffected (Figure 3.10). The early endosome is the first compartment that endocytosed materials are delivered to

and its lumen is mildly acidic at pH 6.0-6.2 (Cain, 1989). Despite the fact that PPAA has potent haemolytic activity at this pH, it does not appear to disrupt early endosomes.

In contrast, Lamp-1 immunofluorescence was significantly affected following uptake of PAAAs (Figure 3.11). Lamp-1 proteins belong to a series of proteins that are located on the surface of late endosomes, lysosomes and the trans Golgi network. This suggests that the polymers were disrupting one or more of these compartments. To identify the precise compartment that the polymers disrupt, various other assays were performed. Changes in LysoTracker Yellow staining suggested that, 4 hours after uptake (when extensive release of calcein from vesicles could be measured), the polymers were effecting changes in the morphology of lysosomes. However, at this same time point, flow cytometric analysis of cells stained with acridine orange (which accumulates inside lysosomes (Zelenin, 1999)) indicated that lysosomes remained structurally intact (Figure 3.14). Extensive lysosomal bursting is known to induce cell death (Brunk *et al.*, 2001); we found that after continuous exposure of cells to 200 μg/ml polymer for 24 hours, >95% of cells remained viable (Figure 3.1). Collectively, these results suggest that the release of calcein and cathepsin B-EGFP fusion protein measured at 4 hours after polymer uptake was occurring from a compartment other than lysosomes. Immunofluorescence analyses indicated that the morphology of the trans-Golgi network was not affected following polymer treatment (Figure 3.12). Therefore, we conclude that late endosomes are likely to be the intracellular compartment that becomes disrupted following constitutive endocytosis of PAAAs.

It is unclear why endocytosed PAAAs alter the morphology of lysosomes but do not physically disrupt them. Two possible explanations are as follows: (1) The lysosomal

membranes may be resistant to the disruptive effects of the polymers. It is known that the lumenal face of the lysosomal membrane is heavily coated with a family of glycoproteins that are thought to provide the membrane with protection from the many lytic enzymes in the lumen (Granger, 1990). This coating may also sterically shield the membrane from the actions of the protonated, hydrophobic polymers; (2) At a pH of less than 5 (which is found in lysosomes), if present at a sufficient concentration, the heavily protonated, hydrophobic polymers may precipitate and become ineffective as membrane disruptants. Supporting the latter possibility, as stated before, PPAA precipitates from aqueous solution at pH<5. The two above explanations may not be mutually exclusive.

Collectively, these results suggest that cells endocytose PAAAs and transport them to late endosomes, where acidification of the lumen by the membrane H^+-ATPase triggers polymer-mediated vesicle disruption and release of endosomal contents to the cytosol. PPAA and PEAA show great potential for use as drug delivery agents for cancer therapies.

Chapter 4

Investigation of Poly[1-(dimethylamino)ethyl methacrylate] as a Potential Delivery Agent for Pro-Apoptotic Cancer Therapeutics

4.1 Introduction

In recent years, many polymers have been tested for their ability to enhance delivery of anti-cancer agents to tumours. A few polymers show great potential and are now in stage I and II clinical trials. Unfortunately, progress is slow due to various limitations *in vivo*, for example, retaining polymer conjugates at tumour sites. Therefore, research continues to search for a suitable delivery agent. Initial investigations of PAAAs were discussed in the previous chapter. Results are promising and indicate that PAAAs disrupt late endosomes in a pH-dependent manner and deliver molecules into the cytosol.

The current chapter describes an investigation of another polymer, poly[1-(dimethylamino)ethyl methacrylate] (pDMAEMA). pDMAEMA was analysed for its ability to (1) induce apoptotic cell death by disruption of lysosomal membranes and (2) deliver molecules into the cytosol of cancer cells. The chemical structure of pDMAEMA is schematically represented in Figure 4.1.

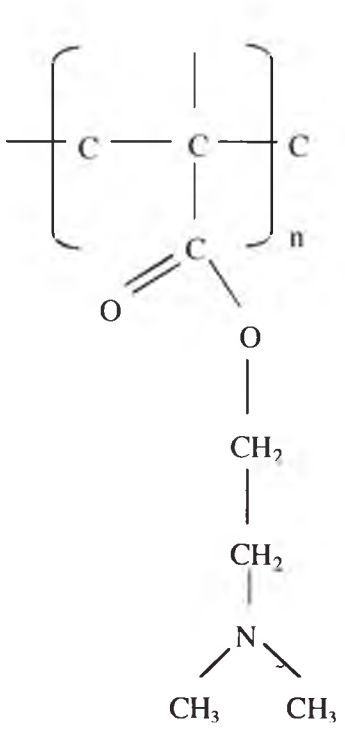

Figure 4.1: Schematic representation of the chemical structure of poly(2-(dimethylamino)-ethyl methacrylate (pDMAEMA). Adapted from van de Wetering *et al.* (1999).

Van de Wetering and colleagues (1999) suggested that pDMAEMA may have properties, similar to PAAAs, which enable it to disrupt endosomal membranes. Currently there is no direct evidence that pDMAEMA disrupts endosomes. Van de Wetering *et al.* (1999) have suggested that at physiological pH, pDMAEMA is partially protonated but at lower pH it becomes completely protonated (i.e. acts as a 'proton sponge'). They have hypothesised that at low pH, the proton sponge action of pDMAEMA causes massive ATPase-driven proton accumulation within endosomes that is followed by passive chloride ion influx to prevent the build up of a charge gradient. The influx of the protons and chloride ions would increase the osmolarity of the endosomal contents and cause water influx resulting in osmotic swelling and subsequent disruption of endosomes (Boussif *et al.*, 1995; van de Wetering *et al.*, 1999, Funhoff *et al.*, 2003).

pDMAEMA, and derivatives thereof, have previously been used as delivery agents in gene therapy to kill cancer cells (Fonseca *et al.*, 1999). In these experiments, pDMAEMA was complexed with plasmids encoding a therapeutic toxin and then used to transfect cancer cells. The pDMAEMA-plasmid complex has shown some favourable results *in vitro*, however, like many other potential cancer therapies, unfavourable complications such as lack of cell specificity have arisen (van Steenis *et al.*, 2003).

Previously, relatively few studies of pDMAEMA have been performed. It has only been characterised in terms of molecular modelling, pKa values, cytotoxicity, and transfection efficiency (Van de Wetering *et al.*, 1999; Arigitia *et al.*, 1999). Therefore, experiments described in the current chapter further characterise pDMAEMA by determining (1) its mechanism of entry into cells, (2) the mode of cell death it induces (i.e. apoptosis or necrosis) and (3) its ability to disrupt endosomes and release molecules into the cytosol of cells. These investigations were intended to identify whether pDMAEMA might by used in the development of novel cancer therapeutics such as a trimolecular construct (section 1.10).

4.2 Materials and Methods

4.2.1 Materials

pDMAEMA (Mw = 22 kDa) and pDMAEMA/AEMA (Mw = 31 kDa; a copolymer of pDMAEMA and aminoethylmethacrylate, polymerised in the ratio 19:1) were gifts from Dr. Wim E. Hennink, Department of Pharmaceutics, Utrecht Institute for Pharmaceutical Sciences (UIPS), Utrecht University, The Netherlands. Propidium iodide and calcein were from Sigma (MO, USA). Annexin V-FITC was purified and conjugated to FITC within the laboratory (see section 2.2.5). CaspACE FITC-VAD-FMK was from Promega (WI, USA). Monoclonal antibodies reactive with early endosomal antigen 1 (EEA1), lysosomal-associated membrane protein-1 (Lamp-1) and cytochrome c were from Pharmingen-Transduction Laboratories (CA, USA). Alexa 488-conjugated goat-anti-mouse Ig and 3,3'-dihexyloxacarbocyanine iodide ($DiOC_6(3)$) were from Molecular Probes (OR, USA).

4.2.2 Methods

4.2.2.1 Determining Cell Viability Following Introduction of pDMAEMA

U937 cells were incubated in polymer buffer (PB; 145 mM NaCl, 5 mM KCl, 0.5 mM HEPES) containing pDMAEMA and constitutive endocytosis allowed to proceed before determining cell viability. U937 cells ($2x10^6$) were centrifuged for 5 minutes at 300 *g*. Cells were resuspended in 0.6 ml of PB, with or without the addition of pDMAEMA to give a final concentration of 1 μg/ml or 2 μg/ml (added from a stock solution at 4 mg/ml). Cell suspensions were incubated for 1 hour at 37°C; at 15, 30 and 60 minutes,

200 μl of the cell suspension was removed. Cell viability was then determined by staining cells with PI as described in section 3.2.2.1.

4.2.2.2 Confirming the Mode of Entry of pDMAEMA into Cells

Previous experiments involving pDMAEMA have presumed that the mode of entry of the polymer into cells was via endocytosis, however, this was not conclusively shown. Endocytosis is a process by which cells internalise material from their external environment (Mellman, 1996). Internalised material is then transported through the cell in a series of compartments called endosomes. Like PAAAs (Chapter 3), we predicted that pDMAEMA, internalised by endocytosis, would pass through the early endosomal compartment. To confirm this, we traced the initial movements of pDMAEMA through the cell. This was achieved by biotinylating pDMAEMA/AEMA (which contains free amine groups), and staining fixed permeabilised cells with anti-EEA1 antibody (EEA1 is used for the detection of early endosomes). Biotinylated pDMAEMA/AEMA (b-pDMAEMA/AEMA) was detected using streptavidin-Alexa 546 and anti-EEA1 antibody was detected using Alexa 488-conjugated goat anti-mouse Ig antibody. Biotinylation, cell fixation and permeabilisation, and confocal analyses were performed as described in section 3.2.2.2.

To further test the hypothesis that pDMAEMA enters cells via endocytosis, the dependence of its cytotoxicity on temperature was determined. Endocytosis works most efficiently at 37 C and is inhibited at lower temperatures, for example, 4 C. Two parallel experiments were performed; one at 37 C and the other at 4 C. For each experiment, cytotoxicity assays were performed as described above (section 4.2.2.1). A

decrease in cytotoxicity at 4 C was expected if the mode of entry of pDMAEMA into cells was by endocytosis.

4.2.2.3 Staining Cells with Annexin V-FITC to Measure Phosphatidylserine Exposure

Phosphatidylserine (PS) is a phospholipid, normally confined to the inner leaflet of the plasma membrane. However, during apoptosis, and in some necrotic cell systems, it is exposed on the outer leaflet of the plasma membrane (Kerr, 1995; Martin *et al.*, 1996). The exposure of PS on the surface acts as a trigger for the recognition of apoptotic cells by phagocytes. Phagocytes contain specific receptors for exposed PS, thereby allowing rapid removal of the cells (Martin *et al.*, 1996). PS externalisation is most commonly measured using a protein known as annexin V. Annexin V has high affinity for aminophospholipids such as PS (Meers and Mealy; 1993, Meers and Mealy, 1994; Martin *et al.*, 1996). Fluorescent conjugates of annexin V (e.g. FITC conjugates) can be used to detect PS exposure on the surface of cells by flow cytometry (Kroemer *et al.*, 1995).

Annexin V labelling solution was made by diluting annexin V-FITC (1 mg/ml) 1:100 in annexin V buffer (10 mM HEPES, pH 7.4, 140 mM NaCl, 5 mM $CaCl_2$). $2x10^6$ cells were centrifuged at 300 *g* and resuspended in 500 μl of PB containing either 1 μg/ml or 2 μg/ml polymer. Cells were incubated for 30 minutes at 37°C to allow constitutive endocytosis to occur. The cells were resuspended in 1 ml of 1x PBS and re-centrifuged as above. The supernatant was removed and cells were resuspended in 50 μl of the annexin V labelling solution, followed by a 15 minute incubation at room temperature in the dark. Immediately before flow cytometric analysis, 500 μl of annexin V buffer

was added and cells stained with PI (see section 3.2.2.1). FSC, SSC, FL1 and FL3 signals were acquired. Increased PS exposure on the cell surface was measured as an increase in FL1 fluorescence. Non-viable (i.e. PI positive) cells were excluded from all analyses. Figure 4.2 shows an example of how flow cytometry data was analysed.

A Control **B pDMAEMA**

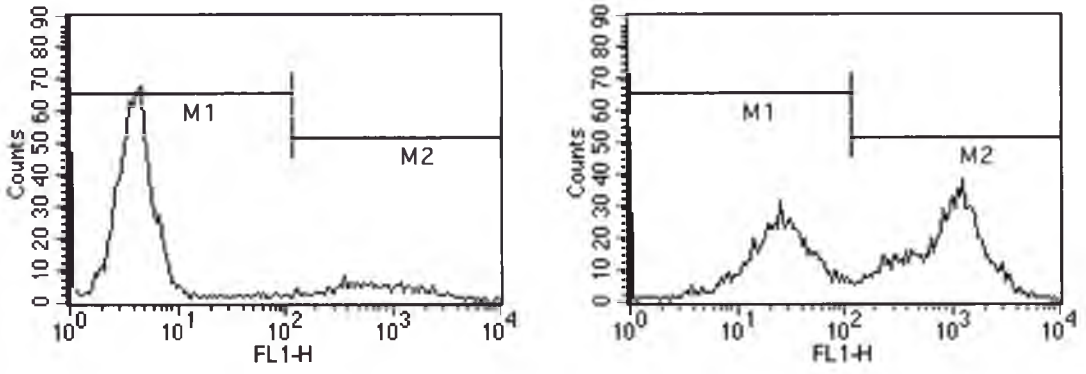

Marker	% Gated
All	100.00
M1	86.32
M2	13.72

Marker	% Gated
All	100.00
M1	44.67
M2	55.36

Figure 4.2: FL1 histograms of U937 cells exposed to 2 μg/ml pDMAEMA for 30 minutes and stained with annexin V-FITC. The margins used for the control cells were the same as those used for cells treated with pDMAEMA. M1 is the population of cells that had not bound annexin V-FITC to their surface. The percentages of cells that bound annexin V-FITC to their surface (M2) are shown under each histogram. Histogram A represents the control cells. Histogram B represents cells exposed to pDMAEMA. Non-viable cells were excluded from all analyses.

4.2.2.4 Staining Cells with 3,3'-Dihexyloxacarbocyanine Iodide ($DiOC_6(3)$) to Measure Mitochondrial Depolarisation

$DiOC_6(3)$ is a cationic lipophilic fluor that accumulates in the matrix of mitochondria. The negative charge of the matrix attracts the positive charge of the fluor, while the

lipophilic properties allow the fluor to diffuse across membranes and enter the matrix. When there is reduced mitochondrial membrane potential (mitochondrial depolarisation), accumulation of the fluor is reduced and is measured by flow cytometry as a decrease in cell-associated fluorescence (Kroemer *et al.*, 1997).

Following loading of polymers by constitutive endocytosis (section 4.2.2.1) cells were centrifuged at 300 *g* for 5 minutes. The supernatant was discarded and the pellet was resuspended in 1 ml of complete medium containing 40 nM $DiOC_6(3)$. This was prepared from a 1 M stock, which was diluted to 1 mM in 500 μl of 1x PBS and then diluted to 40 nM in complete medium. The cells were incubated at 37°C for 15 minutes in the dark. Immediately before flow cytometric analysis, cells were stained with PI (see section 3.2.2.1). FSC, SSC, FL1 and FL3 signals were collected. Non-viable cells were excluded from all analyses. Figure 4.3 is an example of how flow cytometry data was analysed.

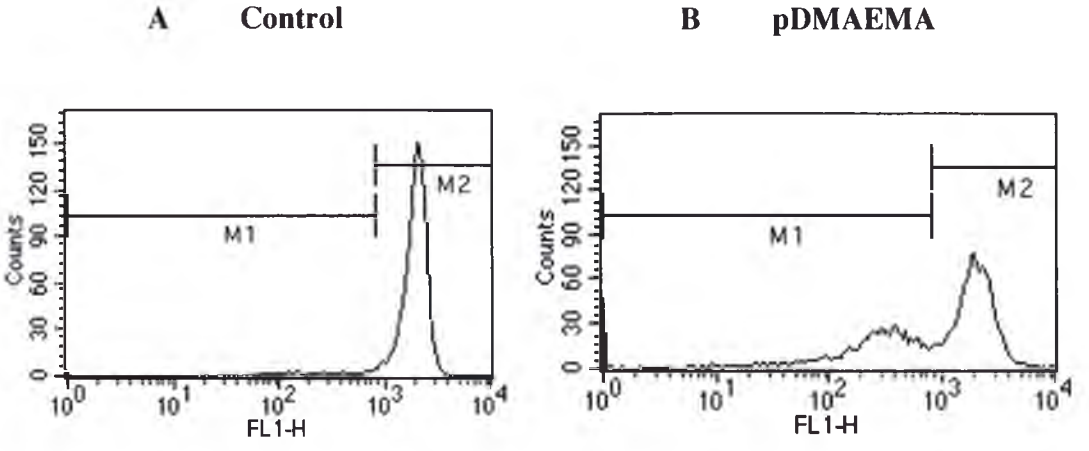

Marker	% Gated
All	100.00
M1	2.71
M2	97.32

Marker	% Gated
All	100.00
M1	38.67
M2	61.46

Figure 4.3: FL1 histograms of U937 cells exposed to 2 μg/ml pDMAEMA for 30 minutes and stained with $DiOC_6(3)$. The margins used for the control cells were the same as those used for cells treated with polymer. M1 is the population of cells with depolarised mitochondria. The percentages of cells with depolarised mitochondria are shown under each histogram. Histogram A represents control cells. Histogram B represents cells exposed to pDMAEMA. Non-viable cells were excluded from all analyses.

4.2.2.5 Measuring Caspase Activation Following Exposure to pDMAEMA

Several caspases, in particular caspase 3, are known to be involved in apoptosis. Caspase 3 has been implicated in virtually all apoptotic systems tested. Caspases interact with proteins normally stored within mitochondria and other intracellular proteins to regulate apoptosis. Following exposure to pDMAEMA, caspase activation was determined using CaspACE™ FITC-VAD-FMK(carbobenzoxy-valyl-alanyl-aspartyl-[O-methyl]-fluormethylketone). CaspACE™ FITC-VAD-FMK is a cell permeable probe that irreversibly binds to a number of activated caspases (Flores and

Macklin, 2000; Perkins *et al.*, 2003). pDMAEMA was loaded by constitutive endocytosis into $2x10^6$ U937 cells (as previously described in section 4.2.2.1). Following loading, cells were washed with DMEM:F12 and resuspended in DMEM:F12 containing 10 μM CaspACE™ FITC-VAD-FMK. Cells were then incubated for 20 minutes at 37°C in the dark. Immediately before flow cytometric analysis, cells were stained with PI (see section 3.2.2.1). FSC, SSC, FL1 and FL3 signals were collected. Caspase activation was measured by an increase in FL1 fluorescence. Non-viable cells were excluded from all analyses.

4.2.2.6 Measuring Cytochrome c Release Following Exposure to pDMAEMA

Cytochrome c is an extrinsic membrane protein, normally associated with the outer surface of the inner membrane of mitochondria (Gastman, 2001). Cytochrome c release from mitochondria to the cytosol has been reported in many different systems of apoptosis (Kluck *et al.*, 1997; Zhaung and Cohen, 1998). Immunofluorescence staining of cells allows the release of cytochrome c from mitochondria to be visualised by fluorescence microscopy as a change from punctate regions of intensely concentrated fluorescence (corresponding to mitochondrial localisation), to diffuse fluorescence located throughout the cell cytosol.

U937 cells ($2x10^6$) were centrifuged (300 *g*, 5 minutes) in a 15 ml tube. Cells were fixed and permabilised as described in section 3.2.2.2. Cells were then diluted with ice-cold 0.1% (w/v) BSA/PBS to pre-block non-specific binding sites and to minimise cell loss during centrifugation. Cells were centrifuged again (900 *g*, 10 minutes), drained and resuspended in 50 μl of 1% (w/v) BSA/PBS containing 2.5 μg/ml mouse anti-

cytochrome c primary antibody. Cell suspensions were transferred to pre-chilled 1.5 ml tubes and incubated on ice for 1 hour. Cells were then diluted to 1.5 ml with 0.1% BSA/PBS, centrifuged (900 *g*, 10 minutes) and thoroughly drained. Cells were then resuspended in 50 μl of goat-anti-mouse Ig-Alexa 488 (diluted to 2 μg/ml in 1% BSA/PBS) and incubated in the dark, on ice, for 1 hour. Cells were subsequently washed twice with PBS, resuspended in 1% PF/PBS and examined by confocal microscopy. Cells were excited at 488 nm and fluorescence collected using an emission window set at 500-540 nm. All signals collected were adjusted to remain within the linear range of the detectors.

4.2.2.7 Determining if pDMAEMA Causes Rupture of Endosomes or Lysosomes

Similar to studies conducted with PAAAs (Chapter 3), a variety of assays were conducted to determine if pDMAEMA disrupted endosomes and/or lysosomes and released their contents to the cytosol. Initially, calcein was simultaneously loaded with pDMAEMA into cells to determine if pDMAEMA induced calcein release from endosomes. Other polymers, such as PAAAs (section 3.2.2.2), have the ability to release molecules from endosomes into the cytosol. pDMAEMA (at 1-2 μg/ml) was co-loaded into cells with calcein as described for PAAAs in section 3.2.2.2. Immunofluorescence assays were then used to examine the morphology and distribution of both early and late endosomes and lysosomes following uptake of pDMAEMA by constitutive endocytosis. Anti-EEA1 and anti-Lamp-1 antibodies were used to visualize early endosomes and late endosomes/lysosomes, respectively. Immunofluorescence assays were conducted as previously described in section 3.2.2.6. Globular regions of fluorescence were measured and scored as before (see section 3.2.2.6). For each

treatment, 50 randomly chosen cells were analysed. To further test the effects of pDMAEMA on lysosomes, cells were stained with the fluorescent acidotropic probes acridine orange and LysoTracker Yellow. This was done as described in section 3.2.2.7, except in these experiments cells were only incubated for 1 hour (as opposed to 4 hours). For each treatment, 50 randomly chosen cells that had been stained with LysoTracker Yellow were analysed.

4.3 Results

4.3.1 Effects of pDMAEMA on U937 Cells

Cell viability was initially tested following exposure of cells to 1 or 2 μg/ml pDMAEMA for 15, 30 and 60 minutes. Non-viable cells were detected by staining with PI. Poniris (2001) previously showed that 80-90% of cells exposed to 10-100 μg/ml pDMAEMA for 15 minutes died. Likewise, substantial cell death was apparent following exposure of cells to 5 μg/ml polymer for 15 minutes (data not shown). At lower concentrations of pDMAEMA (e.g. 1 or 2 μg/ml), the extent of cell death was significantly less. However, 1-2 μg/ml pDMAEMA induced a time-dependent increase in cell death (Figures 4.4 and 4.5). Under these conditions, pDMAEMA caused the appearance of a population of cells that stained with PI to an intermediate level (Figure 4.5, indicated by the rectangle). This population most likely represents cells with 'leaky membranes'- a characteristic that is often associated with cells undergoing apoptosis.

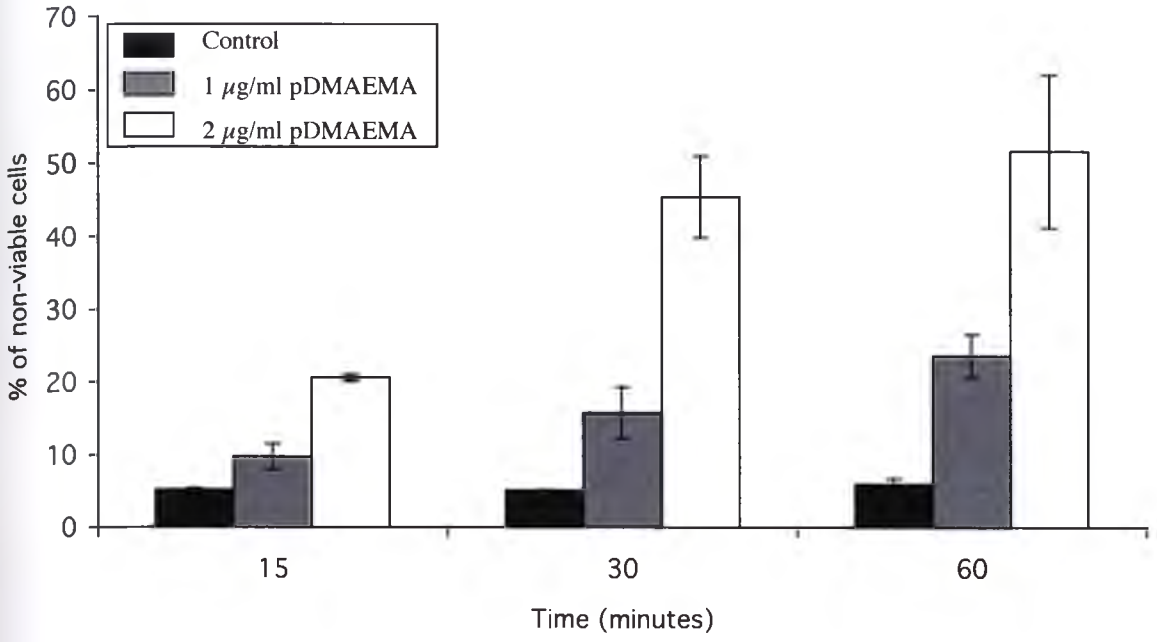

Figure 4.4: Bar graph showing the percentage of non-viable U937 cells, as a function of time, during exposure to 1 μg/ml or 2 μg/ml of pDMAEMA. Each data point represents the mean value from three independent experiments. Error bars represent the standard error of the mean in each case.

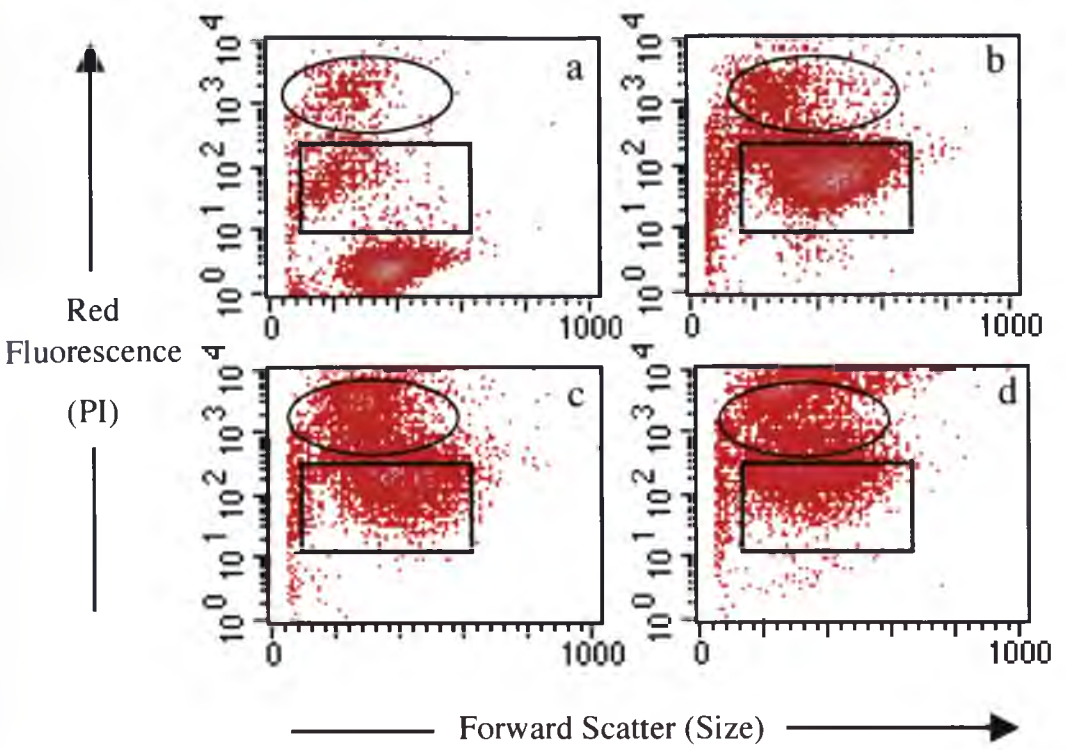

Figure 4.5: Flow cytometry density plots of (a) untreated U937 cells and U937 cells exposed to 2 μg/ml pDMAEMA for (b) 15, (c) 30 and (d) 60 minutes. The elipses indicate dead cells and the rectangles indicate cells with 'leaky' membranes. The results shown are representative of 4 independent experiments.

Cells were exposed to b-pDMAEMA/AEMA and stained with anti-EEA1 to confirm that pDMAEMA is internalised by endocytosis. Cells were exposed to 1 or 2 μg/ml b-pDMAEMA/AEMA for 30 minutes and then stained with anti-EEA1 antibody and Alexa 488-conjugated goat anti-mouse Ig; b-pDMAEMA/AEMA was detected using streptavidin-Alexa 546. Confocal microscopy showed that the polymer was largely at the periphery of the cell. In approximately 40% of cells there was co-localization of the fluorescences associated with b-pDMAEMA/AEMA and early endosomes (Figure 4.6). Approximately 200 cells were analysed in these experiments.

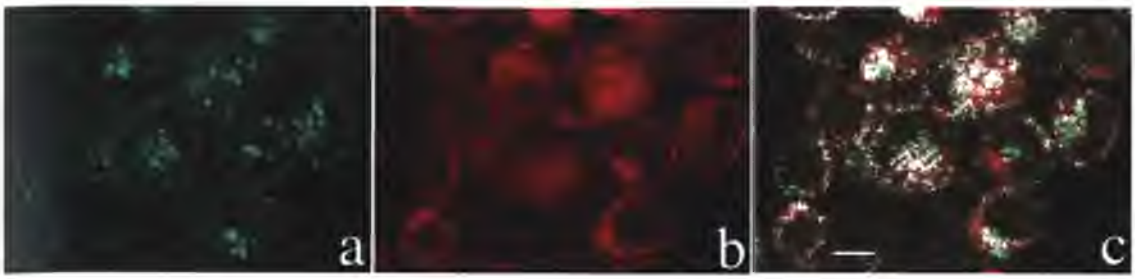

Figure 4.6: Confocal microscopy images of U937 cells exposed to 2 μg/ml b-pDMAEMA/AEMA for 30 minutes. Images show cells stained with (a) anti-EEA1 antibody only (green fluorescence), (b) streptavidin-Alexa 546, and (c) an overlay of the two fluorescence images. In most cells, vesicles show partial co-localisation of green and red fluorescence (white). This result is representative of two independent experiments. 200 cells were scanned to ensure reproducibility. Bar = 10 μm.

The percentage of non-viable cells was reduced considerably when cytotoxic assays were performed at 4°C compared to 37°C. Approximately 50% of cells were non-viable following exposure to 1 μg/ml pDMAEMA for 1 hour at 37°C. In comparison, only 20% of cells were non-viable following exposure to 1 μg/ml pDMAEMA for 1 hour at 4°C (Figure 4.7). Similar results were observed following exposure of cells to 2 μg/ml pDMAEMA (results not shown).

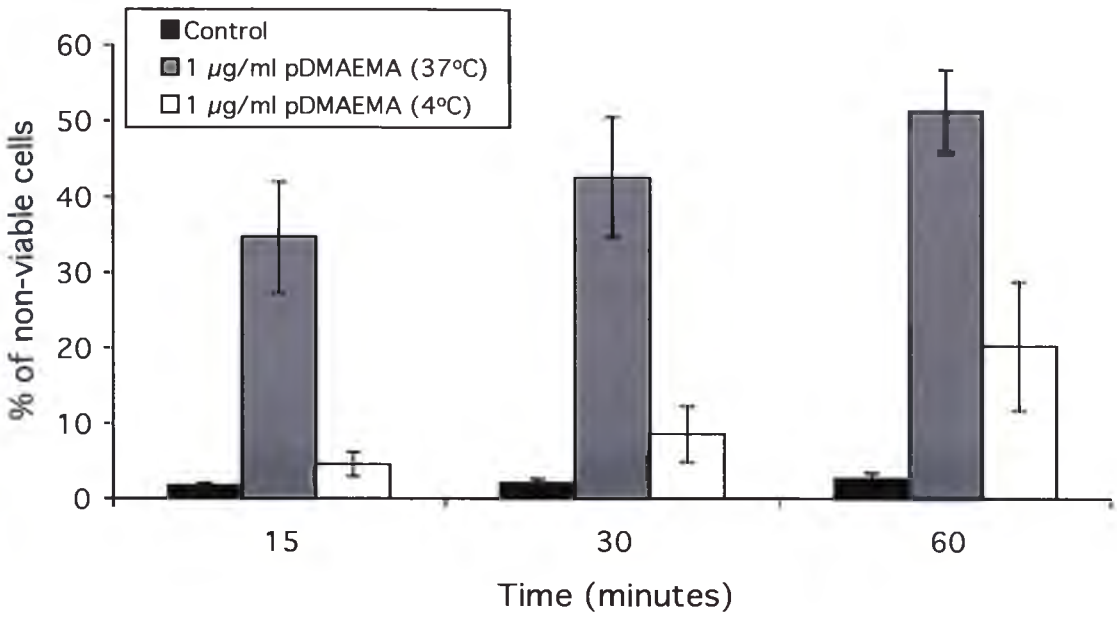

Figure 4.7: Bar graph showing the percentage of non-viable U937 cells, as a function of time, during exposure to 1 μg/ml of pDMAEMA. Parallel experiments were conducted at 37 C (grey bars) and 4 C (white bars). Each data point represents the mean value from three independent experiments. Error bars represent the standard error of the mean in each case.

To determine if death was via apoptosis, measurements of mitochondrial depolarisation, phosphatidylserine exposure, caspase activation and mitochondrial release of cytochrome c were made. Mitochondrial depolarisation was detected by staining control and polymer-exposed cells with $DiOC_6(3)$. Time course experiments were conducted over 60 minutes. Approximately 10% of cells had depolarised mitochondria following exposure of cells to either 1 μg/ml or 2 μg/ml pDMAEMA for 15 minutes. At 60 minutes, this increased to approximately 20% for cells treated with 1 μg/ml pDMAEMA and to 30% in cells treated with 2 μg/ml pDMAEMA (Figure 4.8). Non-viable cells were excluded from all analyses.

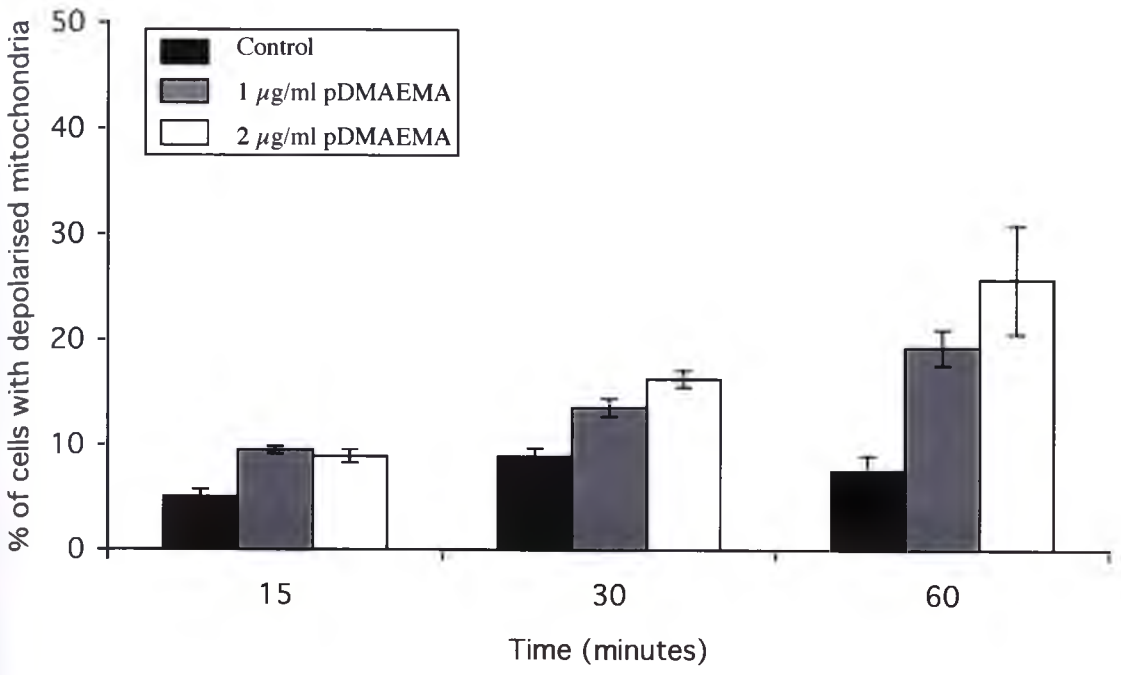

Figure 4.8: The percentage of U937 cells with depolarised mitochondria, as a function of time, during a 60 minute exposure to pDMAEMA. Cells were either left untreated (black bars), or exposed to 1 μg/ml (grey bars) or 2 μg/ml pDMAEMA (white bars) for 15 to 60 minutes. Mitochondrial depolarisation was measured as described in section 4.2.2.4. Each data point represents the mean value from three independent experiments. Error bars represent the standard error of the mean in each case.

Exposure of cells to pDMAEMA also resulted in PS exposure. Following 15 minutes exposure to 1 μg/ml of pDMAEMA, approximately 25% of cells had surface-exposed PS. Approximately 60% of cells had surface-exposed PS following a 60 minute exposure to 2 μg/ml pDMAEMA. The proportion of cells with surface-exposed PS was significantly different between treatments at all time points ($p<0.001$ $F_{14} = 447.55$, pairwise Tukey-Kramer comparisons), however, the differences over time for any one treatment were not significant (Figure 4.9). Non-viable cells were excluded from all analyses.

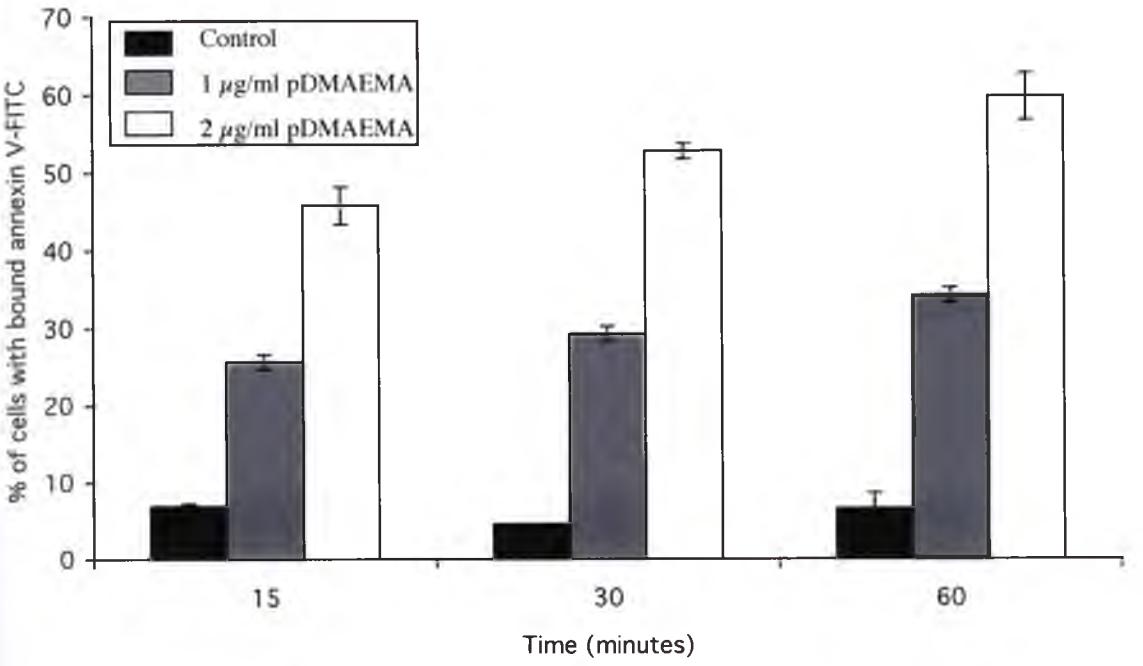

Figure 4.9: Bar graph showing the percentage of cells with surface-exposed PS, as a function of time, following a 15 to 60 minute exposure to either 1 μg/ml or 2 μg/ml pDMAEMA. Each data point represents the mean value from three independent experiments. Error bars represent the standard error of the mean in each case.

Caspase activation was also assayed following the exposure of U937 cells to pDMAEMA but none was detected (Figure 4.10). Caspase activation was detected in U937 cells induced to undergo apoptosis by exposure to TNFα and cycloheximide (Figure 4.10, inset panel A).

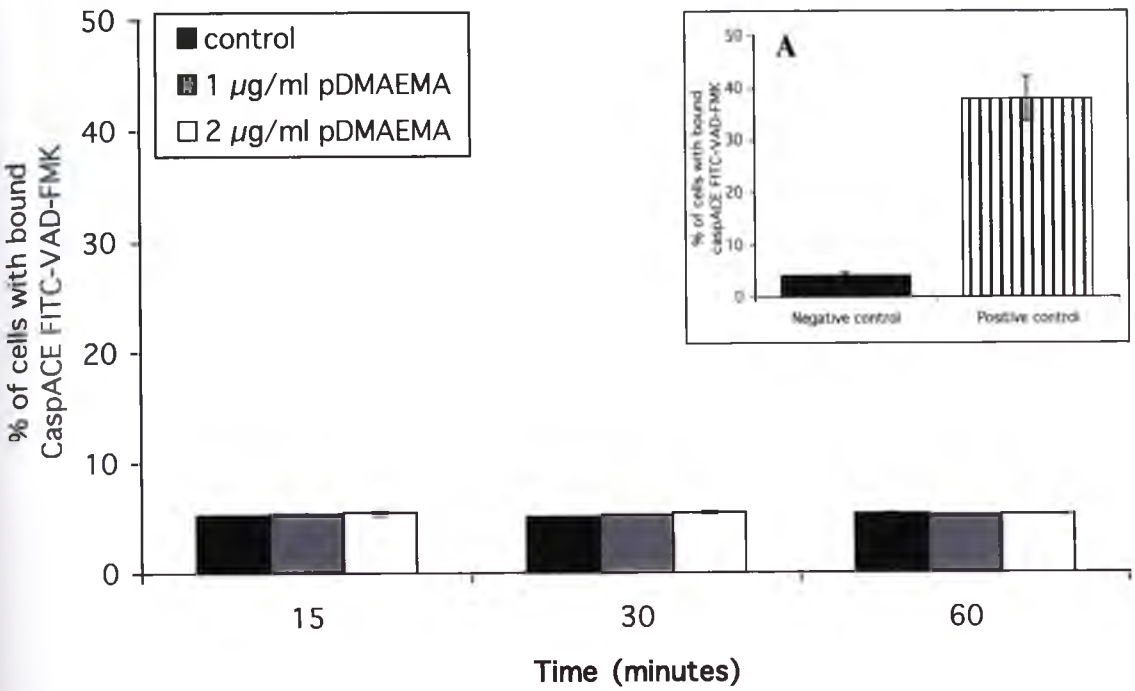

Figure 4.10: Bar graph showing the percentage of cells with bound CaspACE FITC-VAD-FMK, as a function of time, following a 15 to 60 minute exposure to 1 μg/ml or 2 μg/ml pDMAEMA. Panel A: Positive Control; U937 cells exposed to 10 ng/ml TNFα and 10 μg/ml cycloheximide for 4 hours. Each data point represents the mean value from three independent experiments. Error bars represent the standard errors of the mean in each case.

Cytochrome c was not released from mitochondria following exposure of cells to 1-2 μg/ml pDMAEMA for 30 minutes. Immunofluorescence staining of cytochrome c in untreated control cells showed a punctate distribution typical of mitochondrial localisation (Figure 4.11, panel a). A similar pattern of immunofluorescence to that of control cells was observed in cells treated with either 1 μg/ml or 2 μg/ml pDMAEMA (Figure 4.11, panels b and c). Diffuse cytosolic fluorescence was not observed in cells exposed to pDMAEMA. However, a diffuse cytosolic fluorescence was observed when cells were induced to undergo apoptosis by exposure to 10 ng/ml TNFα and 10 μg/ml cycloheximide (Figure 4.11, panel d).

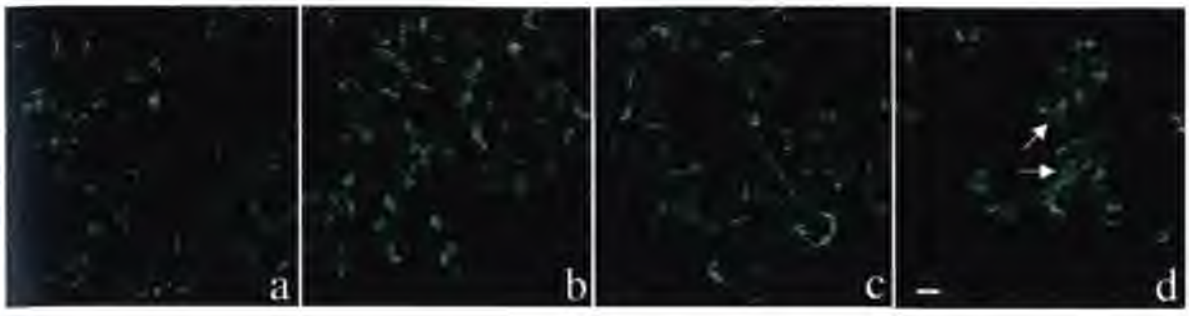

Figure 4.11: Immunofluorescence images obtained by confocal microscopy of U937 cells stained with anti-cytochrome c antibody. A similar punctate pattern of fluorescence was detected in both untreated control cells (a) and cells exposed for 30 minutes to either 1 μg/ml (b) or 2 μg/ml (c) pDMAEMA. However, in some cells exposed to 10 ng/ml TNFα and 10 μg/ml cycloheximide for 4 hours (positive control; d), fluorescence was more diffuse (arrows). These images are representative of cells analysed from two independent experiments. Bar = 5 μm.

Finally, light microscopy was used to examine cells for pDMAEMA-induced changes in the morphology of the cell membrane. Significant membrane blebbing occurs in apoptotic U937 cells (e.g. following exposure to TNFα and cycloheximide). Membrane blebbing was not observed following exposure to pDMAEMA (results not shown).

4.3.2 Characterisation of the Morphology and Distribution of Intracellular Vesicles Following Exposure of Cells to pDMAEMA

A final series of assays, similar to those described in chapter 3, were completed to determine if endocytosed pDMAEMA disrupts endosomes or lysosomes. Following exposure to pDMAEMA, U937 cells were assayed by confocal microscopy for the release of calcein (a small tracer molecule) from endosomes to the cytosol. U937 cells were incubated for 30 minutes in medium containing 2 mg/ml calcein with or without

the addition of 1-2 μg/ml pDMAEMA and subsequently assayed. In both control and polymer-treated cells, fluorescence was in punctate regions around the periphery of the cell (Figure 4.12A). This suggests that pDMAEMA did not induce release of calcein from intracellular vesicles. Results were also quantified by measuring the cytosolic calcein fluorescence of many cells from each treatment (see section 4.2.2.7). There was no significant difference in cytosolic calcein fluorescence of the control and polymer-treated cells ($p>0.7154$ $F_{2,57}=0.3369$, pairwise Tukey-Kramer comparisons). In all treatments, the cytosolic calcein fluorescence was less than 10 arbitrary units (Figure 4.12B). Similar results were obtained when Jurkat cells were used (results not shown). Cytosolic calcein fluorescence of cells treated similarly with PAAAs (discussed in chapter 3) was 4-10 times greater than control cells (section 3.3.3). The level of cytosolic calcein fluorescence for the control cells was similar for these experiments and those described in section 3.3.3.

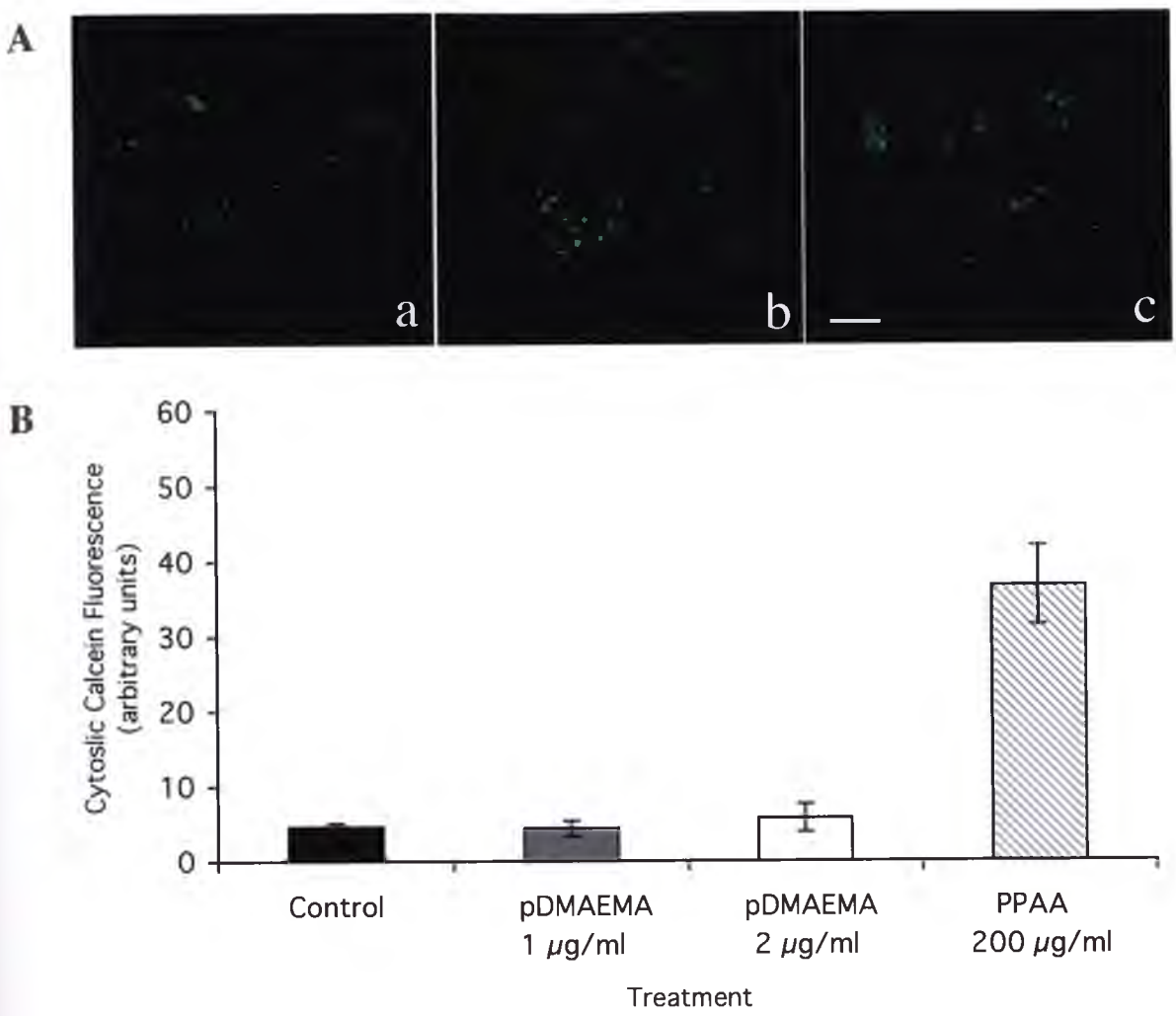

Figure 4.12: **A** Confocal images of U937 cells incubated for 30 minutes in medium containing 2 mg/ml calcein and 1 μg/ml or 2 μg/ml pDMAEMA. Panel a represents control cells (i.e. incubated in the absence of pDMAEMA) and panels b and c represent cells exposed to 1 μg/ml or 2 μg/ml pDMAEMA, respectively. Images are representative of three independent experiments. Bar = 10 μm. **B** Bar graph comparing cytosolic calcein fluorescence of U937 cells exposed for 30 minutes to 1-2 μg/ml pDMAEMA or 200 μg/ml PPAA. Quantitative image analyses were performed as described in section 3.3.3. Data points represent means of values determined for 15-20 cells and error bars shown are standard errors of the mean in each case.

Immunofluorescence assays were conducted to determine the morphology of endosomes and lysosomes following a 30 minute exposure of cells to pDMAEMA.

Anti-EEA1 and anti-Lamp-1 antibodies were used to stain early endosomes and late endosomes/lysosomes, respectively. Following staining with anti-EEA1 antibody, fluorescence within both control and polymer-treated cells was in punctate regions. Early endosomes appeared as roughly circular, bright fluorescent patches distributed mainly at the cell periphery (Figure 4.13). The pattern of fluorescence suggests that the morphology and distribution of early endosomes was not affected by exposure of cells to pDMAEMA.

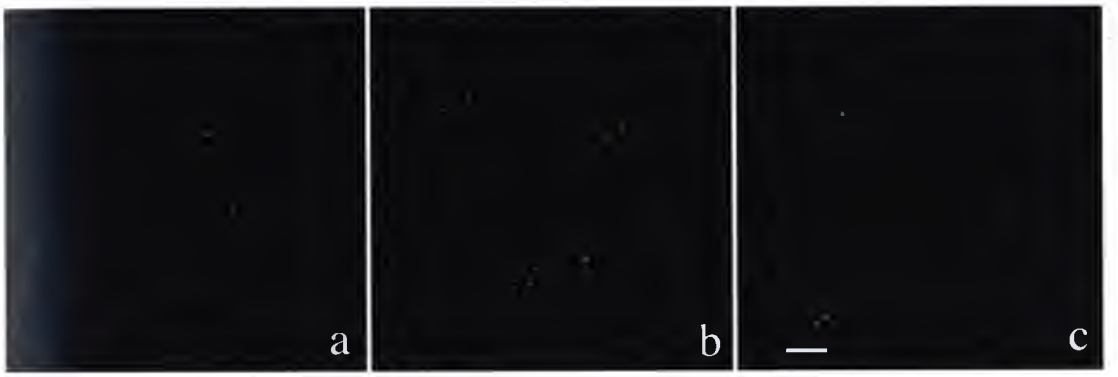

Figure 4.13: Confocal microscopy images showing U937 cells stained with anti-EEA1 antibody following exposure to pDMAEMA. Cells were incubated for 30 minutes with (a) no additions, or 1 μg/ml (b) or 2 μg/ml (c) pDMAEMA. Images are representative of two independent experiments. Bar = 5 μm.

The pattern of Lamp-1 immunofluorescence in untreated control cells was different from that of cells exposed to pDMAEMA. Untreated control cells stained with anti-Lamp-1 antibody showed large globular regions of fluorescence (grf), with approximately 40% of these regions being greater than 3 μm in diameter. A similar pattern of fluorescence was evident in some cells following a 30 minute exposure to 1-2 μg/ml pDMAEMA, however the size of the grf was, on average, considerably smaller (Figure 4.14A). In approximately 25-30% of cells exposed to 1-2 μg/ml of pDMAEMA,

grf were not detected. Quantitative analysis (Figure 4.14B) showed a negative correlation between the concentration of pDMAEMA in which cells were incubated and the size of grf. This indicates that the morphology of late endosomes/lysosomes is affected by exposure of cells to pDMAEMA.

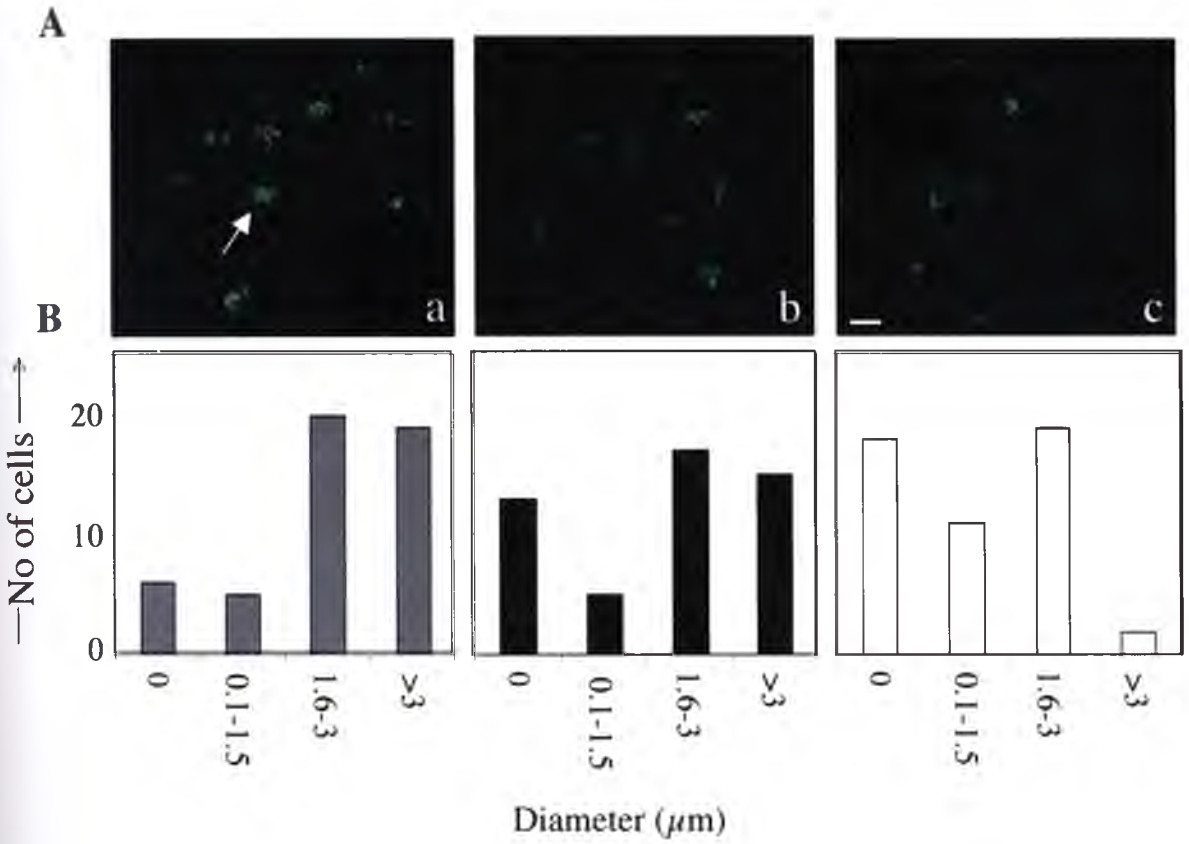

Figure 4.14: **A** Confocal images of U937 cells stained with anti-Lamp-1 antibody following exposure to pDMAEMA. Images shown represent untreated control cells (a), and cells exposed for 30 minutes to 1 μg/ml (b) or 2 μg/ml (c) pDMAEMA. A large globular region of fluorescence (grf) is indicated by the white arrow. These images are representative of three independent experiments. Bar = 5 μm. **B** Histogram plots summarising the results of quantitative image analysis of the diameter of grf of 50 randomly chosen U937 cells treated as in the panel above (see section 3.2.2.7 for more details regarding this analysis).

LysoTracker Yellow and acridine orange were used to further investigate the effects of pDMAEMA on lysosomes. Fluorescence in control cells stained with LysoTracker

Yellow was largely concentrated around the periphery of the cell (Figure 4.15A, panel a). In contrast, following pDMAEMA uptake, cells showed a more diffuse pattern of LysoTracker fluorescence (Figure 4.15A: compare panels b and c), suggesting changes in lysosomal morphology. Image analysis (see section 3.2.2.7) confirmed that pDMAEMA (both at 1 μg/ml and 2 μg/ml) had induced changes in the pattern of LysoTracker Yellow fluorescence (Figure 4.15B). Under the conditions tested, flow cytometric analysis showed that control cells and cells exposed to 1 μg/ml pDMAEMA had similar level of red AO fluorescence (Figure 4.16). Similar results were obtained when cells were exposed to 2 μg/ml pDMAEMA (data not shown). However, in cells exposed to MSDH (a known lysosomal disruptive agent) a population of cells with substantially decreased red AO fluorescence was detected (indicated by the arrow on Figure 4.16). The remaining MSDH-treated cells not in this population had red AO fluorescence slightly lower that that of control or pDMAEMA-treated cells. A substantial decrease in red AO fluorescence indicates lysosomal rupture. Collectively, these results indicate that (1) MSDH caused lysosomal bursting and (2) exposure of cells to pDMAEMA caused changes in lysosomal morphology but did not physically disrupt lysosomes.

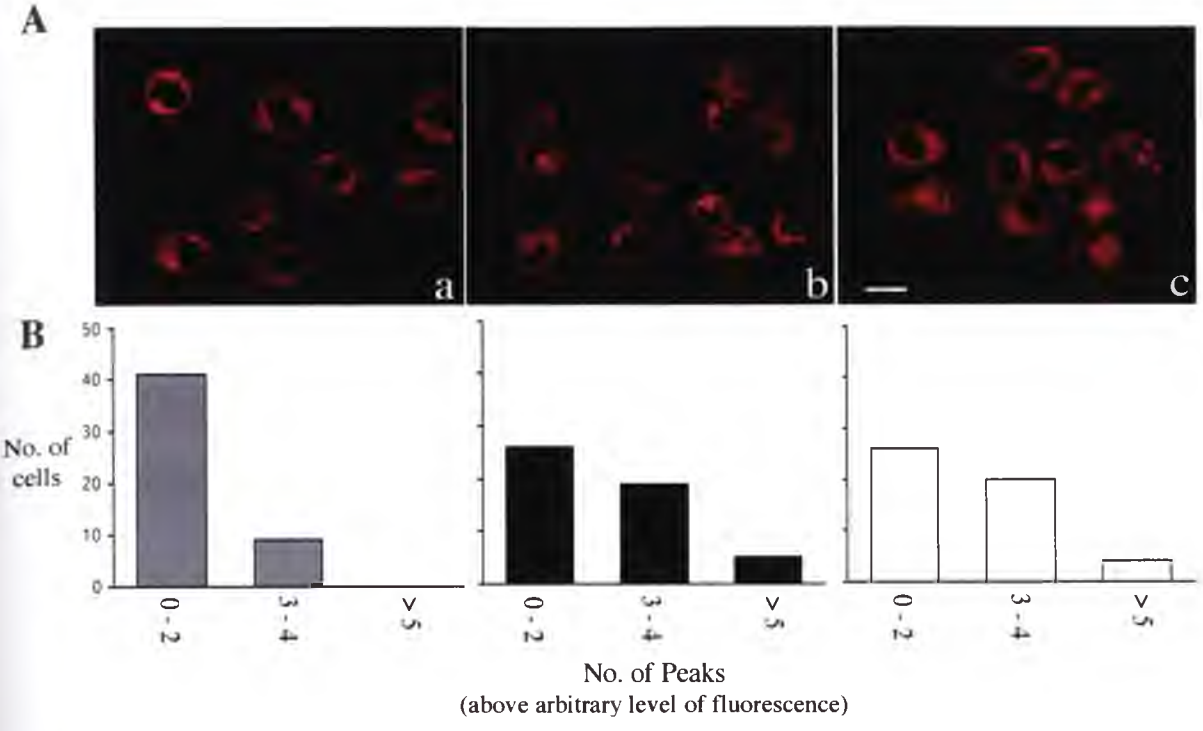

Figure 4.15: **A**: Confocal microscopy images of U937 cells exposed to 1 μg/ml pDMAEMA for 30 minutes and stained with LysoTracker Yellow. See section 4.2.2.7 for details of methods. Images show: (a) control cells (no added polymer) and cells treated with 1 μg/ml or 2 μg/ml pDMAEMA (panels b and c, respectively). The images shown are representative of three independent experiments. Bar = 10 μm. **B**: Each histogram plot summarises the results of quantitative image analysis, performed as described in section 3.2.2.7, for 50 cells treated as in the image above. For the purpose of these analyses, fields of view were selected at random from three independent experiments.

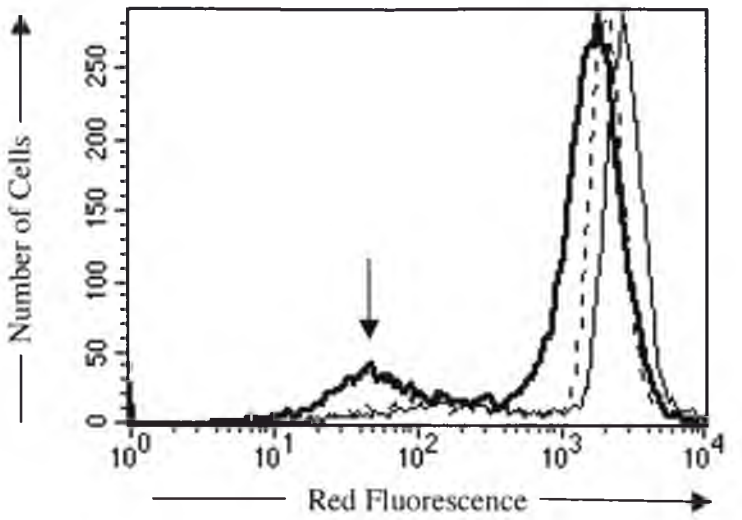

Figure 4.16: Overlay flow cytometry histograms of U937 cells stained with acridine orange following a 30 minute incubation in PB containing no additions (thin solid line) or 1 μg/ml pDMAEMA (dashed line), or after a 4 hour incubation in culture medium containing 70 μM MSDH (thick solid line). In some MSDH-treated cells a substantial decrease in red AO fluorescence was detected (arrow). The results shown are representative of three independent experiments.

4.4 Discussion

In the past few years, pDMAEMA has successfully been used in gene therapy (Foneseca *et al.*, 1999). In these experiments, pDMAEMA was complexed with plasmid DNA to yield polymer/plasmid complexes (polyplexes). OVCAR-3 human ovarian carcinoma and COS-7 cells were then transfected with the polyplexes and the transfection efficiency and cell viability measured (van de Wetering *et al.*, 1999). The most promising results were obtained when low concentrations of polymer, similar to those used in this study, were used. Based on these previous experiments and functional predictions about pDMAEMA, experiments were performed to determine the mechanism of entry of pDMAEMA into cells, the mode of cell death following pDMAEMA internalisation, and finally, the ability of pDMAEMA to disrupt endosomes and release molecules into the cytosol of cells.

Following a 30 minute incubation of cells in 2 μg/ml b-pDMAEMA/AEMA, the biotinylated polymer was detected inside U937 cells primarily at the cell periphery (Figure 4.6). In approximately 40% of the cells, a fraction of the b-pDMAEMA/AEMA co-localised with anti-EEA1 stained vesicles (early endosomes). These results are similar to those from experiments using b-PEAA described in Chapter 3 and suggest that, like PAAAs, pDMAEMA is taken up by endocytosis and transits through early endosomes before moving onto other vesicular compartments (e.g. late endosomes/lysosomes). Endocytic entry of pDMAEMA into cells is also consistent with the effects of temperature on its cytotoxicity. Endocytosis works most efficiently at 37 C and is inhibited at 4 C (Mellman, 1996). Thus, the reduced number of non-viable cells following exposure of cells to pDMAEMA at 4 C compared to 37 C supports the conclusion that entry of pDMAEMA into cells occurs via endocytosis (Figure 4.7).

These results are also supported by Zuidam *et al.* (2000); they showed that internalisation of pDMAEMA-polyplexes was inhibited at 4 C and that internalised pDMAEMA-polyplexes remained contained within what appeared to be endocytic vesicles.

The second aim of this study was to determine the mode of cell death following exposure of cells to pDMAEMA. There was a time-dependent increase in non-viable cells following exposure of cells to either 1 or 2 μg/ml pDMAEMA (Figure 4.4). Cell death did not occur immediately; the cell membranes first became 'leaky' – a characteristic that is often associated with apoptosis (Figure 4.5). The detection of 'leaky cell membranes' following the exposure of cells to pDMAEMA raises the possibility that it may affect cells by directly interacting with cell membranes. The cell surface contains many ion channels that fluctuate between open and closed conformations and that maintain the equilibrium of ions within the cell. The dissipation of ion gradients leads to impairment of essential processes in the cell and finally cell death (Ultee *et al.*, 1999). For example, inappropriate accumulation of Ca^{2+} and Na^{+} ions within rat striatum cells causes abnormalities in energy metabolism by increasing (1) the activity of proteases, lipases and endonucleases, (2) the production of free radicals, and (3) DNA damage that ultimately leads to cell death (McLaughlin *et al*, 1998; Bordelon *et al.*, 1998). Therefore, it is possible that in addition to (or in parallel with) its effects from within the cell following endocytosis, exogenous pDMAEMA may induce cell death by directly interacting with the cell membranes to result in the collapse of ion gradients. Arguing against this possibility is the observation that confocal images of cells incubated with b-pDMAEMA/AEMA do not show a concentration of the polymer

at the cell membrane (Figure 4.6), which would be expected if it were directly exerting its cytotoxic effects at this site.

A series of assays were performed to determine the type of cell death induced by pDMAEMA. Following exposure of cells to pDMAEMA mitochondrial depolarisation (Figure 4.8) and PS exposure (Figure 4.9) were both detected. However, under these same conditions, caspase activation (Figure 4.10), cytochrome c release (Figure 4.11) and changes in cell morphology (data not shown) were not detected. Until recently, mitochondrial depolarisation and PS exposure were both thought to be hallmarks of apoptosis; however, both are now known to sometimes occur during necrosis. For example, mitochondrial depolarisation has been detected in cells induced to undergo necrosis with cyclosporin and trifluoperazine (Lemasters *et al.*, 1999) and PS exposure has been detected in thymocytes (Waring *et al.*, 1999) and mouse leukaemia cells (Bonneau and Poulin, 2000) undergoing death exclusively by necrosis. Therefore, collectively, the results suggest that cell death caused by exposure to pDMAEMA is via necrosis not apoptosis. The fact that cell death was very rapid also supports this conclusion. Following a 60 minute exposure to 2 μg/ml of pDMAEMA, approximately 50% of cells were non-viable (Figure 4.4). Apoptosis generally takes hours and in some cell systems it may take days; necrosis is generally much faster.

Lastly, experiments were performed to determine the ability of internalised pDMAEMA to disrupt endosomes, in particular lysosomes. If pDMAEMA disrupts endosomes it is possible that it could be used as a delivery agent in a novel cancer therapeutic (see section 1.0). The ability of pDMAEMA to disrupt endosomes and release a small membrane-impermeable fluor (calcein) into the cytosol of cells was investigated. When

U937 cells were incubated in buffer containing calcein and pDMAEMA, they showed fluorescent intracellular vesicles (Figure 4.12). This pattern of fluorescence did not change over 60 minutes, suggesting that calcein was not released into the cytosol. Other characteristics associated with calcein release, such as vesicle fusion (Jones *et al.*, 2003; Linhardt and Tirrell 1999), were also not observed. Similar results were obtained with Jurkat cells (data not shown). The results shown in this chapter suggest that pDMAEMA does not have the ability to disrupt endosomes and release small tracer molecules into the cytosol.

The morphology of early/late endosomes and lysosomes following exposure of cells to pDMAEMA was also investigated. It is possible that pDMAEMA may change the morphology of vesicles without physically disrupting their membranes. Similar to PAAAs (Chapter 3), there was no measurable effect of exposing cells to pDMAEMA on the pattern of EEA1 immunofluorescence, suggesting that early endosomes were unaffected (Figure 4.13). In contrast, Lamp-1 immunofluorescence was significantly affected following the exposure of cells to pDMAEMA. Lamp-1 proteins are primarily located on the surface of late endosomes and lysosomes. Results shown in Figure 4.14 suggest that pDMAEMA caused morphological changes to one or both of these compartments. To further characterize the compartment affected following exposure to pDMAEMA, cells were stained with LysoTracker Yellow and AO. Changes in the pattern of LysoTracker Yellow staining were observed following the exposure of cells to pDMAEMA, suggesting that pDMAEMA caused changes in lysosomal morphology (Figure 4.15). However, flow cytometric analysis of cells stained with acridine orange indicated that lysosomes remained structurally intact (Figure 4.16). Therefore, the results suggest that exposure of cells to pDMAEMA changes the morphology of late

endosomes or lysosomes but does not physically disrupt them. This latter result is supported by Zuidam *et al.* (2000); they showed that a large percentage of polyplexes (pDMAEMA bound to DNA) were retained within endosomes following a 24 hour post-transfection incubation.

Results presented in chapter 3 showed that the uptake of PAAAs by constitutive endocytosis disrupted late endosomes in a pH-dependent fashion and released both small and large molecules into the cytosol. Results presented in this chapter demonstrate that exposure of cells to pDMAEMA induced changes in the morphology of endosomes/lysosomes but did not disrupt them. The exposure of cells to pDMAEMA resulted in rapid necrotic death. In contrast, cell viability was maintained following the uptake of PAAAs. The most appropriate polymer to use as a delivery agent for a proposed cancer therapeutic (see section 1.10) must have the ability to disrupt endosomes and release their contents into the cytosol. Results presented in this chapter indicate that pDMAEMA lacks this ability. In addition, the very high toxicity of pDMAEMA could pose a significant risk of bystander cell damage in cancer therapies. Collectively, these results indicate that, of the polymers tested, PAAAs appear to be the best suited to deliver molecules into the cell cytosol.

Chapter 5

Synthesis and Functional Assays of PAAA-X-Bad(140-165) Conjugates

5.1 Introduction

Chapters 3 and 4 describe the effects of two different polymers (PAAA and pDMAEMA) on cells. A variety of assays were performed to determine if these polymers disrupted endosomes/lysosomes and induced apoptosis, and if they might be used as part of a novel cancer therapeutic (see section 1.10). Many morphological and biochemical changes were evident following uptake of PAAAs and pDMAEMA. However, the results obtained suggest that, of the polymers tested, PAAAs are the most suitable to be used as endosomal disruptive agents.

As previously described in chapter 1, the proposed novel cancer therapeutic is comprised of a synthetic polymer conjugated to both a targeting ligand and, via a pH-sensitive linker, to a pro-apoptotic peptide. For several years now, synthetic polymers have been conjugated to anti-tumour agents using a variety of linking mechanisms (Kratz *et al.*, 1999). The linkers that show the greatest potential for *in vivo* cancer therapy are those that are stable in plasma and only cleave within tumours to release the anti-tumour agent. The most promising linkers recently used are pH-sensitive. These linkers are stable at physiological pH (i.e. pH 7.4) but trigger the release of the anti-cancer drug at acidic pH, such as that found in late endosomes and lysosomes (Duncan *et al.*, 1996). Synthesis of such linkers has been slow because the chemistry involved is complicated. More recently, carboxcyclic-hydrazide pH-sensitive linkers have been developed. These linkers are stable at pH 7.4 but not at lower pH values. The chemistry involved in the synthesis of these linkers is considerably simpler than that required for other linkers. Synthesis of a carboxcyclic-hydrazide linker and experiments involving its conjugation to PEAA and PPAA are described in this chapter. Conjugation of the

carboxcyclic-hydrazide linker involves a chemical reaction between the amine group on the linker and a carboxyl group on the polymer.

This chapter also describes a series of assays that were performed to:

1. Determine the percentage of derivatized carboxyls on the polymer (i.e. the number of linkers attached to the polymer). Collaborators from the University of Washington (USA) have previously conjugated specific anti-tumour agents to PAAAs. They found that derivatization of more than 3-5% of carboxyls on the polymers resulted in loss of polymer function (C. Cheung, 2002, *pers. commun.*).
2. Confirm that derivatized PAAAs retained their ability to disrupt endosomes in a pH-dependent manner. One of the greatest risks involved in conjugating molecules to pH-sensitive polymers is the potential loss of function of the polymers. Loss of polymer function would result in the construct being retained within acidic endosomes, risking degradation of the pro-apoptotic peptide by endosomal/ lysosomal proteases.
3. Determine the stability of the carboxcyclic-hydrazide bond joining the linker to the polymer. This bond must be stable at physiological pH to ensure that Bad(140-165) is only released once inside the targeted cancer cells, thereby reducing bystander cell damage.

The final section of this chapter describes (1) the conjugation of Bad(140-165) to PEAA/PPAA via the carboxcyclic-hydrazide linker, and (2) the effects that PEAA/PPAA-linker-Bad(140-165) constructs (PAAA-X-Bad(140-165)) have on cells following uptake by constitutive endocytosis. Assays similar to those described in

chapters 3 and 4 were conducted to determine the morphological and biochemical effects on cells of the uptake of PAAA-X-Bad(140-165) constructs. Based on the results in chapter 3, we predicted that internalisation of PAAA-X-Bad(140-165) would disrupt the morphology of endosomes and release Bad(140-165), which would in turn induce apoptosis. Pro-apoptotic peptides, including Bad(104-182), Bak(82-94) and Bad(140-165)) have previously been shown to bind to Bcl-X_L (an anti-apoptotic protein) and in turn elicit characteristic features of apoptosis, both in isolated mitochondria (Narita *et al.*, 1998) and in intact cells (Kelekar *et al.*, 1997).

5.2 Materials and Methods

5.2.1 Materials

4-aminobenzoic acid, dichloromethane, isobutyl chloroformate, *tert*-butyl carbazate, triethylamine, maleic anhydride, trifluoroacetic acid (TFA), acetronitrile, fluorescamine, sodium phosphate, boric acid and ethylenediamine tetraacetic acid (EDTA) were from Sigma/Aldrich (MO, USA). Hexane and acetone were from Crown Scientific (Sydney, Australia). Anhydrous acetone was from Merck (NJ, USA). Silica gel 60 F_{254} pre-coated aluminium plates (0.2 mm thickness; used for analytical thin layer chromatography) and Silica gel 60 (230-400 mesh; used for flash chromatography) were also from Merck. Methanol, anhydrous sodium acetate, acetic anhydride, HCl and magnesium sulfoxide were from Ajax chemicals (Sydney, Australia). 5-((2-(and-3)-S-(acetylmercapto)succinoyl)amino)fluorescein (SAMSA fluorescein) was from Molecular Probes (OR, USA). Biotin-X-NHS was from Calbiochem (CA, USA). Bad(140-165) was synthesised at the University of Notre Dame (USA) and was provided as a gift from Professor Martin Tenniswood. Bad(140-165) was synthesised with three additions at the C-terminus; firstly, a cathepsin cleavage sequence (Leu Ile Val Arg Tyr Thr Arg), then a triple glycine spacer (Gly Gly Gly) and finally, at the extreme C-terminus, a cysteine residue. This modified peptide is subsequently referred to simply as Bad(140-165). Two strategies were adopted to favour intra-endosomal/lysosomal release of Bad(140-165); the cathepsin cleavage site was one, the acid-labile hydrazide linkers was the second.

5.2.2 Methods

5.2.2.1 Synthesis of Hydrazide Cross Linker

The hydrazide cross linker was synthesised according to Lau *et al.* (1995a, b). 4-aminobenzoic acid (20 g) was suspended in 120 ml of anhydrous acetone. Distilled methanol (20 ml) was then added drop-wise and the suspension was stirred until completely dissolved (Solution A). Solution B was made by adding 40 ml of anhydrous acetone drop-wise to 16.49 g maleic anhydride. Solution B was then added drop-wise to solution A, under nitrogen and stirred at room temperature for 1 hour. The yellow precipitate was then filtered and washed with acetone and vacuum dried. Anhydrous sodium acetate (3.4 g) and 20 g of the yellow precipitate were added together and then treated with 40 ml of acetic anhydride at 50°C for 2 hours. The solution was then evaporated to dryness. Water (500 ml) was added to the solid and stirred at 70°C for 2 hours. Again the solution was filtered off and the precipitate was vacuum dried to yield 4-maleimidobenzoic acid (MBA).

MBA (2.68 g) was suspended in 60 ml of dichloromethane and cooled to 0°C before the addition of 1.89 ml of triethylamine and 1.76 ml of isobutyl chloroformate. The mixture was stirred for 1 hour at 0°C and then 1.26 g of *tert*-butyl carbazate in 10 ml of dichloromethane was added drop-wise. Stirring was continued for 3 hours at room temperature. The reaction mixture was diluted with 150 ml of acetic acid and washed with saturated $NaHCO_3$ (2x50 ml), 0.1 M HCL (2x50 ml), saturated NaCl (2x50 ml), H_2O (50 ml) then dried using $MgSO_4$ and evaporated to give crude protected hydrazide product. The product was purified by flash chromotography, using silica gel 60 (230-400 mesh) and a mixture of solvents: initially 1:2 and then 2:3 Me_2CO:hexane. Thin

layer chromotography (TLC) was then performed on Kieselgel 60 F_{254} pre-coated aluminium plates (0.2 mm) for all samples, using standard techniques. Comparable samples were then pooled, evaporated to produce a solid and analysed by one-dimensional H NMR. A Mercury 300 MHz Fourier Transform spectrometer was used for all NMR analyses. Chemical shifts are reported in parts per million (ppm).

Protected hydrazide (Fraction 3; 500 mg) was dissolved in 5 ml of ice-cold TFA and stirred for 30 minutes in an ice bath. The TFA was then removed under vacuum at room temperature to give the final product. This was again analysed by NMR. Figure 5.1 schematically depicts the chemical reactions and the synthesis of the intermediates and final product.

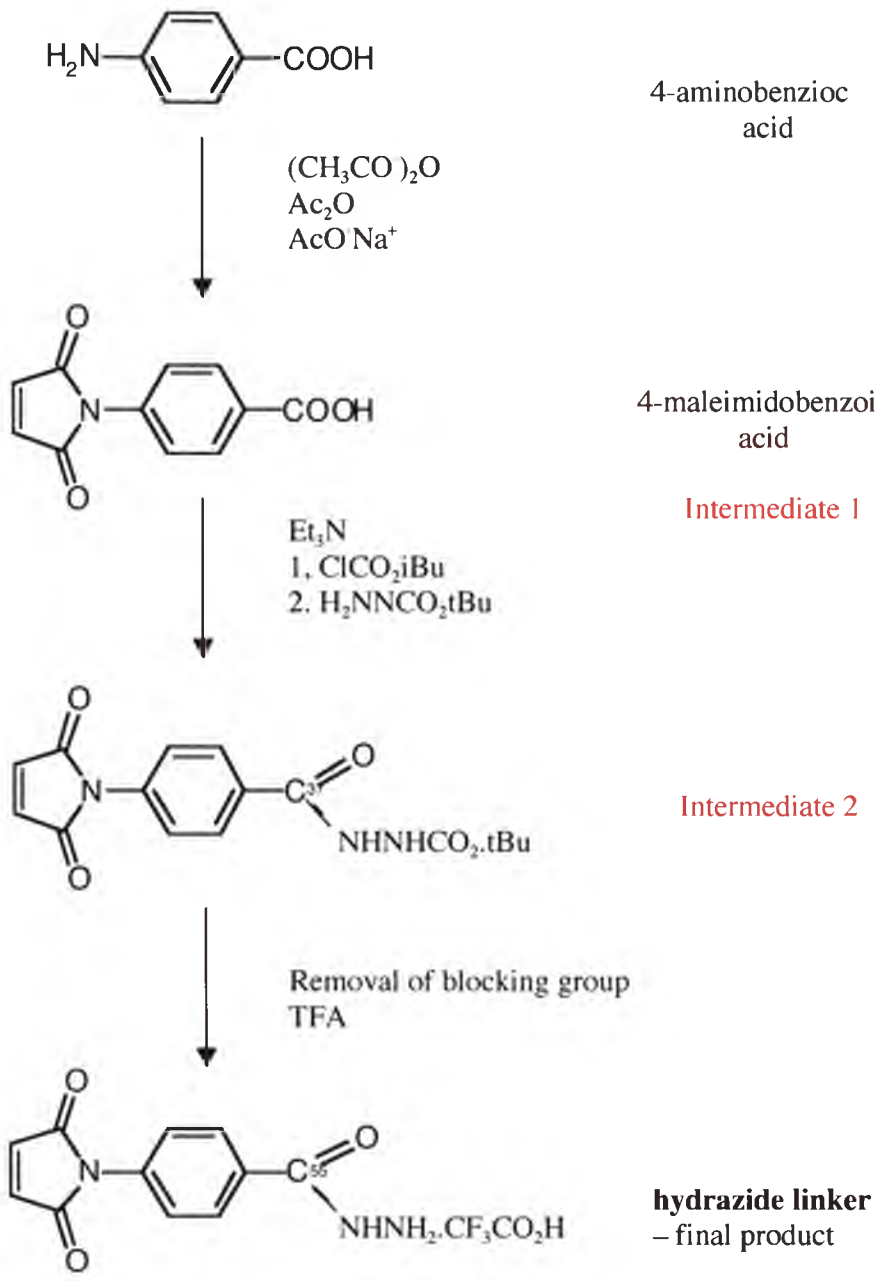

Figure 5.1: Schematic representation of the hydrazide synthesis. The intermediate products are indicated in red.

5.2.2.2 Coupling Polymer and Cross Linker

Previous results suggest that PEAA or PPAA are appropriate polymers to use as endosomal-disruptive agents. Therefore, PEAA and PPAA were conjugated to the hydrazide linker described in 5.2.2.1. Many small-scale experiments were conducted to determine ideal conjugation ratios. This was done to ensure that the ability of the polymer to disrupt membranes in a pH-dependent manner was maintained. The amounts used are summarised in Table 5.1. Once the optimum ratios were determined, the reactions were scaled up.

A basic summary of the conjugation procedure follows. The polymer and the hydrazide linker were dissolved in anhydrous methanol with the addition of TFA and stirred at room temperature, protected from light, for 24 hours. The solution was evaporated under a stream of N_2 gas until a precipitate was formed. The precipitate was resuspended in acetronitrile and allowed to stand at 4°C, protected from light, for a further 24 hours. The precipitate was then centrifuged (800 *g*, 10 minutes), dried under vacuum and analysed by NMR.

Polymer (Molecular weight)	Polymer (mg)	Linker (mg)	Methanol (ml)	TFA (μl)	Acetronitrile (ml)
PEAA (23 kDa)	4.8	10.3	2	0.75	1
PEAA (23 kDa)	5.1	3.8	2	0.75	1
PEAA (23 kDa)	5.0	1.28	2	0.75	1
PPAA (43 kDa)	31.4	2.9	3	1.5	2.5
PEAA (32 kDa)	49.2	3.2	4	2.5	2.5
PEAA (43 kDa)	12.8	2.0	3	1.5	2.5
PPAA (105 kDa)	8.6	2.6	3	1.5	2.5

Table 5.1: Quantities of starting materials used in the small-scale conjugation reactions between PAAAs (PPAA and PEAA, various molecular weights) and hydrazide linker (synthesised as described in section 5.2.2.1).

5.2.2.3 Determining the Number of Hydrazide Linkers Attached to PAAAs Using SAMSA Fluorescein

The number of hydrazide linkers attached to PEAA or PPAA was calculated using SAMSA fluorescein. Activated SAMSA fluorescein reacts with the free malemide group on the linker. The degree of labelling was determined from the absorbance at 495 nm. SAMSA fluorescein was activated by removal of the acetyl-protecting group. This was achieved by dissolving 10 mg of SAMSA in 1 ml of 0.1 M NaOH and incubating the mixture at room temperature for 15 minutes. Following activation, the solution was neutralised with 14 µl of 6 M HCl and buffered with the addition of 0.2 ml of 0.5 M sodium phosphate, pH 7.

To determine the number of derivatized carboxyl groups on the PAAAs, a 200X molar excess of activated SAMSA fluorescein was added to the polymer-linker mixture (200 µg/ml polymer-linker in sodium phosphate buffer containing 0.05 M EDTA). This was

then incubated at room temperature on an orbital shaker for approximately 2 hours to allow conjugation to take place. Samples were then dialysed overnight in the dark against 0.5 M phosphate buffer to remove unbound SAMSA fluorescein. Following dialysis, the degree of labelling was determined from the absorbance of the labelled polymer at 495 nm. The extinction co-efficient of SAMSA fluorescein is approximately 80,000 $cm^{-1}M^{-1}$ at 495 nm (Molecular Probes, OR, USA).

5.2.2.4 Determining if the pH-Dependent Lytic Ability of PAAAs is Retained Following Conjugation with Hydrazide Linker

Following conjugation of the hydrazide linker to PEAA and PPAA, the ability of PEAA-X and PPAA-X to disrupt membranes in a pH-dependent manner was tested by conducting whole cell experiments (as described in section 3.2.2.5). Maintaining this function was crucial (see introduction for more details). Derivatized polymer and control samples (underivatized polymer) were compared in the same assays.

5.2.2.5 Determining the Stability of the Carboxcyclic-Hydrazide Bond Joining the Linker to the Polymer

It was expected that the polymer-linker construct (PAAA-X) would be stable at physiological pH but that the hydrazide bond within the linker would cleave at mildly acidic pH. The stability of PAAA-X was determined using fluorescamine. Fluorescamine is a non-fluorescent molecule that reacts with primary amines to form fluorescent products. The spontaneous cleavage of the hydrazide bond that occurs at mildly acidic pH results in the formation of two primary amine groups. Thus, fluorescamine can be used to measure the extent of hydrazide linker cleavage.

A stock solution of fluorescamine was made (15 mg / 50 ml acetone). PAAA-X was added to 1 ml of 0.2 M phosphate buffer to give a final concentration of 200 μg/ml (from a 6.5 mg/ml stock in 0.1 M NaOH). The pH was then adjusted to either 5 or 7.4 and the samples incubated on a rocker at room temperature for 48 hours. At 0, 24 and 48 hours, 300 μl was removed from each sample and added to 1200 μl of 0.2 M borate buffer (pH 8.5). This was then vortexed and while vortexing, 500 μl of the stock fluorescamine solution was added. Samples were mixed for 5 minutes and allowed to sit for 1 minute. Several 100 μl aliquots were then placed in a black 96-well plate and read on a Biolumin 960 fluorescence plate reader (Molecular Dynamics, Sydney, Australia) with an excitation wavelength of 390 nm and an emission wavelength of 475-490 nm. Negative (polymer only) and positive controls (glycine) were also assayed. All samples were assayed in triplicate.

5.2.2.6 Conjugating Bad(140-165) Peptide to Polymer-Linker Constructs

Bad(140-165) was conjugated to three derivatized polymers (PEAA 23 kDa, PEAA 32 kDa and PPAA 43 kDa). Conjugation was achieved through the spontaneous reaction of the maleimide group on the linker with the C-terminal thiol group on Bad(140-165). PAAA-X (2 mg) and approximately 1.5 mg of Bad(140-165) were dissolved in 460 μl of DMF (dimethyl formamide) and 40 μl of 100 mM TAPS (N-tris[Hydroxymethyl]methyl-3-aminopropane-sulfonic acid) buffer (pH 8.5). This mixture was then incubated for 3 hours at room temperature under nitrogen. Following this, the sample was dialysed for 48 hours at room temperature against 100 mM TAPS buffer (pH 9.5). Dialysis caused some of the conjugate to precipitate; following dialysis the sample was centrifuged (300 *g*, 5 minutes) to pellet the precipitate. The supernatant (containing PAAA-X-Bad(140-165)) was then stored at –20 C. Conjugation of

Bad(140-165) to PAAA-X was confirmed using fluorescamine (see section 5.2.2.5). Bad(140-165) contains 7 free amine groups; successful conjugation of Bad(140-165) to PAAA-X was confirmed by measuring a significant increase in fluorescamine fluorescence compared to that of PAAA-X alone.

A standard curve plotting fluorescamine fluorescence verses the concentration of free amine groups was produced using methylamine. This was the used to calculate the number of Bad(140-165) molecules attached to each of the PAAA-X-Bad(140-165) conjugates.

5.2.2.7 Functional Assays of PAAA-X-Bad(140-165) Constructs

PAAA-X-Bad(140-165) constructs were introduced into U937 cells via constitutive endocytosis. Subsequently, a series of assays were conducted to determine the effects on cells of the uptake of the constructs.

U937 cells ($1x10^6$) were centrifuged at 300 *g* for 5 minutes. Cells were drained thoroughly and resuspended in 1 ml of DMEM:F12 containing 200 μg/ml of PAAA-X-Bad(140-165). Following a 30 minute incubation at 37°C, cells were washed with DMEM:F12 and resuspended in 2 ml of complete medium. Cells were then transferred to a 6-well plate and incubated for a further 4 hours at 37°C. Following this incubation, 4 ml of complete medium was added to each of the cell cultures, which were then incubated for up to 72 hours at 37°C. Cytotoxicity assays were performed (as described in section 3.2.2.1) at 24, 48 and 72 hours.

To determine if PEAA/PPAA-X-Bad(140-165) were internalised and co-localised with early endosomes, immunofluorescence assays were performed. PAAA-X-Bad(140-165) was firstly labelled with biotin. A stock solution of biotinylation reagent (biotin-X-NHS) (40 mg/ml in DMSO) was initially made. 0.25 mg of the stock biotin reagent was added to 1 ml of sodium carbonate buffer (pH 8.5) containing 3 mg of PAAA-X-Bad(140-165). This was then incubated on a rocker for 2 hours at room temperature. Biotinylated PAAA-X-Bad(140-165) (PAAA-X-Bad(140-165)-biotin) was dialysed against PBS for 24 hours and then introduced into U937 cells as described in section 3.2.2.3. Cells were fixed, permeabilised and stained with anti-EEA1 antibody and goat-anti-mouse Ig-Alexa 488 (as described in 3.2.2.6). Cells were also stained with steptavidin-Alexa 546 (as described in 3.2.2.2). Finally, cells were analysed by confocal microscopy (see section 3.2.2.2).

Lastly, experiments similar to those described in section 3.2.2.3 were performed to determine if PAAA-X-Bad(140-165) constructs disrupted endosomes and released their contents into the cytosol. U937 cells were incubated for 30 minutes in PB containing 2 mg/ml of calcein and 200 μg/ml of PAAA-X-Bad(140-165). Cells were analysed 2 and 4 hours after incubation with PAAA-X-Bad(140-165).

5.3 Results

5.3.1 Synthesis of the Hydrazide Linker

Synthesis of the hydrazide linker involved the synthesis of 2 intermediates (see Figure 5.1). Table 5.2 shows the colour and yields of each product. Intermediate 2 was purified by flash chromatography and resulted in several different fractions. These fractions were analysed by TLC. The Rf values were determined for each fraction (Table 5.3). Fractions 1, 2, and 4 contained unwanted by-products. Fraction 3 contained the desired product.

Following TLC, fractions were pooled and then analysed by one-dimensional H NMR. The pattern of resonance peaks for each fraction was analysed; the purified hydrazide was confirmed to be in fraction 3. The spectrum of fraction 3 showed two doublets in the aromatic region (7.998 and 7.969 ppm and 7.614 and 7.586 ppm). These represented the benzene group. A singlet was evident at 7.011 ppm and represented the maleimide group. Other peaks were visible, however these were attributed to either the blocking group (*t*-but) or the solvent. The one-dimensional H NMR spectrum for fraction 3 is shown in Figure 5.2.

The final step in the synthesis involved the removal of the blocking group, which was achieved by the addition of ice cold TFA. The yield of purified hydrazide was 0.79 g (Table 5.2).

Compound	Amount Synthesised (g)	Colour
Starting Material (4-aminobenzoic acid)	20	White
Intermediate 1 (MBA)	15.31	Beige
Intermediate 2	2.88	White
Final Product (Hydrazide linker)	0.79	Yellow/Brown

Table 5.2: Summary of the hydrazide synthesis. Synthesis involved the production of two intermediates and the removal of a protecting group.

Fraction 1	0.222, 0.349, 0.539, 0.603
Fraction 2	0.285, 0.428
Fraction 3	**0.253**
Fraction 4	0.126

Table 5.3: Rf values of the crude hydrazide linker mixture following flash and thin layer chromatography (see section 5.2.2.1). Fractions 1, 2 and 4 contain various by-products of the synthesis. Fraction 3 contained the purified hydrazide linker.

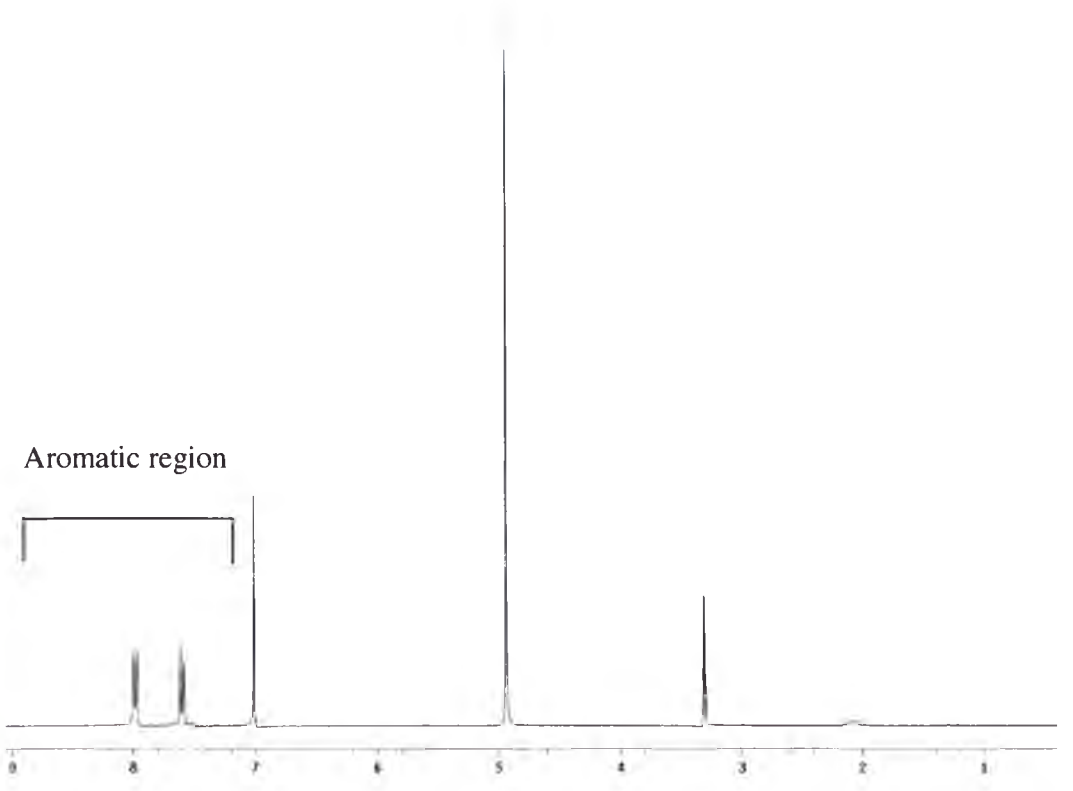

Figure 5.2: One-dimensional H NMR of fraction 3. The two doublets in the aromatic region (7.998 /7.969 ppm and 7.614 /7.586 ppm) represent the benzene group. The singlet at 7.011 ppm represents the maleimide group. Other peaks were visible, however these were attributed to either the blocking group (4.95 ppm) or the solvent (3.36 ppm).

5.3.2 Conjugation of the Hydrazide Linker to PAAAs

Purified hydrazide linker (X) was conjugated to five different PAAAs using the method described in section 5.2.2.2. Three conjugation reactions were successful. These were PEAA(23 kDa), PEAA(32 kDa) and PPAA(43 kDa). The H NMR spectrum obtained for PEAA(23 kDa)-X was similar to that observed for the linker alone, however a downward chemical shift was evident (Figure 5.3). The spectrum of PEAA(23 kDa)-X showed a doublet in the aromatic region (at 7.942 and 7.913 ppm and 7.569 and 7.541 ppm), representing the derivatized benzene ring, and a singlet at 7.000 ppm representing

the maleimide group. A broad range peak was evident at approximately 2 ppm, representing the polymer. This peak was considerably broader than other peaks, due to the heterogeneous mass of PAAA molecules (i.e. PAAAs are a collection of polymers with close but not identical molecular weights). Similar spectra were also obtained for samples of both PEAA(32 kDa)-X and PPAA(43 kDa)-X (results not shown).

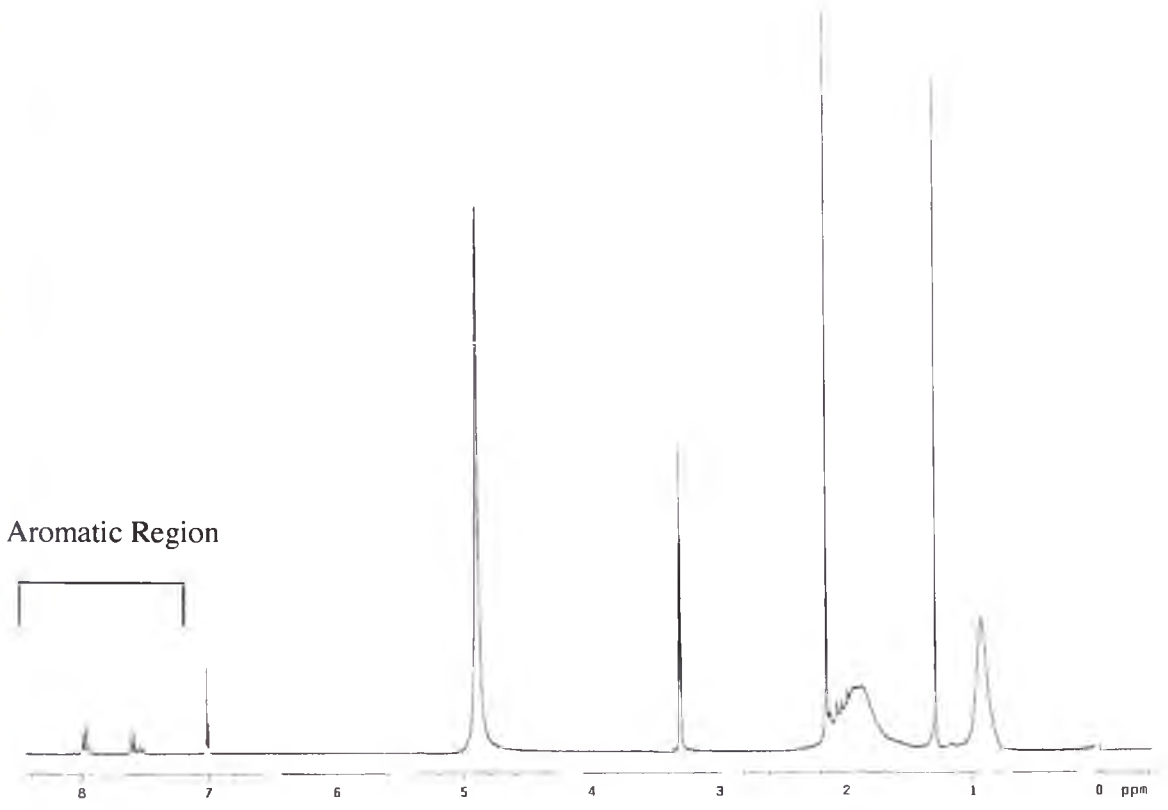

Figure 5.3: One-dimensional H NMR spectrum obtained for PEAA(23 kDa)-X. Two doublets are evident in the aromatic region. These represent the benzene group. A singlet is seen at ~7.000 ppm representing the malemide group. A broad range peak is seen at approximately 2 ppm, representing the polymer. A distinct chemical downward shift is evident for both the doublet and the singlet compared to the linker alone (Figure 5.2). This is caused by conjugation of the polymer to the hydrazide linker. Other peaks were visible, however, these were attributed to either the blocking group, the solvent or the polymer.

5.3.3 Determining the Number of Hydrazide-Linkers Conjugated to PAAAs

At acidic pH, PAAAs are thought to cause membrane rupture by inserting themselves directly into membranes. This is thought to occur following a conformational change of the PAAA from an expanded coil shape to a more complex shape. This conformational change is most likely related to the increased hydrophobic character when the many carboxylate ions become protonated at low pH (Murthy *et al.*, 1999). Therefore, when conjugating the hydrazide linker to a PAAA, a sufficient fraction of carboxylate ions must remain unmodified to ensure that the PAAA retains its ability to disrupt membranes. It was suggested that the ability of these polymers to lyse membranes may be lost if more than 3-5% of carboxyl groups are altered (C. Cheung, 2002, *pers. commun.)*. The number of hydrazide linkers attached to the polymers was determined using SAMSA fluorescein (see section 5.2.2.3 for details). Table 5.4 summarises the number of hydrazides attached to PAAAs and the percentage of carboxyl groups derivatized.

PAAA (Molecular weight)	No. of linkers attached per PAAA molecule	% of COOH derivatized
PEAA (23 kDa)	4	2
PEAA (32 kDa)	6	2
PPAA (43 kDa)	13	3

Table 5.4: Number of carboxcyclic-hydrazide linkers conjugated to three PAAAs. These numbers were calculated on the basis of results from an assay using SAMSA fluorescein (see section 5.2.2.3 for methods).

5.3.4 Determining the pH-Sensitive Membrane-Lytic Ability of PAAAs Derivatized with Hydrazide Linker

Whole cell experiments, similar to those described in section 3.2.2.5, were performed to determine if the derivatized polymers (PAAA-X) retained their ability to disrupt membranes in a pH-sensitive manner. Three derivatized polymers, with molecular weights ranging from 23 kDa to 43 kDa were tested. Cytolysis was detected by flow cytometric analysis of PI-stained cells.

At pH 7, 6.5 and 6, approximately 5% of cells were non-viable following exposure to either PEAA(23 kDa) or PEAA(23 kDa)-X. At pH 5.5, both PEAA(23 kDa) and PEAA(23 kDa)-X lysed approximately 97% of cells; in both cases the extent of cell lysis increased slightly at pH 5 to about 99%. At all pH values tested, there were no significant differences in the extent of cell lysis induced by PEAA(23 kDa) or PEAA(23 kDa)-X (Figure 5.4 A). Similar results were obtained when PEAA(32 kDa) and PEAA(32 kDa)-X were tested, except that at pH 6, both PEAA(32 kDa) and PEAA(32 kDa)-X lysed more cells (15% and 28%, respectively) (Figure 5.4 B). The difference between the percentage of cells lysed by PEAA(32 kDa)-X and PEAA(32 kDa) at pH 6 was not significant ($p > 0.05$ $F_{1,4} = 5.2943$, Students t-test). The results shown in this chapter indicate that derivatization of PEAA with a hydrazide linker had no significant effect on its ability to lyse cells at pH 5-5.5.

Previously, PPAA was shown to disrupt RBC at pH 6.5 and below (Stayton *et al.*, 2000). Similarly, in whole cell experiments described in this chapter, cell lysis induced by PPAA (43 kDa) occurred at pH 6.5 and below. At pH 6.5, PPAA(43 kDa) lysed approximately 90% of cells; this increased to approximately 95% at pH 6. However, at

pH 5.5 and below the percentage of cells lysed by PPAA(43 kDa) decreased. This extent of cell lysis was similar when PPAA(43 kDa)-X was used. Like PEAA polymers, there was no significant difference in the extent of cell lysis induced by either PPAA(43 kDa) or PPAA(43 kDa)-X (Figure 5.4 C).

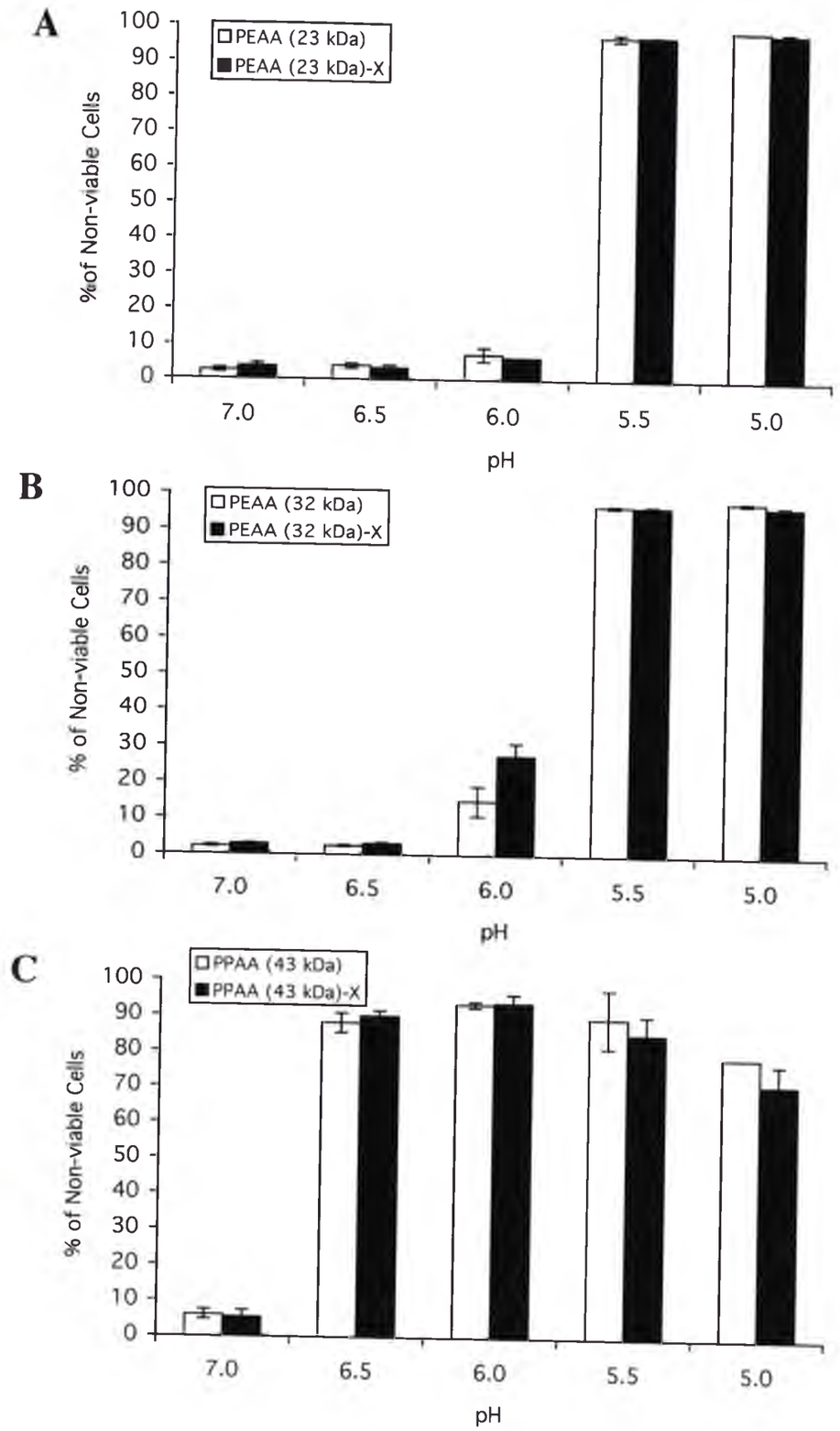

Figure 5.4: Histogram plots showing the percentage of non-viable cells following a 30 minute exposure of U937 cells to either PAAA or PAAA-X. Cytolysis was detected by flow cytometric analysis of PI-stained cells. (A) Cells exposed to 200 μg/ml PEAA(23 kDa) (white bars) or PEAA(23 kDa)-X (black bars). (B) Cells exposed to 200 μg/ml PEAA(32 kDa) (white bars) or PEAA(32 kDa)-X (black bars). (C) Cells exposed to 200 μg/ml PPAA(43 kDa) (white bars) or PPAA(43 kDa)-X (black bars). Each data point represents the mean value from three independent experiments. Error bars represent the standard error (SE) of the mean in each case. In some cases the SE are too small to be visible.

5.3.5 Testing the Effects of pH on the Stability of the Carboxcyclic-Hydrazide Bond in the Linker Used to Derivatize PAAAs

Theoretically, at physiological pH, the carboxcyclic-hydrazide bond within the linker is stable. However at acidic pH, the linker is expected to be cleaved from the polymer, generating free primary amine groups. Stability of the PAAA-X constructs was determined using fluorescamine, a non-fluorescent molecule that reacts with free primary amines to produce a fluorescent product. Stability tests were conducted on three types of PAAA-X, formed from PEAA(23 and 32 kDa) and PPAA(43 kDa). Derivatized polymers were incubated in phosphate buffers at either pH 7 or 5. At 0, 24 and 48 hours, aliquots of these samples were assayed for free amine groups using fluorescamine (see section 5.2.2.5).

In all cases, the resulting fluorescence for aliquots taken from the pH 7 buffer was significantly lower than those obtained for corresponding aliquots taken from the pH 5 buffer (Figure 5.5 A, B and C). For the PAAA-X samples incubated at pH 7, the fluorescence ranged between 2000 and 2500 arbitrary units. Fluorescence did not change significantly during the 48 hour time period for these samples. The fluorescence obtained from aliquots taken from the pH 7 buffer was similar to that of the controls (i.e. buffer containing PAAA plus fluorescamine (data not shown) or fluorescamine alone). These results suggest that the carboxcyclic-hydrazide bond in the linker is stable at pH 7.

For PEAA(23 kDa)-X incubated at pH 5, the level of fluorescence measured for the 0 hour sample was approximately 6000 arbitrary units. Surprisingly, a significantly lower

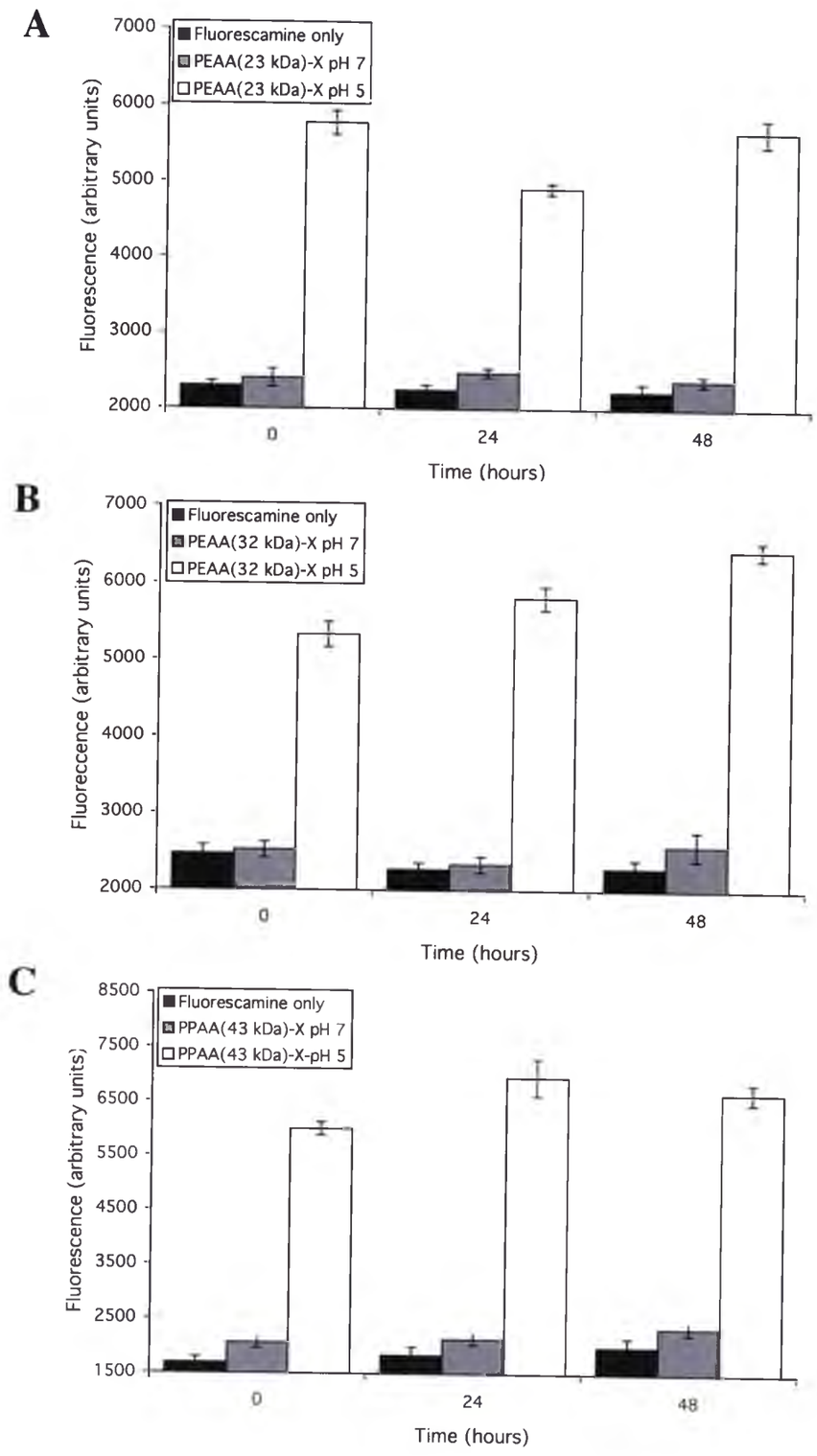

Figure 5.5: Bar graphs showing the level of fluorescamine fluorescence measured for PAAA-X samples incubated in either pH 5 or pH 7 buffers for up to 48 hours. PAAAs were conjugated to a hydrazide linker (X) as described in section 5.2.2.2. Data is shown for (A) PEAA(23 kDa)-X, (B) PEAA(32 kDa)-X, and (C) PPAA(43 kDa)-X incubated in pH 5 or pH 7 buffer. The level of fluorescence measured for samples containing only fluorescamine are also shown. Each data point represents the mean of the values from three independent experiments. Error bars represent the standard errors of the mean in each case.

5.3.6 Conjugation of Bad(140-165) to PAAA-X

Bad(140-165) was conjugated to both PPAA-X and PEAA-X. Bad(140-165) has 7 free amines; conjugation of Bad(140-165) to PAAA-X was confirmed by measuring an increase in primary amine groups associated with the conjugate (by fluorescamine assay; section 5.2.2.5). The fluorescence obtained for PPAA(43 kDa)-X alone was approximately 14000 arbitrary units. The fluorescence obtained for PPAA-X-Bad(140-165) was significantly higher (~17000 arbitrary units) than that obtained for PPAA(43 kDa)-X alone ($p<0.0001$, $F_{1,14} = 93.54$, Student's t-test; Figure 5.6). These results suggest that conjugation between PPAA-X and Bad(140-165) was successful. Conjugation of Bad(140-165) to PEAA-X was also successful (results not shown). (Note: In these experiments the sensitivity settings on the Biolumin fluorescence plate reader were different from those used in previous experiments, hence the fluorescence values shown in Figure 5.6 are considerably higher than those previously displayed in Figure 5.5). The number of Bad(140-165) molecules attached per PAAA molecule were calculated using the results of fluorescamine assays and are shown in Table 5.5.

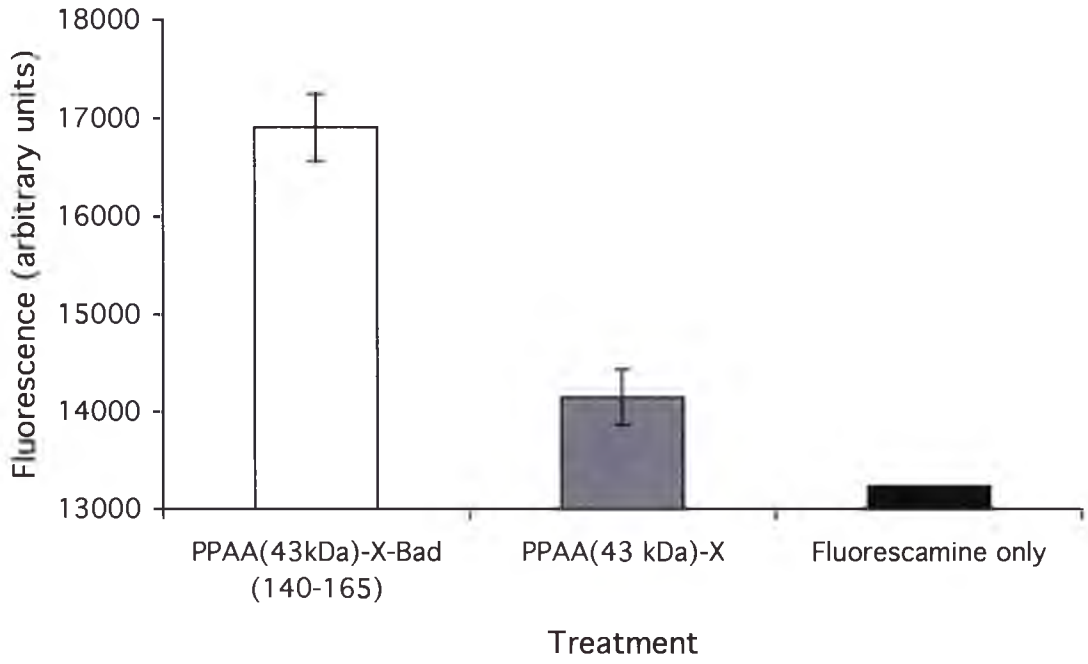

Figure 5.6: Bar graph showing the results of fluorescamine assays testing PPAA-X-Bad(140-165) (white bar), PPAA-X (grey bar) and fluorescamine only (black bar). Each data point represents the mean of values from three independent experiments. Error bars represent the standard errors of the mean in each case and in some cases are too small to be seen.

PAAA (Molecular weight)	**No. of linkers attached per PAAA molecule**	**No. of Bad(140-165) molecules attached per PAAA molecule**
PEAA (23 kDa)	4	2
PEAA (32 kDa)	6	2
PPAA (43 kDa)	13	5

Table 5.5: Number of Bad(140-165) molecules conjugated to PAAA-X.

5.3.7 Introduction of PPAA/PEAA-X-Bad(140-165) into U937 Cells by Constitutive Endocytosis

PEAA(23 kDa)-X-Bad(140-165), PEAA(32 kDa)-X-Bad(140-165) and PPAA(43 kDa)-X-Bad(140-165) were introduced into U937 cells by constitutive endocytosis, using methods described in section 3.2.2.1 (except that, following the initial incubation, cells were incubated in 4 ml of complete medium containing the constructs for 3 days). Cell viability was determined after 24, 48 and 72 hours. Over this time, there was a small, but insignificant, increase in the proportion of dead cells in both control and PAAA-X-Bad(140-165)-treated cells. An increase in cell density over the 72 hours (due to normal cell multiplication) may have resulted in the increase in non-viable cells. Results obtained for PEAA(32 kDa)-X-Bad(140-165) are shown in Figure 5.7.

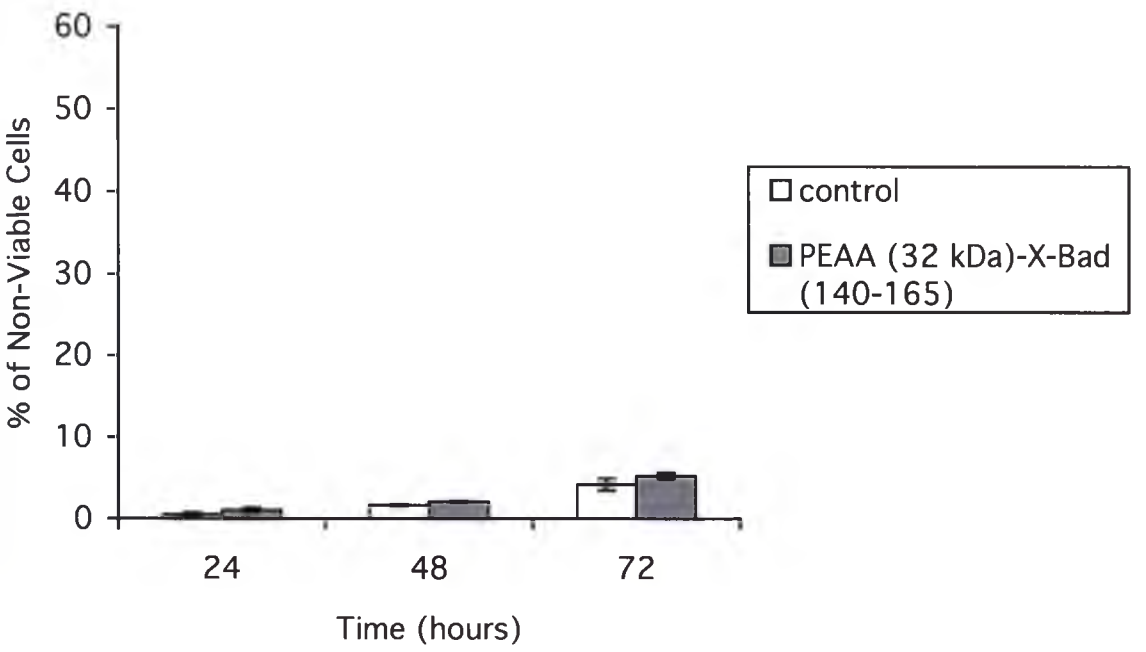

Figure 5.7: Bar graph showing the viability of U937 cells following uptake of PEAA(32 kDa)-X-Bad(140-165) by constitutive endocytosis. Graph shows the percentage of non-viable cells in: control (white bars) and cells incubated with PEAA(32 kDa)-X-Bad(140-165) (grey bars). Each data point represents the mean value from three independent experiments. Error bars represent the standard errors of the mean in each case and in some cases are too small to be seen.

PAAAs are internalised into cells by constitutive endocytosis and transit through early endosomes. To determine if this is also true for PAAA-X-Bad(140-165) constructs, cells were incubated for 30 minutes in PB containing PPAA-X-Bad(140-165)-biotin. U937 cells were then stained with anti-EEA1 antibody and Alexa 488-conjugated goat anti-mouse Ig; PPAA-X-Bad(140-165)-biotin was detected using streptavidin-Alexa 546. Confocal microscopy showed PPAA-X-Bad(140-165)-biotin located primarily at the periphery of the cell. In approximately 50% of cells there was partial overlap of the fluorescences attributable to PPAA-X-Bad(140-165)-biotin and EEA1. This pattern of fluorescence suggests that, like PPAA alone, PPAA-X-Bad(140-165)-biotin enters cells

via endocytosis and transits through early endosomes (Figure 5.8). A similar pattern of fluorescence was observed when PEAA-X-Bad(140-165)-biotin was introduced into U937 cells (data not shown).

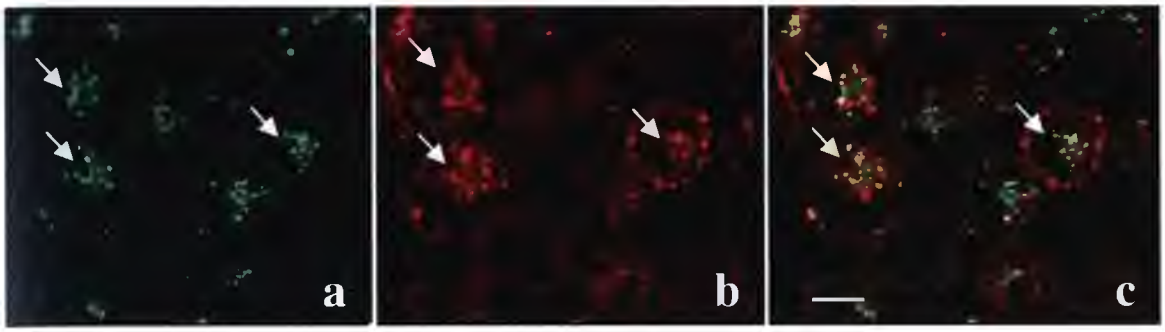

Figure 5.8: Confocal microscopy images of U937 cells incubated for 30 minutes in PB containing PPAA-X-Bad(140-165)-biotin. Images show cells stained with (a) anti-EEA1 antibody only (green fluorescence), (b) streptavidin-Alexa 546, and (c) an overlay of the two fluorescence images. In approximately 50% of cells, vesicles show partial co-localisation of green and red fluorescence (arrows). This result is representative of two independent experiments. Approximately 240 cells were scanned to ensure reproducibility. Bar = 10 μm.

To determine if the membrane disruptive ability of PAAAs is retained following conjugation of Bad(140-165), U937 cells were incubated in PB containing the membrane-impermeable fluor calcein and PEAA(32 kDa)-X-Bad(140-165) (see section 5.2.2.7). There was a time dependent release of calcein from vesicles to the cytosol when cells were incubated in the presence of PEAA(32 kDa)-X-Bad(140-165). Two hours after uptake, fluorescent vesicles were still clearly seen in some PEAA(32 kDa)-X-Bad(140-165)-treated cells while in others the fluorescence was considerably more diffuse (Figure 5.9, panel b). At 4 hours following loading, fluorescence was diffuse in most cells, indicating release of calcein from vesicles to the cytosol (Figure 5.9, panel

c). A similar pattern of fluorescence was detected when cells were incubated in the presence of PPAA-X-Bad(140-165) (data not shown).

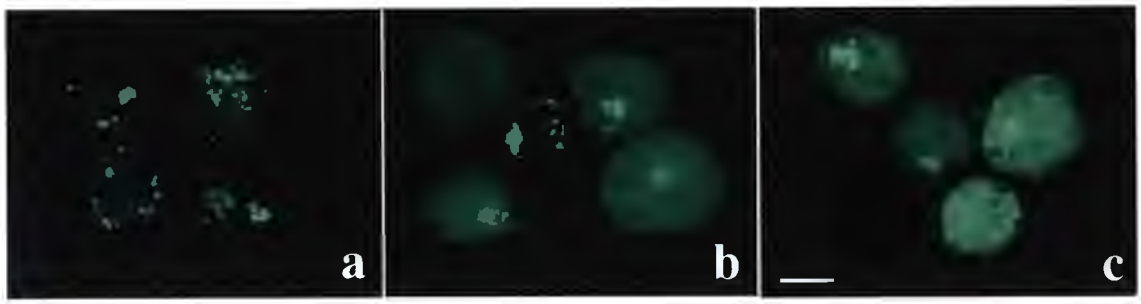

Figure 5.9: Confocal microscopy images of U937 cells incubated in PB containing 200 μg/ml of PEAA(32 kDa)-X-Bad(140-165) and 2 mg/ml calcein. Images show U937 cells immediately after uptake of PEAA(32 kDa)-X-Bad(140-165) and 2 and 4 hours after uptake (b and c, respectively). This result is representative of three independent experiments. 50 cells were scanned to ensure reproducibility. Bar = 10 μm.

5.4 Discussion

This chapter described the synthesis of a pH-sensitive hydrazide linker, the structure of which was confirmed by one-dimensional H NMR. The hydrazide linker was conjugated to various PAAAs. Results presented in this chapter show that approximately 2-3% of the carboxyl groups were conjugated to the linker (Table 5.4). Cheung and colleagues have previously conjugated anti-tumour agents to PAAAs. They found that derivatization of more than 3-5% of the carboxyl groups on the polymers inhibited their ability to disrupt membranes in a pH-sensitive manner (C. Cheung, *pers. commun.*). Therefore, in experiments conducted, the percentage of derivatized carboxylate ions was kept to a minimum.

The ability of the polymer to disrupt membranes in a pH-dependant manner was not affected by the conjugation of hydrazide linker (X) to the polymer (Figure 5.4). In all cases, the cytolytic efficiencies of underivatized PAAAs and the corresponding PAAA-X derivatives were not significantly different (Figure 5.4). The maximum cytolysis for both PPAA and PPAA-X occurred at pH 6.0, while that for PEAA and PEAA-X (irrespective of molecular weight) occurred at pH 5.0-5.5. The efficiency of cytolysis of PPAA and PPAA-X decreased at pH 5.5 and below. The reason for this is not known, however, Stayton and colleagues have recently shown a similar trend in experiments involving PPAA and RBCs. They showed that the haemolytic activity of PPAA was lower at pH 5.5 than at pH 6.5 or 6. At pH 5.5 and below, PPAA has a tendency to precipitate from solution. Stayton *et al.* (2000) have suggested that the greater hydrophobicity of PPAA may explain why it had reduced haemolytic efficiency at pH <6. It is possible that at pH <6, PPAA (and PPAA-X) form micro-aggregates which reduces their cytolytic activity.

To determine the stability of the carboxcyclic-hydrazide bond, PAAA-X samples were incubated in buffer at either pH 5 or pH 7 for up to 48 hours and then assayed using fluorescamine. Fluorescamine reacts with primary amine groups to produce a fluorescent product. Cleavage of the carboxcyclic-hydrazide bond generates two primary amines that are otherwise absent from the structure of PAAA-X. For PAAA-X samples incubated at pH 7, the level of fluorescence measured in the fluorescamine assay was not expected to change over 48 hours; this was found to be the case for all PAAA-X samples tested (Figure 5.5). In contrast, for PAAA-X samples incubated at pH 5, it was expected that the level of fluorescence measured in the fluorescamine assay would increase at each consecutive time point. This was found to be the case for PEAA(32 kDa)-X but not for the other two PAAA-X constructs tested. For PEAA(23 kDa)-X, the fluorescence obtained for the 24 hour sample was about 15% lower than the values obtained for 0 or 48 hours, which were similar (Figure 5.5 A). The anomalously low value for the 24 hour sample may have resulted from the use of an aged stock solution of fluorescamine; several stock solutions were used in these experiments and in some cases they may have been of different ages (up to several days old, stored at 4 C; fluorescamine is known to oxidise slowly in solution). In the case of PPAA(43 kDa)-X, the values obtained for the 24 and 48 hour samples were not significantly different from each other but these values were slightly higher than the value obtained for the 0 hour sample. Overall, the levels of fluorescence measured for all PAAA-X samples incubated at pH 5, irrespective of the time of incubation, were significantly higher than those measured for corresponding samples incubated at pH 7. These results suggest that the carboxcyclic-hydrazide bond is stable at pH 7 (physiological pH) but at pH 5 (which is found inside late endosomes/lysosomes) is very unstable and under these conditions, in many cases, cleaves almost immediately.

The final experiments described in this chapter involved conjugating Bad(140-165) to PAAA-X, and determining the effects on cells of the uptake of PAAA-X-Bad(140-165) conjugates by constitutive endocytosis. Conjugation of PAAA-X and Bad(140-165) was confirmed using fluorescamine (Figure 5.6). Quantitative analyses showed that the number of Bad(140-165) molecules attached per PAAA ranged from 2 to 5, depending on the polymer used (Table 5.5). These results indicate that approximately one third of the linkers attached to the polymer conjugated with Bad(140-165). The reason why Bad(140-165) did not conjugate to all of the attached linker molecules is currently unknown but may be a result of the instability of the reactive maleimide group in aqueous solution.

Surprisingly, uptake of PAAA-X-Bad(140-165) did not induce cell death (Figure 5.7). We expected that endocytosis of PAAA-X-Bad(140-165) would result in apoptosis. This expectation was based on the following:

1. Results shown in chapter 3 demonstrate that PAAAs are taken up by endocytosis and disrupt endosomes to release both small and macro-molecules to the cytosol.
2. Results shown in Figure 5.8 suggest that PPAA-X-Bad(140-165) is taken up by endocytosis and transits through early endosomes before moving onto other vesicular compartments.
3. Results shown in this chapter demonstrate that the pH-sensitive membrane disruptive ability of PAAAs is not affected following conjugation of the linker and Bad(140-165). Results shown in Figure 5.9 demonstrate that uptake of PEAA-X-Bad(140-165) induced physical disruption of endosomes sufficient to release calcein into the cytosol. These results are consistent with those reported by Lackey and colleagues (1999) who demonstrated that PPAA retains its ability

to lyse RBCs following conjugation with streptavidin. They also showed that PPAA-streptavidin complexes have similar haemolytic activity to that of unmodified PPAA (Lackey *et al.*, 1999).

4. Results presented in this chapter show that the linker is stable at physiological pH but not at the pH found in endosomes (Figure 5.5).
5. Work previously performed in this laboratory showed that pinocytic loading (described in section 6.2.2.1) of Bad(140-165) alone into U937 cells induced characteristics of apoptosis (Woods, 2000). Immediately after pinocytic loading of Bad(140-165), approximately: 25% of cells had depolarised mitochondria (compared to 2% of control cells), 40% of cells had PS exposure (compared to 6% of control cells), and 76% of cells showed a diffuse pattern of fluorescence following staining with anti-cytochrome c antibody, suggesting cytochrome c release (only 11% of control cells showed a diffuse pattern of fluorescence). In addition, it was shown that caspase inhibition significantly reduced the extent of cell death induced by pinocytic loading of Bad(140-165). These results demonstrated that cytosolic Bad(140-165) induces apoptosis. Several other research groups have also shown that apoptosis is induced following cytosolic delivery of a variety of pro-apoptotic peptides similar to the one used in this study (Kelekar *et al.*, 1997; Narita *et al.*, 1998).

Collectively, the above results suggest that PAAA-X-Bad(140-165) constructs are internalised by cells into endosomes where the low pH of the lumen would (1) rapidly cleave the carboxcyclic-hydrazide bond in the linker, releasing Bad(140-165), and (2) trigger the polymer to disrupt the endosomal membrane and release its contents (including Bad(140-165)) to the cytosol. So, the question is why did uptake

of PAAA-X-Bad(140-165) not induce apoptosis? The reason(s) for this are not yet known but could include the following:

1. *In vivo*, the linker may not have been completely cleaved from the construct, thereby limiting the amount of Bad(140-165) released into the cytosol.
2. Regardless of the extent of linker cleavage, the amount of Bad(140-165) released may not have been enough to induce apoptosis. To estimate the amount of Bad(140-165) theoretically delivered into cells in the experiments described here, the ratio of the intracellular concentration of a constitutively endocytosed fluorescently-labelled protein to its concentration in the external medium was determined. A standard curve plotting fluorescence versus concentration was produced for FITC-insulin. U937 cells were then allowed to constitutively endocytose FITC-insulin for a period of 20 minutes from an external concentration of 200 μg/ml (as described in section 3.2.2.1). Subsequently, $10x10^6$ U937 cells were disrupted using a series of five freeze/thaw cycles and the lysate centrifuged (16,000 g, 6 minutes) to pellet cell debris. The level of fluorescence in the supernatant was then determined and used to calculate the amount of FITC-insulin internalised by the cells. Assuming that U937 cells are spheres of 24 μm in diameter (estimated from confocal microscopy), it was calculated that the final intracellular concentration of FITC-insulin was only 0.08% of that in the external medium (results not shown). Using this value, it is possible to estimate that after 20 minutes of endocytosis, the concentration of PAAA-X-Bad(140-165) within U937 cells would be about 3.06×10^{-10} M. Assuming complete cleavage of Bad(140-165) from the polymer, and knowing that each PAAA molecule had 2-5 Bad(140-165) peptides attached (Table 5.5),

this predicts that under these conditions the final intracellular concentration of Bad(140-165) would be in the range 0.61 – 1.53 x 10^{-9} M.

The *in vitro* binding affinity (K_D) of Bad(140-165) for Bcl-X_L is 6.0x10^{-9} M (Kelekar *et al.*, 1997); this binding interaction is thought to be involved in exerting the pro-apoptotic effect of Bad. Thus, the calculations outlined above (with all their assumptions), indicate that after 20 minutes of endocytosis from an external concentration of PAAA-X-Bad(140-165) of 200 μg/ml, the intracellular concentration of Bad(140-165) would be, at most, approximately 4 fold lower than that required for significant interaction with Bcl-X_L. Therefore, it is quite feasible that the concentration of PAAA-X-Bad(140-165) released into the cytosol may not have been enough to induce apoptosis.

3. Cleavage of the linker occurs at a double bond (Figure 5.10). This results in the bulk of the structure of the linker remaining attached to the released peptide. Pro-apoptotic peptides interact with anti-apoptotic proteins in a specific manner (see sections 1.3.2.1 and 1.6). Thus, it is possible that the linker structure that remains attached to Bad(140-165) prevents its interaction with Bcl-x_L (an anti-apoptotic protein, see section 1.3.2.1) and inhibits its ability to induce apoptosis. Alternatively, or in addition, it is also possible that the cathepsin cleavage site incorporated into Bad(140-165) may also prevent its interaction with anti-apoptotic proteins.

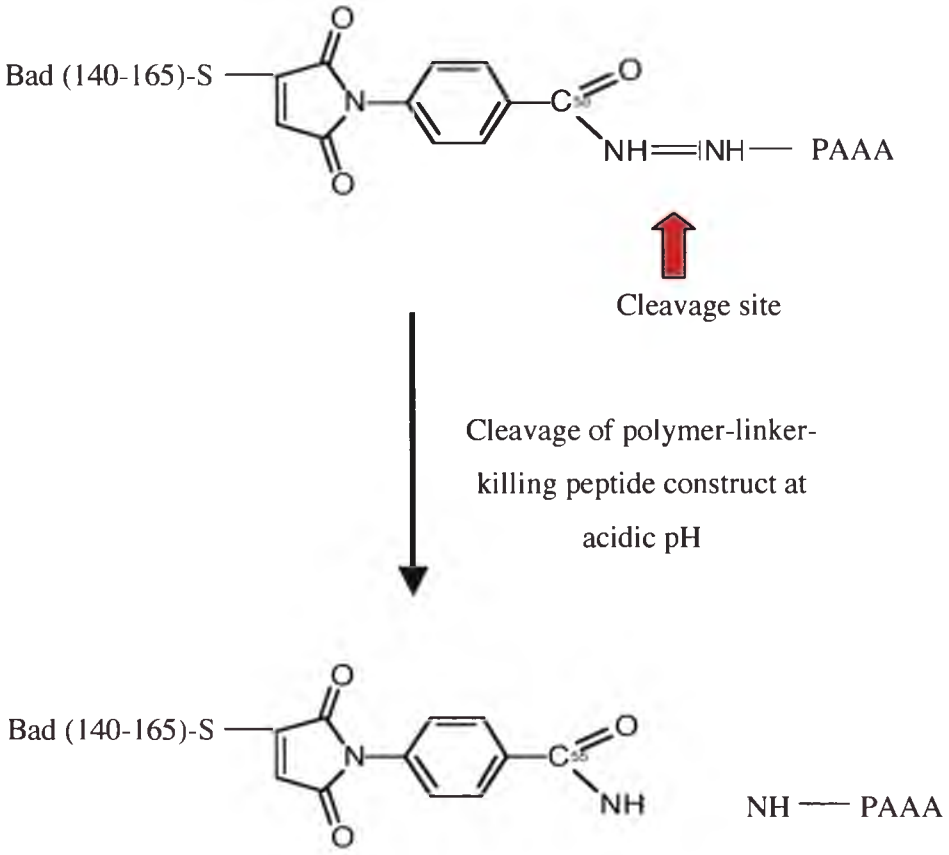

Figure 5.10: Schematic representation of the cleavage of PAAA-X-Bad(140-165) at acidic pH. Cleavage occurs at the double bond (indicated by the arrow) and results in the bulk of the linker structure remaining associated with the released Bad(140-165).

In conclusion, results presented in this chapter describe initial work directed towards the development of a novel cancer therapeutic. Additional experiments (described in chapter 7) will be needed to determine why PAAA-X-Bad(140-165) did not induce apoptosis following uptake by constitutive endocytosis. However, results thus far are positive and show great potential for further development.

Chapter 6

Detection of Mitochondrial Permeability Transition in Intact Cells

6.1 Introduction

Traditional cancer therapeutics don't directly manipulate apoptosis but instead kill cancer cells by indirect methods (e.g. by interfering with DNA replication). However, new cancer therapeutics in development, are now focusing on targeting apoptosis directly. Apoptosis is an ideal mode of killing because apoptotic cells are naturally engulfed and degraded by phagocytes, preventing the release of toxic cellular contents into adjacent healthy tissue. To confirm that the new therapeutics induce apoptosis in intact cells it will be necessary to accurately measure apoptotic process, such as MPT.

MPT has been studied in isolated mitochondria for decades (Zoratti and Szabo, 1995) and more recently in intact cells. In *in vitro* studies, MPT is associated with loss of electrical potential difference across the inner mitochondrial membrane (i.e. the loss of $\Delta\psi_{mit}$) and mitochondrial swelling resulting from an increase in the permeability of mitochondria to solutes up to 1500 Da in mass (Zoratti and Szabo, 1995). MPT is thought to result from the sustained opening of permeability transition pores (PTP) that form at points of contact between the inner and outer mitochondrial membranes. Other studies of mitochondria, both in intact cells and as isolated organelles *in vitro*, have provided evidence that PTP can also undergo rapid transient openings that do not result in MPT (Petronilli *et al.*, 1999; Ichas *et al.*, 1997; Huser *et al.*, 1998).

The precise biological role(s) of MPT have yet to be established. However, it has been implicated as being important in several aspects of cell physiology and pathology, including:

1. Control of mitochondrial calcium homeostasis (Zoratti and Szabo, 1995).
2. Initiation of autophagy (Lemasters *et al.*, 1998).

3. Triggering necrosis in cells undergoing ischemia- and reperfusion-induced injury (Lemasters *et al.*, 1998; Di Lisa *et al.*, 2001).
4. Triggering apoptosis (Loeffler and Kroemer, 2000).

Given the likelihood that MPT performs critical biological functions, it is important to develop a valid technique for measuring this phenomenon in intact cells. Two previous approaches for doing this have been described, however, both have significant limitations. Both of these techniques utilize the membrane-permeable acetoxymethyl ester of calcein (calcein-AM) to stain the cytosol (Nieminen *et al.*, 1995) or the mitochondrial matrix (Petronilli *et al.*, 1999).

The first reported technique measured MPT in hepatocytes by tracing the movement of cytosolic calcein into mitochondria. The movement of calcein into mitochondria was imaged using confocal microscopy. This technique involved introducing calcein-AM into cells via diffusion and subsequently staining them with TMRM (TMRM labels polarised mitochondria with bright red fluorescence). Theoretically, once inside the cytosol, the ester bond is cleaved by non-specific esterases to release free calcein, which is membrane-impermeable. Using this technique, polarised mitochondria fluoresced red due to the accumulation of TMRM and, when viewing calcein fluorescence, appeared as dark voids within a brightly green fluorescent cytosol (Nieminen *et al.*, 1995). In this technique, MPT is detected by a loss of mitochondrial staining with TMRM and an increase in calcein fluorescence inside mitochondria.

Minamikawa *et al.* (1999a) described a second technique for measuring MPT in intact cells. In this technique, calcein-AM is loaded into cells (by diffusion) and stained with

TMRM. Cells are also simultaneously incubated with Co^{2+} ions, which enter the cytosol but not mitochondria to complex with calcein and thereby quench its fluorescence. This technique detects MPT by a loss of mitochondrial staining with TMRM and a decrease in calcein fluorescence inside mitochondria (Minamikawa *et al.*, 1999 a and b).

The following chapter describes the development of an alternative confocal microscopy technique for the detection of MPT in intact cells that is free of the disadvantages associated with the other techniques described above (see discussion for more details). In this new approach, unconjugated calcein is simultaneously introduced into the cytosol of millions of cells by the process of pinocytic loading and, to identify the position of individual mitochondria and to measure $\Delta\psi_{mit}$, the cells are counter-stained with TMRM. A variety of cells types were used and results show that cytosolic calcein, which is initially excluded from polarized mitochondria, gradually enters them in response to transient openings of the MPT pore and that induction of sustained MPT produces a rapid net movement of calcein into mitochondria. Figure 6.1 schematically represents the three techniques for measuring MPT in intact cells.

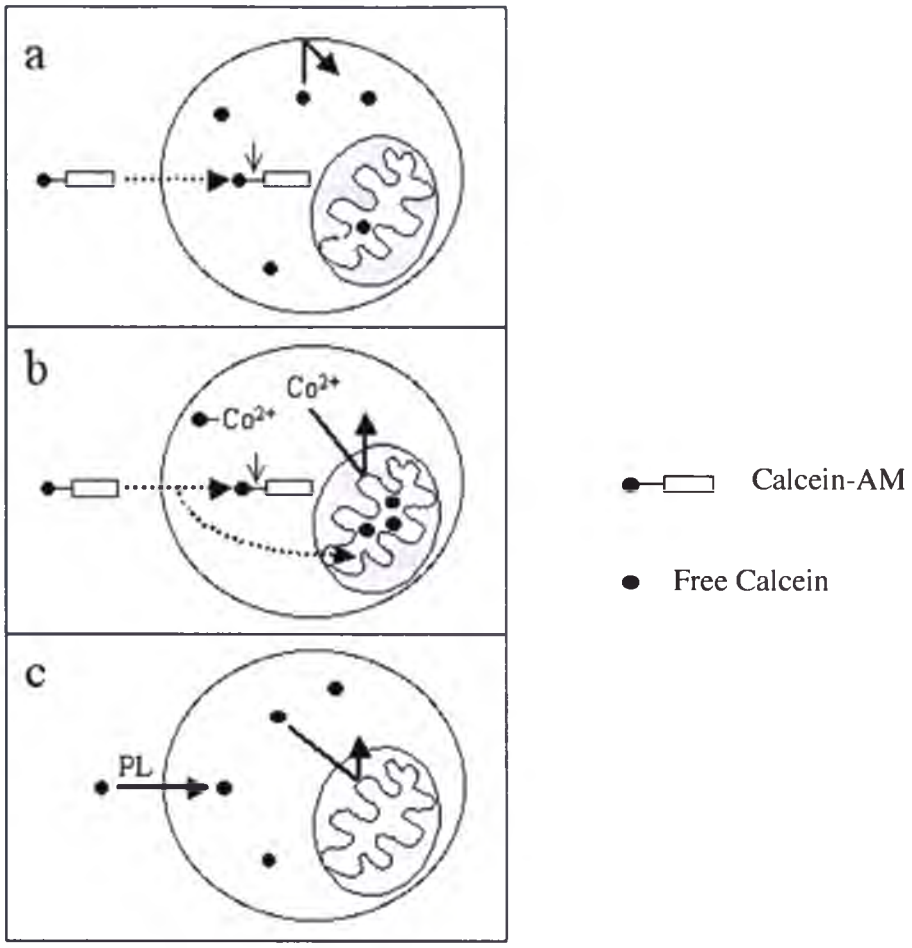

Figure 6.1: Schematic representations of three confocal microscopic techniques for measuring MPT in intact cells. In all cases, cells are stained with TMRM, which label polarised mitochondria with bright red fluorescence. (a) Calcein-AM is loaded into cells via diffusion (straight dotted arrow). Once inside, the ester bond is cleaved by non-specific esterases (thin solid arrow) to release free calcein that is membrane impermeable (thick solid arrow). (b) Calcein is loaded into cells as in (a) but cells are simultaneously incubated with 1 mM Co^{2+} ions, which enter the cytosol but not mitochondria to complex with calcein and thereby quench its fluorescence. (c) Calcein is directly introduced into cells by pinocytic loading (PL) and is largely excluded from the mitochondrial matrix. In these methods, MPT is detected by a loss of mitochondrial staining with TMRM and either an increase (a and c) or a decrease (b) in calcein fluorescence inside mitochondria.

6.2 Materials and Methods

6.2.1 Materials

Polyethylene glycol (molecular mass 1000 Da: PEG1000), sucrose, and 13-*cis*-retinoic acid (RA) were from Sigma (Sydney, Australia). N-(2-hydroxyethyl)piperazine-N'-(2-ethanesulfonic acid) (HEPES) was from United States Biochemical Corp. (OH, USA). Calcein-AM and tetramethylrhodamine methyl ester (TMRM) were from Molecular Probes Inc. (OR, USA). Bongkrekic acid (BA) was a gift from Prof J Duine (University of Delft, the Netherlands). All other chemicals were of analytical reagent grade and were from Ajax Chemicals (Sydney, Australia).

6.2.2 Methods

6.2.2.1 Pinocytic Loading of Intact Cells

Pinocytic loading is a technique that was developed for the introduction of macromolecules into mammalian cells and is a convenient, rapid and simple procedure. Unlike other cell loading methods, such as microinjection and electroporation, pinocytic loading provides a more gentle cell-loading method and does not significantly alter cell function. The pinocytic loading technique is based on the osmotic lysis of pinocytic vesicles (Okada and Rechsteiner, 1982). Macromolecules are firstly taken up by cells via pinocytosis. The cells are then placed in a hypotonic medium, which results in the bursting of pinosomes within the cells and release of their contents to the cytosol (Figure 6.2). Pinocytic loading has previously been used to load macromolecules such as monoclonal antibodies (Chakrabarti *et al.*, 1989), fluoresceinated dextran and horseradish peroxidase (Okada and Rechsteiner, 1982) into intact cells. Cell viability is maintained throughout the procedure.

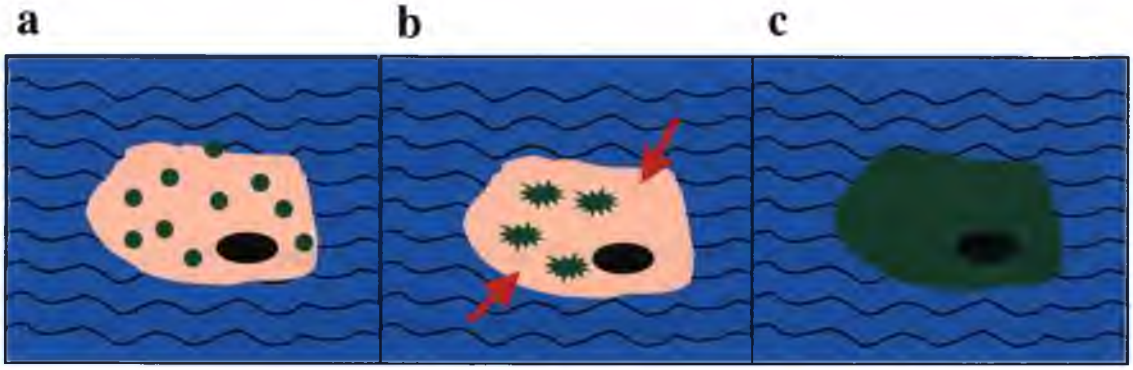

Figure 6.2: Schematic representation of the process of pinocytic loading. (a) Cells are incubated in a hyper-osmotic buffer containing the molecule to be loaded. This causes a loss of water from the cells and the simultaneous uptake of pinocytic vesicles containing the target molecule. (b) During the subsequent incubation in a mildly hypo-osmotic buffer, water re-enters the cells and the hyper-osmolar pinocytic vesicles causing them to burst. (c) Release of macromolecules into the cytosol of the cell.

Cells ($2x10^6$) were centrifuged for 5 minutes at 300 *g* and washed in 1 ml of DMEM:F12. Cells were re-centrifuged as above and the supernatant was thoroughly drained. The cells were then gently resuspended in 100 µl of hyper-osmotic buffer (10 mM HEPES, 10% (w/v) polyethylene glycol (PEG), 0.5 M sucrose, pH 7.4) containing the compound to be loaded at a concentration of 2 mg/ml. The cell suspension was incubated for 10 minutes at 37°C and diluted with hypo-osmotic buffer (60% DMEM:F12 and 40% water (v/v)) to make up a final volume of 10 ml. Cells were then incubated for 2 minutes at 37°C and centrifuged as above. Cells were washed twice with DMEM:F12. For immediate analysis by confocal microscopy, cells were resuspended in 200 μl of complete medium.

In some experiments, pharmacological inhibitors of MPT (100 μM bongkrekic acid or 10 μM cyclosporin A) were added to the calcein/hyper-osomotic buffer solution during

cell loading and to the medium in which cells were incubated for up to 1 hour prior to confocal microscopic analysis. In other experiments, cells were treated with 0.5 mM 13-*cis*-retinoic acid (to induce MPT) immediately before confocal analysis.

6.2.2.2 Staining Cells with a Cationic Fluorescent Dye to Measure Mitochondrial Membrane Potential

Tetramethylrhodamine methyl ester perchlorate (TMRM) is a cationic flurophore that accumulates inside mitochondria in response to the $\Delta\psi_{mit}$ (Heiskanen *et al.*, 1999), thus enabling changes in $\Delta\psi_{mit}$ to be monitored. Depolarisation results in mitochondrial release of TMRM and reduced mitochondrial red fluorescence.

Cells ($1x10^6$) were centrifuged for 5 minutes at 300 *g*. The supernatant was discarded and cells were resuspended in 500 μl of 50 nM TMRM in complete medium. TMRM was added by diluting 1 mM stock (in DMSO) to 1 μM in complete medium and then diluting the 1 μM stock 1:50 in complete medium. Samples were incubated at 37°C for 15 minutes in the dark and then immediately analysed by confocal microscopy and/or flow cytometry.

6.2.2.3 Confocal Microscopy, Flow Cytometry and Image Analysis

Following cell labelling, cells were immediately loaded onto glass slides and examined by a Leica DMIRBE inverted microscope coupled to a Leica TCS SP confocal system (Leica Microsystems, Sydney, Australia). Cells were sequentially excited at 488 nm (calcein) and 543 nm (TMRM) and fluorescence collected using emission windows set at 500-540 nm (calcein) and 560-610 nm (TMRM). All signals collected were adjusted to remain within the linear range of the detectors. Images were collected using TCS NT

software (Leica Microsystems, Sydney, Australia). In some experiments, this software was also used to calculate the average pixel intensity of calcein fluorescence within regions of interest (ROI) drawn onto collected images. In these cases, for each treatment, images of 10-14 individual cells were analysed as follows. For each cell, the mean fluorescence was determined for three ROI drawn to represent (1) mitochondria (these were drawn to be contained within regions stained with TMRM), (2) cytosol (drawn inside the cells but outside those regions stained with TMRM), and (3) background (drawn outside the cell). The values for each set of three ROI were averaged, then the mean background value was subtracted from each of the mean values for mitochondria and cytosol. Finally the background corrected value for mitochondria was divided by the corresponding value for the cytosol and expressed as a percentage. Differences between treatments were analysed using Oneway ANOVA (JMP software, SAS Institute INC, Cary, NC, USA). Images to be incorporated into figures were exported as TIFF files and figures were assembled using Adobe Photoshop v5.0 software (Adobe Systems, Sydney, Australia).

In some experiments, cells stained with 50 nM TMRM (as previously described) were subsequently analysed using a FACSort flow cytometer (Becton Dickinson, Sydney). The cells were excited with a 488 nm Argon laser and fluorescence collected using a 585 +/- 21 nm band pass filter. Acquired data was analysed using CellQuest (v.3.1f) software (Becton Dickinson, Sydney).

6.3 Results

6.3.1 Imaging Mitochondria by Staining Cells with Calcein-AM and TMRM

Results shown in section 6.3.1 were obtained by Alison Smail. They are included in this thesis because they complement other related work (sections 6.3.2 and 6.3.3).

Jurkat cells were loaded with calcein-AM and stained with TMRM. Calcein-AM was loaded into the cytosol and also, to a lesser extent, mitochondria. In the absence of co-staining (Figure 6.3, panel a) mitochondria were detectable as areas of slightly lower fluorescence intensity within a field of bright cytosolic calcein fluorescence. This was also true for cells stained with 50 nM TMRM (Figure 6.3, panel b). The areas of reduced fluorescence levels in cytosolic calcein fluorescence corresponded to red fluorescent mitochondria stained with TMRM (Figure 6.3, panel b-d). However, under these conditions, because of the relatively small difference between the intensity of calcein fluorescence in mitochondria versus the cytosol, it was difficult to visually discriminate mitochondria solely on this basis. Higher concentrations of TMRM were also tested. In cells stained with 100 nM, 500 nM and particularly 2000 nM TMRM, the intensity of green calcein fluorescence detected within mitochondria visibly decreased and they became more easily discernable as darkened voids within the brightly fluorescent cytosol (Figure 6.3 panels e and h). Thus, it is possible that when calcein-AM-loaded cells were stained with TMRM (at 100 nM or 500 nM, but not at 50 nM), mitochondrially-accumulated TMRM caused quenching of intra-mitochondrial calcein fluorescence.

This interpretation was confirmed by quantitative analysis of images collected for cells pinocytically loaded with calcein and stained with a range of concentrations of TMRM. When low concentrations of TMRM were used, the average intensity of calcein fluorescence in ROI drawn within mitochondria was approximately 90% of that in the cytosol, confirming that calcein-AM is poorly excluded by Jurkat cell mitochondria (Figure 6.4). Similar results were obtained for U937 cells (data not shown). As the concentration of TMRM used to stain cells was increased above 100 nM, calcein fluorescence within mitochondria decreased (Figure 6.4). The level of calcein fluorescence within mitochondria in cells stained with 1-2 μM TMRM was significantly reduced from that in cells stained with 10-100 nM TMRM ($p<0.001$, $F_{3,63}=37.0$, Tukey Kramer HSD (Honestly Significant Difference)).

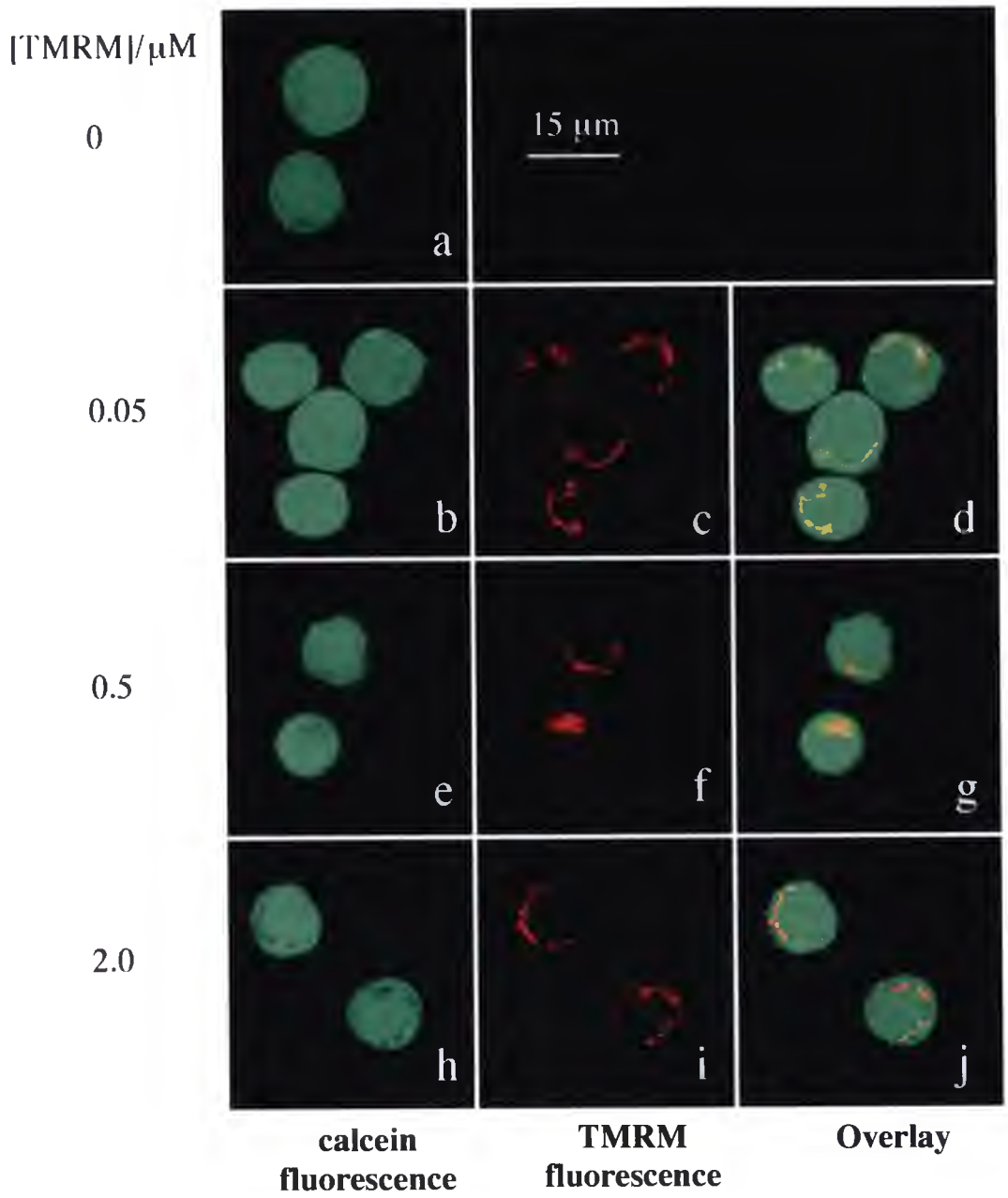

Figure 6.3: Images acquired by confocal microscopy showing Jurkat cells incubated in 1 μM calcein-AM and stained with 0-2000 nM TMRM. Images are representative of several independent experiments.

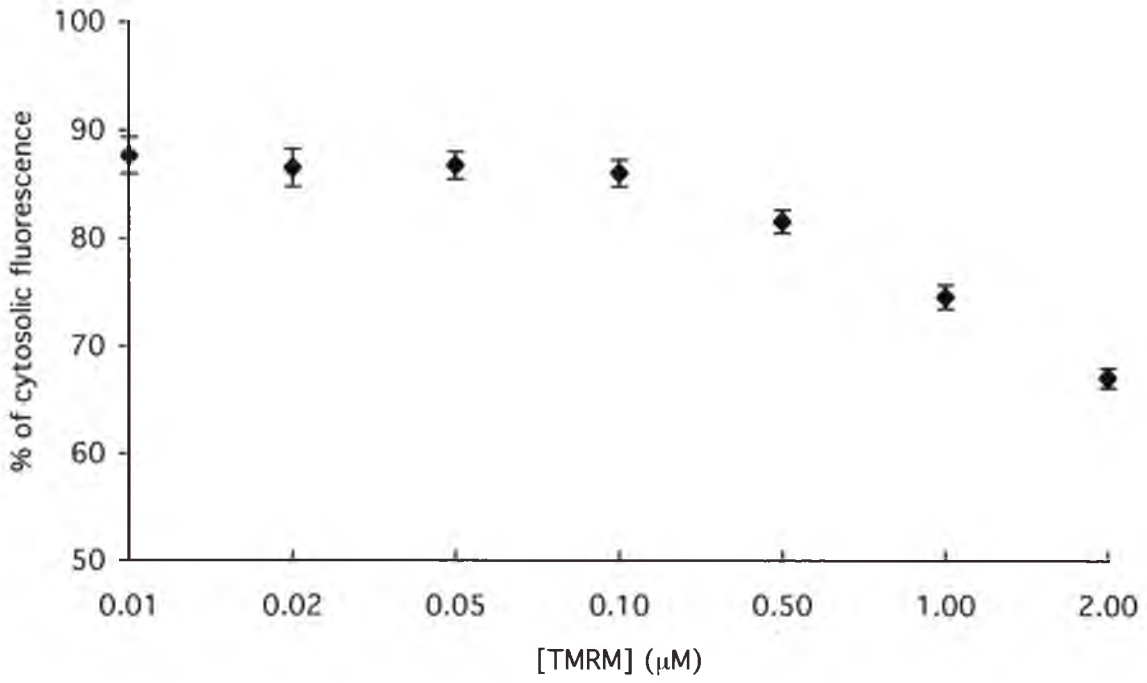

Figure 6.4: Plot showing the level of calcein fluorescence, in ROI drawn within TMRM-stained mitochondria, expressed as a percentage of the cytosolic calcein fluorescence for Jurkat cells loaded with 1 μM calcein-AM and stained with 0.01 – 2 μM TMRM. For each data point, the error bars shown represent the standard errors of the mean of values determined for 10 cells.

6.3.2 Imaging Mitochondria by Pinocytic Loading of Calcein into Cells and Staining with TMRM

Mitochondria were imaged in both suspension-cultured (Jurkat cells) and adherent (HeLa cells) human cells following pinocytic loading of calcein and staining with TMRM. In HeLa cells, mitochondria excluded sufficient calcein to give them the appearance of darkened voids in a bright green background of cytosolic fluorescence (Figure 6.5, panel a). Polarised mitochondria stained with TMRM were clearly discerned by their bright red fluorescence (Figure 6.5, panel b) and corresponded in position to darkened areas in the calcein fluorescence (Figure 6.5, panel c). In some cells, the edges of the darkened areas excluding calcein appeared 'blurred'. Petronilli *et*

al. (1999) reported a similar staining pattern in cells loaded with calcein and suggest that this is probably the result of fluorescence spreading which magnifies the size of emitting objects, while reducing that of dark spots. Similar results were obtained when Jurkat cells were used (Figure 6.6 and Figure 6.7).

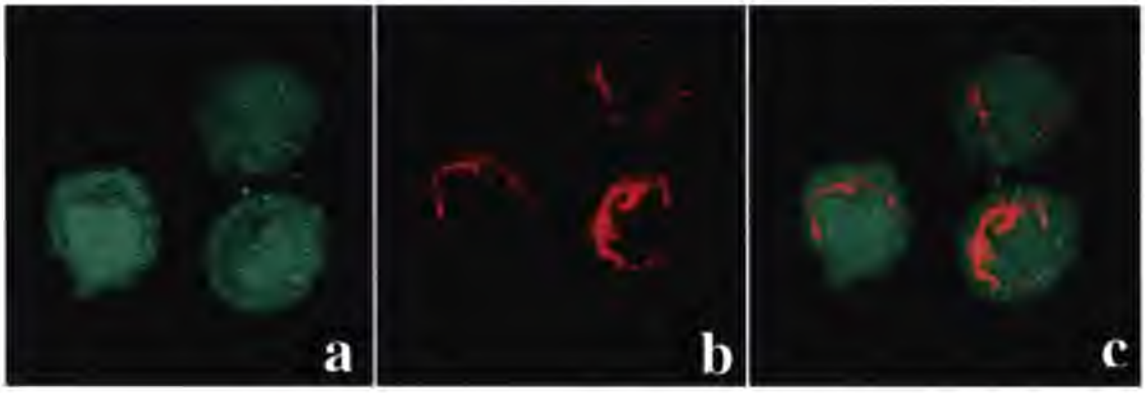

Figure 6.5: Confocal microscopy images showing HeLa cells pinocytically loaded with calcein and stained with 50 nM TMRM. Images show: calcein fluorescence (a), TMRM fluorescence (b), and fluorescence overlay (c). Images shown are representative of many acquired in two independent experiments.

Jurkat cells were pinocytically loaded with calcein and stained with TMRM before subsequently being analysed over a period of 1 hour; cells were analysed immediately after pinocytic loading and again 30 and 60 minutes later. Immediately after staining, calcein was evenly distributed throughout the cytosol and was partly excluded from mitochondria; mitochondria appeared as darkened areas in a background of bright green fluorescence (Figure 6.6). Polarised mitochondria stained with TMRM were clearly discerned by their bright red fluorescence and corresponded in position to darkened areas in the calcein fluorescence (data not shown). Quantitative image analysis indicated that immediately after pinocytic loading with calcein, the level of calcein fluorescence in ROI drawn within mitochondria (defined by staining with TMRM) was

approximately 60% of that of the cytosol (Figure 6.7). A gradual time-dependent in-filling of mitochondria with calcein was observed over the hour time period (Figure 6.6, panels b and c). This was confirmed by quantitative image analysis, which indicated that over a 60 minute period immediately following pinocytic loading, for ROI drawn within mitochondria of control cells, the average intensity of calcein fluorescence increased steadily from 60% to approximately 80% of that in the cytosol (Figure 6.7). These changes in fluorescence were statistically significant ($p<0.001$, $F_{2,39}=24.99$, Tukey-Kramer HSD) and occurred in the absence of any loss of TMRM staining (Figure 6.8).

The slow calcein influx was inhibited by treating cells for 1 hour with bongrekic acid (BA) or cyclosporin A prior to calcein loading and TMRM staining. Bongrekic acid and cyclosporin A are both pharmacological inhibitors of MPT (Marchetti *et al.*, 1996). In contrast to control cells, over a 1 hour period following pinocytic loading of calcein, there was no significant change in the average intensity of calcein fluorescence within ROI drawn within mitochondria of BA-treated cells (Figure 6.7: $p=0.156$, $F_{2,39}=1.95$, Tukey-Kramer HSD). Similar results were obtained using cells treated with cyclosporin A (data not shown).

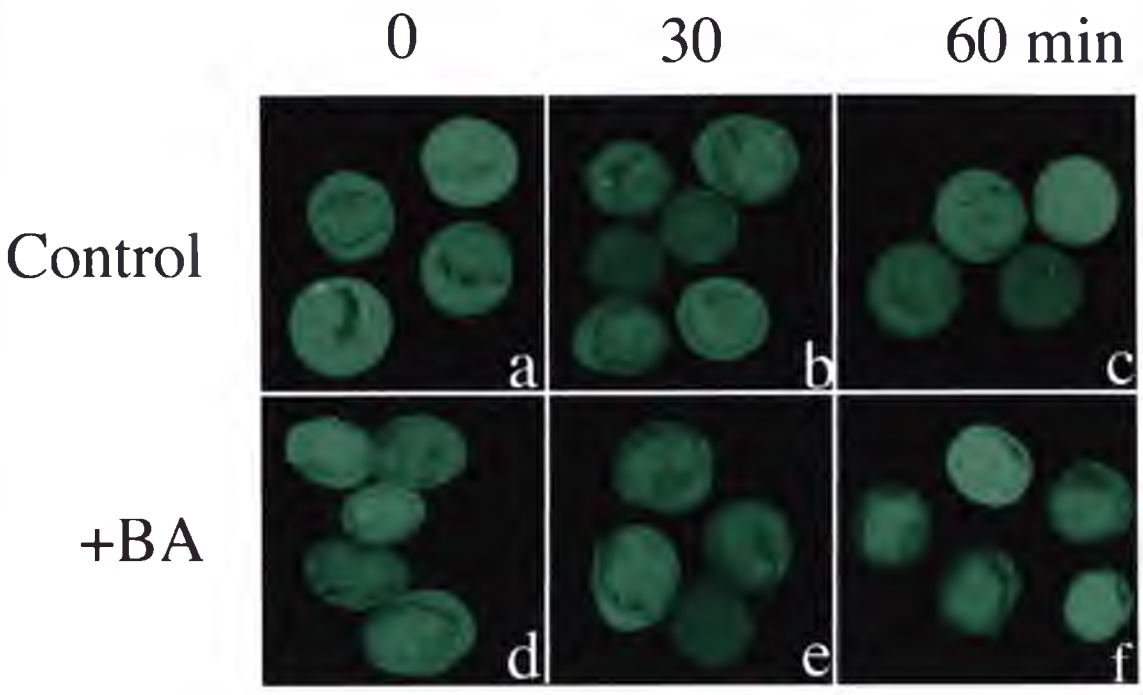

Figure 6.6: Confocal microscopy images showing calcein fluorescence in control (a-c) or BA-treated (d-f) Jurkat cells pinocytically loaded with calcein (and stained with 50 nM TMRM), imaged either immediately after loading (a, d), or 30 minutes (b, e) or 60 minutes (c, f) later.

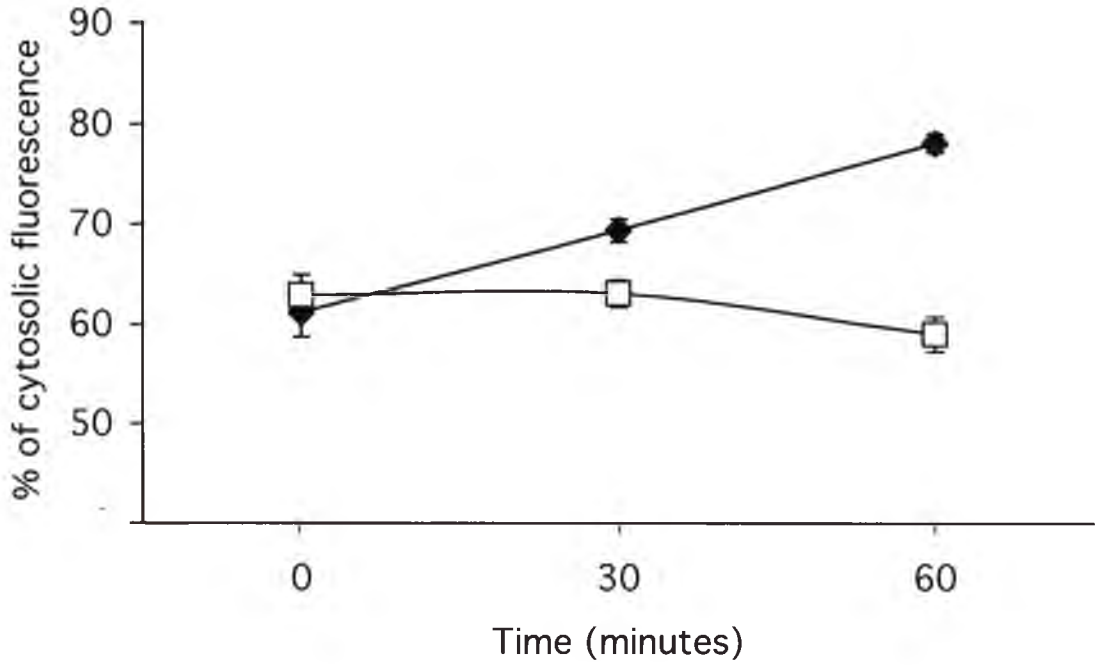

Figure 6.7: Line graph showing the levels of intra-mitochondrial calcein fluorescence in control cells (♦) and BA-treated cells (□), expressed as a percentage of the level of cytosolic calcein fluorescence, as a function of time after pinocytic loading. The error bars shown represent standard errors of the mean of measurements made for 10-14 cells for each data point (see section 6.2.2.3 for more details).

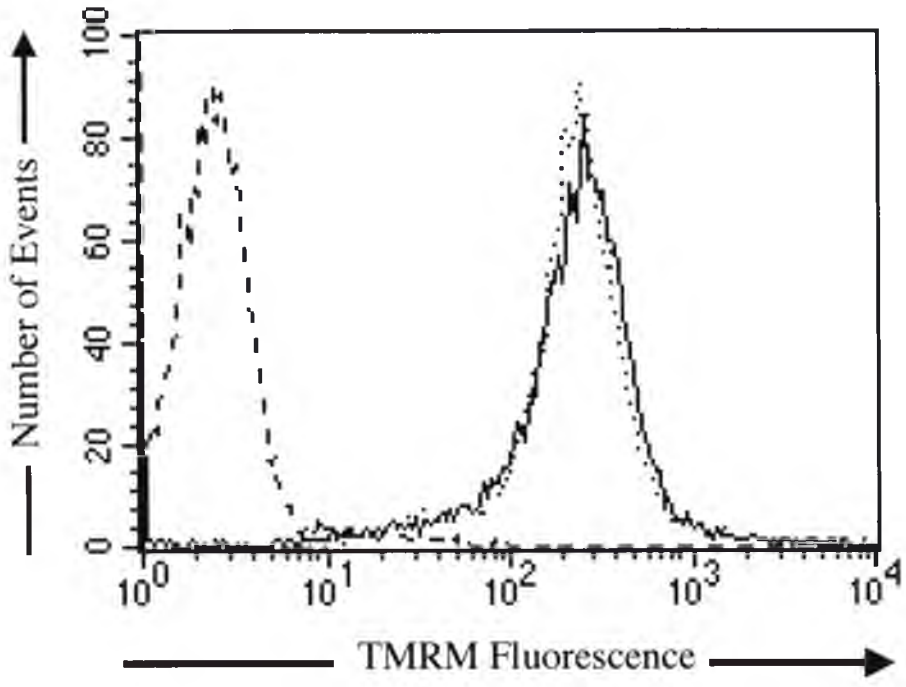

Figure 6.8: Overlay histograms showing the results of flow cytometric analysis of Jurkat cells pinocytically loaded with calcein. The dashed line (the single peak to the left) represents cells that were not stained with TMRM. The dotted and solid lines (which are nearly identical in position) represent cells that were stained with TMRM and analysed either immediately or 60 minutes later, respectively. The results shown are representative of three independent experiments.

6.3.3 Detecting Mitochondrial Permeability Transition Induced by Retinoic Acid

Pinocytic loading of cells with calcein and staining with TMRM was also used to detect MPT induced by brief incubation of cells with retinoic acid (RA). Previous research indicates that RA acts as a mitochondrial uncoupler and induces MPT and cyctochrome c release (Rigobello *et al.*, 1999). Immediately after exposure to RA, calcein fluorescence was uniform throughout the entire cell. Mitochondria were not discernable as dark regions or regions of significantly lower green fluorescence and mitochondria did not stain with TMRM, indicating collapse of $\Delta\Psi_{mit}$ (Figure 6.9). In control cells,

most areas of reduced calcein fluorescence corresponded in position to TMRM-stained mitochondria (e.g. the region indicated by arrow no.1, Figure 6.9, panels a and c). However, occasionally, areas of lower calcein fluorescence did not correspond in position with TMRM-stained, polarised mitochondria (e.g. the region indicated by arrow no.2, Figure 6.9, panel c). This latter type of calcein void was previously reported in hepatocytes microinjected with calcein (Petronilli *et al.*, 1999) but has not been identified. It is possible that such regions may correspond to transiently depolarised mitochondria that have not undergone MPT and that therefore still exclude calcein.

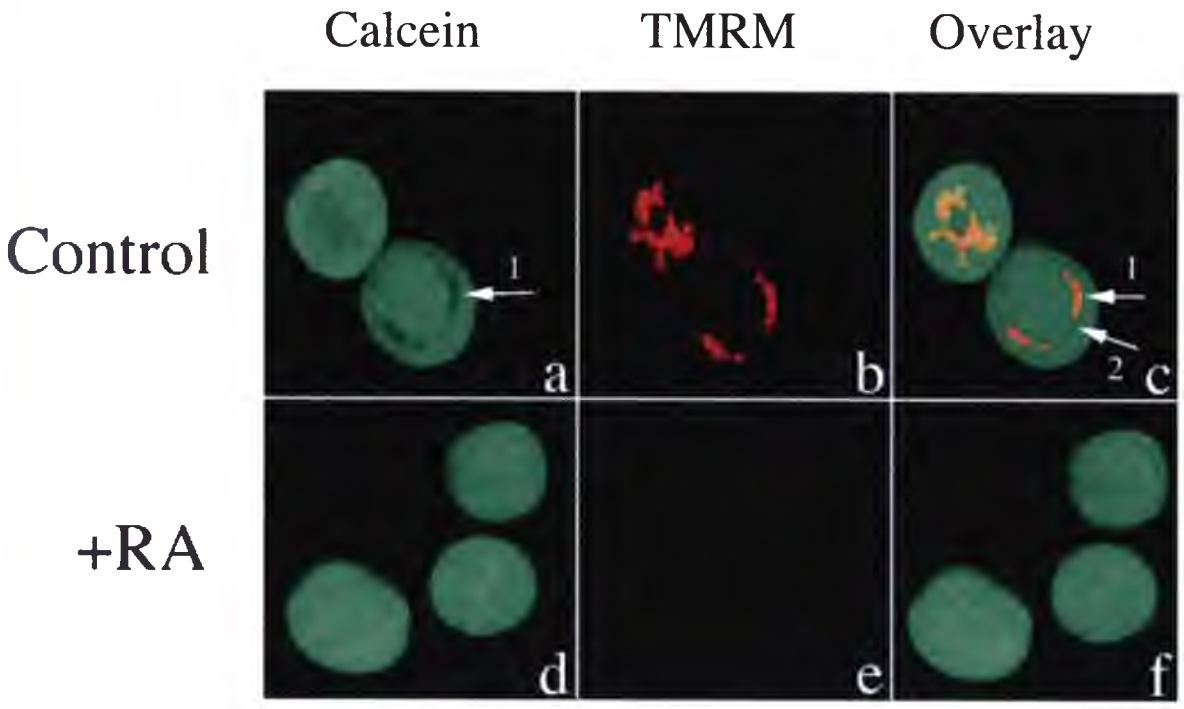

Figure 6.9: Confocal images showing Jurkat cells pinocytically loaded with calcein and stained with 50 nM TMRM. Control cells (a-c) received no further treatment. Other cells (+ RA: d-f) were stained with TMRM in the presence of 0.5 nM RA to induce mitochondrial permeability transition. The arrow numbered 1 (panel a) indicates a 'dark region' that corresponds in position to TMRM-stained mitochondria (see panel c). The arrow numbered 2 (panel c) indicates a 'dark region' that does not correspond in position to TMRM-stained mitochondria.

6.4 Discussion

Results presented here demonstrate that pinocytic loading of calcein into cells and staining with 50 nM TMRM can provide a useful technique for detecting MPT in intact cells. MPT was detected by a loss of mitochondrial staining with TMRM and an increase in calcein fluorescence inside mitochondria. Results show that, in a variety of cell types, cytosolic calcein is excluded from normal polarized mitochondria but enters them during MPT.

Minamikawa *et al.* (1999) and Nieminen *et al.* (1995) describe alternative techniques to measure MPT in intact cells (see section 6.1). The technique described in this chapter is a favourable alternative and avoids the disadvantages associated with the earlier approaches. The advantages of this new technique are:

1. It has successfully been applied to various cell lines including HeLa (human epitheloid carcinoma), Jurkat (human T cell leukemia) and U937 (human myelomonocytic), suggesting that it would be applicable to use in most cell types. The technique described by Nieminen *et al.* (1995) is only applicable to some cell types. Nieminen *et al.* (1995) and Lemasters *et al.* (1998) reported that when calcein-AM only is loaded (by diffusion) into rat hepatocytes and then the cells are stained with TMRM, there appeared to be little calcein fluorescence detected within mitochondria. However, results described in this chapter and those of others (Petronilli *et al.*, 1999) show that this is not the case when other cell types, such as rat hepatoma MH1C1 and Jurkat cells, are loaded with calcein-AM. In these cases, the ability of the technique (described by Nieminen *et al.* (1995)) to image mitochondria as calcein-negative voids, and thereby measure MPT in intact cells, is significantly limited.

2. It does not involve toxic substances. The technique of Minamikawa *et al.* (1999) to measure MPT (Figure 6.1, panel b) involves loading cells with calcein-AM but quenching cytosolic calcein fluorescence with Co^{2+} ions (Minamikawa *et al.*, 1999a; Minamikawa *et al.*, 1999b). Co^{2+} is a heavy metal that is known to cause toxic and other effects on cells. For example Co^{2+} (1) completely stopped growth in murine osteoblast-like MC3T3-E1 cells (Okazaki *et al.*, 1998), (2) had adverse effects on developmental stages of post-blastocyst mouse pre-embryos *in vitro* (Nieminen *et al.*, 1995), and (3) significantly increased lactate production by cultured rat Sertoli cells (Monsees *et al.*, 1998). It is difficult to exclude the possibility that even short exposures of cells to Co^{2+} might induce subtle changes that impact upon mitochondrial physiology.
3. It avoids potential artefacts arising from quenching of intra-mitochondrial calcein fluorescence. The technique described by Nieminen *et al.* (1995), (Figure 6.1, panel a) which stains cells with TMRM at a concentration of 500 nM or above, causes mitochondrially-accumulated TMRM to suppress intra-mitochondrial calcein fluorescence, probably by fluorescence quenching (TMRM has been shown to quench calcein fluorescence both in a mixture of the two fluors in solution and in dual-stained isolated mitochondria (Petronilli *et al.*, 1999)). Even in cell types which do not accumulate intra-mitochondrial calcein following loading from 1 μM calcein-AM, this quenching effect may have important implications. For example, if calcein-AM-loaded cells are stained with TMRM at a concentration of 500 nM or greater, TMRM-mediated quenching is likely to make detection of calcein entry into mitochondria more difficult. This would probably be most problematic when mitochondria remain polarised and therefore retain a high internal concentration of TMRM, as has been reported to

occur when mitochondria undergo transient, reversible openings of the mitochondrial permeability transition pores (Petronilli *et al.*, 1999). Thus, under these conditions, MPT might go undetected.

4. It unambiguously identifies the physical movement of calcein across the inner mitochondrial membrane barrier coincident with MPT. The technique described by Minamikawa and associates (Figure 6.1, panel b), relies on calcein-AM entering mitochondria within cells and being cleaved by esterases to entrap calcein within the matrix. This does not occur when rat hepatocytes are incubated in a solution containing 1 μM calcein-AM (Lemasters *et al.*, 1998). Thus, at least in this cell type, the technique is not successful or it may require cell-specific adjustments to the conditions used. Also Minamikawa's technique can not discriminate between calcein release from mitochondria or Co^{2+} entry into mitochondria.

Importantly, cell viability was maintained when calcein was loaded into cells using the technique described in this chapter. To load calcein into the cytosol, cells were exposed for 10 minutes to a hyperosmotic buffer followed by a 7 minute exposure to a hypoosmotic solution (the effects of which would tend to counter the initial hyperosmotic stress). When measured up to 3 days after treatment, no effects of pinocytic loading on the viability of L929 cells were detected (Okada and Rechsteiner, 1982). Furthermore, in studies of Jurkat and HeLa cells, results confirmed that at 5 hours after pinocytic loading there was no decrease in cell viability (data not shown). Thus, pinocytic loading has no gross effects on cell viability. Furthermore, the demonstration that cytosolic hyperosmolarity induced by uptake of Na^+-co-transported, non-metabolised amino acids did not affect either matrix volume, respiratory rate,

$NADH/NAD^+$ ratio or $\Delta\Psi_{mt}$ in mitochondria within intact hepatocytes (Devin *et al.*, 1998) suggests that the mild osmotic stress associated with pinocytic loading is unlikely to affect mitochondria. It has been shown that osmotic stress sustained for a minimum of 30-100 minutes can induce changes in general cellular metabolism (Brunmair *et al.*, 2000; Ouwens *et al.*, 2001); however, there is no evidence that short (< 10 minutes) exposure to mild osmotic stress produces such changes. Using the technique described in this chapter, measurements of MPT are best performed within 30 minutes of pinocytic loading. Thus, the available information suggests that the brief, mild osmotic stress associated with the procedure is unlikely to result in any major, rapid changes in mitochondria or cell metabolism that would compromise the measurements taken.

Results presented in this chapter show that, when cells were imaged immediately after pinocytic loading of calcein, the level of calcein fluorescence in ROI drawn within TMRM-stained mitochondria of control cells was approximately 60% of that in the cytosol, and increased gradually thereafter. The high level of measured intra-mitochondrial calcein fluorescence is probably a consequence of the following two factors, which relate to features of mitochondrial ultrastructure and the physics of confocal imaging: (1) Electron microscopy indicates that mitochondria are 0.1-0.5 μm thick and, when present as discrete structure, 1-2 μm long (Frey and Mannella, 2000). Confocal imaging collects 'optical sections' through the specimen of about 1 μm in thickness. Mitochondrial ROI were drawn inside areas containing red (TMRM) fluorescence. In some planes, the 1 μm thickness of the confocal optical section would be greater than the dimensions of mitochondria. In these cases, three-dimensional spaces seen (in two-dimensions) on-screen as containing TMRM fluorescence might also contain calcein fluorescence coming from adjacent regions of intermembrane space

or cytosol that have been captured in the same optical section. (2) Recent ultra-structural analysis indicates that the cristae, which may occupy a large fraction of the volume of the mitochondrial interior, are generally connected to the intermembrane space via short tubular junctions 28 nm in diameter (Frey and Mannella, 2000). Calcein would have free access (across the permeable outer mitochondrial membrane) to the intermembrane space and, via the cristae junctions, to the cristae. Confocal microscopy is unable to spatially resolve cristae within mitochondria. Therefore, using the technique described, optical sections through the TMRM-stained mitochondrial matrix will incorporate calcein-containing cristae, even though these are not discerned as discrete visible structures. Therefore, acting together, both these factors probably account for the level of calcein fluorescence measured in mitochondrial ROI immediately after pinocytic loading.

Studies of mitochondria, both in intact cells and as isolated organelles *in vitro*, have established that MPT pores constitutively undergo rapid transient openings (Petronilli *et al.*, 1999; Ichas *et al.*, 1997; Huser *et al.*, 1998). The technique described in this chapter detected constitutive transient MPT as a gradual time-dependent entry of calcein into mitochondria. Furthermore, these results demonstrate that RA, a known inducer of MPT (Rigobello *et al.*, 1999), elicited an influx of calcein into the matrix and a loss of mitochondrial staining with TMRM. Thus, the technique described here can be used to measure the occurrence of MPT 'flickering' and also the bulk entry of calcein into mitochondria associated with sustained MPT. The latter is most easily detected when cells are imaged soon after calcein loading.

Although this new technique has many advantages over previously described methods, two limitations have been identified. These are: (1) the measurement of sustained MPT (detected as complete in-filling of mitochondria with calcein) is best performed within 30 minutes of pinocytic loading, and, more importantly, (2) detection of MPT in cells undergoing apoptosis is not possible. When cells were pinocytically loaded with calcein several hours after induction of apoptosis, it was not possible to induce release of calcein from pinocytic vesicles by incubating cells in hypoosmotic media, even when conditions were varied to increase the osmotic gradient imposed. This result was obtained when apoptosis was induced in either (1) Jurkat cells with staurosporine or anti-Fas antibody, or (2) U937 cells with tumour necrosis factor α and cycloheximide (results not shown). The reason(s) underlying the difference in behaviour between normal and apoptotic cells is unknown, but it may relate to an increase in the permeability of the cell membrane that occurs during apoptosis (Zamai *et al.*, 1996). Unfortunately, due to this latter limitation, this technique would not be appropriate to determine if novel cancer therapeutics, including that described in section 1.10, induce apoptosis in intact cells. Despite these limitations, this technique will be valuable in studies investigating the cellular functions of MPT.

Chapter 7

Conclusions

Apoptosis is a highly regulated form of cell death. Minor changes in the process can result in diseases, such as cancer. For many years now, clinical treatment of cancer has involved chemotherapy, radiotherapy and surgery. However, despite the wide use of these conventional treatments, there are still many disadvantages associated with them. These disadvantages have led to development of novel cancer therapeutics some of which are now in stage I and II clinical trials. This thesis describes work directed towards the development of a novel cancer therapeutic comprised of an endosomal-disruptive polymer conjugated to both a targeting ligand and, via a pH-sensitive linker, to a pro-apoptotic peptide (Bad(140-165)).

Two different types of synthetic polymer (PAAAs and pDMAEMA) were investigated for their potential use as endosomal-disruptive agents. PAAAs were found to be endocytosed into cells and then transported to late endosomes, where acidification of the lumen by the membrane H^+-ATPase triggered polymer-mediated vesicle disruption and release of endosomal contents to the cytosol. pDMAEMA was also found to be endocytosed into cells and transported to endosomes where it induced morphological changes in late endosomes/lysosomes (but did not physically disrupt them). pDMEAMA induced rapid necrotic death. PAAAs were chosen as the most appropriate endosomal-disruptive agents for use in the novel cancer therapeutic because (1) the very high toxicity of pDMAEMA could pose a significant risk of bystander cell damage in cancer therapies, and (2) under the conditions tested, pDMAEMA did not have the ability to disrupt endosomes.

A pH-sensitive hydrazide linker (X) was successfully synthesised and conjugated to PEAA and PPAA. Whole cell experiments indicated that the pH-sensitive membrane

disruptive ability of the polymers was retained following conjugation with the hydrazide linker. The stability of the carboxcyclic-hydrazide bond incorporated into the linker was then determined. At pH 7, the bond was stable; however, at pH 5, it was very unstable and the linker was cleaved almost immediately from the polymer. Lastly, Bad(140-165) was conjugated to PAAA-X and then introduced into cells by constitutive endocytosis. Following uptake, in approximately 50% of cells, PAAA-X-Bad(140-165) partially co-localised with early endosomes. Also, uptake of PAAA-X-Bad(140-165) induced a time-dependent release of calcein from endosomes into the cytosol. These results showed that PAAA-X-Bad(140-165) was internalised by constitutive endocytosis and retained the ability to disrupt endosomes. Cells were expected to undergo apoptosis following uptake of PAAA-X-Bad(140-165), however, cell viability was retained. A number of possibilities (discussed in section 5.4) have been proposed to explain why apoptosis was not induced. Experimental strategies to investigate these possibilities are discussed in section 7.1.

Lastly, a new technique was developed to measure MPT in intact cells. Two techniques of measuring MPT in intact cells have previously been described (Nieminen *et al.*, 1995; Minamikawa *et al.*, 1999). However, both these techniques have several disadvantages. The new technique involves loading cells with calcein using the process of pinocytic loading. This technique simultaneously loads millions of cells with calcein, and subsequently visualises mitochondria as darkened voids within a bright green fluorescent cytosol. MPT is measured as an in-filling of the dark voids. This new technique has several advantages compared to the other techniques, including (1) it is applicable to many types of cells, (2) it avoids the use of toxic substances, (3) it avoids potential artefacts arising from quenching of intra-mitochondrial calcein fluorescence,

and (4) it unambiguously identifies the physical movement of calcein across the inner mitochondrial membrane barrier coincident with MPT.

This new technique was initially developed to allow accurate measurement of MPT in intact cells following uptake of PAAA-X-Bad(140-165). Unfortunately, technical limitations prevent the use of this method to measure MPT in cells undergoing apoptosis (see section 6.4). Despite this limitation, this technique will be useful in functional studies of MPT.

7.1 Contributions of this Work

We hypothesised that uptake of PAAA-X-Bad(140-165) into cells by constitutive endocytosis would induce apoptosis, however, this was not the case. Further experiments will be needed to determine why apoptosis was not induced. These experiments could include:

1. Dual staining of PAAA-X-Bad(140-165). PAAA-X could firstly be conjugated with a fluorescent molecule that reacts specifically with carboxyl groups (e.g. 5-(aminoacetamido) fluorescein). Bad(140-165) could then be conjugated to the fluorescently labelled PAAA-X and biotinylated (as described in this thesis). The dual labelled construct could then be introduced into cells by constitutive endocytosis and the location of PAAA and Bad(140-165) traced using confocal microscopy. These experiments would indicate if Bad(140-165) is cleaved from PAAA-X-Bad(140-165) following uptake.
2. Increasing the number of Bad(140-165) molecules released into the cytosol. Assuming complete intracellular cleavage of Bad(140-165) from PAAA-X-Bad(140-165), calculations indicated that the maximum intracellular

concentration of Bad(140-165) delivered by a 20 minute period of constitutive endocytosis of PAAA-X-Bad(140-165) from an external concentration of 200 μg/ml was 4 fold less than the known K_D for the *in vitro* binding of Bad(140-165) to Bcl-X_L (see Discussion in Chapter 5). Increasing the number of hydrazide linkers and/or Bad(140-165) peptides conjugated to PAAA molecules might overcome this potential problem.

3. Determining if Bad(140-165) conjugated to the hydrazide linker alone (X-Bad(140-165)) induces apoptosis. These experiments would indicate if the linker conjugated to Bad(140-165) prevents the interaction of Bad(140-165) with Bcl-X_L and in turn prevents apoptosis. X-Bad(140-165) could be introduced into cells by pinocytic loading (as described in section 6.2.2.1) or using PEP 1. PEP 1 is a 21-mer amphipathic peptide. It has the ability to efficiently deliver a variety of peptides and proteins into several cell types in a fully biological active form, without the need for prior chemical coupling or denaturing steps (Morris *et al.*, 2001). Following introduction of X-Bad(140-165), a variety of assays for apoptosis could be performed, including measurements of mitochondrial depolarisation, MPT, caspase activation, PS exposure and cytochrome c release.

Once the factors(s) responsible for the inability of the initial PAAA-X-Bad(140-165) constructs to induce apoptosis are identified and resolved, the chosen targeting ligand could be conjugated to PAAA-X-Bad(140-165) to produce the desired novel cancer therapeutic (as described in section 1.10). The effects of receptor-mediated endocytosis of the trimolecular construct on cells could then be established using assays similar to those described in this thesis.

At present, cancer is the second most common cause of death in highly developed countries (Szekeres and Novotny, 2002). The development of new cancer therapeutics, to be used in conjunction with traditional treatments, will be invaluable in treating cancer in the future. Hopefully, this thesis will provide information that will aid in the future development of a new and novel cancer therapeutic.

Literature Cited

Akasaki K (1995) Biosynthetic transport of a major lysosomal membrane glycoprotein, lamp-1: convergence of biosynthetic and endocytic pathways occurs at three distinctive points. *Experimental Cell Research* **220**: 464-473

Ali S, Joao H, Hammerschmid F, Eder J and Steinkasserer A (1999) Transferrin trojan horses as a rational approach for the biological delivery of therapeutic peptide domains. *Journal of Biological Chemistry* **274**: 24066-24073

Antonsson B, Conti F, Ciavatta A, Montessuit S, Lewis S, Martinou I, Bernasconi L, Bernard A, Mermod J, Mazzei G, Maundrell K, Gambale F, Sadoul R and Martinou J (1997) Inhibition of Bax channel-forming activity by Bcl-2. *Science* **277**: 370-372

Antunes F, Cadenas E and Brunk U (2001) Apoptosis, induced by exposure to a low steady-state concentration of H_2O_2 is a consequence of lysosomal rupture. *Biochemical Journal* **356**: 549-555

Arap W, Haedicke W, Bernasconi M, Kain R, Rajotte D, Krajewski S, Ellerby H, Bredesen D, Pasqualini R and Ruoslahti E (2002a) Targeting the prostate for destruction through a vascular address. *Proceedings of the National Academy of Sciences of the United States of America* **99**: 1527-1531

Arigita C, Zuidam N, Crommelin D and Hennink W (1999) Association and dissociation characteristics of polymer/DNA complexes used for gene delivery. *Pharmaceutical Research* **16**: 1534-1541

Baell J and Huang D (2002) Prospects for targeting the Bcl-2 family of proteins to develop novel cytotoxic drugs. *Biochemical Pharmacology* **46**: 851-863

Balakirev M and Zimmer G (1998) Gradual changes in permeability of inner mitochondrial membrane precede the mitochondrial permeability transition. *Archives of Biochemistry & Biophysics* **356**: 46-54

Basanez G, Nechushtan A, Drozhinin O, Chanturiya A, Choe E, Tutt S, Wood K, Hsu Y, Zimmerberg J and Youle R (1999) Bax, but not Bcl-xL, decreases the lifetime of planar phospholipid bilayer membranes at subnanomolar concentrations. *Proceedings of the National Academy of Sciences of the United States of America* **96**: 5492-5497

Bernardi P, Petronilli V, Di Lisa F and Forte M (2001) A mitochondrial perspective on cell death. *Trends in Biochemical Sciences* **26**: 112-117

Bi X, Yong A, Zhou J, Gall C and Lynch G (2000) Regionally selective changes in brain lysosomes occur in the transition from young adulthood to middle age in rats. *Neuroscience* **97**: 395-404

Bonneau M and Poulin R (2000) Spermine oxidation leads to necrosis with plasma membrane phosphatidlyserine redistribution in mouse leukaemia cells. *Experimental Cell Research* **259**: 23-34

Boise L and Thompson C (1997) Bcl-x(L) can inhibit apoptosis in cells that have undergone Fas-induced protease activation. *Proceedings of the National Academy of Sciences of the United States of America* **94**: 3759-3764

Bordelon Y, Chesselet M, Erecinska M and Silver I (1998) Effects of intrastriatal injection of quinolinic acid on electrical activity and extracellular ion concentrations in rat striatum in vivo. *Neuroscience* **83**: 459-69

Boussif O, Lezoualc'h F, Zanta M, Mergny M, Scherman D, Demeneix B and Behr J (1995) A versatile vector for gene and oligonucleotide transfer into cells in culture and *in vivo*: polyethylenimine. *Proceedings from the National Academy of Science of the United States of America* **92**: 7297-7301

Boustead C, Brown R and Walker J (1993) Isolation, characterisation and localisation of annexin V from chicken liver. *Biochemical Journal* **291**: 601-608

Boya P, Roques B, and Kroemer G (2001) Bacterial and viral proteins regulating apoptosis at the mitochondrial level. *EMBO Journal* **20**: 4326-4331

Brunk U, Neuzil J and Eaton J (2001) Lysosomal involvement in apoptosis. *Redox Report* **6**: 1-7

Brunk U and Svensson I (1999) Oxidative stress, growth factor starvation and fas activation may all cause apoptosis through lysosomal leak. *Redox Report* **4**: 3-11

Brunmair B, Neschen S, Gras F, Roden M, Norwotny P, Waldhausl W and Furnsinn C (2000) Metabolic response to anisoomolarity or rat skeletal muscle *in vitro*. *Hormone Metabolism Research* **32**: 251-255

Cain C (1989) Regulation of endocytic pH by the Na^+,K^+-ATPase in living cells. *Proceedings of the National Academy of Science of the United States of America* **86**: 544-548

Cande C, Cohen I, Daugas E, Ravagnan L, laochette N, Zamzami N and Kroemer G (2002) Apoptosis inducing factor (AIF): a novel caspase-independent death effector released from mitochondria. *Biochimie* **84**: 215-222

Carter N and Meyer E (1994) Introduction to the Principles of Flow Cytometry *Flow Cytometry: A Practical Approach*. Ed. MG Ormerod. P. 12. Oxford University Press, Oxford, UK

Cassarino D, Parks J, Parker W and Bennett J Jr (1999) The parkinsonian neurotoxin MPP+ opens the mitochondrial permeability transition pore and releases cytochrome c in isolated mitochondria via an oxidative mechanism. *Biochimica et Biophysica Acta*. **1453**: 49-62

Chai J, Du C, Wu J, Kyin S, Wang X and Shi Y (2000) Structural and biochemical basis of apoptotic activation by Smac/DIABLO. *Nature* **406**: 855-862

Chakrabarti R, Pfeiffer N, Wylie D and Schuster S (1989) Incorporation of monoclonal antibodies into cells by osmotic permeabilization. Effect on cellular metabolism. *Journal of Biological Chemistry* **264**: 8214-21

Cheung C, Murthy N, Stayton P and Hoffman A (2001) A pH-sensitive polymer that enhances cationic lipid-mediated gene transfer. *Bioconjugate Chemistry* **12**: 906-910

Clarke H (1998) The introduction of cytochrome into intact cell; influence on apoptosis. *Honours Thesis* Department of Biological Sciences University of Wollongong

Cory S and Adams J (2002) The Bcl2 family: regulators of the cellular life-or-death switch. *Nature Reviews. Cancer* **2**: 647-56

Darynkiewicz Z and Li X (1996) Measurements of flow cytometry techniques in Apoptosis: A User's Giude. Ed. TJ Cotter and SJ Martin. P.73-76. Portland Press Ltd., London, UK.

Datta S, Katsov A, Iiu L, Petros A, Fesik S, Yaffe M and Greenerg M (2000) 14-3-3 proteins and survival kinases cooperate to inactivate BAD by BH3 domain phosphorylation. *Molecular Cell* **6**: 41-51

Daugas E, Nochy D, Ravagnan L, Loeffler M, Susin S, Zamzami N and Kroemer G (2000) Apoptosis-inducing factor (AIF): a ubiquitous mitochondrial oxidoreductase involved in apoptosis. *FEBS Letters* **476**: 118-123

Dengy Y and Wu X (2000) Peg3/Pw1 promotes p53-mediated apoptosis by inducing Bax translocation from cytosol to mitochondria. *Proceedings of the National Academy of Science of the United States of America* **97**: 12050-12055

Desagher S and Martinou J (2000) Mitochondria as the central control point of apoptosis. *Trends in Cell Biology* **10**: 369-377

Devin A, Espie P, Guerin B and Rigoulet M (1998) Energetics of swelling in isolated hepatocyted: a comprehensive study. *Molecular and Cellular Biochemistry* **184**: 107-121

Di Lisa F, Menabo R, Canton M, Barile M and Bernardi P (2001) Opening of the mitochondrial permeability transition pore causes depletion of mitochondrial and cytosolic NAD^+ and is a causative event in the death of myocytes in post-ischemic reperfusion of the heart. *Journal of Biological Chemistry* **276**: 2571-2575

Du C, Fang M, Li Y and Wang X (2000) Smac, a mitochondrial protein that promotes cytochrome c-dependent caspase activation during apoptosis. *Cell* **102**: 33-42

Duncan R (1997) Drug targeting: where are we now and where are we going? *Journal of Drug Targeting* 5:1-4

Duncan R (1992) Drug-polymer conjugates: potential for improved chemotherapy. *Anti-Cancer Drugs* **3**: 175-210

Duncan R, Dimitrijevic S and Evagorou EG (1996) The role of polymer conjugates in the diagnosis and treatment of cancer. *S.T.P. Pharma Sciences* **6**: 237-363

Duncan R, Gac-Breton S, Keane R, Musila R, Sat Y, Satchi R and Searle F (2001) Polymer-drug conjugates, PDEPT and PELT: Basic principles for design and transfer from laboratory to clinic. *Journal of Controlled Release* **74**: 135-146

Etrych T, Jelinkova M, Rihova and Ulbrich K (2001) New HPMA copolymers containing doxorubicin bound via pH-sensitive linkage: synthesis and preliminary *In Vitro* and *In Vivo* biological properties. *Journal of Controlled Release* **73**: 89-102

Ferri K and Kroemer G (2001) Mitochondria - the suicide organelles *Bioessays* **23**: 111-115

Finnegan N, Curtin J, Prevost G, Morgan B and Cotter T (2001) Induction of apoptosis in prostate carcinoma cells by BH3 peptides which inhibit Bak/Bcl-2 interactions. *British Journal of Cancer* **85**: 115-121

Finucance D, Bossy-Wetzel E, Waterhouse N, Cotter T and Green D (1999) Bax-induced caspases activation and apoptosis via cytochrome c release from mitochondria is inhibitable by Bcl-xL. *Journal of Biological Chemistry* **274**: 2225-2233

Flores A and Macklin W (2000) Akt-mediated survial of oligodendrocytes induced by neuregulins. *Journal of Neuroscience* **20**: 7622-7630

Fonseca M, Storm G, Hennink W, Gerritsen W and Haisma H (1999) Cationic polymeric gene delivery of beta-glucuronidase for doxorubicin prodrug therapy. *Journal of Gene Medicine* **1**: 407-14

Frey T and Mannella C (2000) The internal structure of mitochondria. *Trends in Biochemical Science* **25**: 319-324

Funhoff A, Van Nostrum C, Koning G, Schuurmans-Niewenbroek N, Crommelin D and Hennink W (2003) Endosomal escape of polymeric gene delivery complexes is not always enhanced by polymers buffering at low pH. *In press*

Fulda S, Scaffidi C, Susin S, Krammer P, Kroemer G, Peter M and Debatin K (1999) Activation of mitochondria and release of mitochondrial apoptogenic factors by betulinic acid. *Journal of Biological Chemistry* **273**: 33942-8

Gardner A, Xu F, Fady C, Jacoby F, Duffey D, Tu Y and Lichtenstein A (1997) Apoptotic vs nonapoptotic cytoxicity induced by hydrogen peroxide. *Free Radical Biology and Medicine* **22**: 73-83

Gastman B (2001) Apoptosis and its clinical impact. *Head and Neck* **23**: 409-425

Gilmore K, Quinn H and Wilson M (2001) Pinocytic loading of cytochrome c into intact cells specifically induces caspase-dependent permeabilization of mitochondrial: evidence for a cytochrome c feedback loop. *Cell Death and Differentiation* **8**: 631-639

Goldstein J, Waterhouse N, Juin P, Evan G and Green D (2000) The coordinate release of cytochrome c during apoptosis is rapid, complete and kinetically invariant. *Nature Cell Biology* **2**: 156-62

Gottlieb E, Vander Heiden M and Thompson C (2000) Bcl-xL prevents the initial decrease in mitochondrial potential and subsequent reactive oxygen species production during tumour necrosis factor alpha-induced apoptosis. *Molecular and Cellular Biology* **20**: 5680-5689

Granger B (1990) Characterization and cloning of lgp110, a lysosomal membrane glycoprotein from mouse and rat cells. *Journal of Biological Chemistry* **265**: 12036-12043

Green D and Evan G (2002) A matter of life and death. *Cancer Cell* **1**: 19-30

Green D and Kroemer G (1998) The central executioners of apoptosis: caspases or mitochondria? *Trends in Cell Biology* **8**: 267-271

Green D and Reed J (1998) Mitochondria and apoptosis. *Science* **5381**: 1309-1312

Goping I, Gross A, Lavoie J, Nguyen M, Jemmerson R, Roth K, Korsmeyer S and Shore G (1998) Regulated targeting of BAX to mitochondria. *Journal of Cell Biology* **143**: 207-215

Gross A, Jockel J, Wei M and Korsmeyer S (1998) Enforced dimerization of BAX results in its translocation, mitochondrial dysfunction and apoptosis. *EMBO* **17**: 3878-3885

Gross A, McDonnell J and Korsmeyer S (1999) Bcl-2 family members and the mitochondria in apoptosis. *Genes and Development* **381**: 335-341

Guicciardi M, Deussing J, Miyochi H, Bronk S, Svingen D, Peters C, Kaufmann S and Gores G (2000) Cathepsin B contributes to TNF-Alpha mediated hepatocyte apoptosis by promoting mitochondrial release of cytochrome c. *Journal of Clinical Investigation* **106**: 1127-1137

Harris M and Thompson C (2000) The role of the Bcl-2 family in the regulation of outer mitochondrial membrane permeability. *Cell Death & Differentiation.* **7**: 1182-1191

Hegde R, Srinivasula S, Zhang Z, Wassell R, Mukattash R, Cilenti L, DuBois G, Lazebnik Y, Zervos A, Fernandes-Alnemri T and Alnemri E (2002) Identification of Omi/HtrA2 as a mitochondrial apoptotic serine protease that disrupts inhibitor of apoptosis protein-caspase interaction. *Journal of Biological Chemistry* **277**: 432-438

Heiskanen K, Bhat M, Wang H, Ma J and Nieminen A (1999) Mitochondrial depolarization accompanies cytochrome c release during apoptosis in PC6 cells. *Journal of Biological Chemistry* **274**: 5654-5658

Hellquist H, Svensson I, Brunk U (1997) Oxidant-induced apoptosis: A consequence of lethal lysosomal leak. *Redox Report* **3**: 65-70

Hengartner M (2000) The biochemistry of apoptosis. *Nature* **407**: 770-776

Hirsch T, Marzo I and Kroemer G (1997) Role of the mitochondrial permeability transition pore in apoptosis. *Bioscience Reports* **17**: 67-76

Hsu Y, Wolter K and Youle R (1997) Cytosol-to membrane redistribution of Bax and Bcl-xL during apoptosis. *Proceedings of the National Academy of Sciences of the United States of America* **94**: 3668-3672

Hughes J, Aronsohn A, Avrutskaya A and Juliano R (1996) Evaluation of adjuvants that enhance the effectiveness of antisense oligodeoxynucleotides. *Pharmaceutical Research* **13**: 404-10

Huser J, Rechenmacher C and Blatter L (1998) Imaging the permeability pore transition in single mitochondria. *Biophysical Journal* **74**: 2129-2137

Ichas F, Jouaville L and Mazat J (1997) Mitochondria are excitable organelles capable of generating and conveying electrical and calcium signals. *Cell* **89**: 1145-1153

Igney F and Krammer P (2002) Death ad anti-death:tumour resistance to apoptosis. *Nature Reviews* **2**: 277-288

Jones R, Cheung C, Black F, Zia J, Stayton P, Hoffman A and Wilson M (2003) Poly(2-alkylacrylic acid) polymers deliver molecules to the cytosol by pH-sensitive disruption of endosomal vesicles. *Biochemical Journal* **372**: 65-75

Kagedal K, Zhao M, Svensson I and Brunk U (2001) Sphingosine-induced apoptosis in dependent of lysosomal proteases. *Biochemical Journal* **359**: 335-343

Kelekar A, Chang B, Harlan J, Fesik S and Thompson C (1997) Bad is a BH3 domain-containing protein that forms an inactivating dimer with Bcl-xL. *Molecular and Cellular Biology* **17**: 7040-7046

Kelekar A and Thompson C (1998) Bcl-2-family proteins: The role of the BH3 domain in apoptosis. *Trends in Cell Biology* **8**: 324-330

Kerr J (1995) Neglected opportunities in apoptosis research. *Trends in Cell Biology* **5**: 55-57

Kessel D and Horwitz J (2001) Pro-apoptotic interactions between XK469 and the peripheral benzodiazepine receptor. *Cancer Letters* **168**: 141-144

Kim J and Tirrell D (1999) Synthesis of well-defined poly(2-ethylacrylic acid). *Macromolecules* **32**: 945-948

Kluck R, Bossy-Wetzel E, Green D and Newmeyer D (1997) The release of cytochrome c from mitochondria: a primary site for Bcl-2 regulation of apoptosis. *Science* **275**: 1132-1136

Knudson C and Kormeyer S (1997) Bcl-2 and Bax function independently to regulate cell death. *Nature Genetics* **16**: 358-363

Kratz F, Beyer U and Schutte M (1999) Drug-polymer conjugates containing acid-cleavable bonds. *Critical Reviews in Therapeutic Drug Carrier Systems* **16**: 245-88

Kreitman R (1999) Immunotoxins in cancer therapy. *Current Opinion in Immunology* **11**: 570-578

Kroemer G, Dallaporta B and Resche-Rigon M (1998) The mitochondrial death/life regulator in apoptosis. *Annual Review of Physiology* **60**: 619-642

Kroemer G, Petit P, Zamzami N, Vayssiere J-L and Mignotte B (1995) The biochemistry of programmed cell death. *The FASEB Journal* **9**: 1277-1287

Kroemer G and Reed D (2000) Mitochondrial control of cell death. *Nature Medicine* **6**: 513-519

Kroemer G, Zamzami N and Susin S (1997) Mitochondrial control of apoptosis. *Immunology Today* **18**: 44-51

Lackey C, Murthy N, Press O, Tirrell D, Hoffman A and Stayton P (1999) Hemolytic activity of pH-responsive polymer-streptavidin bioconjugates. *Bioconjugate Chemistry* **10**: 401-405

Lackey C, Press O, Hoffman A and Stayton P (2002) A biometric pH-responsive polymer directs endosomal release and intracellular delivery of an endocytosed antibody complex. *Bioconjugate Chemistry* **13**: 996-1001

Lau A, Berube G and Ford C (1995a) Conjugation of doxorubicin to monoclonal anti-carcinoembryonic antigen antibody via novel thiol-directed cross-linking reagents. *Bioorganic and Medicinal Chemistry* **3**: 1299-1304

Lau A, Berube G, Ford C and Gallant M (1995b) Novel doxorubicin-monoclonal anti-carcinoembryonic antigen antibody immunoconjugate activity *in vitro*. *Bioorganic and Medicinal Chemistry* **3**: 1305-1312

Lemasters, J, Nieminen A, Qian T, Trost, L Elmore S, Nishimura Y, Crowe R, Cascio W, Bradham C, Brenner D and Herman B (1998) The mitochondrial permeability transition in cell death- a common mechanism in necrosis, apoptosis and autophagy. *Biochimica et Biophysica Acta* **1366**: 177-196

Lemasters J, Qian T, Trost L, Herman B, Cascio W, Bradham C, Brenner D and Niemen A (1999) Confocal microscopy of the mitochondrial permeability transition in necrotic and apoptotic cell death. *Biochemical Society Symposia* **66**: 205-222

Li H, Kolluri S, Gu J, Dawson M, Cao X, Hobbs P, Lin B, Chen G, Lu J, Lin F, Xie Z, Fontana J, Reed J and Zhang X (2000) Cytochrome c release and apoptosis induced by mitochondrial targeting of nuclear orphan receptor TR3. *Science* **289**: 1159-1164

Li K, Li Y, Shelton J, Richardson J, Spencer E, Chen Z, Wang X and Williams R (2000) Cytochrome c deficiency causes embryonic lethality and attenuates stress-induced apoptosis. *Cell* **101**:389-99

Li S, Zhao Y, He X, Kim T, Kuharsky D, Rabinowich H, Chen J, Du C and Yin X (2002) Relief of extrinsic pathway inhibition by Bid-dependent mitochondrial release of Smac in Fas-mediated hepatocyte apoptosis. *Journal of Biological Chemistry* **277**: 26912-26920

Li W, Yuan X, Nordgren G, Dalen H, Dubowchik G, Firestone R and Brunk U (2000) Induction of cell death by the lysosomotropic detergent MSDH. *FEBS Letters* **470**: 35-39

Linhardt J, Thomas J and Tirrell D (1999) Free-radical synthesis of poly(2-ethylacrylic acid) fractions of low polydispersity: Effects of molecular weight and polydispersity on the pH-dependent conformational transition in aqueous solutions. *Macromolecules* **32**: 4457-4459

Linhardt J and Tirrell D (1999) Free radical synthesis of poly(2-ethylacrylic acid) fractions of low polydispersity: effects of molecular weight and polydispersity on the pH-dependent conformational transition in aqueous solutions. *Macromolecules* **32**: 4457-4459

Linhardt J and Tirrell D (2000) pH induced fusion and lysis of phosphatidylcholine vesicles by the hydrophobic polyelectrolyte poly(2-ethylacrylic acid). *Langmuir* **16**: 122-127

Liu X, Zou H, Slaughter C and Wang X (1997) DFF a heterodimeric protein that functions downstream of caspase-3 to trigger DNA fragmentation during apoptosis. *Cell* **89**: 175-184

Liu Z, Sun C, Olejniczak E, Meadows R, Betz S, Oost T, Herrmann J, Wu J and Fesik S (2000) Structural basis for binding of Smac/DIABLO to the XIAP BIR3 domain. *Nature*. **408**: 1004-8

Loadman P, Bibby M, Double J, Al-Shakhaa W and Duncan R (1999) Pharmacokinetics of PK1 and doxorubicin in experimental colon tumour models with differing responses to PK1. *Clinical Cancer Research* **5**: 3682-3688

Loeffler M and Kroemer G (2000) The mitochondrion in cell death control: certainties and incognita. *Experimental Cell Research* **256**: 19-26

Lorenzo H, Susin A, Penninger J and Kroemer G (1999) Apoptosis inducing factor (AIF): a phylogenetically old, caspase-independent effector of cell death. *Cell Death and Differentiation* **6**: 516-524

Luo Y and Prestwich G (2002) Cancer-targeted polymeric drugs. *Current Cancer Drug Targets* **2**: 209:226

Maeda H (2001) SMANCS and polymer-conjugated macromolecular drugs: advantages in cancer chemotherapy. *Advanced Drug Delivery Reviews* **46**: 169-185

Maeda H, Sano Y, Takeshita J, Iwai Z, Kosaka T, Marubayashi Y and Matsukado A (1981) A pharmacokinetic simulation model for chemotherapy of brain tumour with an antitumour protein antibiotic, necarzinostatin. Theoretical considerations behind a two-compartment model for continuous infusion via an internal carotid artery. *Cancer Chemotherapy and Pharmacology* **5**: 243-249

Maeda H, Sawa T and Konno T (2001) Mechanism of tumour-targeted delivery of macromolecular drugs, including the EPR effect in solid tumour and clinical overview of the prototype polymeric drug SMANCS. *Journal of Controlled Release* **74**: 47-61

Mai J, Mi Z, Kim S, Ng B and Robbins P (2001) A proapoptotic peptide for the treatment of solid tumours. *Cancer Research* **61**: 7709-7712

Mancini M, Machamer C, Roy S, Nicholson D, Thornberry N, Casciola-Rosen L and Rosen A (2000) Caspase-2 is localized at the Golgi complex and cleaves golgin-160 during apoptosis. *Journal of Cell Biology* **149**: 603-612

Marchetti P, Castedo M, Susin S, Zamzami N, Hirsch T, Macho A, Haeffner A, Hirsch F, Geuskens M and Kroemer G (1996) Mitochondrial permeability transition is a central coordinating event in apoptosis. *Journal of Experimental Medicine* **184**: 1155-1160

Martin S, Finucane D, Amarante-Mendes G, O'Brien G and Green D (1996) Phosphatidylserine externalisation during CD95-induced apoptosis of cells and cytoplasts requires ICE/CED-3 protease activity. *Journal of Biological Chemistry* **271**: 28753-28756

Martins L, Iaccarino I, Tenev T, Gschmeissner S, Totty N, Lemoine N, Savopoulos J, Gray C, Creasy C, Dingwall C and Downward J (2002) The serine protease Omi/HtrA2 regulates apoptosis by binding XIAP through a reaper-like motif. *Journal of Biological Chemistry* **277**: 439-444

McLaughlin B, Nelson D, Silver I, Erecinska M and Chesslet M (1998) Methylmalonate toxicity in primary neuronal cultures. *Neuroscience* **86**: 276-290

Mechtold B and Radbruch A (1992) Glossary in flow cytometry and cell sorting. Ed. A Radbruch. P.212. Springer Verlag, Berlin, Germany

Meers P and Mealy T (1993) Calcium-dependent annexin V binding to phospholipids: stoichiometry, specificity, and the role of negative charge. *Biochemistry* **32**:11711-21

Meers P and Mealy T (1994) Phospholipid determinants for annexin V binding sites and the role of tryptophane 187. *Biochemistry* **33**: 5829-5837

Mehendale H, Roth R, Gandolfi A, Klaunig J and Lemasters J (1994) Novel mechanism in chemically induced hepatotoxicity. *The FASEB Journal* **8**:1285-1295

Mellman I (1996) Endocytosis and molecular sorting. *Annual Review of Cell and Developmental Biology* **12**: 575-625

Meyer O, Papahadjopulos D, Leroux J (1998) Copolymers of N-isopropylacrylamide can trigger pH sensitivity to stable liposomes. *FEBS* **421**: 61-64

Mignotte B and Vayssiere J (1998) Mitochondria and apoptosis. *European Journal of Biochemistry* **252**: 1-15

Miller L (1999) An exegesis of IAPs: salvation and surprises from BIR motifs. *Trends in Cell Biology* **9**: 323-328

Minamikawa T, Sriratana A, Williams D, Bowser D, Hill J and Nagley P (1999) Chloromethyl-X-rosamine (mitoTracker Red) photosensitises mitochondria and induces apoptosis in intact human cells. *Journal of Cell Science* **112**: 2419-2430

Minamikawa T, Williams D, Bowser D and Nagley P (1999) Mitochondrial permeability transition and swelling can occur reversibly without inducing cell death in intact human cells. *Experimental Cell Research* **246**: 26-37

Monsees T, Winterstein U, Hayatpour J, Schill W and Miska W (1998) Effect of heavy metals on the secretory function of testicular cells in culture. *Journal of Trace Microprobe Technology* **16**: 427-435

Morris M, Depollier J, Mery J, Heitz F and Divita G (2001) A peptide carrier for the delivery of biologically active proteins into mammalian cells. *Nature Biotechnology* **19**: 1173-1176

Muchmore S, Sattler M, Liang H, Meadows R, Harlan J, Yoon H, Netteshein D, Chang B, Thompson C, Wong S, Ng S and Fesik S (1996) X-ray and NMR structure of human Bcl-xL, an inhibitor of programmed cell death. *Nature* **381**: 335-341

Mukherjee S, Ghosh R and Maxfielf F (1997) Endocytosis. *Physiological Reviews* **77**: 759-803

Murthy N, Robichaud J, Tirrell D, Stayton P, Hoffman S (1999) The design and synthesis of polymers for eukaryotic membrane disruption. *Journal of Controlled Release* **61**: 137-143

Muzio M, Stockwell B, Stennicke H, Salvesen G and Dixit V (1998) An induced proximity model of caspase-8 activation. *Journal of Biological Chemistry* **273**: 2926-2930

Narita M, Shimizu S, Ito T, Chittenden T, Lutz R, Matsuda H and Tsujimoto Y (1998) Bax interacts with the permeability transition pore to induce permeability transition and cytochrome c release in isolated mitochondria. *Proceedings of the National Academy of Sciences of the United States of America* **95**:*14681-14686*

Neuzil J, Svesson I, Weber T, Weber C and Brunk U (1999) Alpha- tocopheyl succinate-induced apoptosis in Jurkat T cells involves caspase-3 activation and both lysosomal and mitochondrial destabilisation. *FEBS Letters* **445**: 295-300

Ng S, Nguyen M, Kwan T, Brantob P, Nicholson P, Comlish J and Shore G (1997) T28 Bap 31 a Bcl2/Bclx$_L$ pro-caspase-8-associated protein in the endoplasmic reticulum. *Journal of Cell Biology* **139**: 327-338

Nieminen A, Byrne A, Herman B and Lemasters J (1997) Mitochondrial permeability transition in hepatocytes induced by t-BuOOH-HAD(P)H and reactive oxygen species. *American Journal of Physiology* **41**: C1286-C1294

Nieminen A, Saylor A, Tesfai S, Herman B and Lemasters J (1995) Contribution of the mitochondrial permeability transition to lethal injury after exposure of hepatocytes to *t*-butylhydroperoxide. *Biochemical Journal* **307**: 99-106

Normura M, Shimizu S, Ito T, Narita M, Matsuda H and Tsujimoto Y (1999) Apoptotic cytosol facilitates Bax translocation to mitochondria that involves cytosolic factor regulated by Bcl-2. *Cancer Research* **59**: 5542-5548

Ohkuma S, Shimizu S, Noto M, Sai Y, Kinoshita K and Tamura H (1993) Inhibition of cell growth by bafilomycin A (1), a selective inhibitor of vacuolar H^+-ATPase. *In Vitro Cell and Development Biology* **29A**: 862-866

Okada C and Rechsteiner M (1982) Introduction of macromolecules into cultured mammalian cells by osmotic lysis of pinocytic vesicles. *Cell* **29**: 33-41

Okazaki K, Endou M and Okumura F (1998) Involvement of barium-sensitive K+ channels in endothelium-dependent vasodilation produced by hypercapnia in rat mesenteric vascular beds. *British Journal of Pharmacology* **125**: 168-74

Olejnicka B, Dalen H and Brunk U (1999) Minute oxidative stress is sufficient to induce apoptotic death of NIT-1 insulinoma cells. *APMIS* **107**: 747-761

Orth M and Schapira A (2001) Mitochondria and degenerative disorders. *American Journal of Medical Genetics* **106**: 27-36

Ott M, Robertson J, Gogvade V, Zhivotovsky B and Orrenius S (2002) Cytochrome c release from mitochondria proceeds by a two-step process. *Proceedings of the national Academy of Sciences of the United States of America* **99**: 1259-1263

Ouwens D, Gomes de Mesquita D, Dekker J and Maassen J (2001) Hyperosmotic stress activates the insulin receptor in CHO cells. *Biochimica et Biophysica Acta.* **1540**: 97-106

Paddock S (1999) An introduction to confocal imaging *in* methods in molecular biology, Vol. 122: Confocal microscopy: Methods and protocols. Ed. SW Paddock. P.1-2. Hummana press Inc., New Jersey, USA

Pan G, Himke E and Dixit V (1998) Activation of caspases triggered by cytochrome c *In Vitro*. *FEBS Letters* **426**: 151-154

Parone P, James D and Martinou J (2002) Mitochondria: regulating the inevitable. *Biochimie* **84**: 105-111

Pastorino J, Chen S, Tafani M, Snyder J and Farber J (1998) The over-expression of Bax produces cell death upon induction of the mitochondrial permeability transition. *Journal of Biological Chemistry* **273**: 7770-7775

Patel T, Gores G and Kaufmann S (1996) The role of proteases during apoptosis. *The FASEB Journal* **10**: 587-597

Perkins D, Pereira E and Aurelain L (2003) A herpes simplex virus type 2 protein (ICP10 PK) inhibits caspase-activation in hippocampal neurons. *Journal of Virology* **77**: 1292-1305

Petit P, Susin S, Zamzami N, Mignotte B and Kroemer G (1996) Mitochondria and programmed cell death: Back to the future. *FEBS Letters* **396**: 7-13

Petronilli V, Miotto G, Canton M, Brini M, Colonna R, Bernardi P and Di Lisa F (1999) Transient and long-lasting openings of the mitochondrial permeability transition pore can be monitored directly in intact cells by changes in mitochondrial calcein fluorescence. *Biophysical Journal* **76**: 725-734

Pimm M, Perkins A, Strohalm J, Ulbrich K and Duncan R (1996) Gamma scintigraphy of the biodistribution of ^{123}I-Labelled N-(2 Hydroxypropyl)methacrylamide copolymer-doxorubicin conjugates in mice with transplanted melanoma and mammary carcinoma. *Journal of Drug Targeting* **3**: 375-383

Plank C, Oberhauser B, Mechtler K, Koch C and Wagner E (1994) The influence of endosome-disruptive peptides on gene transfer using synthetic virus-like gene transfer systems. *Journal of Biological Chemistry* **269**: 12918-12924

Polster B, Kinnally K and Fiskum G (2001) BH3 death domain peptide induces cell type-selective mitochondrial outer membrane permeability. *The Journal of Biological Chemistry* **276**: 37887-37894

Poniris M (2001) Preliminary work towards a pro-apoptotic cancer therapeutic based on a synthetic polymer. *Honours Thesis* Department of Biological Sciences, University of Wollongong

Raso V, Brown M, McGrath J, Liu S and Stafford W (1997a) Antibodies capable of releasing diptheria toxin in response to low pH found in endosomes. *Journal of Biological Chemistry* **272**: 27618-27622

Raso V, Brown M and McGarth J (1997b) Intracellular targeting with low pH triggered bispecific antibodies. *Journal of Biological Chemistry* **272**: 27623-27628

Reed J (1997) Double identity for proteins of the Bcl-2 family. *Nature* **387**: 773-776

Reed J (2002) Apoptosis-targeted therapies for cancer. *Cancer Cell* **3**: 17-22

Rigobello M, Scutari G, Friso A, Barzon E, Artusi S and Bindoli A (1999) Mitochondrial permeability transition and release of cytochrome c induced by retinoic acids. *Biochemical Pharmacology* **58**: 665-670

Roberg K (2001) Relocalization of cathepsin D and cytochrome c early in apoptosis revealed by immunoelectron microscopy. *Laboratory Investigation.* **81**: 149-58

Roberg K, Johansson U and Ollinger K (1999) Lysosomal release of cathepsin D precedes relocation of cytochrome c and loss of mitochondrial transmembrane potential during apoptosis induced by oxidative stress. *Free Radical Biology and Medicine* **27**: 1228-1237

Roberts L, Kurosawa H, Bronk S, Fesmier P, Agellon L, Leung W, Mao F and Gores G (1997) Cathepsin B contributes to bile salt-induced apoptosis of rat hepatocytes. *Gastroenterology* **113**: 1714-26

Rodriguez J and Lazebnik Y (1999) Caspase-9 and apaf-1 form an active holoenzyme. *Genes and Development* **13**: 3179-3184

Ruttter G and Rizzuto R (2000) Regulation of mitochondrial metabolism by ER Ca2+ release: an intimate connection. *Trends in Biochemical Science* **25**: 215-221

Saleh A, Srinivasula S, Acharya S, Fishel R and Alnemri E (1999) Cytochrome c and dATP-mediated oligomerization of apaf-1 is a prerequisite for procaspase-9 activation. *Journal of Biological Chemistry* **274**: 17941-17945

Scheffler I (2001) Mitochondria make a come back. *Advanced Drug Delivery Reviews* **49**: 3-26

Schoonderwoert V, Holthuis J, Tanaka S, Tooze S and Martens G (2000) Inhibition of the vacuolar H+-ATPase perturbs the transport, sorting, processing and release of regulated secretory proteins. *European Journal of Biochemistry* **267**: 5646-54

Schotte P, Van Criekinge W, Van de Craen M, Van Loo G, Desmedt M, Grooten J, Cornelissen M, De Ridder L, Vandekerckhove J, Fiers W, Vandenabeele P and Beyaert R (1998) Cathepsin B-mediated activation of the proinflammatory caspase-11. *Biochemical & Biophysical Research Communications* **251**: 379-87

Seaman, M. N. J. and Luzio, J. P. (2001) Lysosomes and other late compartments of the endocytic pathway. In: Endocytosis (Marsh, M., Ed.), pp. 111-148, Oxford University Press, London

Sedlak T, Oltvai Z, Yang E, Wang K, Boise L, Thompson C and Korsmeyer S (1995) Multiple Bcl-2 family members demonstrate selective dimerization with Bax. *Proceedings from the National Academy of Sciences of the United States of America* **92**: 7834-7838

Seymour L (1991) Synthetic polymers with intrinsic anticancer activity. *Journal of Bioactive and Compatible Polymers* **6**: 178-216

Skulachev V (1996) Why are mitochondria involved in apoptosis? Permeability transition pores and apoptosis as selective mechanisms to eliminate superoxide-producing mitochondria and cell. *FEBS Letters* **397**: 7-10

Shi Y (2001) A structural view of mitochondria-mediated apoptosis. *Nature Structural Biology* **8**: 394-401

Shimizu S, Ide T, Yanagida T and Tsujimoto Y (2000) Electrophysiological study of a novel large pore formed by Bax and the voltage-dependent anion channel that is permeable to cytochrome c. *Journal of Biological Chemistry* **275**: 12321-12325

Shimizu S, Narita M and Tsujimoto Y (1999) Bcl-2 family proteins regulate the release of apoptogenic cytochrome c by the mitochondrial channel VDAC. *Nature* **399**: 483-487

Stayton R, Hoffman A, Murthy N, Lackey C, Cheung C, Tan P, Klimb L, Chilkoti F, Wilbur S and Press, O (2000) Molecular engineering of proteins and polymers for targeting and intracellular delivery of therapeutics. *Journal of Controlled Release* **65**: 203-220

Steller H (1995) Mechanisms and genes of cellular suicide. *Science* **267**: 1445-1449

Stoka V, Turk B, Schendel S, Kim TH, Cirman T, Snipas S, Ellerby L, Bredesen D, Freeze H, Abrahamson M, Bomme D, Krajewski S, Reed J, Yin X, Turk V and Salvesen G (2001) Lysosomal protease pathways to apoptosis. *Journal of Biological Chemistry* **276**: 3149-3157

Sullivan P (1987) Effects of temperature, pH elevators, and energy production inhibitors on horseradish peroxidase transport through endocytic vesicles. *Journal of Cell Physiology* **131**: 58-63

Susin S, Lorenzo H, Zamzami N, Marzo I, Brenner C, Larocrette N, Prevost M, Alzari P and Kroemer G (1999a) Mitochondrial release of caspase-2 and –9 during the apoptotic process. *Journal of Experimental Medicine* **189**: 381-394

Susin S, Zamzami N, Castedo M, Daugas E, Wang H, Geley S, Fassy F, Reed J and Kroemer G (1997) The central executioner of apoptosis-multiple connections between protease activation and mitochondria in Fas-Apo-1 / CD95- and ceramide-induced apoptosis. *Journal of Experimental Medicine* **186**: 25-37

Szekeres T and Novotny L (2002) New targets and drugs in cancer chemotherapy. *Medical Principles and Practice* **11**: 117-125

Terman A, Abrahamsson N and Brunk U (1999) Ceroid/lipofuscin-loaded human fibroblasts show increased susceptibility to oxidative stress. *Experimental Gerontology.* **34**: 755-70

Terman A, Dalen H and Brunk U (1999) Ceriod/lipofusion-loaded human fibroblasts show decreased survival time and diminished autophagocytosis during amino acid starvation. *Experimental Gerontology* **34**: 943-957

Thompson C (1995) Apoptosis in the pathogenesis and treatment of disease. *Science* **267**: 1456-1462

Tolstikov V, Cole R, Fang H and Dincus S (1997) Influence of endosome destabilising peptides in efficacy of anti-HIV immunotoxins. *Bioconjugate Chemistry* **8**: 38-43

Trail P and Bianchi A (1999) Monoclonal antibody drug conjugates in treatment of cancer. *Current Opinion In Immunology* **11**: 584-588

Tsujimoto Y and Shimizu S (2000) VDAC regulation by the Bcl-2 family of proteins. *Cell Death & Differentiation* **7**: 1174-1181

Ulbrich K, Strohalm J, Subr v and Plocova D (1996) Polymeric conjugated of drug and antibodies for site-specific drug delivery. *Macromolecular Symposium* **103**: 177-192

Ultee A, Kets E and Smid E (1999) Mechanisms of action of carvacrol on the food-borne pathogen Bacillus cereus. *Applied & Environmental Microbiology* **65**: 4606-4610

Vander Heiden M, Chandel N, Williamson E, Schumacker P and Thompson C (1997) Bcl-x_L regulates the membrane potential and volume homeostasis of mitochondria. *Cell* **91**: 627-637

Vandeurs B, Holm PK and Sandvig K (1996) Inhibition of the vascular H^+-ATPase with bafilomycin reduces delivery of internalised molecules from mature multivescular endosomes to lysosomes in Hep-2 cells. *European Journal of Cell Biology* **69**: 343-350

Van de Wetering P, Moret E, Schuurmans-Nieuwenbroek E, van Steenbergen M and Hennik W (1999) Structure-activity relationships of water-soluble cationic methacrylate/methacrylamide polymers for nonviral gene delivery. *Bioconjugate Chemistry* **10**: 589-597

Van Loo G, van Gurp B, Depuydt S, Srinivasula I, Rodriguez E, Alnemri K, Gevaert J, Vandekerckhove W, Declercq and Vandenabeele P (2002) The serine protease Omi/HtrA2 is released from mitochondria during apoptosis. Omi interacts with caspase-inhibitor XIAP and induces enhanced caspase activity *Cell Death & Differentiation* **9**: 20-26

Van Steenis J, van Maarseveen W, Verbaan F, Verrijk R, Crommelin D, Storm G and Hennink W (2003) Preparation and characterization of folate-targeted pEG-coated pDMAEMA-based polyplexes. *Journal of Controlled Release* **87**: 167-176

Vaux D and Strasser A (1996) The molecular biology of apoptosis. *Proceedings of the National Academy of Sciences of the United States of America* **93**: 2239-2244

Verhagen A, Ekert P, Pakusch M, Silke J, Connolly L, Reid G, Moritz R, Simpson R and Vaux D (2000) Identification of DIABLO, a mammalian protein that promotes apoptosis by binding to and antagonizing IAP proteins. *Cell* **102**: 43-53

Verhagen A, Silke J, Ekert P, Pakusch M, Kaufmann H, Connolly L, Day C, Tikoo A, Burke R, Wrobel C, Moritz R, Simpson R and Vaux D (2002) HtrA2 promotes cell death through its serine protease activity and its ability to antagonize inhibitor of apoptosis proteins. *Journal of Biological Chemistry* **277**: 445-54

Villa P, Kaufmann S and Earnshaw W (1997) Caspases and caspase inhibitors. *Trends in Biological Sciences* **22**: 388-393

Waterhouse. N, Ricci J and Green D (2002) And all of a sudden it is over: mitochondrial outer membrane permeabilzation in apoptosis. *Biochimie* **84**: 113-121

Waring P, Lambert D, Sjaarda A, Hurne A and Beaver J (1999) Increased cell surface exposure of phosphatidylserine on propidium iodide negative thymocytes undergoing death by necrosis. *Cell Death and Differentiation* **6**: 624-637

White E (1993) Death-defying acts: a meeting review on apoptosis. *Genes and Development* **7**: 2277-2284

Wilson M (1998) Apoptosis: unmasking the executioner. *Cell Death and Differentiation* **5**: 646-652

Wood (2000) Development of a novel cancer therapeutic involving the targeted delivery of pro-apoptotic peptides. *Honours Thesis* Department of Biological Sciences, University of Wollongong

Wu G, Chai J, Suber T, Wu J, Du C, Wang X and Shi Y (2000) Structural basis of IAP recognition by Smac/DIABLO. *Nature **408***: 1008-12

Yang J, Liu X, Bhalla K, Kim C, Ibrado A, Cai J, Peng T, Jones D and Wang X (1997) Prevention of apoptosis by Bcl-2: release of cytochrome c from mitochondria blocked. *Science* **275**: 1129-1132

Ye H, Cande C, stephanou NC, Jiang S, Gurbuxani S, Larochette N, Daudas F, Garrido C, Kroemer G and Wu H (2002) DNA binding is required for the apoptogenic action of apoptosis inducing factor. *Nature Structural Biology* **9**: 680-684

Yin X (2000) Signal transduction mediated by Bid, a pro-death Bcl-2 family proteins, connects the death receptor and mitochondria apoptosis pathway. *Cell Research* **10**:161-167

Zamai L, Falcieri E, Marhefka G and Vitale M (1996) Supravital exposure to propidium iodide identifies apoptotic cells in the absence of nucleosomal DNA fragmentation. *Cytometry* **23**: 303-311

Zamzami N, Brenner C, Marzo I, Susin S and Kroemer G (1998) Subcellular and submitochondrial mode of action of Bcl-2-like oncoproteins. *Oncogene* **16**: 2265-82

Zamzami N, Hirsch T, Dallaporta B, Petit P and Kroemer G (1997) Mitochondrial implication in accidental and programmed cell death: apoptosis and necrosis. *Journal of Bioenergetics and Biomembranes* **29**: 185-192

Zamzami N, Marzo I, Susin S, Brenner C, Larochette N, Marchetti P, Reed J, Kofler R and Kroemer G (1998) The thiol crosslinking agent diamide overcomes the apoptosis-inhibitory effect of Bcl-2 by enforcing mitochondrial permeability transition. *Oncogene* **16**: 10551063

Zelenin A (1999) Acridine orange as a probe for cell and molecular biology. In: fluorescent and luminescent probes (Mason, W. T., Ed.), pp. 117-135, Academic Press, Sydney

Zhai D, Huang X, Han X and Yang F (2000) Characterisation of tBid-induced cytochrome c release from mitochondria and liposomes. *FEBS Letters* **472**: 293-296

Zhao M, Eaton J and Brunk U (2000) Protection against oxidant-mediated lysosomal rupture: A new anti-apoptotic activity of Bcl-2? *FEBS Letters* **485**: 104-108

Zhuang J and Cohen M (1998) Release of mitochondrial cytochrome c is upstream of caspase activation in chemical-induced apoptosis in human monocytic tumour cells. *Toxicology Letters* **103**: 121-129

Zoratti M and Szabo I (1995) The mitochondrial permeability transition. *Biochimica et Biophysica Acta* **1241**: 139-179

Zou H, Li Y, Lui X and Wang X (1999) An Apaf-1-cytochrome c multiplex complex is a functional apoptosomes that activates procaspases-9. *Journal of Biological Chemistry* **274**: 11549-11556

Zuidam N, Posthuma G, de Vries E, Crommelin D, Hennink W and Storm G (2000) Effects of physicochemical characteristics of poly(2-(dimethylamino)ethyl methacrylate)-based polyplexes on cellular association and internalization. *Journal of Drug Targeting* **8**: 51-66

Appendix

Jones, R. A., Cheung, C., Black, F., Zia, J., Stayton, P., Hoffman, A. & Wilson, M. R. (2003). Poly(2-alklacrylic acid) polymers deliver molecules to the cytosol by pH-sensitive disruption on endosomal vesicles. *Biochemical Journal, 372 (Part 1), 65-75.*